MIXED-FREQUENCY TESTING OF INDUCTION MACHINES USING INVERTERS

İLHAMİ ÇOLAK

Doctor of Philosophy

THE UNIVERSITY OF ASTON IN BIRMINGHAM

OCTOBER 1994

THE UNIVERSITY OF ASTON IN BIRMINGHAM

MIXED-FREQUENCY TESTING OF INDUCTION MACHINES USING INVERTERS

İLHAMİ ÇOLAK

Doctor of Philosophy
OCTOBER 1994

SUMMARY

This work has concentrated on the testing of induction machines to determine their temperature rise at full-load without mechanically coupling to a load machine. The achievements of this work are outlined as follows.

1. Four distinct categories of mixed-frequency test using an inverter have been identified by the author. The simulation results of these tests as well as the conventional 2-supply test have been analysed in detail.

2. Experimental work on mixed-frequency tests has been done on a small (4 kW) squirrel cage induction machine using a voltage source PWM inverter. Two out of the four categories of test suggested have been tested and the temperature rise results were found to be similar to the results of a direct loading test. Further, one of the categories of test proposed has been performed on a 3.3 kW slip-ring induction machine for the conformation of the rotor values.

3. A low current supply mixed-frequency test-rig has been proposed. For this purpose, a resonant bank was connected to the DC link of the inverter in order to maintain the exchange of power between the test machine and the resonant bank instead of between the main supply and the test machine. The resonant bank was then replaced with a special electro-mechanical energy storage unit. The current of the main power supply was then reduced in amplitude.

4. A variable inertia test for full load temperature rise testing of induction machines has been introduced. This test is purely mechanical in nature and does not require any electrical connection of the test machine to any other machine. It has the advantages of drawing very little net power from the supply.

5. The computation time of the phase equation model of the machine has been improved by using the explicit form of the inverse of the inductance matrix of the machine. In addition, this basic phase equation model has been expanded by including core loss, saturation of mutual and leakage fluxes of both stator and rotor and rotor deep-bar effect.

KEY-WORDS:
Induction Machines, Mixed-Frequency Testing, Temperature Rise, Inverter, Saturation.

To My Family

Acknowledgement

I would like to thank to my colleagues in the office and many members of staff in the department.

Most particularly, I would like to thank Dr. Seamus Garvey for his excellent supervision and friendly attitudes, and Professor M. T Wright for providing the project for me.

Finally, I would like to thank Gazi University for its financial support.

CONTENTS

LIST OF FIGURES

Titles **Page Numbers**

List of Tables **Page Numbers**

CHAPTER 1

INTRODUCTION

1.1. Literature Survey of Full-Load Temperature Rise Testing of Induction Machines

Induction machines have been widely used in industry for about 150 years. They are relatively inexpensive machines from very small to very large rates of power (from a few hundred watts to several megawatts). Induction machines are generally used as motors to convert electrical energy to mechanical energy. Though it is also possible to use them as generators. Naturally, when the machine is energised, it dissipates power. The dissipated power is composed of two parts, electrical losses and mechanical losses. The electrical losses are the stator copper loss, the rotor copper loss, the core loss and the stray load losses. Windage and friction losses are collectively called mechanical loss. The testing of induction machines to determine the temperature rise as well as the power dissipated inside the machines as heat is a matter of interest to both customers and manufacturers. This is important since it affects the insulation materials, the cooling systems and the efficiency of the machine.

There are several methods commonly used to establish, approximately, the full-load temperature rise of the induction machine. Some of these methods are combined and summarised in ERA Report (1993). The most accurate and basic heat run of the induction machine is to load the machine shaft directly with a mechanical or an electrical load. This test is capable of producing the full-load current flowing into the machine and the full-load mechanical losses occurring inside the machine as well as the full-load rotor current flowing in the rotor bars at rated rotor speed. However coupling of a load to the machine shaft is not easy and hence the test is expensive due to the following reasons:

- The different size of half-couplings is needed for the different shaft size of machines.
- The load for the large machines occupies space and costs a lot of money.

- The load consumes energy.
- A large amount of current is drawn from the supply during the test.

Romeira (1948) proposed the "superimposed frequency test" for the full load heat run of slip-ring induction machines. This test involves feeding harmonic currents into the rotor from an auxiliary supply through a set of auxiliary rotor resistances as shown in Fig. 1-1. However, due to the slip-rings and the brushes of the slip-ring induction machines, the use of slip-ring induction machines is decreasing, whilst the squirrel-cage machine is increasing in popularity.

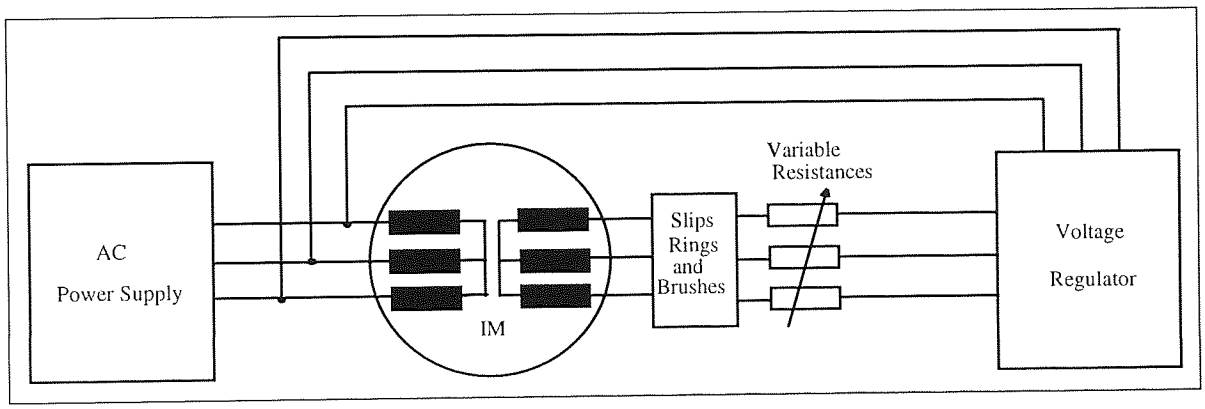

Fig. 1-1 Superimposed frequency test.

The back-to-back test is one of the other testing methods for the full-load heat run of an induction machine. This test has two distinct merits, which are the economy and the accuracy. Because, in this test, the full-load size plant is not needed for loading and the major part of the test power is circulated rather than dissipated. Further, the loss is measured as a net input rather than as the small difference between two separately measured large powers. However, it requires coupling of two induction machines which will run at different speeds when generating or motoring. Thus direct coupling of two induction machines is not possible if two induction machines are operated from a constant frequency supply.

Christofides and Adkins (1966) suggested a method of back-to-back test to overcome this problem as shown in Fig. 1.2, in where, the two induction machines are fed from the same power supply and coupled to two DC machines which are fixed on a stationary bedplate.

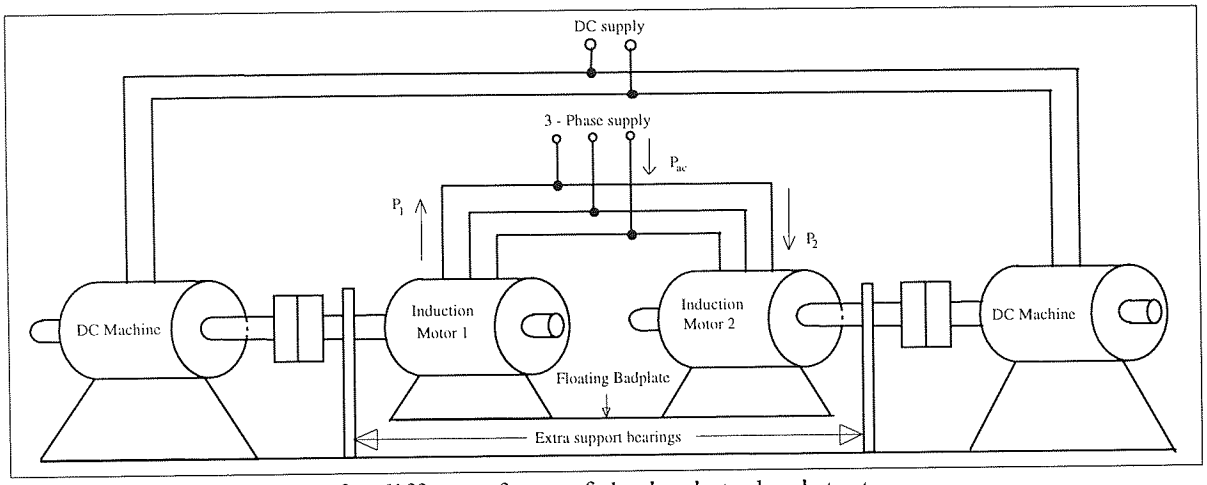

Fig. 1.2 Block diagram of a different form of the back-to-back test.

The stators of the two induction motors are strapped together and are free to rotate on their own bearings. The induction machine 1 is driven as generator at speed of ω_G while the induction machine 2 runs as a motor at speed of ω_M. The speeds of these two induction machines can be adjusted until the stator frames have no tendency to rotate, which means that the torques in two couplings are equal. At this point of balance, the electrical input power to the two induction machines is P_{ac} and the total electrical losses P_t of the two induction machines are given as:

$$P_t = P_{ac} + T(\omega_G - \omega_M) \tag{1.1}$$

They concluded that, the input power P_{ac} supplies the stator losses and very nearly the whole of the load losses. The mechanical power input $T(\omega_G - \omega_M)$ supplies the fundamental rotor I^2R losses and negligible part of the load losses. Thus the load losses P_{ll} can be calculated accurately as:

$$P_{ll} = P_{ac} - (P_{fe1} + 3I_1^2R_1) \tag{1.2}$$

Since the measurement of the rotor I^2R loss is usually the most unreliable and inaccurate for the conventional measurements, it is an advantage of this method that the rotor fundamental loss is not included into the calculation of the load losses.

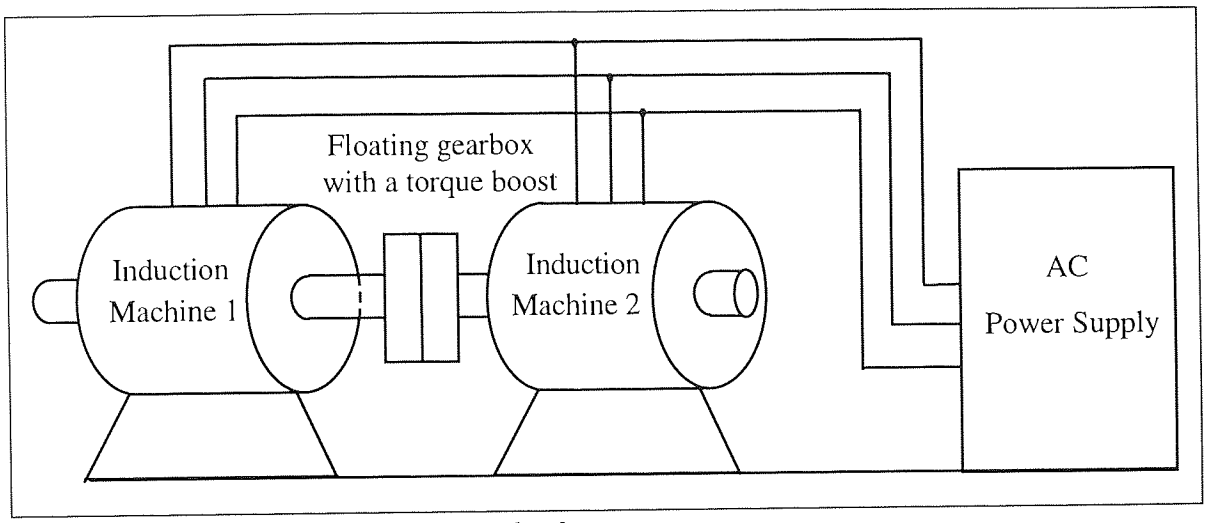

Fig. 1-3 Block diagram of the back-to-back test.

Morris (1968) suggested connecting "a floating gear box with a torque boost" between the test machine and the load machine as given in Fig. 1-3. This method of back-to-back test does not require two extra DC machines as Christofides and Adkins (1966) suggested. Thus the two identical machines are connected as back-to-back to each other through a special gearbox so that the speed differences between the two induction machines can be adjusted with the gearbox. The power loss in the gearbox is of the same order as the load loss in the induction motors. Thus, the gearbox loss must be compensated by the addition of a torque boost to the gearbox housing which ensures that the torques on both sides of the gearbox are equal.

$$T_M = T_G = T \tag{1.3}$$

$$P_M - P_G = \omega_M T_M - \omega_G T_G = (\omega_M - \omega_G)T \tag{1.4}$$

Since $(\omega_M - \omega_G)$ can be measured accurately, the difference power to the same accuracy is as the torque T. This torque balance technique can be applied in variety of ways.

Another approximate form of the heat run of induction machines was called the "phantom loading" introduced by Fong (1972). In this test, the test machine is connected electrically to another auxiliary machine. A DC power supply is also connected between the terminals of two machines as shown in Fig. 1-4. The full-load current flows in both stator and rotor, the full flux circulates in the magnetic circuits and both machines rotate at synchronous speed without being mechanically coupled to each other or a third machine.

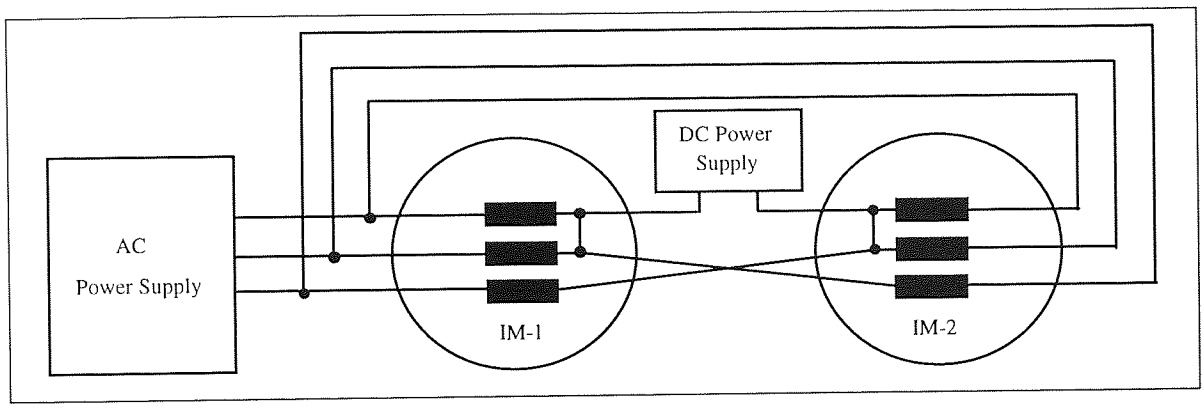

Fig. 1-4 Phantom loading test.

Fong tested both a squirrel-cage induction motor (3 kW at 1450 rpm) and a slip-ring induction motor (3.7 kW at 1430 rpm) respectively. The temperature rise was found to be similar from both phantom loading test and actual test for the squirrel-cage motor. However an increase in speed (about 40 rpm) for both machines used in the test was observed during the phantom loading test. A value of 66.5 °C temperature rise was recorded from the phantom loading test while normal loading test produced 61.5 °C temperature rise for the slip-ring induction machine. Ho (1988) improved the phantom loading test further for the testing of delta connected machines by using a current injector again between the terminals of the two machines. Ho applied the phantom loading test on a 330 kW and 2.2 kW motors. Ho then found the test results for the 2.2 kW induction motor very encouraging.

According to Plevin (1988), a method called "the forward short circuit test" has been developed by GEC ALSTHOM Large Machines Ltd and has been used for the testing of

large machines of ratings up to 21 MW for more than 40 years. This test involves a separate machine to drive the test machine and an alternator or a variable frequency power supply to feed the test machine as shown in Fig. 1-5. The machine is driven at rated speed by feeding its stator from an unexcited alternator. The speed difference between the test machine and alternator can be corrected by playing the excitation of the alternator. Since the induction machine is fed from the reduced frequency of the alternator and driven as an induction generator by a DC machine, the slip of the induction machine can be adjusted to be beyond the slip corresponding to maximum power. Under these conditions, the effective rotor resistance is relatively small such that the machine impedance is dominated by reduced frequency leakage reactance requiring only relatively small voltage for rated current to circulate. Because of the small effective rotor resistance, it may be said that it is approaching short circuit and the rotating speed will be faster than the reduced frequency synchronous speed. Hence it is named as "the forward short circuit test". Finally, it is reported that this test produces a temperature rise which is very close to that obtained by direct loading test at the rated stator current and the rated rotor speed.

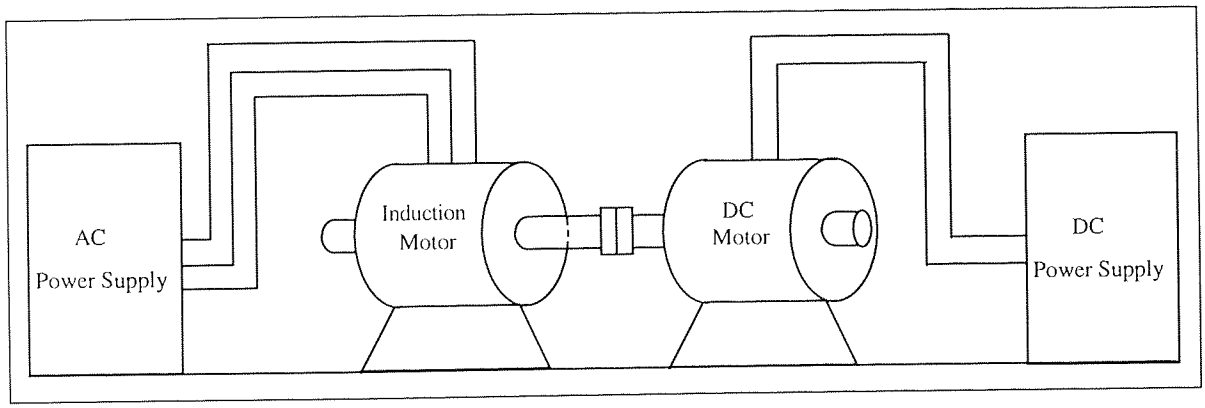

Fig. 1-5 Forward short circuit test.

All the testing methods mentioned above require the use of an extra machine as load or excitation or extra power supplies (to produce mixed-frequency power). Mechanical coupling of large machines on the test-bed (especially in the case of vertical machines) is very difficult and increases the cost of the test. The mixed-frequency test does not require an extra machine or mechanical load. The conventional mixed-frequency test requires the

use of two different power supplies of different frequencies and amplitudes. It is a method that can be applied for testing all types of machine with the advantages of being economic and accurate.

1.2. Structure and Content of the Thesis

This thesis consists of 8 chapters and 5 appendices. The structure of thesis is summarised chapter by chapter as follows:

Chapter 2 deals with the mixed-frequency testing of induction machines. It starts by giving the historical background of mixed-frequency testing of induction machines and continues by explaining the different supply arrangements which can be used for mixed-frequency testing. Furthermore, this chapter also outlines the concepts behind the mixed-frequency test and briefly discusses the low and high frequency contents of voltage waveforms from inverters.

Chapter 3 describes, in brief, the methods which can be used for simulation of induction machines on mixed-frequency testing. In particular it explains the phase equation model and the d-q axis model in detail. The arguments for using the phase equation model in preference to the d-q axis model are outlined.

Chapter 4 deals with the establishment of model parameters from straightforward tests on the induction machine. The appropriate tests themselves are described briefly and the method by which parameters are extracted from the results is outlined.

Chapter 5 investigates different forms of the mixed-frequency test. The degrees of modulation of frquency, amplitude and torque are defined and related. The mixed-frequency testing of one particular induction machine is studied in detail in simulation by applying four different voltage waveforms to the terminals of the induction machine.

In chapter 6, test results from the mixed-frequency testing of two different induction machines are given - one squirrel-cage and one slip-ring machine. The results obtained from simulations and tests are compared.

Chapter 7 introduces two new methods to reduce the effects of the large amount of energy exchanging (between the power supply and the load) on the power supply. In the one, a variable inertia test for full-load temperature rise testing of induction machines was introduced. This proposed test is purely mechanical in nature and it does not require any electrical connections of the test machine to any other machine. In the other one, an electromechanical energy storage unit was proposed. In addition to this, the use of a resonant bank between the source and the inverter as a energy storage unit was studied.

Chapter 8 concludes the thesis and sets out suggestions for further work.

Appendix 1 gives the parameters of the test machines.

Appendix 2 introduces a method for reducing the computational time of simulation of induction machines in phase equation model. In this proposal, the explicit form of inverse of the inductance matrix of an induction machine is explained. In addition, incorporation of the saturation, the deep-bar effect and the core losses into the basic phase equation model is given.

Appendix 3 gives the descriptions of equipment used in the test.

Appendix 4 explains the calibration of the tachometer used for the speed measurement.

Appendix 5 includes all the publications which have resulted from this study.

1.3. Machines Investigated in this Thesis

Three different sizes of induction machines have been used in this thesis. One of them is a 4 kW squirrel-cage induction machine which was used as a test machine. The second one is a 3.3 kW slip-ring induction machine which was used to calculate the rotor parameters and to see the effects of the mixed-frequency test on the rotor parameters. Mixed-frequency testing of induction machines has been suggested for the large machines rather than small, therefore a 12.6 MVA squirrel-cage induction machine was used in most of the thesis for the general analysis. The reason for simulating the small machines was simply that experimental mixed-frequency tests were carried out on them. The reason for considering large machines is that they display different dynamic properties to small ones.

CHAPTER 2

MIXED-FREQUENCY TESTING OF INDUCTION MACHINES

2.1. Introduction

In chapter 1, a number of different methods have been given for the testing of induction machines. A substantial subset of these, though are referred to by different names, belong to one "family" of full-load temperature rise testing of induction machines, namely mixed-frequency testing. This chapter involves a detailed historical background of the mixed-frequency testing of induction machines. In addition, supply arrangements for the mixed-frequency testing of induction machines are discussed and the fundamental concepts of the mixed-frequency testing are examined along with low and high-frequency contents of voltage waveforms from inverters used to supply test machines.

2.2. Historical Background of Mixed-Frequency Testing

Mixed-frequency testing of induction machines achieves two outcomes; the losses in the machine and the temperature rise of the machine when those losses are present. Proportionately, its purpose is probably about 1/5 for establishing power losses and about 4/5 for temperature rise since reasonably accurate methods exist for computing power losses in advance. One of the biggest areas of uncertainty remaining in the design of any electrical machine is the effectiveness of the cooling system.

The broadest definition of mixed-frequency testing of induction machines is that a non-sinusoidal voltage pattern consisting of two (or more) harmonic components is applied to the terminals of the induction machine. This produces a full-load rms current flowing into the machine at rated speed, without loading the machine mechanically. The net input power measured is then equal to the total full-load losses of the motor and under such conditions the temperature rise of the machine can be accurately measured.

The mixed-frequency has not been used intensively in the machine industry and there are relatively few publications dealing with it, although it is a long-established method. Kron (1973), Meyer and Lorenzen (1979) and Plevin (1988) all asserted that the mixed-frequency test was first proposed by Ytterberg in 1921. Hill (1965) attributed the test to Lilljeblad who used this method extensively on vertical machines or others that could not be coupled physically to a load.

Hill (1965) also claimed that this method offered a higher accuracy than other methods, because the following conditions were satisfied;

- Full-load values of current and rated voltage were present at the same time.
- Normal leakage flux and main flux occur at the same time.
- The total power loss was measured directly by a wattmeter and not as the difference between two very much larger readings.

Schwenk (1975) tested a large induction machine rating of 11000 hp by applying a mixed-frequency test. The voltages applied to the machine were obtained from two different alternators that were driven by two different DC motors. Schwenk used two types of connection for the test. In one, the coils of the two alternators were connected in series, in the other a transformer was used to isolate these two alternators. Schwenk stated that the mixed-frequency test results were slightly higher than the results obtained from normal load conditions. The main advantages of this test perceived by Schwenk are that coupling of the machine shaft is eliminated and the rated voltage and currents are applied to the test machine rather than rated power. Schwenk also mentioned that the mixed-frequency test had been used for several years by his company (Westinghouse Electric Corporation, East Pittsburgh Pa.) to test large induction motors. They have found this test to be a very practical method especially for measuring temperature rises of large vertical machines, and it had been found invaluable for the testing of efficiency, power factor and various motor torques.

After that, Radic and Strupp (1976) analysed the mixed-frequency (or continuously varied frequency) test. They also employed this method in testing induction machines of all ratings up to 12 MVA. In addition they checked the accuracy of the method for temperature rise measurements on different motors. They noted that at frequency differences (i.e. below 5 Hz), the needles of the analogue instruments swing with significant amplitude, thus reducing the accuracy of the test. With digital instrumentation and recording this frequency limit is removed. Furthermore, they concluded that the continuously varied frequency test gives good accuracy for determination of no-load temperature rise in the windings of the induction motors.

Jordon et al. (1977) recommended the mixed-frequency test is an acceptable method for determining the temperature rise of the induction motors. They stated that the mixed-frequency test result (4292 Watts) was very close to the 4078 Watts obtained from the full-load test of a 300 hp induction machine. They also concluded that the mixed-frequency test can only be used to determine temperature rise, but not for measuring the efficiency or power factor of the induction machines.

The study of mixed-frequency heat runs was continued by Meyer and Lorenzen (1979). Then they measured the temperature rise of an induction machine by using the mixed-frequency method and compared the results with conventional heat run results. As a conclusion, they mentioned that the two-frequency method is suitable for determining the temperature rise of the windings and enables the efficiency of the motor to be determined with a high degree of accuracy.

Plevin (1988) analysed the mixed-frequency test in detail. He stated that in the mixed-frequency test, the dominant effect is the beating of stator voltages. When the stator voltage increases, there is an increase in the torque tending to pull the rotor speed closer to synchronous speed. Thus depending on whether the rotor speed is greater than or less than synchronous speed, an increase in voltage will cause the machine to generate or motor

respectively. It is also the case that shifting the synchronous frequency can cause the machine to motor or generate. Plevin found that for a particular mixed-frequency test involving 2 supplies, the effect of the variation in voltage magnitude was the dominant one. He found that the mixed-frequency test results exceeded those obtained from the full-load test and the vibration was abnormal due to the oscillation of torque.

Peebles Electrical Machines reported that the total loss occurring during a mixed-frequency testing heat run will always be found to exceed that under normal steady full-load conditions. They concluded that this test cannot be used to calculate accurately the efficiency of the motor since it is not possible to measure full-load power factor.

Palit B. B. (1980) observed that the two frequency method is equivalent to the conventional loading method, so far as the temperature rise is concerned. However, he stated that the vibration of the machine was abnormal and the backward and forward movement of the motor shaft in the axial direction caused unwanted trust on the machine bearings.

All the methods of the mixed-frequency testing of induction machines examined above require more than one power supply. Recently, an inverter has been suggested as a mixed-frequency power supply (Çolak et al. (EPE'93)). Grantham and Rahman (1993) and Grantham (1993) introduced a novel machineless dynamometer for load testing three phase induction motors. In this paper, Grantham and Rahman (1993) tested the induction machine by using a microprocessor controlled inverter. Similarly, Grantham et al. (1990) and Spooner et al. (1986) used microprocessor controlled power electronics to replace the electrical machines of an existing equivalent load technique and to rapidly change the machine's supply frequency. In fact, all four references mentioned here are the same although they were published in different conferences by the same author, Grantham, with some different co-authors and the methods which they called microprocessor controlled

power electronic techniques, are parts of the forms of the mixed-frequency testing of induction machines as Çolak et al. (EPE'93) mentioned.

2.3. Supply Arrangements for Mixed-Frequency Testing

The main idea of the mixed-frequency testing of induction machines is to run the machine at the rated speed, drawing the full-load current from the supply and inducing full-load current on the rotor without connecting its shaft mechanically to any load. The only distinction between the various mixed-frequency tests is the method of production of the non-sinusoidal voltage waveform. Thus, only two functions need to be controlled for the production of the mixed-frequency voltage waveforms. Appropriate choice of these two periodic functions causes the rotor to accelerate and decelerate and causes the machine to run alternately as a motor and as a generator. The test machine draws large currents from the supply. The rms value of the current can be adjusted to the rated value by modifying the parameters governing amplitude and frequency as functions of time.

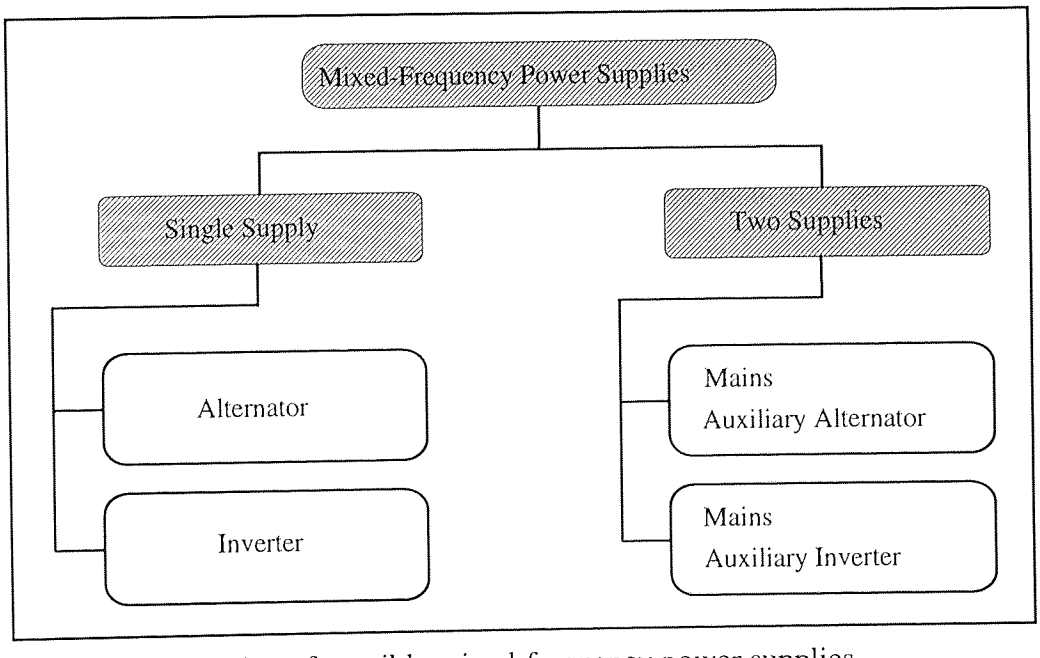

Fig. 2.3-1 Illustration of possible mixed-frequency power supplies.

An alternator or an inverter can be used as a single mixed-frequency power supply as illustrated in Fig. 2.3-1. If an alternator is used to produce different types of voltage waveforms whose amplitudes and frequencies are varied arbitrarily, the field current or

rotor speed of the alternator must be controlled either separately or together. The use of an alternator requires a DC machine or any other machine to drive the rotor of the alternator and a DC source to feed the field windings of the alternator. The use of inverter as a single mixed-frequency power supply provides a wide range of control over the output voltage and frequency as well as eliminating the use of extra DC machines to drive the alternator. The inverter is capable of producing so many different voltage waveforms (sine-wave, square-wave, triangular-wave or different combinations of these waveforms) at different frequencies. The rated power of the inverter is related with the rated power of the semi-conductor used to build the power stack. The use of a single mixed-frequency power supply will be analysed in detail in chapter 5 by giving obtainable voltage equations and simulation results obtained by applying these voltage waveforms.

In the case of using two supplies as a mixed-frequency power supply, there are two possible options given in Fig. 2.3-1. In the first option, both supplies can be two different size of alternators (or the mains and the auxiliary alternator) whose outputs are connected to each other through a specially designed transformer as shown in Fig. 2.3-2 or the coils of the two alternators are connected to each other in serial as shown in Fig. 2.3-3. One of them is the main, the other one is the auxiliary alternator. Generally, the main alternator produces rated amplitude of voltage at rated frequency of the test machine and the auxiliary one produces lower amplitude of voltage at lower frequency. The use of one or two alternators as a mixed-frequency power supply requires one or two more DC machines to drive the alternators.

In the second option, a combination of an inverter as an auxiliary supply and an alternator as a main supply can also be used to supply a mixed-frequency test. In this case the outputs of both inverter and alternator must be connected to each other through a transformer. The use of an inverter as an auxiliary supply eliminates the use of an alternator and a DC machine.

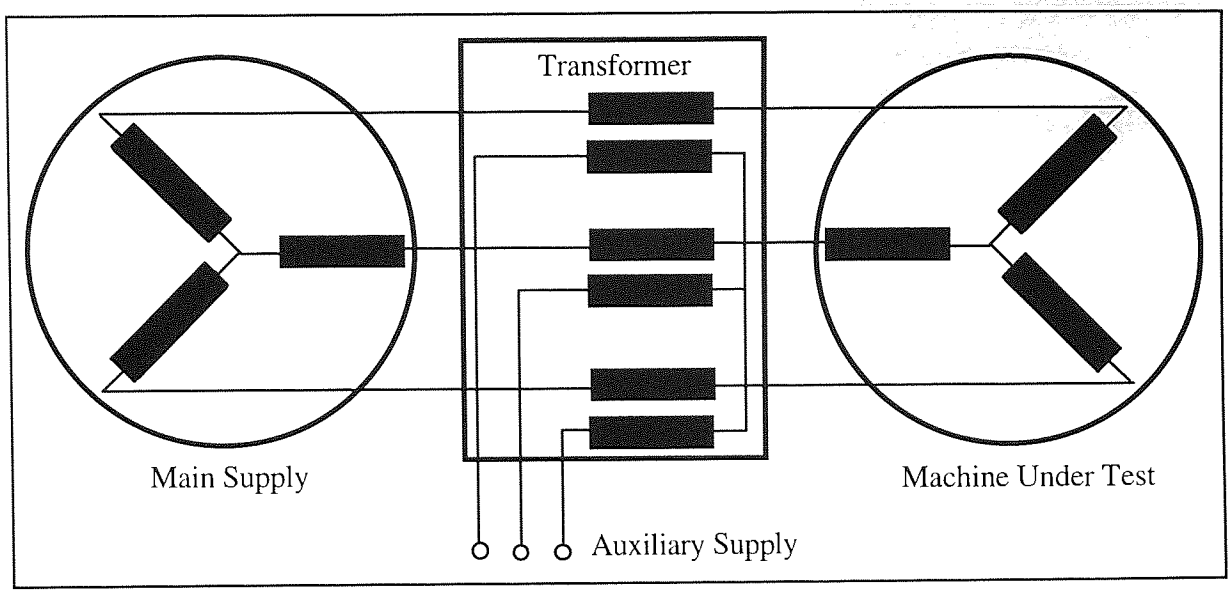

Fig. 2.3-2 Generic connection arrangement for conventional mixed-frequency test through a transformer.

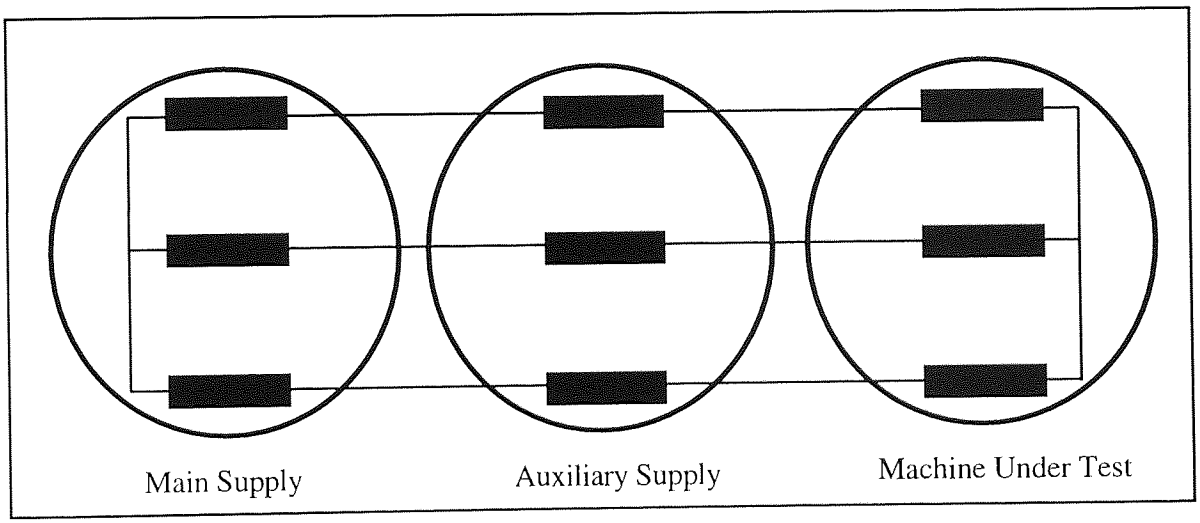

Fig. 2.3-3 Generic serial connection arrangement for conventional mixed-frequency test.

The voltage equation for the use of two supplies (case 1) can be written as:

Case 1:

$$V_{sa}(t) = V_0\left[(\sin(\omega_0 t) + \delta\sin((1-\Re)\omega_0 t))\right] \Rightarrow \Re = \frac{\omega_b}{\omega_0} \qquad (2.3\text{-}1)$$

where

V_{sa}= Resultant voltage,

V_0= Amplitude of base voltage,

δ= Degree of voltage modulation,

ω_0= Angular base frequency,

ω_b= Angular beat frequency,

$\Re$ = Ratio of beat frequency over base frequency.

It can be said that, in the case of using two supplies as a mixed-frequency power supply, various voltage waveforms can be produced in any form as long as one of the supplies used is either alternator or inverter due to the control capabilities of inverter and alternator.

If an inverter is used as an auxiliary power supply and an alternator is used as a main supply, the inverter must be capable of carrying the same current as the main supply. The main supply feeds the inverter through the test machine, so that the average power going into the machine is the sum of both main and inverter powers. Fig.'s 2.3-4a and 2.3-4b are the simulation results of a particular case of the mixed-frequency test (f_b = 10 Hz, δ = 0.084 p.u.).

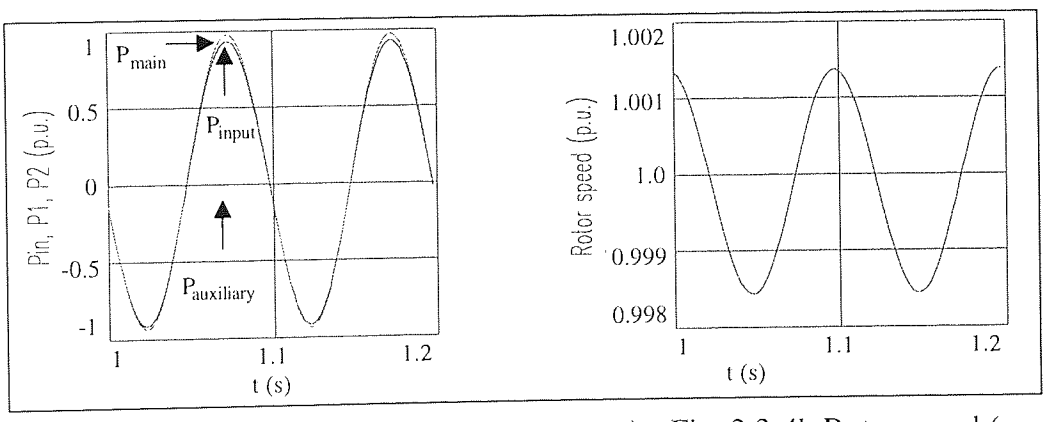

Fig. 2.3-4a Input, main and auxiliary powers (p.u.). Fig. 2.3-4b Rotor speed (p.u.)

As seen from Fig. 2.3-4a, the inverter must be capable of delivering a maximum instantaneous power of 0.26 MW (0.02 p.u.) and absorbing a maximum instantaneous power of -0.544 MW (-0.043 p.u.). If the inverter has no external source of power, it must have an ability to store quantities of energy of the order of 6.088 kJ.

Some of the voltage waveforms for the use of single power supply can be defined respectively, as pure frequency modulation (case 2), pure amplitude modulation (case 3), and simultaneous frequency and amplitude modulation (case 4). These voltage waveforms can also be obtained from the following equations respectively:

Case 2:

$$\left.\begin{aligned} V_{sa}(t) &= V_0 \sin\big(\theta(t)\big) \Rightarrow \frac{d\theta(t)}{dt} = \omega_0 \alpha(t) \Rightarrow \alpha(t) = 1 + \delta\cos(\Re\omega_0 t) \\ \text{or alternatively} \quad \theta(t) &= \omega_0 \int_0^t \alpha(t)dt = \omega_0 t + \frac{\delta \sin(\Re\omega_0 t)}{\Re} \end{aligned}\right\} \quad (2.3\text{-}2)$$

Case 3:

$$V_{sa}(t) = V_0 \alpha(t) \sin\big(\omega_0 t\big) \Rightarrow \alpha(t) = 1 + \delta\cos(\Re\omega_0 t) \quad (2.3\text{-}3)$$

Case 4:

$$\left.\begin{aligned} V_{sa}(t) &= V_0 \alpha(t) \sin\big(\theta(t)\big) \\ \frac{d\theta(t)}{dt} &= \omega_0 \alpha(t) \Rightarrow \alpha(t) = 1 + \delta\cos(\Re\omega_0 t) \\ \text{or alternatively} \quad \theta(t) &= \omega_0 \int_0^t \alpha(t)dt = \omega_0 t + \frac{\delta \sin(\Re\omega_0 t)}{\Re} \end{aligned}\right\} \quad (2.3\text{-}4)$$

where

V_{sa}= Resultant voltage,

V_0= Maximum value of resultant voltage,

ω_0= Angular base frequency of main supply,

ω_b= Angular beat frequency,

$\Re$= Ratio of beat frequency over base frequency, (ω_b/ω_0),

δ= Degree of either voltage or frequency modulation.

2.4. Concept of the Mixed-Frequency Test

The fundamental principles of the full-load temperature rise testing of induction machines are the same for all the methods discussed in chapter 1. However, only the mixed-frequency test allows the possibility of running the induction machine at the rated speed while drawing the rated current from the supply without loading machine mechanically or electrically using identical machine.

There are potentially, an infinite number of different mixed-frequency tests that could be applied to any induction machine. However, all mixed-frequency tests share two parameters namely the "beat frequency", ω_b (Rad/s), and the "degree of torque modulation" δ_T. The beat frequency can be defined as the frequency of the fundamental component of the rotor speed function.

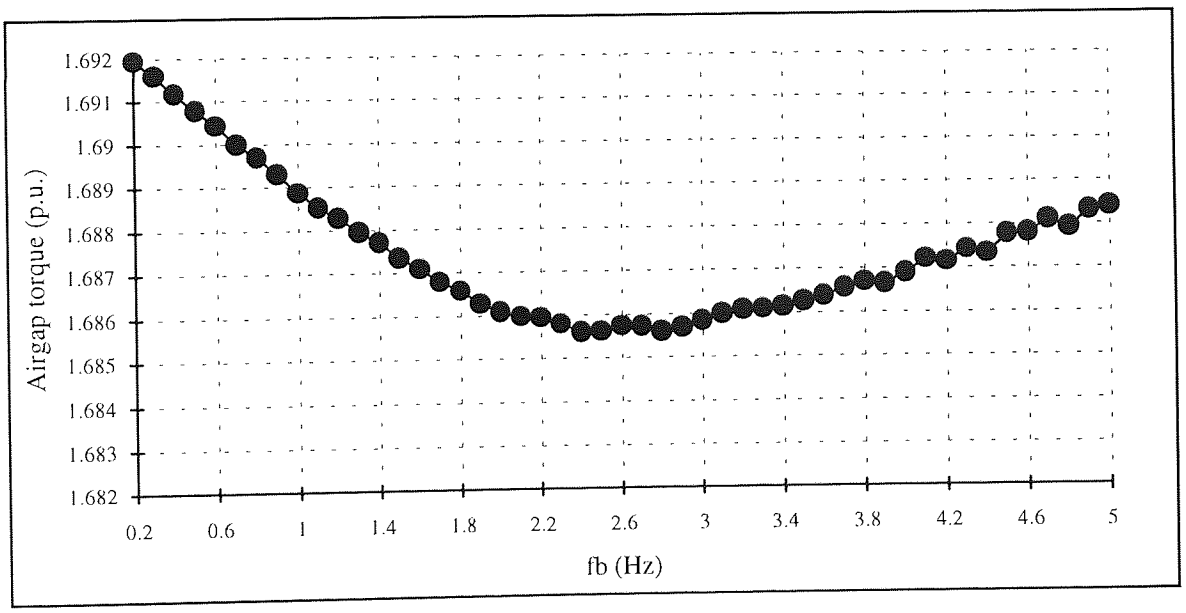

Fig. 2.4-1 Variation of airgap torque with respect to the beat frequency for case 1 with constant degree of voltage modulation and rotor speed.

The degree of the torque modulation can be defined as the rms airgap torque that would be experienced in the machine on test if its rotor speed was held constant and if ω_b was taken to be very low. Fig. 2.4-1 shows the variation of airgap torque for case 1 with $\delta_v = 0.03567$

and ω_r = 154 Rad/s at various beat frequencies. At low beat frequencies, between 0.2 Hz and 2.6 Hz, the rms airgap torque decreases gradually, but then it increases.

It was stated earlier that for all practical mixed-frequency tests, the voltage waveform can be characterised by two functions of time, amplitude and frequency. By judiciously setting these two functions, it must be possible to obtain desired rms values for two variables inside the machine. The obvious variables to set are the stator current and the rate of change of flux. Thus, it is reasonable to impose a restriction at this stage that forces all modulation to be sinusoidal and thereby allows a mixed-frequency test to be characterised very concisely. Within this constrained space, the mixed-frequency test will be allowed to take one of only four forms, constant-voltage varying-frequency, varying-voltage constant-frequency, varying-voltage varying-frequency and sum of two sine-waves from two different power supply. No matter which supply arrangement is used to produce these four modes, the concept of the test is still the same. However, there are differences in terms of producing these modes. In the first, as the amplitude of the voltage is kept constant, the frequency of the voltage is varied. In the second, as the amplitude of voltage is varied, the frequency is kept constant. In the third, both the amplitude and the frequency of the voltage are varied. In the fourth, the mains has the rated amplitude of voltage at the rated frequency as the auxiliary one has the lower amplitude of voltage at the lower frequency so that, both the amplitude and the frequency of resultant voltage are varied. The merits and disadvantages of each four forms henceforth allowed for the mixed-frequency test are throughly investigated in chapter 5.

2.5. Low and High-Frequency Contents of Voltage Waveforms From Inverters

An inverter provides a non-sinusoidal voltage waveform unless its output is filtered. Every inverter output voltage is a combination of PWM signals that have constant magnitude in the positive and negative regions with a variable frequency. Inverters are widely used as

power supplies in industry, due to the wide range of control capability over the output voltage and frequency.

The use of an inverter as a mixed-frequency power supply has much to recommend it over the use of alternators. The main disadvantages of using an alternator can be outlined as:

- Requirement of an extra DC machine to drive the alternator (mechanical coupling is also needed).
- Requirement of a separate DC supply to feed the field windings of alternator.
- Requirement of a special controller for the DC machine.

There are some high frequency harmonics in the inverter output voltage due to the switching frequency of the inverter. These high frequency harmonics will increase the core losses (Cecconi et al. (1986), Mohan et al. (1989)). It is possible, and quite sensible to include some form of filter in the line between inverter and induction machine to eliminate the high frequency harmonics in the voltage applied to the test machine.

2.6. Summary

A detailed historical background of the mixed-frequency testing of induction machines has been summarised, from 1921 up to 1993. In these studies, the mixed-frequency testing was applied to different sizes of machines from a few kilowatts to 12 MVA. Different supply arrangements for mixed-frequency testing of induction machines as well as the concepts of mixed-frequency testing have been given. In addition, the main parameters for the mixed-frequency testing have been explained. Further, besides the conventional mixed-frequency testing power supplies, low and high-frequency contents of voltage waveforms from inverters have been briefly discussed. It is recognised that the high frequency harmonics from inverters do increase the core losses of machines, but measures can be taken to prevent these harmonics from reaching the machine.

CHAPTER 3

MODELLING OF INDUCTION MACHINES

3.1. Introduction

The first priority of this research is the mixed-frequency testing of induction machines. A reliable simulation program is therefore essential to predict the stator currents, the rotor currents, the input power and the rotor speed before testing the induction machine. The first step towards a good simulation program is to choose a suitable model for the induction machine.

A considerable amount of research has been done on mathematical models of the induction machines, using both frequency domain and time domain representations. The frequency domain machine representations are limited to steady-state performance studies. The time domain representations can be used for both steady-state and transient performance studies. There are different types of time domain induction machine models such as the *three phase machine model*, (3-phase stator, 3-phase rotor), (Robertson and Hebbar (1969), Koopman and Trutt (1969), Sarkar and Berg (1970), Jacovides (1973), Rajan et al. (1974), Nath and Berg (1981), Smith and Yacamini (1993)), *hybrid models* (3-phase stator, 2-phase rotor), (Bowes and Clare (1988)), *two axis or d-q axis machine models* (Krause and Thomas (1965), Jordan (1965), Jordan (1967), Krause (1968), Lloyd (1982), Bowes and Clements (1983), Kerkman (1985), Bowes and Clare (1988), Andrade et al. (1994)). In addition, Bowes and Clare (1988) produced a *network equivalent* for the motor based on the d-q axis reference frames. *Space vector modelling* of induction motors is another time domain model that offers notational convenience and facilitates application of modern control theory (Vas (1990), Illango and Ramamoorty (1974), Brown et al. (1983), Salvatore and Stasi (1994), Bresnahan et al. (1994), Andrade et al. (1994)).

Slemon (1989) presented different *equivalent circuit models*, which are simpler than the *conventional T form of circuit*, for induction machines for transient and steady state operations. Russel and Pickup (1982) used the *integral equation method*, which was driven from the phase equation model, for the analysis of the unbalanced induction motor such as single phase stator, polyphase rotor or polyphase stator, single phase rotor.

In this study, the basic phase equation model is used for modelling a three phase induction machine, but the d-q axis model is also given in detail as an alternative model. A discussion of the advantages and the disadvantages of these two models justifies the use of the phase-equation model in this case. A full explanation of each model is given after this discussion.

3.2. Discussion of the phase equation model and the d-q axis model

It is relatively common view that, modelling of induction machines using phase equation model is conceptually simpler than using d-q axis model (Krause and Thomas (1965), Krause (1968), Robertson and Hebbar (1969), Sarkar and Berg (1970)). The machine equations are written for each phase separately in terms of the flux linkages or current in normal phase configuration. Transformation of the equations from one reference frame to another is not needed. Due to non-linearity, the equations are solved in open form, and the mutual effects between stator and rotor phases are updated at each step since they are position dependent. Taking space harmonics into account, analysing machines fed with unsymetrical supplies, and including mixed terminal constraints are all more simply done for the phase equation model than for the d-q axis model.

As explained in appendix 2.1., the principal disadvantage of the phase equation model is that *the inverse of the inductance matrix must be computed at least once during every step in the solution of the differential equations of the induction machine* (Robertson and Hebbar (1969), Sarkar and Berg (1970), Ramshaw and Padiyar (1973), Illango and Ramamoorty (1974), Lloyd (1982)). As a result of this, the computation time associated with using the phase equation model directly is longer than that associated with the use of the d-q axis

model. However, Çolak et al. (1993, IEE, Part-B) have shown that the inverse can be obtained directly in most cases - thereby removing the principal objection to use of the phase equation model.

It is well known (e.g. Ramshaw and Padiyar (1973)) that, the generalised two-axis machine, that is based on the two-reaction theory introduced by Kron in 1934 consists a basic model, that is applicable to many types of machines. In the two axis model, the machine is represented by two phases (the direct and quadrature axes) by transforming the three phase values to the two phases. By doing that the number of electrical equations of the machine is reduced from six (one equation for each phase of stator and rotor) to four and the angle between the rotor and the stator is also eliminated (Jordan (1965-1967), Krause and Thomas (1965), Krause (1968), Sarkar and Berg (1970), Lloyd (1982), Bowes and Clements (1983)). These four equations can be solved by writing them in terms of either flux linkages or current. The solutions are then transformed back into the three axis model to find the individual phase values of the stator and rotor. Most researchers dealing with the simulation of induction machines use the d-q axis model to reduce the computational time associated with the three axis (or phase equation) model.

The d-q axis model is certainly more computationally efficient than phase equation model, but it imposes constraints on the model that may not be present in the actual machine. In particular, analysing the machines under unbalanced conditions and considering mixed terminal constraints are not easy in the two axis model (Jacovides (1973), Illango and Ramamoorty (1974), Rahman and Shepherd (1977), Nath and Berg (1981), Lloyd (1982)). The effect of the variation of the inductance matrix with flux levels can be built into d-q axis models (Brown et al. (1983)) but arguably, it is more straightforward with the phase equation model.

There appears to be a consensus in the literature that the d-q-0 axis modelling is to be favoured because of its computational speed for most analyses of induction machines but

that many situation exist where the additional cost of using phase equations models is justified. Robertson and Hebbar (1969) noted that, with certain types of inverter drives, one or more of the machine terminals will be open circuited for various periods during each cycle. Therefore, the d-q equations must be modified to account for the constraint of zero phase currents during these periods. Illango and Ramamoorty (1974) observed that the continuous monitoring of phase currents, as required in the transient analysis of inverter-fed or phase controlled induction motors, involves transformations back and forth from d-q-0 variables to phase variables. Nath and Berg (1981) expressed the view that because of the complications arising from the in-line switching constraints, the transient analysis of three-phase SCR controlled induction motors was best performed using phase equation model rather than the two-axis model. Bowes and Clements (1983) reported that, the d-q axis modelling of induction machines can be used in the vast majority of operational circumstances where the terminal constraints on voltage or current are known explicitly. Fudeh and Ong (1983) stated that the polyphase to rotating d-q transformation was applicable when only one harmonic from each α-β component was to be considered, otherwise a new problem of separating the harmonic voltages within each α-β component was created. Furthermore, for those situations where the terminal constraints on voltage and current are mixed, and only partly known, the direct three phase simulation model must be more appropriate (Jacovides (1973), Bowes and Clements (1983)). Finally, Smith and Yacamini (1993) reported that, the d-q axis modelling of induction machines can be programmed in MAST, the modelling language used by the Saber simulator, assuming that the machine is balanced and there are no zero sequence components present in the supply voltage. However the initial attempts showed that, using a two-axis machine model with the three phase converter models took longer computer run times than those obtained using direct three phase machine model due to the backward and forward conversions between phase and two-axis quantities.

For the perposes of this study, it was decided that a phase equation model would be utilised from the outset. The rationale was, essentially, that it was known for certain that this

modelling could accomodate, directly, all of the effects which might be significant for simulating induction machines on mixed-frequency test. Since d-q axis model is obtained from the phase equation model by a simple co-ordinate transformation involving the application of at least 2 constraints it was realised that changing models from phase equation form to d-q axis form would always remain an option. With the direct inversion of the inductance matrix in phase equation model, it transpires that there is little computation penalty in using the phase equation form directly.

The simple phase equation model for induction machines is presented briefly in the following section and d-q axis model is presented briefly in the section following that. This simple (phase equation) model has been used for almost all of the simulations reported in the thesis. Appendix 2 reports some work done on extending the simple phase equation model to include the effects of the saturation, deep-bar and core loss.

3.3. The Phase Equation Model of Induction Machines

In the phase co-ordinate reference frame, the voltage balance equations for both stator and rotor of the induction machine can be written in matrix form as (Sarkar and Berg (1970), Ramshaw and Padiyar (1973), Krause (1986)):

$$\mathbf{v} = \frac{d\psi}{dt} + \mathbf{Ri} \tag{3.3-1}$$

where $\mathbf{v}$ is the voltage vector, ψ is the vector of flux linkages, $\mathbf{i}$ is the current vector and $\mathbf{R}$ is the 6x6 resistance matrix of the induction machine as given below:

$$\mathbf{v} = \begin{bmatrix} V_{sa} \\ V_{sb} \\ V_{sc} \\ V_{ra} \\ V_{rb} \\ V_{rc} \end{bmatrix}, \quad \mathbf{i} = \begin{bmatrix} i_{sa} \\ i_{sb} \\ i_{sc} \\ i_{ra} \\ i_{rb} \\ i_{rc} \end{bmatrix}, \quad \psi = \begin{bmatrix} \psi_{sa} \\ \psi_{sb} \\ \psi_{sc} \\ \psi_{ra} \\ \psi_{rb} \\ \psi_{rc} \end{bmatrix}, \quad \mathbf{R} = \begin{bmatrix} r_s & 0 & 0 & 0 & 0 & 0 \\ 0 & r_s & 0 & 0 & 0 & 0 \\ 0 & 0 & r_s & 0 & 0 & 0 \\ 0 & 0 & 0 & r_r & 0 & 0 \\ 0 & 0 & 0 & 0 & r_r & 0 \\ 0 & 0 & 0 & 0 & 0 & r_r \end{bmatrix} \tag{3.3-2}$$

If the effects of the core losses, saturation and space harmonics are ignored on the behaviour of the machine, the relationship between phase currents and phase flux linkages can be written as:

$$\boldsymbol{\psi} = \mathbf{L}\mathbf{i} \quad \text{...or...} \quad \mathbf{i} = \mathbf{L}^{-1}\boldsymbol{\psi} \tag{3.3-3}$$

$$\mathbf{L}(\theta) = \begin{bmatrix} L_{ss} & -\frac{L_{sm}}{2} & -\frac{L_{sm}}{2} & M_{sr}\cos(\theta) & M_{sr}\cos(\theta+\frac{2\pi}{3}) & M_{sr}\cos(\theta-\frac{2\pi}{3}) \\ -\frac{L_{sm}}{2} & L_{ss} & -\frac{L_{sm}}{2} & M_{sr}\cos(\theta-\frac{2\pi}{3}) & M_{sr}\cos(\theta) & M_{sr}\cos(\theta+\frac{2\pi}{3}) \\ -\frac{L_{sm}}{2} & -\frac{L_{sm}}{2} & L_{ss} & M_{sr}\cos(\theta+\frac{2\pi}{3}) & M_{sr}\cos(\theta-\frac{2\pi}{3}) & M_{sr}\cos(\theta) \\ M_{sr}\cos(\theta) & M_{sr}\cos(\theta-\frac{2\pi}{3}) & M_{sr}\cos(\theta+\frac{2\pi}{3}) & L_{rr} & -\frac{L_{rm}}{2} & -\frac{L_{rm}}{2} \\ M_{sr}\cos(\theta+\frac{2\pi}{3}) & M_{sr}\cos(\theta) & M_{sr}\cos(\theta-\frac{2\pi}{3}) & -\frac{L_{rm}}{2} & L_{rr} & -\frac{L_{rm}}{2} \\ M_{sr}\cos(\theta-\frac{2\pi}{3}) & M_{sr}\cos(\theta+\frac{2\pi}{3}) & M_{sr}\cos(\theta) & -\frac{L_{rm}}{2} & -\frac{L_{rm}}{2} & L_{rr} \end{bmatrix} \tag{3.3-4}$$

A complete dynamic model of an induction machine must implicitly involve equations for the mechanical behaviour as for the electrical behaviour (Sarkar and Berg (1970), Ramshaw and Padiyar (1973), Rajan et al. (1974), Çolak et al. (1993, IEE-Part-B)). These equations are summarised as (3.3-5) for a simple model:

$$\left.\begin{aligned} &\frac{d\boldsymbol{\psi}}{dt} = \mathbf{v} - \mathbf{R}\mathbf{L}^{-1}\boldsymbol{\psi} \quad \text{...or...} \quad \frac{d\mathbf{i}}{dt} = \mathbf{L}^{-1}\left[\mathbf{v} - \mathbf{R}\mathbf{i} - \omega_r\frac{d\mathbf{L}}{d\theta}\mathbf{i}\right] \\ &\qquad\qquad \text{and} \\ &\frac{d\omega_r}{dt} = \frac{d^2\theta}{dt^2} = \frac{P}{2J}\left[(T_e - T_L) - F\frac{d\theta}{dt}\right], \qquad T_e = \frac{P}{4}\mathbf{i}^T\frac{d\mathbf{L}}{d\theta}\mathbf{i} \end{aligned}\right\} \tag{3.3-5}$$

where

ω_r = Rotor speed,

θ = Angle between stator and rotor,

T_e = Electromagnetic torque,

T_L = Load torque,

F = Friction constant,

P = Number of poles.

The response of any given induction machine to a given voltage waveform and load torque can be determined using equation (3.3-5). There are several methods, such as Runge-Kutta and Euler, to numerically solve the first order differential equations given in (3.3-5). Note that irrespective of whether the vector of currents $\mathbf{i}$ or the vector of flux linkages $\boldsymbol{\psi}$ is taken as being independent, it is necessary to find the product of $\mathbf{L}^{-1}$ times a 6x1 vector ($\mathbf{y}$) at least once during each step of the simulation (possibly several times per step depending on the integration routine chosen). To evaluate $\mathbf{L}^{-1}\mathbf{y}$ there are several options (Gerald and Wheatley (1994), Hoffman (1992)), for example:

- Compute $\mathbf{L}^{-1}$ and multiply $\mathbf{L}^{-1}\mathbf{y}$.
- Use a direct method to solve $\mathbf{L}^{-1}\mathbf{y}$ (such as Cramer, Gaussian elimination or Gauss Jordan).
- Use an iteration method to solve $\mathbf{L}^{-1}\mathbf{y}$.

Appendix 2 explains the explicit form of inductance matrix of an induction machine as well as incorporating the saturation, the deep-bar effects and the core losses into the basic phase equation model.

3.4. Reference-Frame Theory

There are several reference frames; arbitrary, stationary, rotor and synchronously rotating reference frames. The arbitrary reference frame theory is the general one. Once the arbitrary reference frame theory is given, the others can be obtained easily by changing the angular speed of the reference frame.

3.5. Arbitrary Reference Frame Theory

In this reference frame theory, the angular speed of the frame is chosen arbitrarily. The variables (voltages, currents and flux linkages) of stator and rotor are given in general form and represented by **f**. The subscripts *abc* denote the three phase values respectively (with 120° between phases) and *s* denotes variables and parameters associated with the stator circuit. The subscript *r* denotes the rotor circuit variables and parameters. The three phase subscripts, *abc,* are represented as *qd0* in arbitrary reference frame. The relationship between the three phase and the arbitrary reference frame for the stator may be expressed as (Adkins and Harley (1975), Krause (1986), Krause and Wasynczuk (1989)):

$$\mathbf{f}_{qd0s} = \mathbf{K}_s \mathbf{f}_{abcs} \tag{3.5-1}$$

where

$$\mathbf{f}_{qd0s}^{T} = \begin{bmatrix} f_{qs} & f_{ds} & f_{0s} \end{bmatrix}, \quad \mathbf{f}_{abcs}^{T} = \begin{bmatrix} f_{as} & f_{bs} & f_{cs} \end{bmatrix} \tag{3.5-2}$$

$$\mathbf{K}_s = \frac{2}{3}\begin{bmatrix} \cos(\theta_{dq}) & \cos(\theta_{dq} - \frac{2\pi}{3}) & \cos(\theta_{dq} + \frac{2\pi}{3}) \\ \sin(\theta_{dq}) & \sin(\theta_{dq} - \frac{2\pi}{3}) & \sin(\theta_{dq} + \frac{2\pi}{3}) \\ \frac{1}{2} & \frac{1}{2} & \frac{1}{2} \end{bmatrix}, \quad (\mathbf{K}_s)^{-1} = \begin{bmatrix} \cos(\theta_{dq}) & \sin(\theta_{dq}) & 1 \\ \cos(\theta_{dq} - \frac{2\pi}{3}) & \sin(\theta_{dq} - \frac{2\pi}{3}) & 1 \\ \cos(\theta_{dq} + \frac{2\pi}{3}) & \sin(\theta_{dq} + \frac{2\pi}{3}) & 1 \end{bmatrix} \tag{3.5-3}$$

The three phase stator variables are transformed into the two axis or *q-d* arbitrary reference frame in Fig. 3.5-1. The reference frame is chosen as if there was an angle of θ_{dq} between the phase *as* and phase *qs*. The value θ_{dq} is defined from the integration of the speed (ω) of the reference frame.

$$\theta_{dq} = \int_0^t \omega(t)dt + \theta_{dq}(0) \tag{3.5-4}$$

Fig. 3.5-2 shows transformation of three phase rotor variables to the arbitrary reference frame. If θ_{dq} and ω are replaced by β and ω-ω_r respectively, the equations given for the stator can be used for the rotor. The angle (β) between the phase *ar* and the phase *qr* is given as:

$$\left.\begin{aligned} \beta &= \theta_{dq} - \theta \\ \theta &= \int_0^t \omega_r(t)dt + \theta(0) \end{aligned}\right\} \qquad (3.5\text{-}5)$$

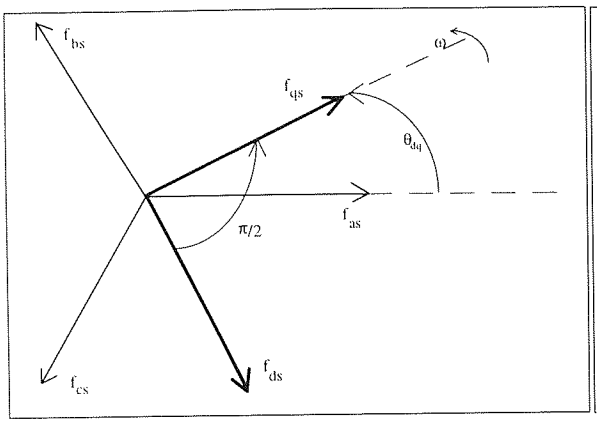

Fig. 3.5-1 Transformation of 3-phase stator variables to arbitrary reference frame.

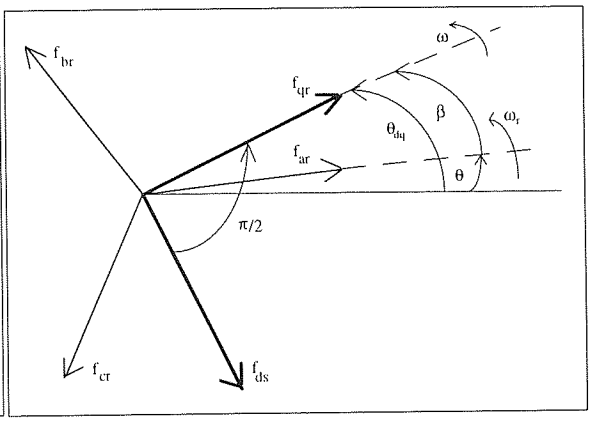

Fig. 3.5-2 Transformation of 3-phase rotor variables to arbitrary reference frame.

Three phase voltages for the stator and the rotor respectively can be written as:

$$\left.\begin{aligned} \mathbf{v}_{abcs} &= \mathbf{r}_s\mathbf{i}_{abcs} + \frac{d\psi_{abcs}}{dt} \\ \mathbf{v}_{abcr} &= \mathbf{r}_r\mathbf{i}_{abcr} + \frac{d\psi_{abcr}}{dt} \end{aligned}\right\} \qquad (3.5\text{-}6)$$

In equation (3.5-6), it was assumed that all the rotor variables and parameters were referred to stator with an appropriate transformation ratio of 1.

In (3.5-6)

$$\left.\begin{aligned} \mathbf{v}_{abcs} &= \begin{bmatrix} v_{as} \\ v_{bs} \\ v_{cs} \end{bmatrix}, \quad \mathbf{i}_{abcs} = \begin{bmatrix} i_{as} \\ i_{bs} \\ i_{cs} \end{bmatrix}, \quad \psi_{abcs} = \begin{bmatrix} \psi_{as} \\ \psi_{bs} \\ \psi_{cs} \end{bmatrix}, \quad \mathbf{r}_{abcs} = \begin{bmatrix} r_s & 0 & 0 \\ 0 & r_s & 0 \\ 0 & 0 & r_s \end{bmatrix} \\ \mathbf{v}_{abcr} &= \begin{bmatrix} v_{ar} \\ v_{br} \\ v_{cr} \end{bmatrix}, \quad \mathbf{i}_{abcr} = \begin{bmatrix} i_{ar} \\ i_{br} \\ i_{cr} \end{bmatrix}, \quad \psi_{abcr} = \begin{bmatrix} \psi_{ar} \\ \psi_{br} \\ \psi_{cr} \end{bmatrix}, \quad \mathbf{r}_{abcr} = \begin{bmatrix} r_r & 0 & 0 \\ 0 & r_r & 0 \\ 0 & 0 & r_r \end{bmatrix} \end{aligned}\right\} \qquad (3.5\text{-}7)$$

The relation between the flux and the current for three phase model can be written as:

$$\begin{bmatrix} \psi_{abcs} \\ \psi_{abcr} \end{bmatrix} = \begin{bmatrix} \mathbf{L}_{ss} & \mathbf{L}_{sr} \\ \mathbf{L}_{sr}^{T} & \mathbf{L}_{rr} \end{bmatrix} \begin{bmatrix} \mathbf{i}_{abcs} \\ \mathbf{i}_{abcr} \end{bmatrix} \tag{3.5-8}$$

where

$$\left.\begin{aligned} \mathbf{L}_{ss} &= \begin{bmatrix} L_{ss} & -\frac{1}{2}L_{sm} & -\frac{1}{2}L_{sm} \\ -\frac{1}{2}L_{sm} & L_{ss} & -\frac{1}{2}L_{sm} \\ -\frac{1}{2}L_{sm} & -\frac{1}{2}L_{sm} & L_{ss} \end{bmatrix}, \qquad \mathbf{L}_{rr} = \begin{bmatrix} L_{rr} & -\frac{1}{2}L_{rm} & -\frac{1}{2}L_{rm} \\ -\frac{1}{2}L_{rm} & L_{rr} & -\frac{1}{2}L_{rm} \\ -\frac{1}{2}L_{rm} & -\frac{1}{2}L_{rm} & L_{rr} \end{bmatrix} \\ \mathbf{L}_{sr}(\theta) &= M_{sr} \begin{bmatrix} \cos(\theta) & \cos(\theta+\frac{2\pi}{3}) & \cos(\theta-\frac{2\pi}{3}) \\ \cos(\theta-\frac{2\pi}{3}) & \cos(\theta) & \cos(\theta+\frac{2\pi}{3}) \\ \cos(\theta+\frac{2\pi}{3}) & \cos(\theta-\frac{2\pi}{3}) & \cos(\theta) \end{bmatrix} = \left[\mathbf{L}_{rs}(\theta)\right]^{T} \end{aligned}\right\} \tag{3.5-9}$$

where

$$L_{sm} = L_{rm} = M_{sr}\,; \quad L_{ss} = L_{sl} + L_{sm}\,; \quad L_{rr} = L_{rl} + L_{rm} \tag{3.5-10}$$

The three phase variables, voltages, currents and flux linkages, can be written in terms of the two axis model by using equation (3.5-1) as:

$$\left.\begin{aligned} \mathbf{v}_{abcs} &= \mathbf{K}_s^{-1}\mathbf{v}_{qd0s}\,, & \mathbf{i}_{abcs} &= \mathbf{K}_s^{-1}\mathbf{i}_{qd0s}\,, & \psi_{abcs} &= \mathbf{K}_s^{-1}\psi_{qd0s} \\ \mathbf{v}_{abcr} &= \mathbf{K}_r^{-1}\mathbf{v}_{qd0r}\,, & \mathbf{i}_{abcr} &= \mathbf{K}_r^{-1}\mathbf{i}_{qd0r}\,, & \psi_{abcr} &= \mathbf{K}_r^{-1}\psi_{qd0r} \end{aligned}\right\} \tag{3.5-11}$$

When equation (3.5-11) is inserted into equation (3.5-6), then the results will be the two-axes' voltages as given in equation (3.5-12).

$$\left.\begin{aligned} \mathbf{v}_{qd0s} &= \mathbf{K}_s \mathbf{r}_s \mathbf{K}_s^{-1} \mathbf{i}_{qd0s} + \mathbf{K}_s \frac{d\mathbf{K}_s^{-1} \boldsymbol{\psi}_{qd0s}}{dt} \\ \mathbf{v}_{qd0r} &= \mathbf{K}_r \mathbf{r}_r \mathbf{K}_r^{-1} \mathbf{i}_{qd0r} + \mathbf{K}_r \frac{d\mathbf{K}_r^{-1} \boldsymbol{\psi}_{qd0r}}{dt} \end{aligned}\right\} \qquad (3.5\text{-}12)$$

The resistance matrices of the stator and the rotor are diagonal and all the diagonal elements are equal to each other. Therefore, the multiplication of the resistance matrices with the $\mathbf{K}_{sr}$ and the $\mathbf{K}_{sr}^{-1}$ is equal to the resistance matrices themselves as given in equation (3.5-13).

$$\left.\begin{aligned} \mathbf{K}_s \mathbf{r}_s \mathbf{K}_s^{-1} &= \mathbf{r}_s \\ \mathbf{K}_r \mathbf{r}_r \mathbf{K}_r^{-1} &= \mathbf{r}_r \end{aligned}\right\} \qquad (3.5\text{-}13)$$

The second parts of the right hand side of equation (3.5-12) are partial differentials. So it will be convenient to rewrite them as:

$$\left.\begin{aligned} \mathbf{K}_s \frac{d\mathbf{K}_s^{-1} \boldsymbol{\psi}_{qd0s}}{dt} &= \mathbf{K}_s \frac{d\mathbf{K}_s^{-1}}{dt} \boldsymbol{\psi}_{qd0s} + \mathbf{K}_s \mathbf{K}_s^{-1} \frac{d\boldsymbol{\psi}_{qd0s}}{dt} \\ \mathbf{K}_r \frac{d\mathbf{K}_r^{-1} \boldsymbol{\psi}_{qd0r}}{dt} &= \mathbf{K}_r \frac{d\mathbf{K}_r^{-1}}{dt} \boldsymbol{\psi}_{qd0r} + \mathbf{K}_r \mathbf{K}_r^{-1} \frac{d\boldsymbol{\psi}_{qd0r}}{dt} \end{aligned}\right\} \qquad (3.5\text{-}14)$$

When equations (3.5-13) and (3.5-14) are put into equation (3.5-12), then the two axis voltage equations can be rewritten as:

$$\left.\begin{aligned} \mathbf{v}_{qd0s} &= \mathbf{r}_s \mathbf{i}_{qd0s} + \mathbf{K}_s \frac{d\mathbf{K}_s^{-1}}{dt} \boldsymbol{\psi}_{qd0s} + \frac{d\boldsymbol{\psi}_{qd0s}}{dt} \\ \mathbf{v}_{qd0r} &= \mathbf{r}_r \mathbf{i}_{qd0r} + \mathbf{K}_r \frac{d\mathbf{K}_r^{-1}}{dt} \boldsymbol{\psi}_{qd0r} + \frac{d\boldsymbol{\psi}_{qd0r}}{dt} \end{aligned}\right\} \qquad (3.5\text{-}15)$$

The second terms of the right hand side of equation (3.5-15) contain the multiplication of the $\mathbf{K}_{sr}$ with the derivative of $\mathbf{K}_{sr}^{-1}$. These terms are worked out as below for the simplicity of equation (3.5-15).

$$\left.\begin{aligned}
\mathbf{K}_s \frac{d\mathbf{K}_s^{-1}}{dt} &= \mathbf{K}_s \omega \begin{bmatrix} -\sin(\theta_{dq}) & \cos(\theta_{dq}) & 0 \\ -\sin(\theta_{dq}-\frac{2\pi}{3}) & \cos(\theta_{dq}-\frac{2\pi}{3}) & 0 \\ -\sin(\theta_{dq}+\frac{2\pi}{3}) & \cos(\theta_{dq}+\frac{2\pi}{3}) & 0 \end{bmatrix} = \omega \begin{bmatrix} 0 & 1 & 0 \\ -1 & 0 & 0 \\ 0 & 0 & 0 \end{bmatrix} \\
\mathbf{K}_r \frac{d\mathbf{K}_r^{-1}}{dt} &= \mathbf{K}_r (\omega - \omega_r) \begin{bmatrix} -\sin(\beta) & \cos(\beta) & 0 \\ -\sin(\beta-\frac{2\pi}{3}) & \cos(\beta-\frac{2\pi}{3}) & 0 \\ -\sin(\beta+\frac{2\pi}{3}) & \cos(\beta+\frac{2\pi}{3}) & 0 \end{bmatrix} = (\omega - \omega_r) \begin{bmatrix} 0 & 1 & 0 \\ -1 & 0 & 0 \\ 0 & 0 & 0 \end{bmatrix}
\end{aligned}\right\} \qquad (3.5\text{-}16)$$

As seen from equation (3.5-16) a 3x3 matrix is multiplied by ω for the stator and by $(\omega-\omega_r)$ for the rotor. The term $(\omega-\omega_r)$ for the rotor is given as below:

$$\frac{d\beta}{dt} = \frac{d(\theta_{dq} - \theta_r)}{dt} = \omega - \omega_r \qquad (3.5\text{-}17)$$

When equation (3.5-16) is inserted into equation (3.5-15), the two axis voltage equations become as:

$$\left.\begin{aligned}
\mathbf{v}_{qd0s} &= \mathbf{r}_s \mathbf{i}_{qd0s} + \omega \psi_{dq0s} + \frac{d\psi_{qd0s}}{dt} \\
\mathbf{v}_{qd0r} &= \mathbf{r}_r \mathbf{i}_{qd0r} + (\omega - \omega_r)\psi_{dq0r} + \frac{d\psi_{qd0r}}{dt}
\end{aligned}\right\} \qquad (3.5\text{-}18)$$

where

$$\left.\begin{aligned}
\psi_{dq0s}^T &= \begin{bmatrix} \psi_{ds} & -\psi_{qs} & 0 \end{bmatrix} \\
\psi_{dq0r}^T &= \begin{bmatrix} \psi_{dr} & -\psi_{qr} & 0 \end{bmatrix}
\end{aligned}\right\} \qquad (3.5\text{-}19)$$

$$\begin{bmatrix} \psi_{qdos} \\ \psi_{qdor} \end{bmatrix} = \begin{bmatrix} \mathbf{K}_s\mathbf{L}_s\mathbf{K}_s^{-1} & \mathbf{K}_s\mathbf{M}_{sr}\mathbf{K}_r^{-1} \\ \mathbf{K}_r\mathbf{M}_{sr}^{T}\mathbf{K}_s^{-1} & \mathbf{K}_r\mathbf{L}_r\mathbf{K}_r^{-1} \end{bmatrix} \begin{bmatrix} \mathbf{i}_{qdos} \\ \mathbf{i}_{qdor} \end{bmatrix} \tag{3.5-20}$$

$$\left.\begin{aligned} \mathbf{K}_s\mathbf{L}_s\mathbf{K}_s^{-1} &= \begin{bmatrix} L_s & 0 & 0 \\ 0 & L_s & 0 \\ 0 & 0 & L_{ls} \end{bmatrix}, \quad \mathbf{K}_r\mathbf{L}_r\mathbf{K}_r^{-1} = \begin{bmatrix} L_r & 0 & 0 \\ 0 & L_r & 0 \\ 0 & 0 & L_{lr} \end{bmatrix} \\ \mathbf{K}_r\mathbf{M}_{sr}^{T}\mathbf{K}_s^{-1} &= \mathbf{K}_s\mathbf{M}_{sr}\mathbf{K}_r^{-1} = \begin{bmatrix} L_{sr} & 0 & 0 \\ 0 & L_{sr} & 0 \\ 0 & 0 & 0 \end{bmatrix} \end{aligned}\right\} \tag{3.5-21}$$

where

$$L_{sr} = \frac{3}{2}M_{sr}, \quad L_s = L_{ls} + L_{sr}, \quad L_r = L_{lr} + L_{sr} \tag{3.5-22}$$

If the currents in voltage equations are chosen as state variables, the relationship between the flux linkages and currents are then given as:

$$\begin{bmatrix} \psi_{qs} \\ \psi_{ds} \\ \psi_{0s} \\ \psi_{qr} \\ \psi_{dr} \\ \psi_{0r} \end{bmatrix} = \begin{bmatrix} L_s & 0 & 0 & L_{sr} & 0 & 0 \\ 0 & L_s & 0 & 0 & L_{sr} & 0 \\ 0 & 0 & L_{ls} & 0 & 0 & 0 \\ L_{sr} & 0 & 0 & L_r & 0 & 0 \\ 0 & L_{sr} & 0 & 0 & L_r & 0 \\ 0 & 0 & 0 & 0 & 0 & L_{lr} \end{bmatrix} \begin{bmatrix} i_{qs} \\ i_{ds} \\ i_{0s} \\ i_{qr} \\ i_{dr} \\ i_{0r} \end{bmatrix} \tag{3.5-23}$$

If the flux linkages in voltage equations are chosen as state variables, the currents are calculated as:

$$\begin{bmatrix} i_{qs} \\ i_{ds} \\ i_{0s} \\ i_{qr} \\ i_{dr} \\ i_{0r} \end{bmatrix} = \frac{1}{D} \begin{bmatrix} L_r & 0 & 0 & -L_{sr} & 0 & 0 \\ 0 & L_r & 0 & 0 & -L_{sr} & 0 \\ 0 & 0 & \frac{D}{L_{ls}} & 0 & 0 & 0 \\ -L_{sr} & 0 & 0 & L_s & 0 & 0 \\ 0 & -L_{sr} & 0 & 0 & L_s & 0 \\ 0 & 0 & 0 & 0 & 0 & \frac{D}{L_{lr}} \end{bmatrix} \begin{bmatrix} \psi_{qs} \\ \psi_{ds} \\ \psi_{0s} \\ \psi_{qr} \\ \psi_{dr} \\ \psi_{0r} \end{bmatrix} \tag{3.5-24}$$

where

$$D = L_s L_r - L_{sr}^2 \tag{3.5-25}$$

The voltage equations in matrix form for an arbitrary reference frame can be written as below since the flux linkages are chosen as state variables:

$$\begin{bmatrix} v_{qs} \\ v_{ds} \\ v_{0s} \\ v_{qr} \\ v_{dr} \\ v_{0r} \end{bmatrix} = \begin{bmatrix} \frac{r_s L_r}{D} + \frac{d}{dt} & \omega & 0 & -\frac{r_s L_{sr}}{D} & 0 & 0 \\ -\omega & \frac{r_s L_r}{D} + \frac{d}{dt} & 0 & 0 & -\frac{r_s L_{sr}}{D} & 0 \\ 0 & 0 & \frac{r_s}{L_{ls}} + \frac{d}{dt} & 0 & 0 & 0 \\ -\frac{r_r L_{sr}}{D} & 0 & 0 & \frac{r_r L_s}{D} + \frac{d}{dt} & \omega - \omega_r & 0 \\ 0 & -\frac{r_r L_{sr}}{D} & 0 & -(\omega - \omega_r) & \frac{r_r L_s}{D} + \frac{d}{dt} & 0 \\ 0 & 0 & 0 & 0 & 0 & \frac{r_r}{L_{lr}} + \frac{d}{dt} \end{bmatrix} \begin{bmatrix} \psi_{qs} \\ \psi_{ds} \\ \psi_{0s} \\ \psi_{qr} \\ \psi_{dr} \\ \psi_{0r} \end{bmatrix} \tag{3.5-26}$$

It is also possible to choose the currents as state variables, but this causes each q and d voltage equations to contain two different first derivatives of current. Therefore, it is always convenient to select the flux linkages as state variables.

Equation (3.5-26) can be written in the form of state space as:

$$\begin{bmatrix} \frac{d\psi_{qs}}{dt} \\ \frac{d\psi_{ds}}{dt} \\ \frac{d\psi_{0s}}{dt} \\ \frac{d\psi_{qr}}{dt} \\ \frac{d\psi_{dr}}{dt} \\ \frac{d\psi_{0r}}{dt} \end{bmatrix} = \begin{bmatrix} -\frac{r_s L_r}{D} & -\omega & 0 & \frac{r_s L_{sr}}{D} & 0 & 0 \\ \omega & -\frac{r_s L_r}{D} & 0 & 0 & \frac{r_s L_{sr}}{D} & 0 \\ 0 & 0 & -\frac{r_s}{L_{ls}} & 0 & 0 & 0 \\ \frac{r_r L_{sr}}{D} & 0 & 0 & -\frac{r_r L_s}{D} & -(\omega - \omega_r) & 0 \\ 0 & \frac{r_r L_{sr}}{D} & 0 & \omega - \omega_r & -\frac{r_r L_s}{D} & 0 \\ 0 & 0 & 0 & 0 & 0 & -\frac{r_r}{L_{lr}} \end{bmatrix} \begin{bmatrix} \psi_{qs} \\ \psi_{ds} \\ \psi_{0s} \\ \psi_{qr} \\ \psi_{dr} \\ \psi_{0r} \end{bmatrix} + \begin{bmatrix} v_{qs} \\ v_{ds} \\ v_{0s} \\ v_{qr} \\ v_{dr} \\ v_{0r} \end{bmatrix}$$

(3.5-27)

The values of the v_{os} and v_{or} in (3.5-27) are the average values of the three phase voltages of stator and rotor respectively and equal to zero (since the stator and rotor phases are symmetrical and balanced) as calculated below, by using equation (3.5-3).

$$\left.\begin{aligned} v_{0s} &= \frac{2}{3}\left(\frac{v_{as}}{2} + \frac{v_{bs}}{2} + \frac{v_{cs}}{2}\right) = \frac{v_{as} + v_{bs} + v_{cs}}{3} = 0 \\ v_{0r} &= \frac{2}{3}\left(\frac{v_{ar}}{2} + \frac{v_{br}}{2} + \frac{v_{cr}}{2}\right) = \frac{v_{ar} + v_{br} + v_{cr}}{3} = 0 \end{aligned}\right\} \quad (3.5\text{-}28)$$

Therefore equation (3.5-27) can be rewritten as below, by eliminating the v_{os} and v_{or} for simplicity.

$$\begin{bmatrix} \frac{d\psi_{qs}}{dt} \\ \frac{d\psi_{ds}}{dt} \\ \frac{d\psi_{qr}}{dt} \\ \frac{d\psi_{dr}}{dt} \end{bmatrix} = \begin{bmatrix} -\frac{r_s L_r}{D} & -\omega & \frac{r_s L_{sr}}{D} & 0 \\ \omega & -\frac{r_s L_r}{D} & 0 & \frac{r_s L_{sr}}{D} \\ \frac{r_r L_{sr}}{D} & 0 & -\frac{r_r L_s}{D} & -(\omega - \omega_r) \\ 0 & \frac{r_r L_{sr}}{D} & \omega - \omega_r & -\frac{r_r L_s}{D} \end{bmatrix} \begin{bmatrix} \psi_{qs} \\ \psi_{ds} \\ \psi_{qr} \\ \psi_{dr} \end{bmatrix} + \begin{bmatrix} v_{qs} \\ v_{ds} \\ v_{qr} \\ v_{dr} \end{bmatrix} \quad (3.5\text{-}29)$$

The expression for electromagnetic torque of the induction machine in the two axis model can be given in terms of the currents as:

$$T_e = \left(\frac{3}{2}\right)\left(\frac{P}{2}\right) L_{sr}\left(i_{qs} i_{dr} - i_{ds} i_{qr}\right) \quad (3.5\text{-}30)$$

It is also possible to write the torque equation in terms of the rotor currents and fluxes or the stator currents and fluxes.

$$T_e = \left(\frac{3}{2}\right)\left(\frac{P}{2}\right)\left(\psi_{qr} i_{dr} - \psi_{dr} i_{qr}\right) \quad (3.5\text{-}31)$$

$$T_e = \left(\frac{3}{2}\right)\left(\frac{P}{2}\right)\left(\psi_{ds} i_{qs} - \psi_{qs} i_{ds}\right) \quad (3.5\text{-}32)$$

The relation between the torque and the rotor speed can be written as:

$$\frac{d\omega_r}{dt} = \frac{P}{2}\,\frac{(T_e - T_L)}{J} \quad (3.5\text{-}33)$$

where

P = Number of poles,

J = Total inertia of rotor and load ($kg.m^2$),

T_L = Load torque (N.m).

An induction machine can be simulated in the two axis model by using electrical equation (3.5-29) and mechanical equation (3.5-33). As mentioned before, this modelling of an induction machine eliminates the angle between the stator and the rotor. Thus it reduces the number of electrical equations from 6 to 4 as given in equation (3.5-29). Therefore, the computation time of the two axis model will be shorter than three axis (phase equation) model.

Although the behaviour of a symmetrical induction machine is given in the arbitrary reference frame, there are three common reference frames used. These are the stationary reference frame, the rotor (Park) reference frame and the synchronously rotating field reference frame. The voltages or differentials of the flux equations for these reference frames can be obtained easily from the arbitrary reference frame by defining an appropriate speed for ω. It can be defined as $\omega = 0$ for the stationary, $\omega = \omega_r$ for the rotor and $\omega = \omega_s$ for the synchronously rotating reference frame.

The reference frames mentioned above have been proposed for different purposes. The stationary reference frame has been proposed for simulation of induction machines that have balanced or discontinuous stator voltages and balanced or zero rotor voltages. If the stator voltages are balanced and external rotor circuits are unbalanced, then the rotor reference frame is most convenient. The stationary or synchronous reference frame is generally used to analyse balanced or symmetrical conditions. The synchronously reference frame is also convenient for variable frequency applications since the stator voltages are balanced.

3.6. Summary

The discussions on the phase equation model and d-q axis model were followed by a detailed explanation of the machine model in both the three phase and two phase (d-q axis) models in this chapter.

It has been highlighted that the computation of the inverse of the inductance matrix at every step of the simulation and having six differential equations for the induction motor in the phase equation model increase the computation time, however the mixed terminal constraints in the phase equation model can be considered easier than those in the d-q axis model.

CHAPTER 4

ESTIMATION OF THE MOTOR PARAMETERS

4.1 Introduction

In chapter 3 it was shown that the induction motor can be simulated using either a three axis or a two axis model and that the same effects can be built into either model. If the form of the model is appropriate for the machine being represented, the validity of the simulation results depends on the accuracy of the parameters in the numerical model. It is essential therefore to estimate the parameters of the test machine before starting a simulation.

There are various ways of calculating the motor parameters using the tests results performed on the motor. If the motor parameters are not varied continuously during the operation of the motor, they can be estimated by using any off-line estimation methods. However, there are certain applications, where the machine parameters are considered to vary during the operation of the motor, so that the parameters must be estimated continuously using on-line estimation methods.

On-line estimation is a large area of determining the machine parameters and encompasses the use of observers for determining machine states from output variables as well as parameter estimators. Some examples include Kalman Filtering (Atkinson et al. (1989), Bal and Grant (1992)), the perturbation method (Acarnley et al. (1991), the stator current trajectory method (Holtz and Thimm (1991)), the mathematical methods based directly on the machine dynamic equations (Artime et al. (1987), Sull (1989), Ansuj et al. (1989), Grzesiak and Reichert (1992)), and the injection of low magnitude, high frequency voltage sets into the machine's supply (Holliday (1994)).

The philosophy aimed at in this work has been to create a model framework in which sufficient detail is incorporated into the model that the parameters need not to be considered variable. The context of mixed-frequency testing does not require use of observers.

Off-line parameter estimation methods are also based on the machine's dynamic equations and the measurements from the test are required only once for a certain period of time. They are suitable for the estimation of the constant parameters. The basic off-line estimation method for simple models of induction machines involves the DC, locked-rotor, no-load and run-up and run-down tests. Timar et al. (1992) developed a computer program, on the basis of the reference frame being fixed to the stator, to calculate the motor parameters using the two line voltages and currents obtained from the run-up and run-down tests. Ramminger and Andresen (1992) proposed a combined method of parameter estimation and correction based on the principle of parameter estimation of dynamic systems. Khenfer et al. (1992) used the data obtained from the locked-rotor test and the no-load test to deduce the motor parameters from the equations based on the equivalent T circuit of the induction motor. They also calculated the rotor inertia from the run-down test and frictional power from the un-loaded and non-fed tests driving the test motor with an auxiliary machine at synchronous speed.

In this chapter motor parameters are estimated for one of the two small induction machines tested in chapter 6. The DC test, no-load test and locked-rotor test were performed on the induction motor as well as run-up and run-down tests. It has been possible to find a set of parameters to reproduce the measured characteristics reasonably accurately.

4.2. Normal Tests for the Steady State Parameters

Steady state parameters of the induction motor can be estimated from the DC test, no-load test and locked-rotor test (Fitzgerald et al. (1983), Chapman (1987), O'Kelly (1991)). The DC test determines the DC resistance of the stator windings. The rotor resistance and the

stator and rotor leakage inductance of the motor are measured by the no-load test and the locked-rotor test based on the equivalent circuit model of the induction motor.

4.2.1. DC Test of Induction Motors

The DC test of an induction motor determines the DC resistance of the stator windings. This test can be performed by applying low value of DC voltage (just enough to flow the rated stator current) to one of the stator phase windings at rated temperature of motor. The DC resistance of the stator winding can then be calculated using the measured voltage and current. In the case of the slip-ring motor, the rotor resistance can be measured as the stator resistance using the DC test method.

4.2.2. No-Load Test of Induction Motors

No-load test of the induction motor must be performed at rated frequency and rated voltage for the correct calculation of the stator reactance, rotational losses and parameters of the magnetising branch. The readings of voltage, currents and powers must be recorded when the motor temperature is at rated value. No-load test arrangements and one phase equivalent circuit of induction motor are shown in Figs. 4.2.2-1 and 4.2.2-2 respectively.

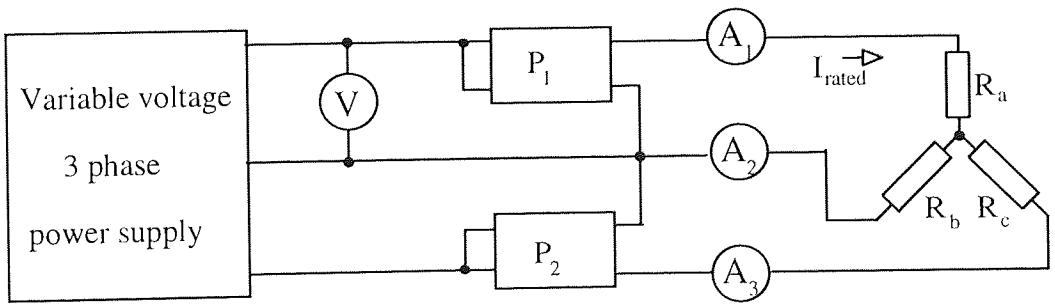

Fig. 4.2.2-1 No-load test of the induction motor.

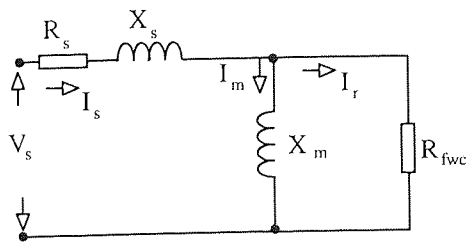

Fig. 4.2.2-2 One phase equivalent circuit of the induction motor.

The resistance R_c and slip resistance are then connected in parallel with each other, so that they can be shown with an equivalent resistance R_{fwc}, which represents the friction, the windage and the core losses. No-load power, P_{nl}, is the sum of two powers measured. The resistance R_{fwc} is much larger than the magnetising reactance, X_m, and overall input power factor will be very small. Therefore the phase impedance, Z_{nl}, of the motor is the sum of stator leakage reactance, X_s, and mutual reactance, X_m. Subtraction of the stator copper losses from the no-load losses gives the rotating losses $P_{rotating}$. Mutual reactance and rotating losses are defined in equation (4.2.2-1).

$$Z_{nl} = \frac{V_{nl}}{\sqrt{3}I_{nl}} = X_s + X_m \quad \text{and} \quad P_{rotating} = P_{fwc} = P_{nl} - P_{sc} \qquad (4.2.2\text{-}1)$$

4.2.3. Locked-Rotor Test of Induction Motors

The circuit diagram for the locked-rotor test of an induction motor is similar to the no-load test circuit diagram, shown in Fig. 4.2.2-1. In this test, the slip of the motor is equal to 1, and the rotor resistance and reactance is much smaller than that of the magnetising circuit. Therefore, it can be assumed that the magnetising circuit is eliminated, and the stator and rotor circuits are connected in series.

This test is carried out by locking the rotor of the test motor with a safe mechanism. Then a small amount of voltage is applied to the terminals of the machine in order that full load current flows into the stator of the motor. When the temperature of the motor is at the rated value, currents, voltage and powers are recorded. Total locked-rotor power P_{lr} is sum of the two powers measured.

The phase impedance Z_{lr}, the power factor, ϕ, sum of the stator and rotor resistances and leakage reactances of the test motor are calculated as:

$$\left.\begin{aligned} Z_{lr} &= \frac{V_{lr}}{\sqrt{3}I_{lr}} \quad \text{and} \quad \phi = \cos^{-1}\left(\frac{P_{lr}}{\sqrt{3}V_{lr}\,I_{lr}}\right) \\ R_{lr} &= R_s + R_r = Z_{lr}\cos(\phi) \\ X_{lr} &= X_s + X_r = Z_{lr}\sin(\theta) \end{aligned}\right\} \qquad (4.2.3\text{-}1)$$

At this point, the relationship between the stator and the rotor leakage reactances must be decided according to Table 4.2.3-1.

Motor class	Description	X_s	X_r
A	Normal starting torque, normal starting current	$0.5X_{lr}$	$0.5X_{lr}$
B	Normal starting torque, low starting current	$0.4X_{lr}$	$0.6X_{lr}$
C	High starting torque, low starting current	$0.3X_{lr}$	$0.7X_{lr}$
D	High starting torque, high slip	$0.5X_{lr}$	$0.5X_{lr}$
Slip-ring		$0.5X_{lr}$	$0.5X_{lr}$

Table 4.2.3-1 Empirical distribution of leakage reactances of induction motors.

In the case of the test motor used, the stator and the rotor leakage reactances are assumed to be equal to each other and calculated as the half of the total leakage reactances. Subtraction of the stator leakage reactance from the no-load impedance gives the mutual reactance of the motor. X_s, X_r and X_m are given in equation (4.2.3-4).

$$X_s = X_r = \frac{X_{lr}}{2} \quad \text{and} \quad X_m = Z_{nl} - X_s \qquad (4.2.3\text{-}4)$$

4.2.4. Calculation of Leakage and Mutual Inductances for Steady State

In the model of the induction motor the resistances and inductances were used, rather than reactances of the motor. Therefore it is necessary to calculate the leakage and mutual inductances of the motor.

The relationship between the reactance and the leakage inductance is given as below for the stator, rotor and magnetising circuit respectively.

$$X_s = 2\pi f_s L_{sl} \Rightarrow L_{sl} = \frac{X_s}{2\pi f_s};\ X_r = 2\pi f_r L_{rl} \Rightarrow L_{rl} = \frac{X_r}{2\pi f_r};\ X_m = 2\pi f_s L_{sr} \Rightarrow L_{sr} = \frac{X_m}{2\pi f_s} \qquad (4.2.4\text{-}1)$$

Apparent rotor self inductance, mutual inductance between stator and rotor, stator self inductance, rotor self inductance, stator mutual inductance, and rotor mutual inductance are calculated as in equation (4.2.4-2) respectively;

$$\left.\begin{aligned} &L_s = L_{sl} + L_{sr};\quad L_r = L_{rl} + L_{sr};\quad M_{sr} = \frac{2}{3}L_{sr};\\ &L_{sm} = L_{rm} = M_{sr};\ L_{ss} = L_s - \frac{1}{2}L_{sm};\ L_{rr} = L_r - \frac{1}{2}L_{rm} \end{aligned}\right\} \qquad (4.2.4\text{-}2)$$

4.3. Additional Tests for Dynamic Model

The normal steady state tests for determining the parameters of the squirrel-cage induction motor were given in section 4.2. Clearly the saturation and rotor deep-bar effects cannot be detected with the normal steady state tests. Therefore, additional tests must be performed on the test motor to estimate the parameters for an accurate dynamic model which would include saturation and rotor deep-bar effects.

The no-load and locked-rotor tests can be repeated at different frequencies and voltages to find the variation of the impedance of the fundamental harmonic as well as to obtain information on the saturation of stator leakage inductance, the saturation of main flux, the

magnetising inductance and the rotor deep-bar effects. An inverter can be used as a supply for these tests. The run-up-down tests can be performed on the test motor to calculate the rotor inertia and mechanical losses of the motor.

4.3.1. No-Load Test at Different Voltages and Frequencies

The no-load test of the squirrel-cage induction machine can be performed at different voltages and different frequencies using an inverter in order to obtain the variation of machine impedance of the fundamental harmonic as a function of the supply voltage and frequency. The no-load impedance gives information on the stator reactance and the reactance of the magnetising branch. As the voltage/frequency ratio rises in the no-load test, the main flux rises and a drop in impedance is observed when the main flux path begins to saturate. Hence the variation in voltage/frequency ratio provides data for main saturation. Varying the frequency provides some information on magnetising inductance. To perform this test, the inverter is set up to deliver a "constant flux" by setting a fixed ratio between voltage and frequency. For each value of this ratio, the inverter output frequency can be varied and then the impedance (voltage/current) of the fundamental harmonic can be recorded by extracting the fundamental harmonics of voltage and current waveforms with a signal analyser.

4.3.2. Locked-Rotor Test at Different Voltages and Frequencies

The locked-rotor test can be performed on the induction machine at different voltages and different frequencies to identify the locked-rotor machine impedance as a function of voltage and frequency. The locked-rotor impedance gives information primarily on the stator and rotor reactances and resistances. In the locked-rotor test, currents are high compared with rated and as such, leakage fluxes are high. The variation of voltage frequency ratio provides different currents and these in turn produce different leakage flux levels and so information is gleaned about leakage path saturation. Variation of frequency in this test gives information on the rotor deep-bar effects. To perform this test, the inverter is set up to deliver a "constant flux" by setting a fixed ratio between voltage and frequency.

For each value of this ratio, the inverter output frequency can be varied and then the impedance (voltage/current) of the fundamental harmonic can be recorded by extracting the fundamental harmonics of voltage and current waveforms with a signal analyser.

4.3.3. Run-Up and Run-Down Tests

Run-up and run-down tests can be performed on test machines to provide the necessary information for the torque-speed curve, current-speed curve and mechanical loss of the test motors. Torques of the test motor can be deduced from the rates of change of speed using the motor inertia if the run-up test was performed at low voltage. The value of the voltage must be chosen just enough to produce the necessary torque for the acceleration of the motor. Providing that the applied voltage and frequency are constant during the acceleration and mechanical time constants are much larger than electrical time constants, then the motor is electrically in steady-state condition, but is mechanically in a transient condition. The motor may then be regarded as progressing through a series of Pseudo-Steady-State during the acceleration period.

The mechanical time constant of an induction motor for small values of slip can be expressed from the electromagnetic torque equation obtained from one phase T equivalent circuit as:

$$T_e = \frac{3V_o^2}{\omega_0 R_r'} s \quad \text{where } \omega_0 = \frac{4\pi f}{\text{poles}} \quad \text{and } s << 1 \qquad (4.3.3\text{-}1)$$

If the applied voltage amplitude and frequency are constant and the motor is electrically in a steady-state condition, and if the slip is small, then the airgap torque produced is directly proportional to slip. If the constants in equation (4.3.3-1) are represented by "κ" and the motor inertia, "J", is known, the mechanical time constant of the induction motor for small values of slip can be defined as below:

$$T_e = \kappa s \quad \Rightarrow \quad \tau_m = \frac{J\omega_0}{\kappa} \qquad (4.3.3\text{-}2)$$

The mechanical time constant for the induction machine for slips which are not very small is always greater than the value obtained for small slip. Since the mechanical time constant is determined by the slope of the torque-speed curve and the inertia, it is clear that it is sometimes negative and that its absolute value is always less than or equal to the time constant for low values of slip.

If the motor inertia is not known, it can be calculated using the run-up and run-down curves obtained from the normal inertia test and the increased inertia test which can be done by adding some known inertia on the shaft of the rotor.

4.3.4. Deducing Rotor Inertia and Mechanical Torque of the Motor

The rotor inertia of the test motor can be deduced using a known additional inertia coupled to the rotor shaft. If two run-down tests are performed on the test motor with and without additional inertia, due to the two different inertias, J_a+J_n and J_n, there will be two different slopes, α_{a+n} and α_n,. The values of these two slopes can be calculated from the run-up and run-down tests done with normal inertia and with additional inertia. The ratio of additional inertia plus normal inertia, J_a+J_n, to normal inertia, J_n, equals to the ratio of slope, α_n, to slope, α_{a+n}, as:

$$\frac{J_a + J_n}{J_n} = \frac{\alpha_n}{\alpha_{a+n}} \qquad (4.3.4\text{-}1)$$

Since the two slopes are calculated and the additional inertia is known, the rotor inertia can be found from equation (4.3.4-1). Provided that the additional inertia has a simple geometry, the value of its inertia can be computed very easily.

If the inertia and the slope are known, the mechanical loss torque of the motor near synchronous speed can be calculated by multiplying the slope with the corresponding inertia as:

$$T_L = (J_a + J_n)\alpha_{a+n} \quad \text{or} \quad T_L = J_n \alpha_n \tag{4.3.4-4}$$

4.4. Matching the Simulation Results With the Experimental Results

A complete dynamic model of an induction machine given in equation 3.3-5 in chapter 3 can be used for the simulation of an induction machine. The DC, no-load, locked-rotor, run-up and run-down tests can easily be applied to the simulation program by using a set of initially obtained machine parameters to get the necessary results for the comparison purposes. Since the importance of each parameter with respect to the test performed is known, good agreement can be achieved between the simulation and test results by manually making small adjustments to the related parameter. When the error between the test and the simulation obtained from all the tests performed has been minimised, the parameters at this stage can be used as the best estimates. It is possible to automate this procedure as follows:

1. Compute predicted impedance and run-up / run-down curves from the present set of parameters.
2. Compute the root-mean-square (rms) errors in each of the three characteristics.
3. Combine the three rms errors into one using a linear combination which has the desired weighting.
4. Make small changes in each of the machine parameters in turn and compute the change in total "error" resulting from each.
5. Assemble the gradient vector and estimate what multiple of this gradient vector should be subtracted from the vector of parameters to approximately minimise the error.
6. Check convergence and if not converged, return to 1 above.

4.5. Experimental Results for Parameters of Test Motors

4.5.1. Experimental Results for Estimation of Squirrel-Cage Motor Parameters

The normal DC, locked-rotor and no-load tests were performed on a 4 kW squirrel-cage induction motor with 50 Hz supply frequency and rated smooth supply voltage. As a result of these tests, the following initial estimates for the parameters were calculated.

First set of parameters of 4 kW motor:

$R_s = 5.26\ \Omega,\ R_r \approx 4.7\ \Omega,\ L_{sl} \approx 0.031$ H, $L_{rl} \approx 0.031$ H, $L_{sr} \approx 0.93$ H.

Fig. 4.5.1-1 shows run-down tests performed on the motor with normal and additional inertia. The initial angular deceleration, α_n, for the run-down test (with normal inertia) was 41.015 rad/s^2. The additional inertia had been calculated as 0.010516 kgm^2. The initial angular deceleration, α_{a+n}, for the run-down test with increased inertia was 18.616 rad/s^2. Using equation 4.3.4-1, the actual inertia of the motor was computed as 0.00478 kgm^2. Knowing this, the mechanical loss torque at a rotor speed 302.4 rad/s was evaluated as 0.196 Nm. The mechanical power losses for this motor can be represented as $T_L\omega_r$ = (0.196)(302.4) = 59.27 W.

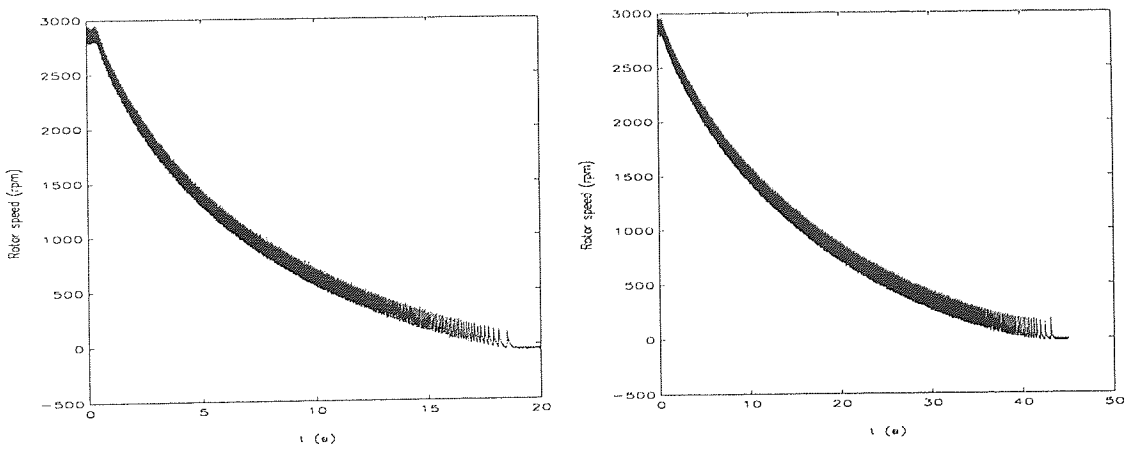

Fig. 4.5.1-1 Run-down rotor speeds of the squirrel-cage induction motor with normal and increased inertia.

A run-up test was performed on the motor on low voltage at 50 Hz frequency which provides a run-up speed curve of the motor that is in steady state electrically. The voltage value was chosen as 25% of rated value which was more than enough for the motor to

produce necessary torque for the acceleration but sufficiently small that the ratio between mechanical and electrical time constants was large.

The run-up speed waveform was then filtered and averaged (Szabados et al. (1989)) to obtain a smooth speed waveform for the calculation of angular accelerations. The measured electrical and mechanical torque-speed curves, in Figure 4.5.1-2, were obtained directly using the inertia and the run-up and run-down slopes at every speed of the motor.

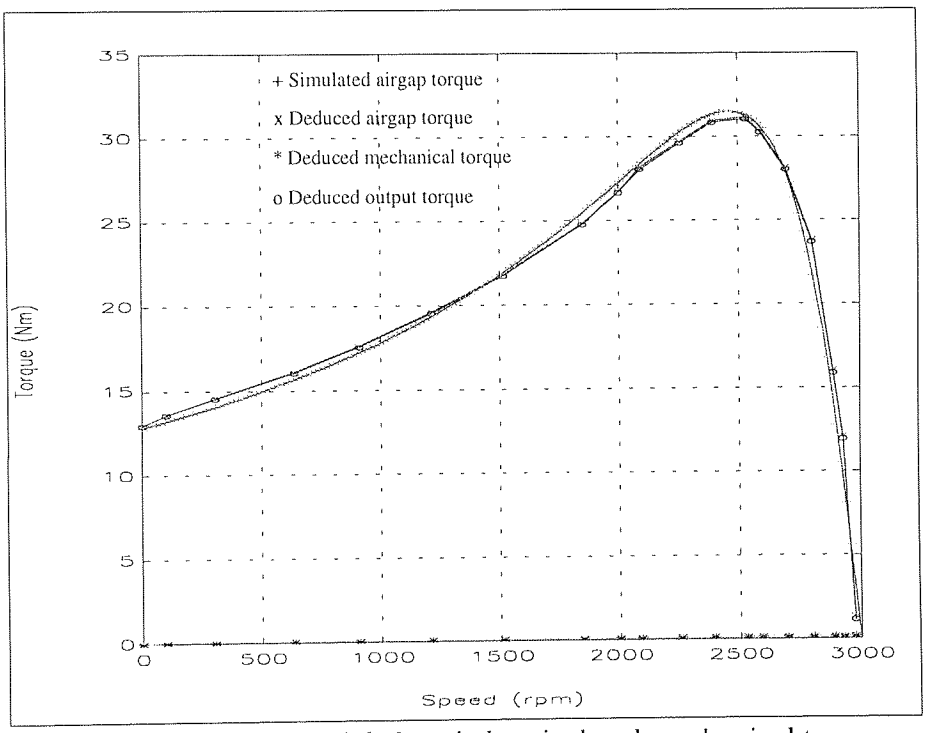

Fig. 4.5.1-2 Simulated and deduced electrical and mechanical torque-speed curves of the squirrel-cage induction motor.

As well as the measured airgap torque-speed curve, Fig. 4.5.1-2 shows the predicted curve based on a rotor resistance of 3.1 ohms. This value was found by simple iterative searching, to obtain the best match between torque-speed curves. The simulated torque speed curve was obtained using the basic phase equations, given in 3.3-5, in the simulation program. The speed of the machine was varied from 0 to 3000 rpm in steps of 2 rpm. At each step, the simulation program was run for a certain time, to get to the steady state and then the produced torque was recorded. This process was repeated for each step of the rotor speed. The measured torque-speed curve in Fig. 4.5.1-2 was multiplied by 16 to obtain the steady

state airgap torque-speed curve for the machine on full volts which would exist if the machine iron was perfectly linear.

It is obvious that, the rotor resistance of 3.1 Ω clearly does not agree with the value obtained from the locked rotor test (4.7 Ω). For a simple simulation, discounting core losses and saturation, the model is now considered to be as good as it can be a simulation not incorporating saturation and core losses connot represent this machine with complete accuracy. In fact, for the bulk of the simulation reported in the remainder of the thesis, R_r was taken to be 3.1 ohms and simple model was used. However in the remainder of this chapter, efforts to estimate a parameter set for a more powerful model are described.

Because the original intention was that core losses and saturation would be included in all simulations (although subsequently, time did not allowed this) the test described in 4.3.1 and 4.3.2 were performed and results were matched, with a simulation incorporating the above effects.

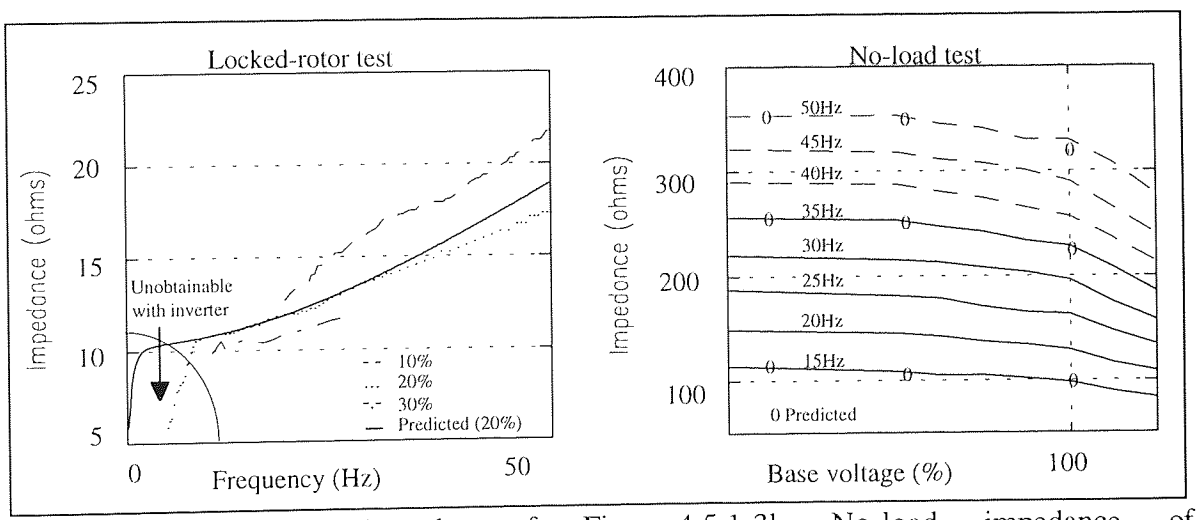

Fig. 4.5.1-3a Locked-rotor impedance of fundamental fundamental harmonic at different freq.

Fig. 4.5.1-3b No-load impedance of harmonic at different base voltages.

The motor was then connected to an inverter which has a facility of producing variable-voltage, variable-frequency or constant-voltage, variable-frequency. The locked-rotor test was performed 3 times setting the flux level of the machine (i.e. the voltage/frequency ratio)

to 10%, 20% and 30% of rated value. At each one of these settings the output frequency of inverter was varied between very low frequencies and 50 Hz. The phase voltage and current of the test machine were recorded by a signal analyser at each step of these locked-rotor test and the impedance of the fundamental harmonic was calculated. Fig. 4.5.1-3a shows the results of locked-rotor test.

A series of no-load tests was also performed by changing the output frequency of the inverter from 50 Hz to 15 Hz in 5 Hz steps. For each frequency, the inverter voltage was varied from a very small value to 120% of the rated machine voltage. The phase voltage and current of the test machine were recorded by a signal analyser at each step of these locked-rotor and no-load tests and the impedance of the fundamental harmonic was calculated. Figs. 4.5.1-3b shows the results of the no-load tests.

Using the procedure outlined in 4.4, a number of iteration of simulation and adjustment led to set of parameters containing saturation and core loss quantities. The enhanced simulation produced results which closely reproduced the test results. The parameter found are as follows. A full explanation of the modelling of saturation and core losses is given in appendix A.2.2 and A.2.3.

Second set of parameters of 4 kW motor (including saturation and core losses):

R_s=5.2Ω, R_r≈5.3Ω, R_c≈540Ω, L_{sr}≈0.92H, L_{sl}≈0.0256H, L_{rl}≈0.0256H

ϕ_m≈0.55p.u., S_m≈0.9H/weber-turn, ϕ_l≈0.15p.u., S_l≈0.6H/weber-turn.

where ϕ_m, S_m, ϕ_l and S_l are parameters describing saturation of main and leakage flux paths.

Using the above set of parameters of 4 kW induction motor in the simulation model, a close match between model and machine was obtained for all areas of Figs. 4.5.1-3a and 4.5.1-3b except at the high frequency end of the locked-rotor test as Figs. 4.5.1-3a and 4.5.1-3b show.

4.5.2. Experimental Results for Estimation of Slip-Ring Motor Parameters

For a 3.3 kW slip-ring induction motor only the DC test, the no-load test and the locked-rotor test were performed. The DC resistance of the motor was calculated from the DC test. During the no-load and the locked-rotor tests the motor was directly fed from the main supply. In the no-load test the rated voltage and the frequency were applied to the motor. In the locked-rotor test the frequency was still kept at rated value, but only 105 volts stator voltage was applied to the motor in order to produce the rated stator current. The inertia, the maximum slope of run-down curve and the mechanical torque of the slip-ring induction motor were found as to be 0.074 kgm^2, 14.294 rad/s^2 and 1.0577 Nm respectively. As a result of above tests, the parameters of the slip-ring induction motor were calculated as:

$R_s = 1.58\ \Omega,\ R_r = 1.5\ \Omega, L_{sl} \approx 0.0245$ H, $L_{rl} \approx 0.0245$ H, $L_{sr} \approx 0.62$ H.

4.6. Summary

In this chapter the DC test, no-load test, and locked-rotor test were explained and performed on the test motors using the mains. The no-load test of a squirrel-cage induction motor using an inverter was also performed at different frequencies and different levels of fluxing to calculate the no-load motor impedance at different flux levels. The locked-rotor test using an inverter was repeated at different voltages and frequencies to calculate the locked-rotor impedance of the motor.

For the slip-ring induction machine only the DC test, the no-load test and the locked-rotor test were performed. The run-up and the run-down tests were applied to the both squirrel-cage and slip-ring induction motors to calculate the mechanical losses and the inertia of machines. As a result of the above tests the parameters of both test motors were calculated.

CHAPTER 5

INVESTIGATION INTO DIFFERENT FORMS OF MIXED-FREQUENCY TEST

5.1. Introduction

In Chapter 2, various practical arrangements were discussed which can be or have been used for conducting mixed-frequency tests of induction machines. It was noted that different arrangements provided different voltage waveforms but that virtually identical power losses could be achieved in every case by judicious choice of the parameters which govern the voltage waveforms. In chapter 2, the supplies were considered to have very low output impedances compared with the input impedance of the induction machine so that the voltage applied to the terminals of the induction machine were independent of the currents drawn (or generated). Because the possibility of using inverters was broached in chapter 2, it was recognised that an infinite number of different voltage waveforms could be generated all of which could meet the criteria of correctly disposing the power losses between rotor and stator.

Even ideal induction machines are not 'linear' in the same way that an idealised DC machine is linear and so it is not possible to extrapolate infinitely from a set of representative cases for which full solutions have been carried out. (For a linear machine like the ideal DC machine, the complete dynamic response of any one of the machine state variables could be determined as the convolution of the impulse response and the input voltage). Therefore, in order to carry out some representative studies of the behaviour of the induction machine on mixed-frequency test, it is necessary to restrict the possibilities by imposing certain constraints. This was mentioned in Chapter 2 where it was noted that when a single variable-speed and variable excitation alternator could be used to generate the requisite voltage waveform for the mixed-frequency test, it would be adequate to consider that either the amplitude or the frequency of the voltage waveform (or both) is

slowly varying functions of time. In this case, slowly varying would be defined as having no substantial frequency components greater than one-half of the mean frequency of the voltage waveform. This led to the identification of three simple types of voltage waveform that were described as CVVF, (Constant Voltage, Variable Frequency), VVCF, (Variable Voltage, Constant Frequency) and VVVF, (Variable Voltage, Variable Frequency).

In this Chapter, the efficiency of CVVF, VVCF and VVVF tests is investigated through simulation and the effects observed are explained. Because there is one common type of voltage waveform used for mixed-frequency tests which is not closely represented by any of the afore-mentioned three types, this type of waveform is also investigated. It is referred to as sum of two sinewaves.

5.2. Simulation Results of Various Possible Forms of the Mixed-Frequency Test

An induction machine, 3 phase, 11 kV/line, 12.6 MVA, 4 pole, whose parameters are given in appendix 1 was used in the simulation to analyse four different forms of mixed-frequency test, each form being associated with a different voltage waveform. Since inertia has a major significance in the mixed-frequency test, three different values of inertia were used. In each case, an equation is given for the voltage waveform, followed by a plot illustrating its waveform and harmonic spectrum. The equation contains two base parameters, base voltage, V_0, and base angular frequency, ω_0, and two other parameters which are dimensionless, the beat frequency ratio, $\Re$, and degree of torque modulation, δ_T. The base voltage and the base angular frequency are the same for all four cases and they are determined by the machine on test. The beat frequency ratio is defined as:

$$\Re = \frac{\omega_b}{\omega_0}, \quad \text{...where...} \ \omega_b = \text{Angular beat frequency} \tag{5.2-1}$$

The degree of voltage modulation defines the instantaneous amplitude envelope of the voltage between $V_0+\delta_v V_0$ and $V_0-\delta_v V_0$ as the degree of frequency modulation defines the

instantaneous variation of frequency between $\omega_0+\delta_f\omega_0$ and $\omega_0-\delta_f\omega_0$. The degrees of voltage and frequency modulations are explained in terms of the degree of torque modulation in section 5.3.

For each of the four possible forms of mixed-frequency test, the simulation program was run for numerous values of, $\Re$, between 0 and 30 % of base frequency. For each value of the $\Re$, a value of δ_T was found such that the rms stator current was equal to its rated value.

The results for each of the four voltage waveforms are presented individually. It will be seen that depending on which waveform was used, the value of $\Re$, and the value of the motor's inertia, J, were obtained for δ_T between 0 and 20.

5.3. Determination of Degree of Amplitude Modulation and Degree of Frequency Modulation

In chapter 2, the degree of torque modulation, δ_T, was defined as the variation in torque which would occur if the beat frequency was low and rotor speed was held constant.

In this chapter, four different waveform types are compared for applicability to mixed-frequency test. Each of these waveform types is characterised by a degree of modulation of the frequency or the amplitude or both. It is therefore necessary to establish relationships between the degrees of modulation of amplitude and frequency and the absolute degree of modulation, δ_T, which is based on torque.

The torque equation of an induction motor can be written from the one phase "T" equivalent circuit of the motor as:

$$T_e = \frac{1}{\omega_0}\frac{3V_0^2}{\left(R_s+\frac{R_r'}{s}\right)^2+X_e^2}\frac{R_r'}{s} \quad \text{where} \quad \omega_0 = \frac{4\pi f}{\text{poles}} \qquad (5.3\text{-}1)$$

5.3.1. Relationships Between the Degrees of Modulation of Amplitude and Torque

If the slip, s, remains constant and the base voltage, V_0, is variable in the torque equation, then the nominal torque across the airgap can be re-written as:

$$T_e = \kappa V_0^2 \tag{5.3.1-1}$$

The derivative of torque with respect to the base voltage is then:

$$\frac{dT_e}{dV_0} = 2\kappa V_0 = \frac{2T_e}{V_0} \tag{5.3.1-2}$$

If a small variation, ΔV_0, occurs on the voltage, a corresponding variation, ΔT_e, will be present in the torque and ΔV_0, ΔT_e are related as:

$$\left.\begin{aligned} \frac{\Delta T_e}{\Delta V_0} = \frac{2T_e}{V_0} \Rightarrow \\ \frac{\Delta T_e}{T_e} = \frac{2\Delta V_0}{V_0} \end{aligned}\right\} \tag{5.3.1-3}$$

The degree of base voltage modulation, δ_v, and the degree of torque modulation, δ_T, are defined in (5.3.1-4).

$$\delta_v = \frac{\Delta V_0}{V_0}, \quad \delta_T = \frac{\Delta \text{ Nominal Torque}}{\text{Rated Torque}} \tag{5.3.1-4}$$

Then the relationship between degree of voltage modulation and degree of torque modulation can be given as below using equations (5.3.1-3) and (5.3.1-4).

$$\delta_v = \frac{\delta_T}{2} \tag{5.3.1-5}$$

5.3.2. Relationships Between the Degrees of Modulation of Frequency and Torque

The relationship between slip and torque in the region very close to the zero slip can be excepted as linear when the base voltage, V_0, remains constant. The stator resistance R_s and the equivalent reactance X_e in the torque equation are very small comparing with the R_r'/s due to the very small value of the slip. Therefore, they can be eliminated for the simplicity of the torque equation as given below.

$$T_e = \frac{1}{\omega_0}\frac{3V_0^2 s}{R_r'} = \kappa s \qquad (5.3.2\text{-}1)$$

If a small change, Δs, occurs on the slip, a corresponding change, ΔT_e, will be present in the torque and δ_T is defined as:

$$\delta_T = \frac{\Delta T_e}{T_e} \qquad (5.3.2\text{-}2)$$

The degree of frequency modulation, δ_f, is defined as:

$$\delta_f = \frac{\Delta \text{ Nominal Frequency}}{\text{Rated Frequency}} \Rightarrow \frac{\Delta\omega_0}{\omega_0} = \Delta s \qquad (5.3.2\text{-}3)$$

The relationship between the degree of frequency modulation, δ_f ,and degree of torque modulation, δ_T, can be written as below using equations (5.3.2-1), (5.3.2-2) and (5.3.2-3):

$$\frac{\Delta s}{s_{rated}} = \frac{\Delta T_e}{T_e} = \delta_T \quad \Rightarrow \quad \delta_f = \delta_T s_{rated} \qquad (5.3.2\text{-}4)$$

5.4. Case 1

This form of the mixed-frequency test has a voltage waveform comprising the sum of two sinewaves as given in equation (5.4-1).

$$V_{sa}(t) = V_0\left[\sin(\omega_0 t) + \delta_v \sin((1-\Re)\omega_0 t)\right] \quad (5.4\text{-}1)$$

where

V_{sa}= Resultant voltage,

V_0= Amplitude of base voltage,

δ_v= Degree of voltage modulation,

ω_0= Angular base frequency,

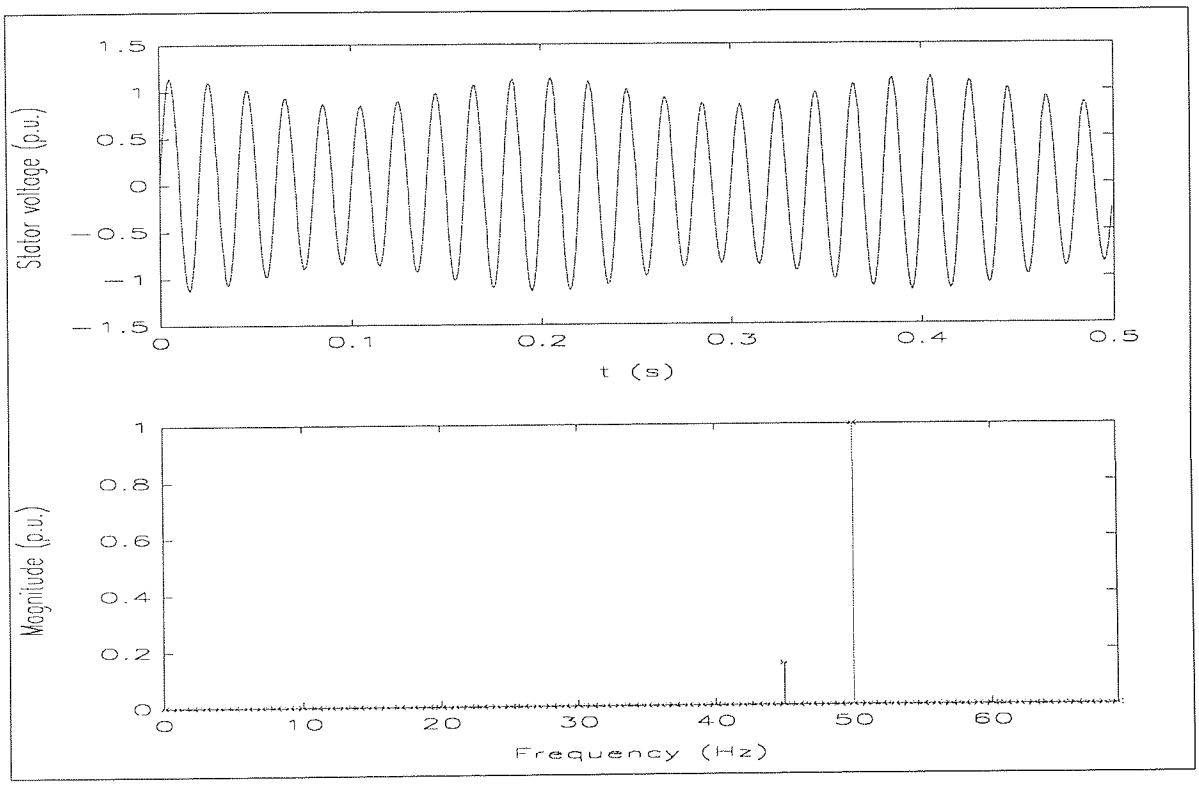

Fig. 5.4-1 Stator phase voltage and its harmonic spectrum for case 1 (V_0=1.0 p.u., δ_v= 0.15, $\Re$=0.1).

Fig. 5.4-1 shows the phase voltage and its harmonic spectrum for case 1 with $\Re$= 0.1 and δ_v = 0.15. The modulation of the amplitude and the variation of the frequency are both smooth. Two harmonics appear at 45 Hz and 50 Hz as values of 0.15 p.u. and 1.0 p.u. respectively.

In this case ($\Re$= 0.1, δ_v= 0.15), the instantaneous amplitude envelop changes between V_0+ δ_v V_0 and V_0-$\delta_v V_0$, and the instantaneous frequency f_{ins} can be calculated as (Kron (1969,1973), Radic and Strupp (1976), Plevin (1988)):

$$\left.\begin{aligned} V_{env}(t) &= V_0\sqrt{\left(1+\delta_v{}^2+2\delta_v\cos(\Re\omega_0 t)\right)} \\ f_{ins}(t) &= \frac{\frac{\omega_0}{2\pi}\left(\left(1+\delta_v{}^2(1-\Re)\right)+\delta_v(2-\Re)\cos(\Re\omega_0 t)\right)}{\left(1+\delta_v{}^2+2\delta_v\cos(\Re\omega_0 t)\right)} \end{aligned}\right\} \qquad (5.4\text{-}2)$$

Kron (1973) has shown that the speed of the rotating field varies between the limits given below:

$$\frac{\omega_0(1+\beta\delta_v)}{1+\delta_v} < \omega_{res} < \frac{\omega_0(1-\beta\delta_v)}{1-\delta_v} \qquad (5.4\text{-}3)$$

where

ω_{res} = Angular velocity of resultant rotating field,

$\beta = (\omega_0-\omega_b)/\omega_0$.

Simulation of the induction machine was carried out with three different machine inertia and then the degree of voltage modulation (δ_v), rotor current and resultant voltage were calculated at wide range of swing frequencies with the condition that the machine input current was at the rated value. That requires the simulation program to run at least three or more times. At each run of the simulation program, the degree of voltage modulation is varied several times to get the rated stator current at each beat frequency.

Fig.'s 5.4-2a, 5.4-2b and 5.4-2c show these results for the three different values of the rotor inertia. All the curves given in these figures look like an odd function of the torque-speed

curve of an induction machine. At low frequency ratios, below 0.01, the variations of degree of voltage modulation, voltage and rotor current are very sharp. The voltage is always over the rated value during the test, because, in this test, one sinewave with a lower magnitude and lower frequency is superimposed on to the another sinewave that has a higher magnitude and higher frequency. It is possible to obtain the rated rms rotor current below 0.01 frequency ratio with the normal inertia of the rotor. At about 0.04 frequency ratio, the rotor current has its

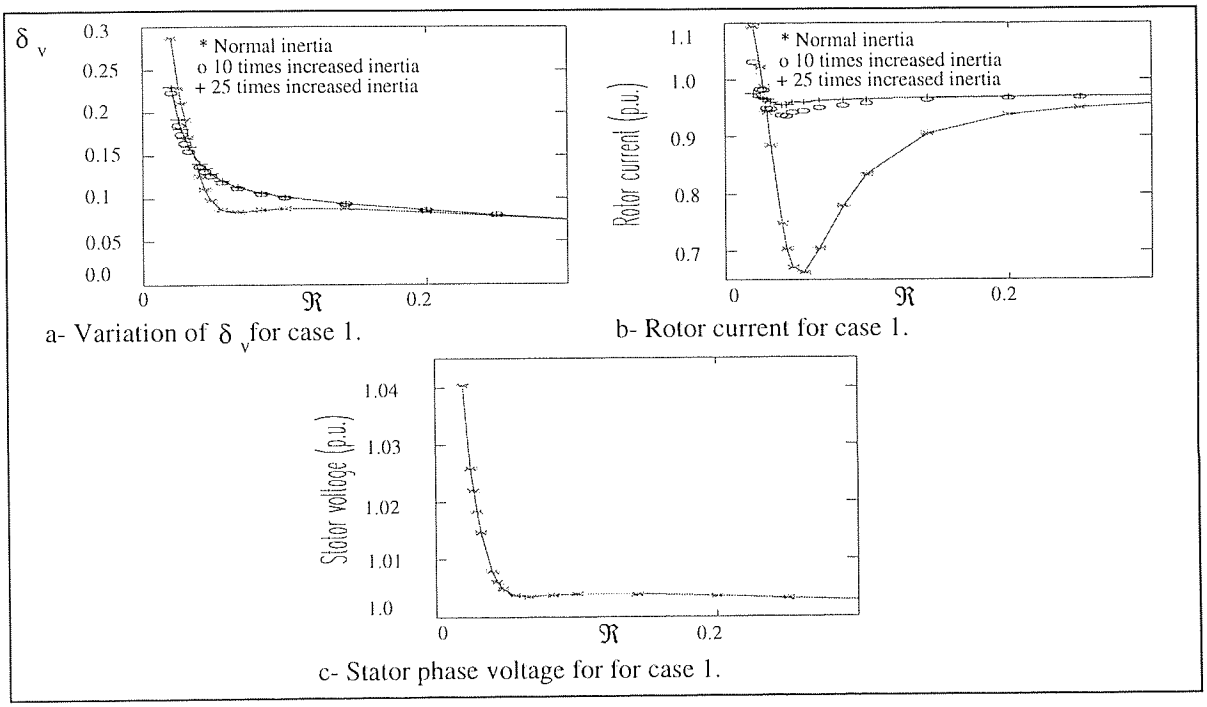

a- Variation of δ_v for case 1.

b- Rotor current for case 1.

c- Stator phase voltage for for case 1.

Fig. 5.4-2 Variations of δ_v, rotor current and stator phase voltage with respect to the f_b for case 1.

minimum value and this is a critical point, because above and below this critical point, the rotor current increases. If the rotor inertia is increased 10 times or 25 times of the normal inertia, the rms rotor current closes to the rated rms value at all the values of frequency ratio. Furthermore, the increment of the rotor inertia changes the degree of voltage modulation, but does not affect the stator voltage.

5.5. Case 2, CVVF Test

In this case, the amplitude of the voltage is constant as its frequency varies with respect to the frequency ratio, $\Re$, as given in equation (5.5-1). In fact, $\Re$ is related with the angular beat frequency, ω_b, as given in (5.2-1), therefore the frequency variation of voltage is due to the variation of the beat frequency.

$$\left.\begin{aligned} V_{sa}(t) &= V_0 \sin(\theta(t)) \Rightarrow \frac{d\theta(t)}{dt} = \omega_0 \alpha(t) \Rightarrow \alpha(t) = 1 + \delta_f \cos(\Re\omega_0 t) \\ \text{or alternatively } \theta(t) &= \omega_0 \int_0^t \alpha(t)dt = \omega_0 t + \frac{\delta_f \sin(\Re\omega_0 t)}{\Re} \\ \delta_T &= \frac{\omega_1}{\omega_0}\frac{1}{s_{rated}} = 2\delta_f \end{aligned}\right\} \quad (5.5\text{-}1)$$

Fig. 5.5-1 shows the phase voltage and its harmonic spectrum of the CVVF test. The frequency variation can be seen easily although the voltage magnitude is constant. However, it was found that, the voltage of the CVVF test consists of more than one harmonics of 0.115 p.u., 0.44 p.u., 0.765 p.u., 0.44 p.u. and 0.115 p.u. at 40 Hz, 45 Hz, 50 Hz, 55 Hz and 60 Hz respectively with 5 Hz steps. The reason for that, the main angular frequency is varied between $(\omega_0+\delta_f\omega_0)$ and $(\omega_0-\delta_f\omega_0)$, therefore, it can be called a pure frequency modulation. Furthermore, all the harmonics of case 2 are symmetric. They are starting to appear at 40 Hz with a small magnitude and then increase as the frequency increases. At 50 Hz, the harmonic has its maximum magnitude, but after 50 Hz, its magnitude reduces gradually in the same order and the same steps as it increases.

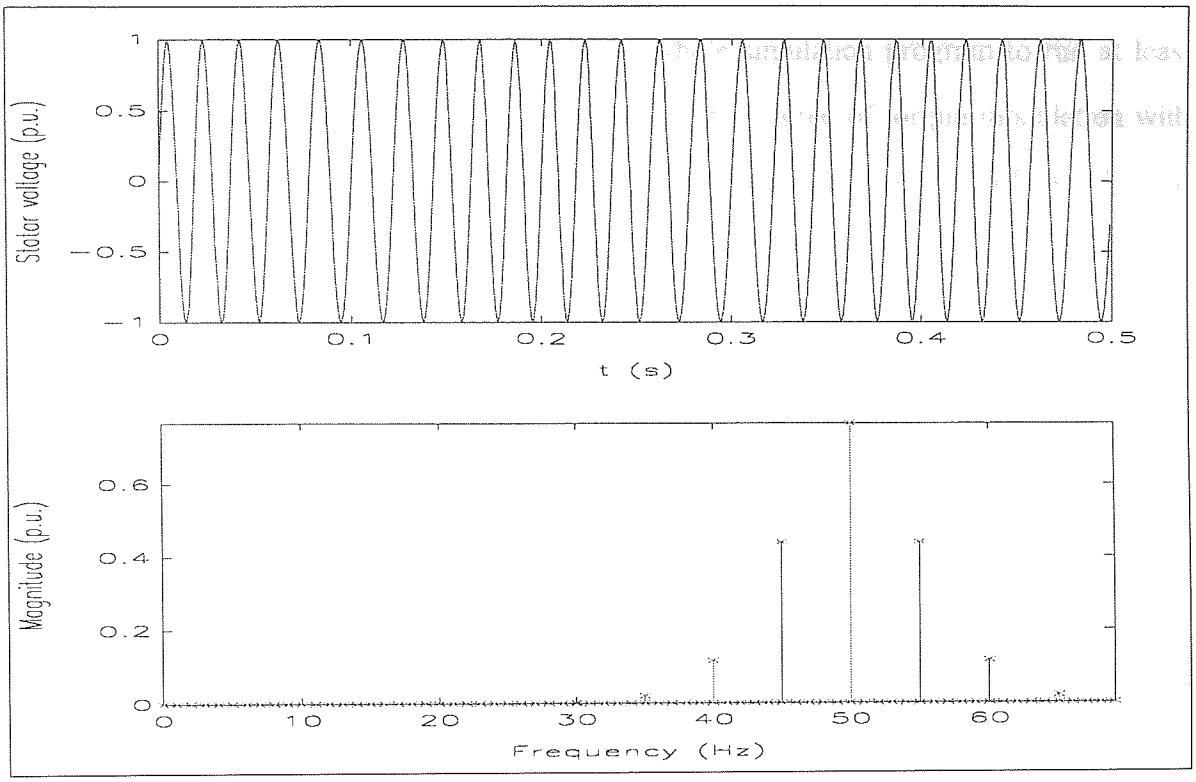

Fig. 5.5-1 Stator phase voltage of CVVF test (V_0 = 1.0 p.u., δ_f = 0.1, $\Re$ = 0.1).

The variations of the degree of torque modulation, the stator voltage and the rotor current with respect to the frequency ratio are illustrated in Fig.'s 5.5-2a and 5.5-2b respectively. Each of the points in these figures were obtained at every step of the frequency ratio by varying the degree of torque modulation providing that, the rms stator current is equal to rated value.

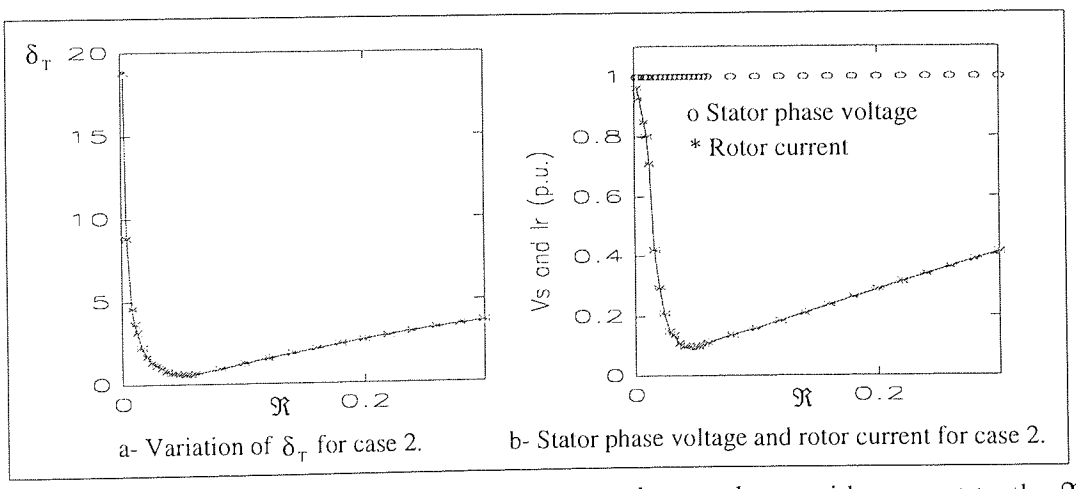

a- Variation of δ_T for case 2.

b- Stator phase voltage and rotor current for case 2.

Fig. 5.5-2 Variations of δ_T, rotor current and stator phase voltage with respect to the $\Re$ for case 2.

Therefore, calculation of each point requires the whole simulation program to run at least three or more times. In Fig. 5.5.-2a, the variation of the degree of torque modulation with respect to the frequency ratio is an odd function of the torque-speed curve of an induction motor. At low frequency ratios, below 0.02, the degree of torque modulation increases very sharply as the frequency ratio decreases. At 0.04 frequency ratio, δ_f has its minimum value, but after 0.04, it increases slowly as the frequency ratio increases. Variation of the rotor current with respect to the frequency ratio in Fig. 5.5-2b is also similar to the variation of the degree of torque modulation. Furthermore, below 0.02 frequency ratio, the CVVF test provides the rms rotor current very close to the rated rms value. The phase voltage is the same during the CVVF test, because it was already kept constant as given in equation (5.5-1).

5.6. Case 3, VVCF Test

In this case, the amplitude of the voltage is varied with respect to the frequency ratio, $\Re$, as given in equation (5.6-1) below, but the frequency of voltage is kept to be constant. Therefore, this case can be called as a pure amplitude modulation.

$$\left.\begin{aligned} V_{sa}(t) &= V_0\alpha(t)\sin(\omega_0 t) \Rightarrow \alpha(t) = 1+\delta_v\cos(\Re\omega_0 t) \\ \delta_T &= 2\delta_v \end{aligned}\right\} \qquad (5.6\text{-}1)$$

Fig. 5.6-1 shows the phase voltage and its harmonic spectrum of the VVCF test. The VVCF test produces three significant harmonics of 0.05 p.u. 1.0 p.u. and 0.05 p.u. at 45 Hz, 50 Hz and 55 Hz respectively, due to the changes in amplitude of voltage between $(V_0+\delta_v V_0)$ and $(V_0-\delta_v V_0)$. Furthermore, all the harmonics of case 3 are symmetric, because there is only one smoothly varying component in the voltage equation.

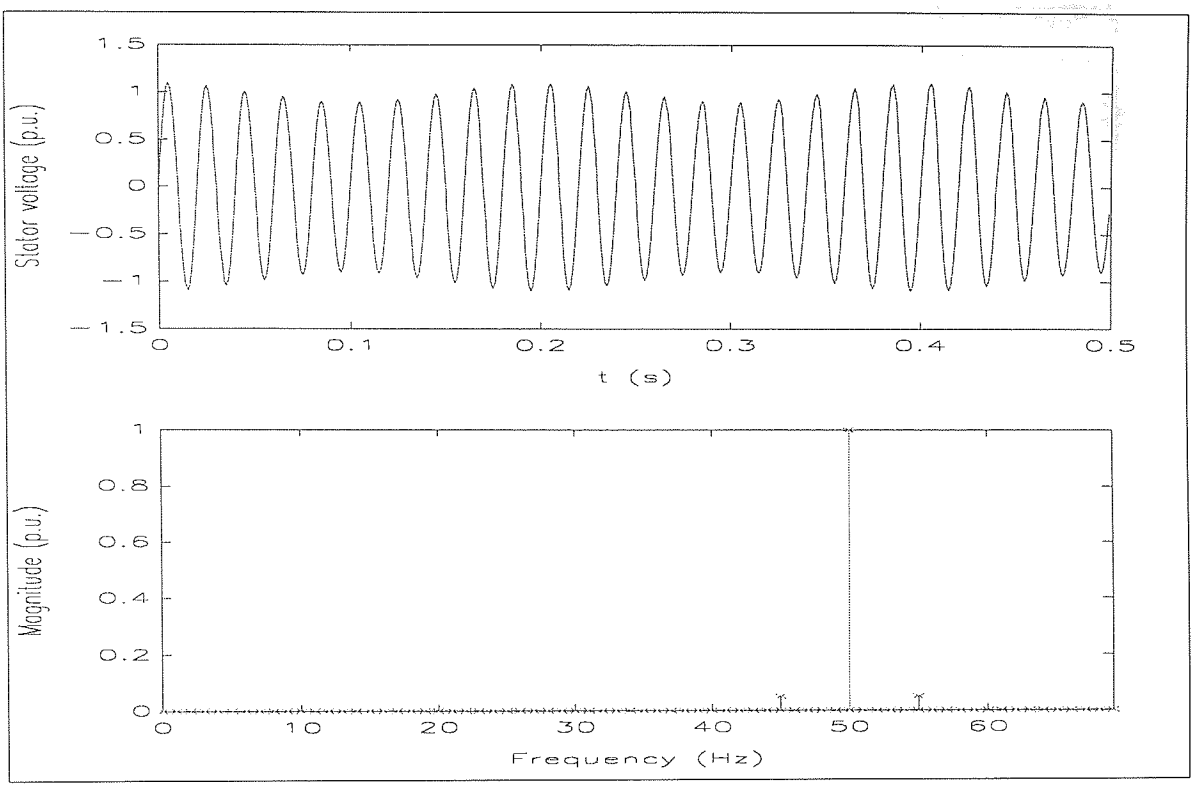

Fig. 5.6-1 Stator phase voltage of CVVF test (V_0 = 1.0 p.u., δ_v = 0.1, $\Re$ = 0.1).

Fig. 5.6-2 shows the variations of degree of voltage modulation, stator voltage and rotor current of case 3 with respect to the frequency ratio. In these figures all the points at each frequency ratio were obtained by running the simulation program repeatedly with different degree of frequency modulation to get the correct value of rms stator current. The shape of these figures is an odd function of torque-slip curve of an induction motor. The stator phase voltage is always over the rated value due to the degree of voltage oscillation. It is possible to obtain the rated rotor current at about 0.1 frequency ratio.

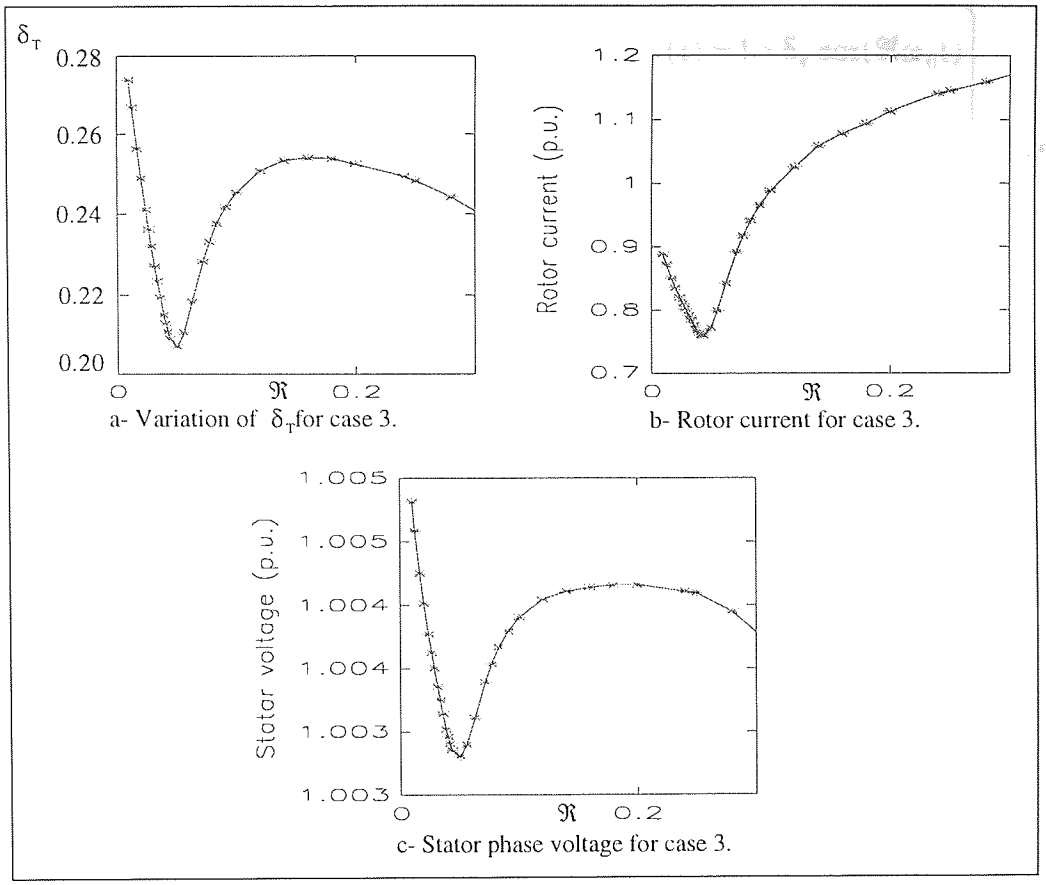

Fig. 5.6-2 Variations of δ_T, rotor current and stator phase voltage with respect to the $\Re$ for case 3.

5.7. Case 4, VVVF Test

The case 4 produces a stator voltage waveform which is frequency dependent rather than the sum of two different voltages. In addition to the degree of voltage modulation, δ_v, the frequency modulation, δ_f, of the voltage is also modulated. There are two main and two dimensionless components of this voltage as described in equation (5.7-1). The base voltage (V_0) and the base frequency (ω_0) are known for a test motor and does not change during the test, but the degree of torque modulation (δ_T) and the frequency ratio ($\Re$) are both varied depending on the beat frequency (ω_b).

$$\left.\begin{aligned} V_{sa}(t) &= V_0\alpha(t)\sin\big(\theta(t)\big) \Rightarrow \frac{d\theta(t)}{dt} = \omega_0\alpha(t) \Rightarrow \alpha(t) = 1+\delta_f\cos(\Re\omega_0 t) \\ \text{or alternatively}\quad \theta(t) &= \omega_0\int_0^t \alpha(t)dt = \omega_0 t + \frac{\delta\sin(\Re\omega_0 t)}{\Re} \\ \delta_f &= \frac{f_1}{f_0},\ \delta_f = \delta_v,\ \delta_T = \frac{\delta_f}{s_{rated}} \text{ and } \delta_T = 2\delta_v \Rightarrow \delta_T = \frac{2f_1}{f_0} + \frac{f_1}{f_0 s_{rated}} = 1.945 f_1 \end{aligned}\right\} \quad (5.7\text{-}1)$$

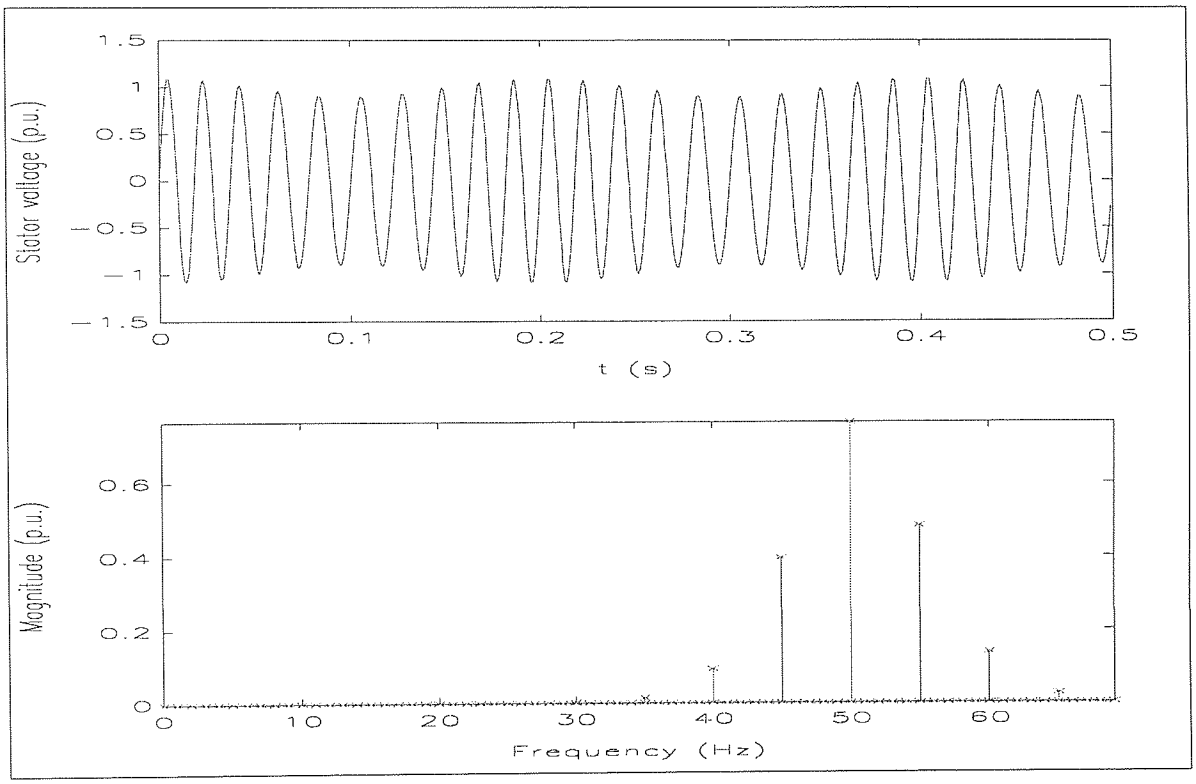

Fig. 5.7-1 Stator phase voltage of VVVF test (V_0 = 1.0 p.u., δ_f = 0.1, δ_v = 0.1, $\Re$ = 0.1).

Fig. 5.7-1 shows the phase voltage and its harmonic spectrum of the VVVF test. The variation of voltage waveform is similar to case 1, but the harmonic content of the VVVF test is totally different. At least there are more than two harmonics of 0.092 p.u., 0.396 p.u., 0.765 p.u., 0.48 p.u. and 0.137 p.u. at 40 Hz, 45 Hz, 50 Hz, 55 Hz and 60 Hz respectively with 5 Hz steps. The magnitudes of harmonics are increasing gradually until 50 Hz and then decreasing in the same order.

Fig. 5.7-2 shows variations of degree of torque modulation, rotor current and stator voltage with respect to the frequency ratio. Note that, at every point of the frequency ratio, the

degree of torque modulation was varied by running the simulation program several times until to get the rated stator current of the motor.

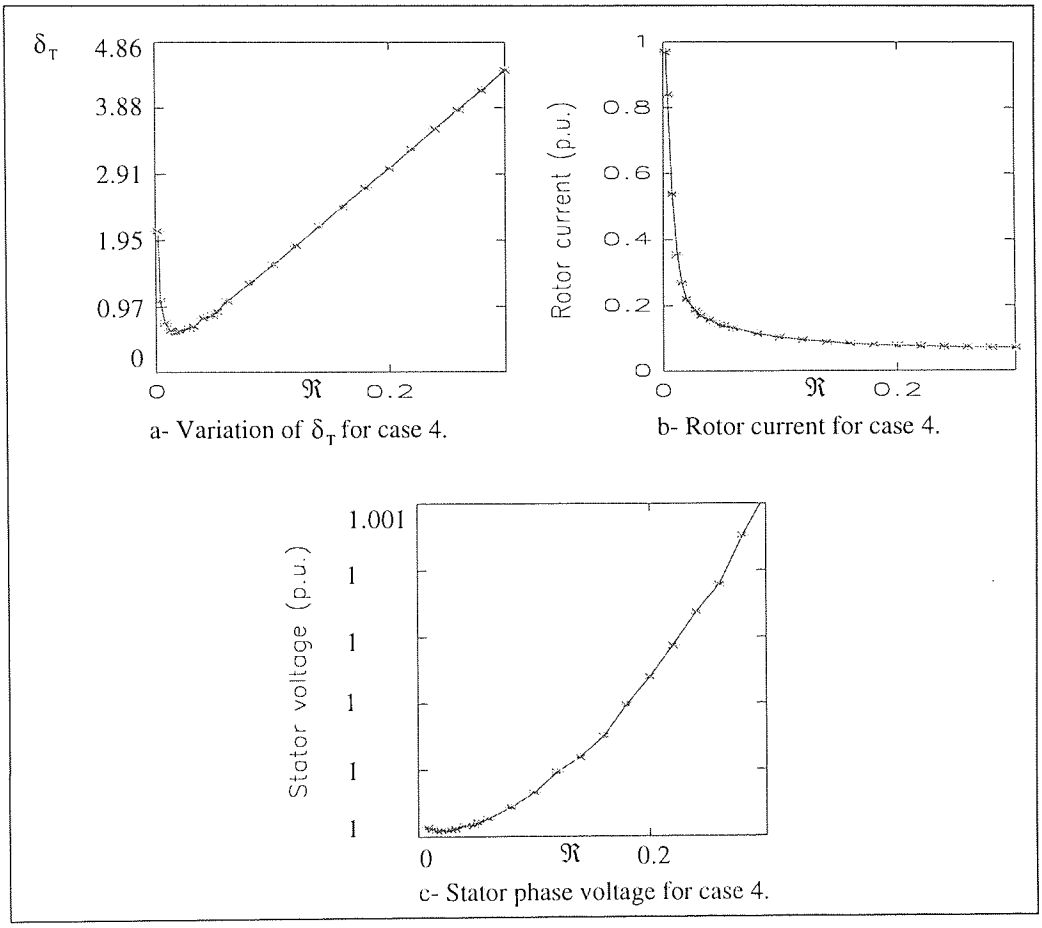

Fig. 5.7-2 Variations of δ_T, rotor current and stator phase voltage with respect to the $\Re$ for case 4.

The degree of torque modulation varies linearly above 0.02 frequency ratio and the stator voltage remains almost constant during the whole range of frequency ratio. However, the rotor current is very close to the rated value at low frequency ratios below 0.02, but above 0.02, the rotor current decreases as the frequency ratio increase.

5.8. Summary

In this chapter, four different forms of the mixed-frequency test have been investigated. First of all, the voltage equations were given in closed form for each case of the mixed-frequency test. The degree of voltage and frequency modulation given in these equations

were expressed in terms of the degree of torque modulation. As an example of each form, the voltage waveforms and their harmonic spectra were analysed for a given frequency ratio and degree of torque modulation. It has been shown that in cases 2, 3 and 4 the voltage waveforms were symmetrical and their harmonics increased between 40 Hz and 50 Hz then decreases between 50 Hz and 60 Hz gradually in the same order with the same steps due to the same frequency ratio. The case 1 has only two harmonics at 45 Hz and 50, because, in case 1, one of the sinewaves, with a low amplitude at low frequency, was superimposed on to the other one which has rated amplitude at rated frequency.

In addition, the investigation on each case was carried on by running the simulation program for wide range of frequency ratio, from zero to 0.3. At each step of the frequency ratio, the simulation program was run several times with different values of the degree of torque modulation to get the rated rms stator current. After every successful running of the simulation program, the degree of torque modulation, the stator voltage and the rotor current were recorded. The variations of these three components with respect to the frequency ratio were found as an odd function of the torque-speed curve of an induction motor. So that each of the curves of these component has a deep point where they have their minimum values. The stator voltage was to be found above the rated value for case 1 and case 3, but it was to be found equal to the rated value for case 2 and case 4. The rotor current was found to be close to the rated value at low frequency ratios below 0.02 for all the three cases. At about 0.04 the rotor current has its minimum value, but above 0.04 it starts to increase. In case 3, the rotor current always decreases as the frequency ratio increases. Furthermore, the effects of the increased inertia test on the rotor current are also given by increasing the rotor inertia to 10 and 25 times the normal inertia for case 1. It has been shown that, the increased rotor inertia test provides the rated rotor current at almost every step of the frequency ratio.

CHAPTER 6

EXPERIMENTAL WORK ON INDUCTION MACHINES AND COMPARISON OF SIMULATION AND TEST RESULTS

6.1. Introduction

Before starting the experimental tests, the test-rig was prepared as required. Firstly a 4 kW squirrel-cage induction machine was coupled to a DC generator, to perform the direct loading test, using a mechanical coupling. The test machine was then fed from both the main power supply and the inverter[1] depending on the requirements of the test. The inverter is capable of delivering constant-voltage, varying-frequency (CVVF) and varying-voltage, varying-frequency (VVVF) output. It has another facility of external analogue speed demand input. A wavetek arbitrary waveform generator[1] was used to input the necessary speed demand into the external analogue input of the inverter. The machine phase voltages were recorded through a power oscilloscope[1] which reduces the voltage to a recordable value. Two phase currents were recorded through two hall-effect current transducers[1]. The rotor speed was detected by a tachometer[1] which counts the black and white colours on the shaft and produces related signals for rotor speed. A data acquisition toolbox[1] was used to record the voltages, currents and speed. Temperature rises at different points within the machine were measured with a thermometer[1] and thermocouples.

In this chapter, the direct loading test and the two different versions of the mixed-frequency (VVVF and CVVF) testings of the squirrel-cage induction machine are analysed in detailed. The same versions of the mixed-frequency test are also analysed with the increased rotor inertia. In addition, in order to validate rotor variables, the direct loading and the varying-voltage, varying-frequency tests are applied to a slip-ring induction machine (3.3 kW) and

[1]Description of the equipment used in the test is given in appendix 3.

then the test results are compared with the simulation results in each section. Further, the losses of the induction machine are given and the losses of the test machine are identified.

6.2. Direct Loading Test of the Squirrel-Cage Induction Machine

A 4 kW squirrel-cage induction machine, whose parameters are given in appendix 1, was connected directly to the supply and tested by loading it with a DC generator so that the rated full-load stator current (7.2 A) was drawn. The test was continued for several hours to warm up the machine to the rated winding temperature rise of 57 °C. After that, the temperature rises at various points (windings, airgap, core, end windings and rotor) within the machine were measured by using 5 different thermocouples and a temperature label for the rotor temperature. Table 6.2-1 shows the rated temperature rises of windings, airgap, core, end windings and rotor of the squirrel-cage induction machine.

Windings (°C)	Airgap (°C)	Core (°C)	End windings (°C)	Rotor (°C)
57	70	32	66	81

Table 6.2-1 Full load temperature rise test results of the squirrel-cage induction machine.

While the machine was running at rated rotor speed and drawing rated stator current from the supply under rated winding temperature, the voltages and the currents of lines *a* and *c* as well as the rotor speed were recorded continuously for several seconds.

Fig. 6.2-1 shows one of the full-load line voltage and current waveforms. Not surprisingly, they appear to be reasonably sinusoidal. The line voltage has a value of 415 Volts rms and the current has a value of 7.2 Amperes rms. Harmonic spectra of the full-load voltage and current are also shown in Fig. 6.2-2.

Fig. 6.2-3 illustrates the full-load instantaneous rotor speed and its harmonic spectrum. The rotor speed was measured using an electronic tachometer and recorded through a data acquisition board into a PC.

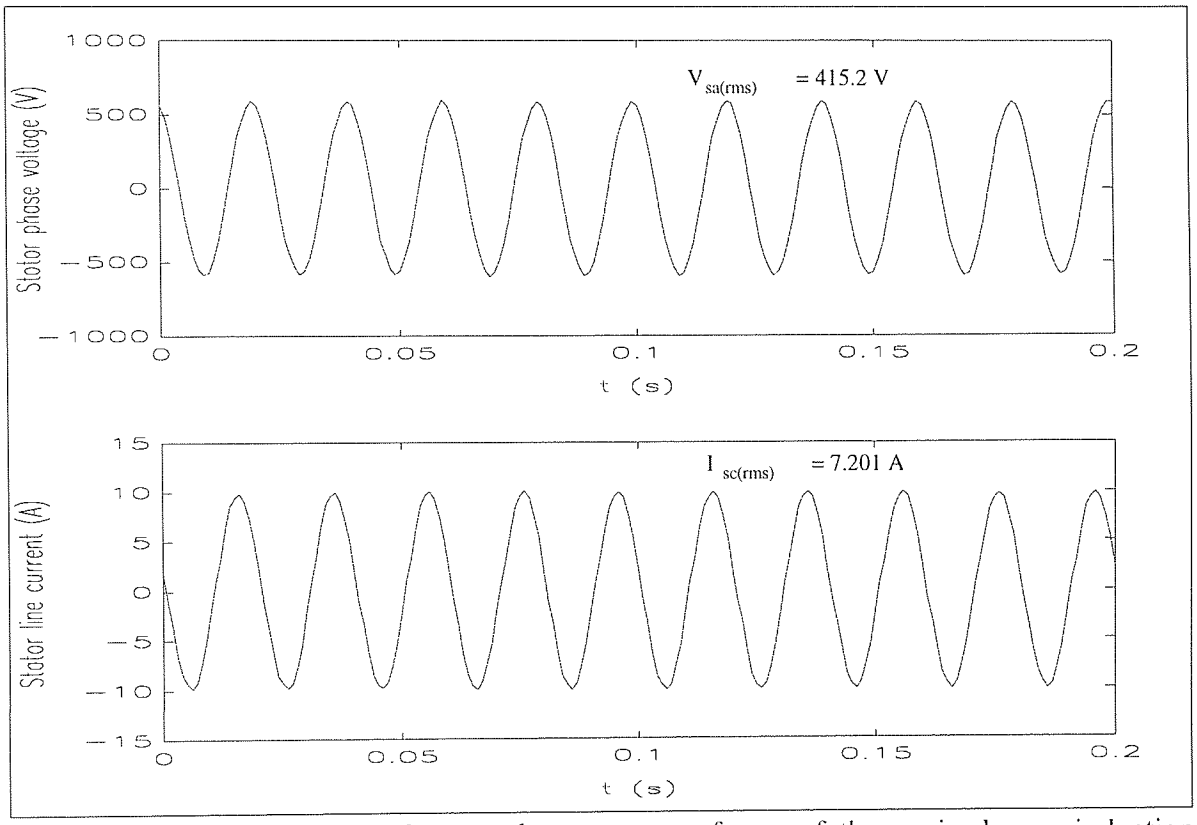

Fig. 6.2-1 Full-load stator voltage and current waveforms of the squirrel-cage induction machine.

As seen from Fig. 6.2-3, the waveform of the rotor speed is varying around the rated speed of 302.6 Rad/s, the DC value of the rotor speed was found to be 302.484 Rad/s.

Simulation results of full-load stator phase current, rotor speed and rotor current with their harmonic spectra are shown in Fig. 6.2-4, Fig. 6.2-5 and Fig. 6.2-6 respectively. The rms value of stator line current was found to be 7.08 A with a peak of 9.99 A harmonic at 50 Hz. The average value of full-load rotor speed was found 302.4 Rad/s. The rotor phase current has an rms value of 3.32 A. These simulation results were found to be similar to the test results.

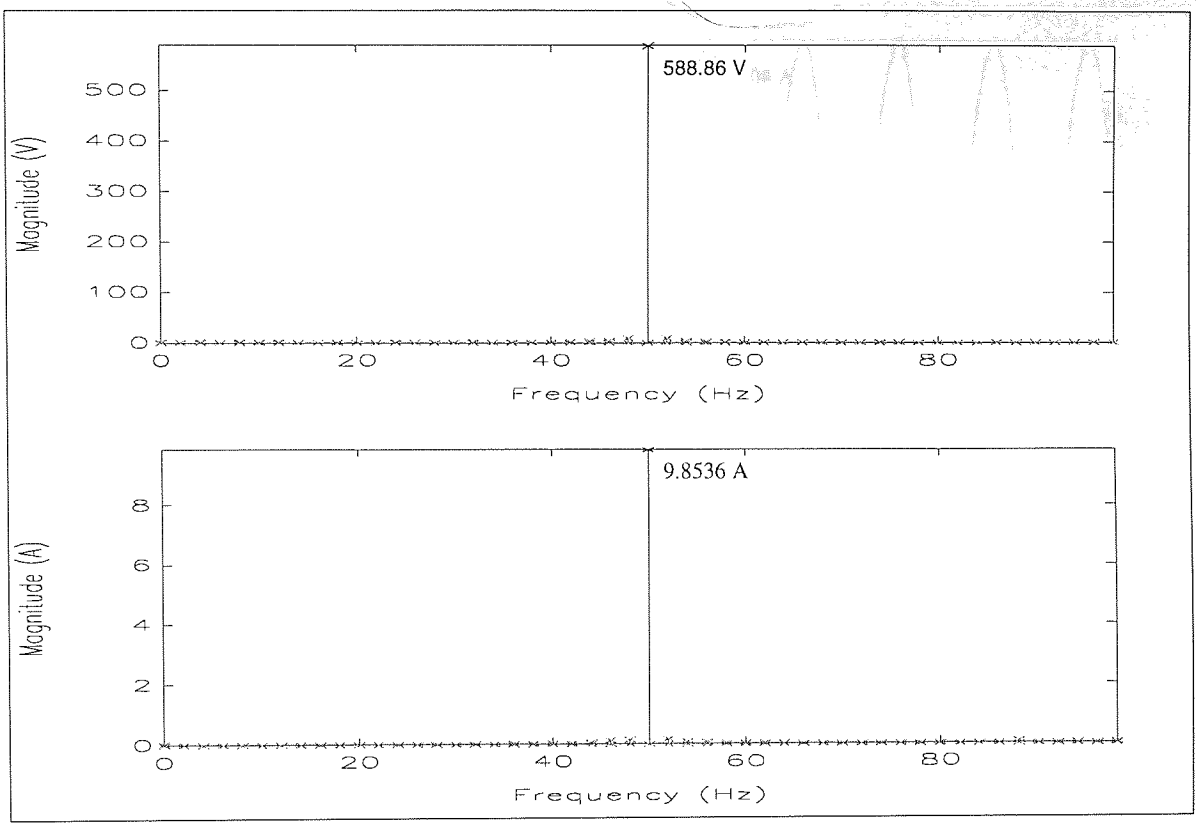

Fig. 6.2-2 Harmonic spectra of full-load stator voltage and current of the squirrel-cage induction machine.

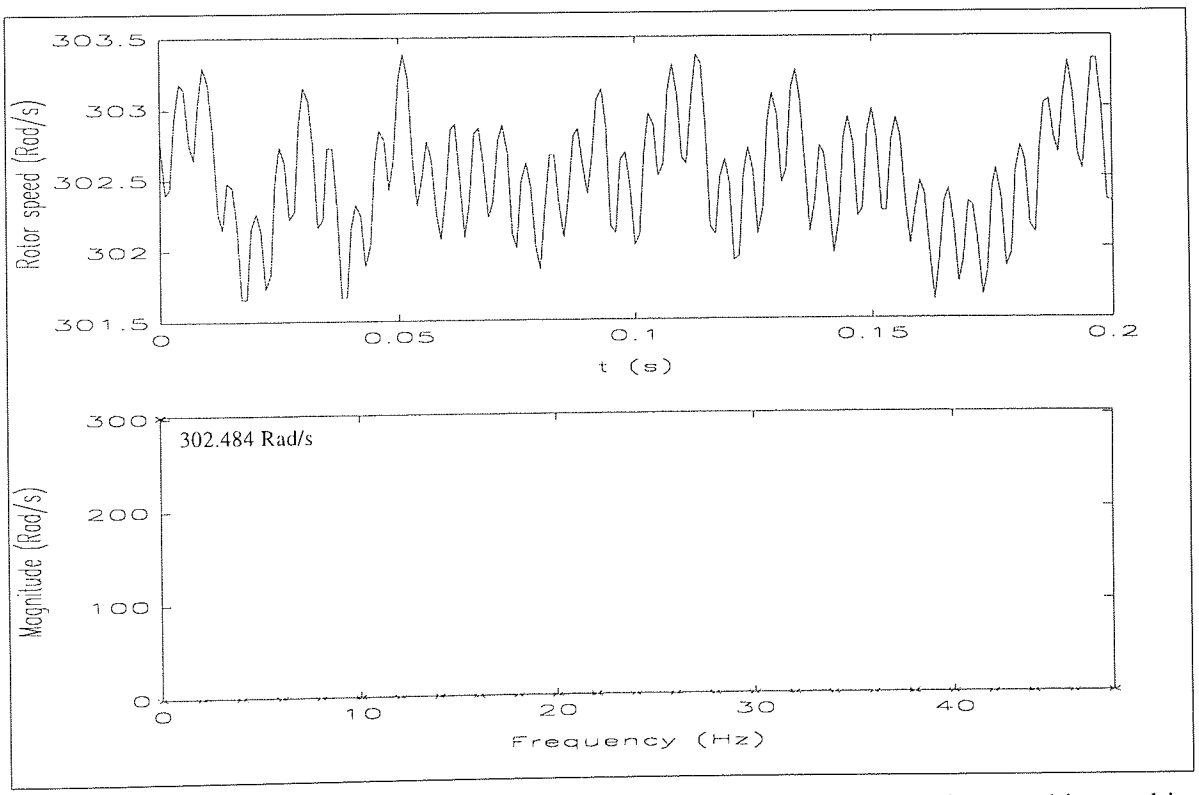

Fig. 6.2-3 Full-load instantaneous rotor speed of the squirrel-cage induction machine and its harmonic spectrum.

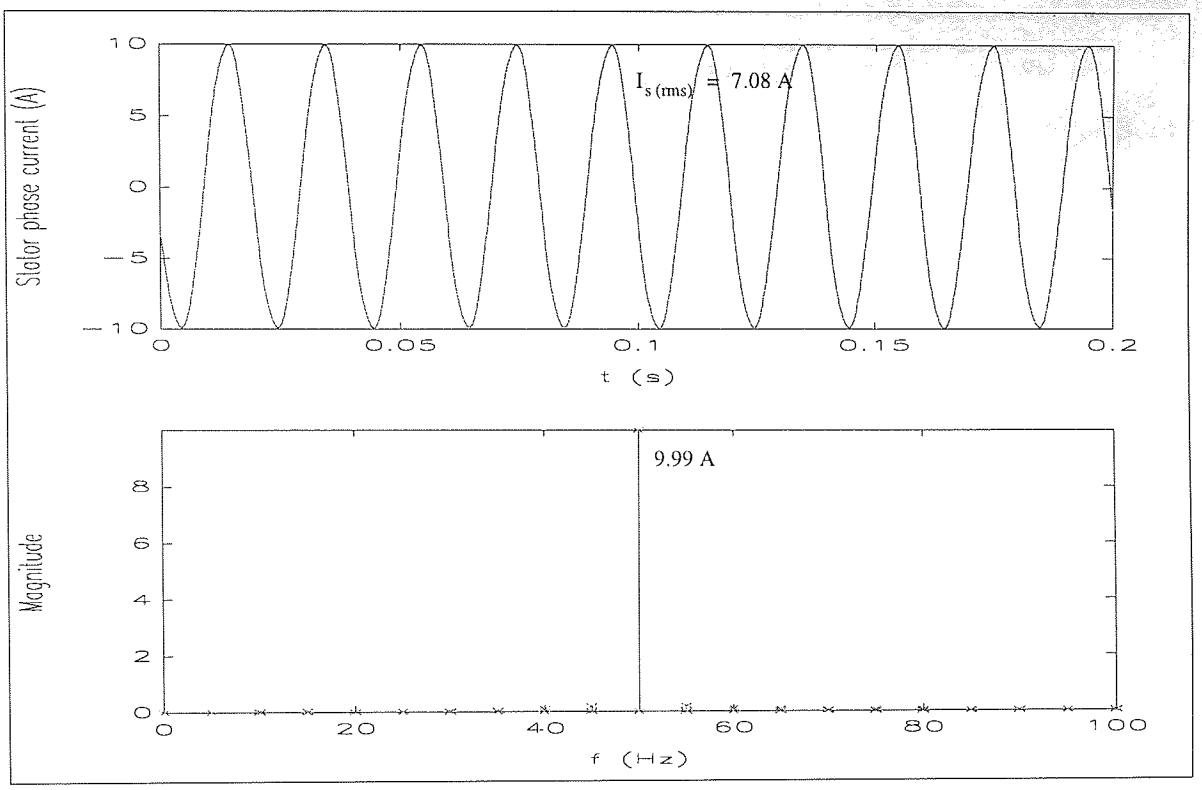

Fig. 6.2-4 Simulation result of full-load stator phase current of the squirrel-cage induction and its harmonic spectrum.

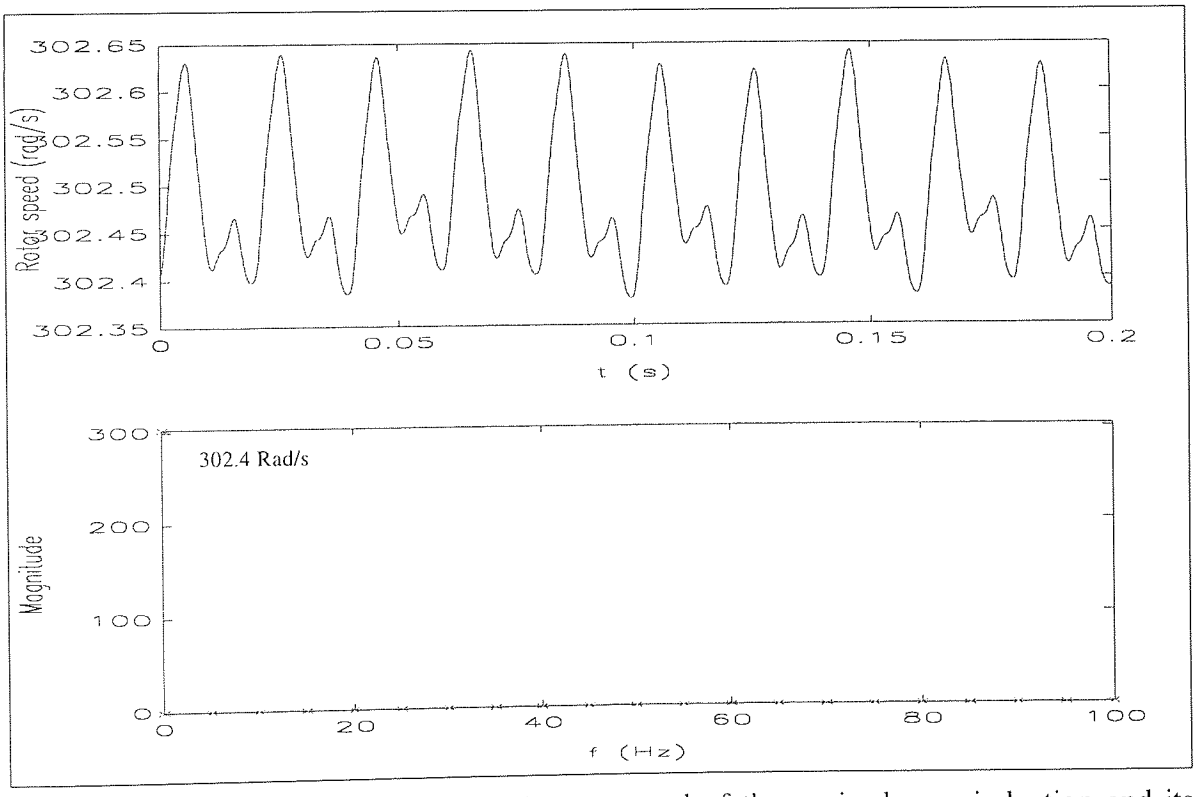

Fig. 6.2-5 Simulation result of full-load rotor speed of the squirrel-cage induction and its harmonic spectrum.

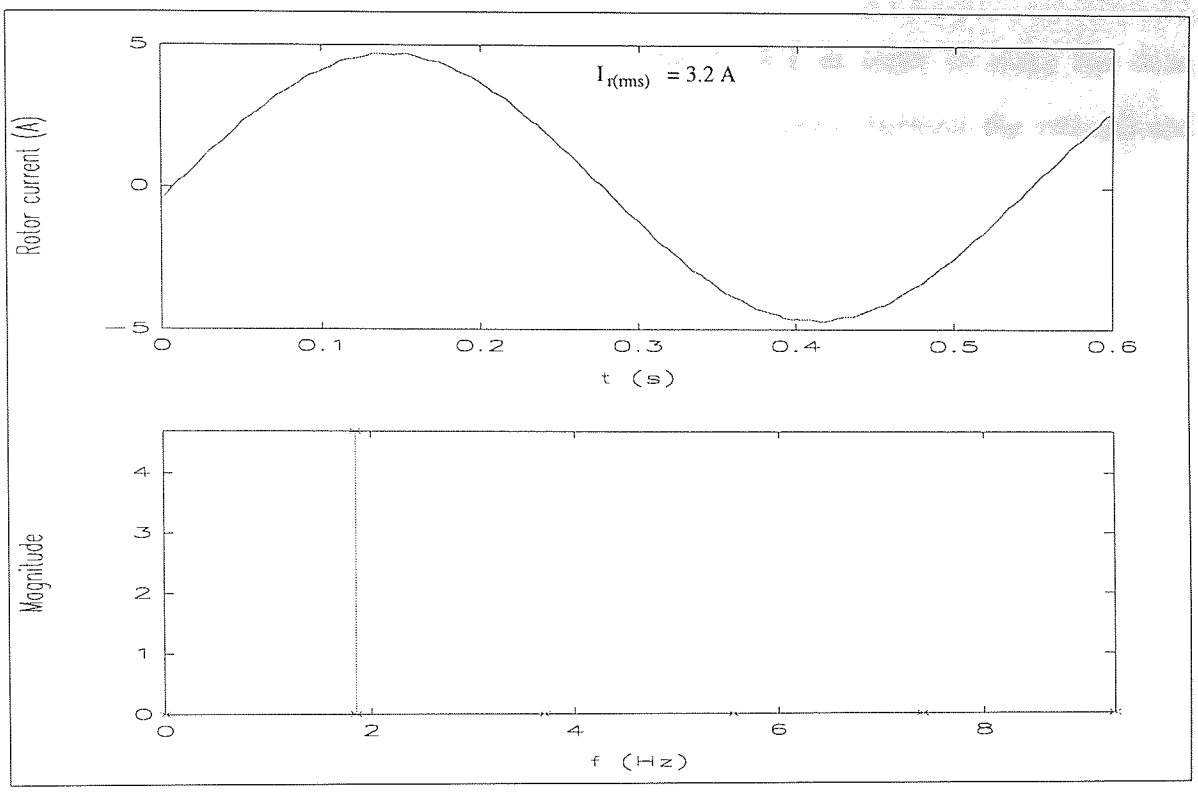

Fig. 6.2-6 Simulation result of full-load rotor current of the squirrel-cage induction and its harmonic spectrum.

6.2.1. Computing Input Power

The electrical connection of the test machine is shown in Fig. 6.2.1-1.

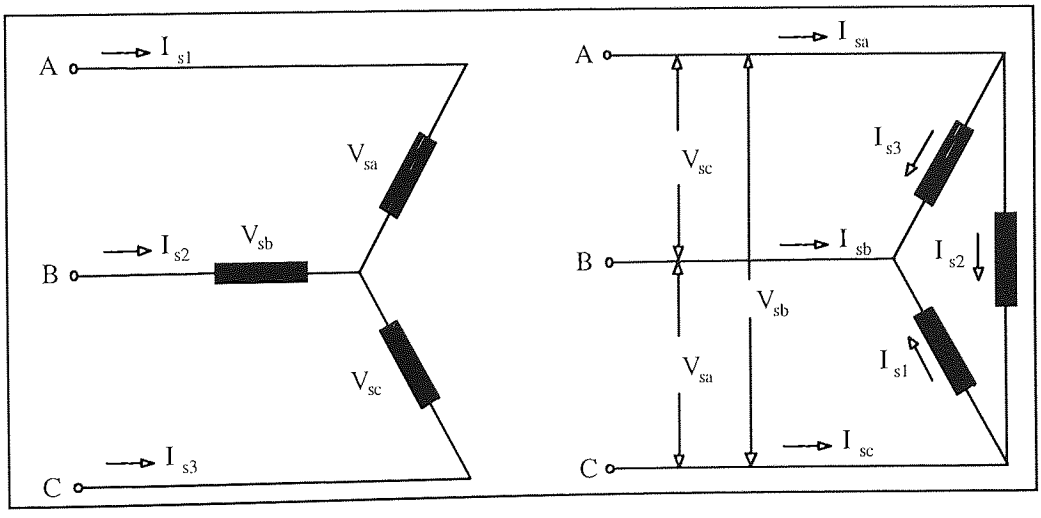

Fig. 6.2.1-1 Star and delta-connections of the machine.

The measurements of the stator line voltage and stator line current from the delta connection were used for the calculation of the instantaneous input power. The star

connection of the machine is also shown in Fig. 6.2.1-1 in order to make the delta connection more understandable. Fig. 6.2.1-2 shows the relations between the voltages and the currents in delta connection.

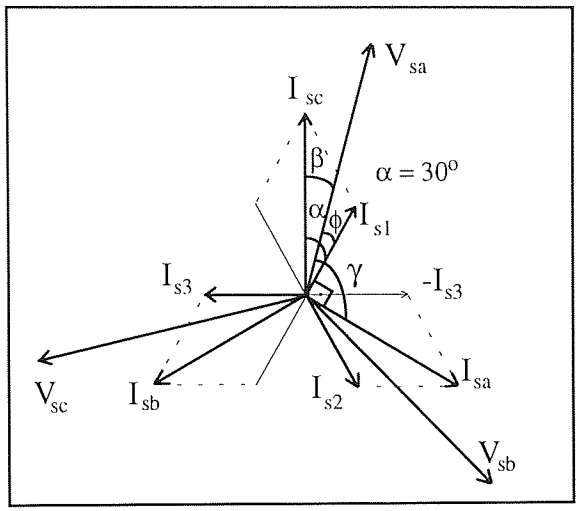

Fig. 6.2.1-2 Vector diagram of the squirrel-cage induction machine.

The instantaneous input power of the machine was calculated according to the two wattmeters method. However, the summation of individual powers of each phase also gives the total instantaneous input power.

Rated input power of the machine is calculated as:.

$$P_{in} = \sqrt{3} V_{sa(rms)} I_{sa(rms)} \cos(\phi) \qquad (6.2.1\text{-}1)$$

The power factor, cos(ϕ), is the cosine of the angle between the stator line voltage and line current when the machine is running under the full-load conditions as explained above. Fig. 6.2.1-3 shows the angle between the full-load line voltage and the line current. In this figure, the line current has been magnified by 50 times in order to show the angle between voltage and current clearly.

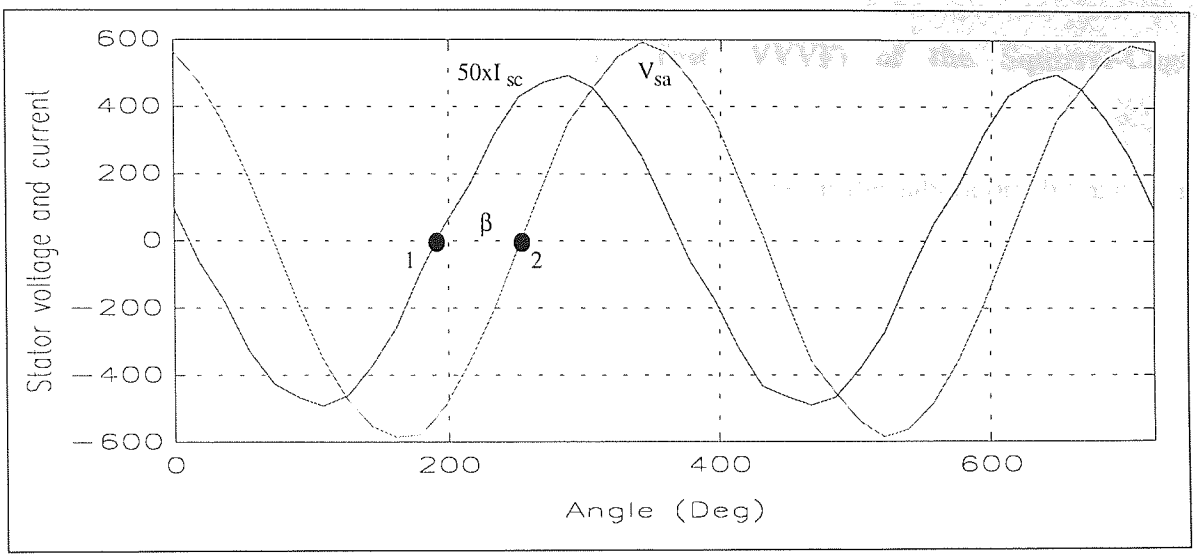

Fig. 6.2.1-3 Illustration of the angle, β, of the squirrel-cage induction machine.

The angle, β, between point 1 and point 2 in Fig. 6.2.1-3 was found to be 57°. If $\beta = 57°$ and $\alpha = 30°$ then, the angle (ϕ) between phase voltage (V_{sa}) and phase current (I_{s1}) can be calculated from Fig. 6.2.1-2 as -27° with respect to $-I_3$.

Since the power factor ($\cos(\phi)$), the rms line voltage (V_{sa}) and the rms line current (I_{sc}) are known, the input power of the induction machine is calculated as 4611.28 W.

The output power is calculated by multiplying the measured angular rotor speed (302.6 Rad/s) with measured torque (13.2 Nm) as:

$$P_{out} = \omega_r T_L = (302.6)(13.2) = 3994.32 \text{ Watts.}$$

The efficiency of the machine is defined:

$$\eta = \frac{P_{out}}{P_{in}} = \frac{3994.32}{4611.28} = 86.62\ \% \qquad (6.2.1\text{-}3)$$

This figure shows that the test machine has losses of 616.96 Watts when it is running under full-load. A breakdown of these losses is given later in this chapter.

6.3. Varying-Voltage, Varying-Frequency Test (VVVF) of the Squirrel-Cage Induction Machine

The VVVF test was carried out using the inverter available in the laboratory by applying sinusoidal speed demand signals from an arbitrary waveform generator to the inverter's external analogue speed demand terminals. The frequency of the speed demand was varied from 2.0 Hz to 15 Hz. In every case, the sinusoidal speed demand had two components, amplitude and DC offset, and sum of these components is limited to 10.4 Volts by the arbitrary waveform generator.

fb (Hz)	Amplitude (V)	DC Offset (V)	Windings °C	Airgap °C	Core °C	End Windings °C	Rotor °C
2	2.92	7.48	57	71	38	63	81
3	2.06	8.34	57	71	37	64	81
4	1.64	8.76	57	72	37	65	81
5	1.40	9.00	57	71	37	65	81
6	1.12	9.28	57	72	37	64	81
7	0.92	9.48	57	72	38	64	81
8	0.74	9.66	57	71	37	64	81
9	0.68	9.72	57	71	38	64	81
10	0.66	9.74	57	71	38	64	81
11	0.60	9.80	57	71	38	64	81
12	0.54	9.86	57	71	38	64	81
13	0.46	9.94	57	71	37	64	81
14	0.44	9.96	57	70	36	64	81
15	0.40	10.0	57	70	36	64	81
Full-load temperature rises			**57**	**70**	**32**	**66**	**81**

Table 6.3-1 Data for VVVF test of the squirrel-cage induction machine.

When the speed demand is 10 Volts DC, the output frequency of voltage of the inverter is equal to 50 Hz which causes the rotor to run at rated speed. As the test motor (4 kW induction machine) was drawing the rated rms stator current of 7.2A from the supply at the rated winding temperature rise of 57 °C, the temperature rises at various points within the motor were recorded as well as the stator voltage, the stator current, the rotor speed and the instantaneous speed demands at different beat frequencies. Table 6.3-1 shows the speed demands and the temperature rises at different beat frequencies for the VVVF test of the induction motor.

Variation of the speed demand with respect to the beat frequency is shown in Fig. 6.3-1.

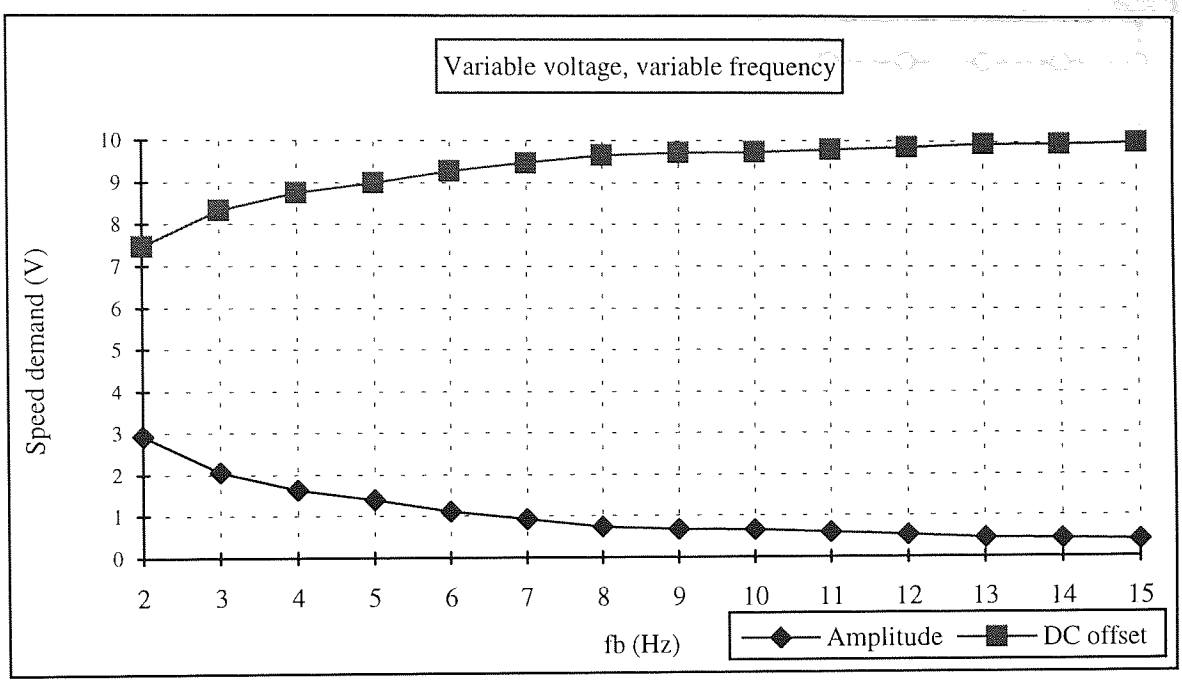

Fig. 6.3-1 Illustration of DC offset and amplitude of speed demand for VVVF test of the squirrel-cage induction machine.

As shown in Fig. 6.3-2, only the winding and the rotor temperature rises are constant at 57 °C and 81 °C respectively during the test, which are the same as for the direct full-load test temperature rises, given in Table 6.3-1. Temperature rises of the airgap are 1 or 2 °C higher than the full-load test temperature rise. Temperature rises of end windings are between 1 and 3 °C less then the full-load result. The VVVF test produces between 4 and 6 °C higher core temperature rises than the full-load core temperature rises as given in Table 6.3.1. This happens due to the low and high frequency harmonic components of the voltage waveform applied to the test machine. The low frequency components appear due to the beat frequency, as the high frequency components appear due to the high switching frequency of the inverter.

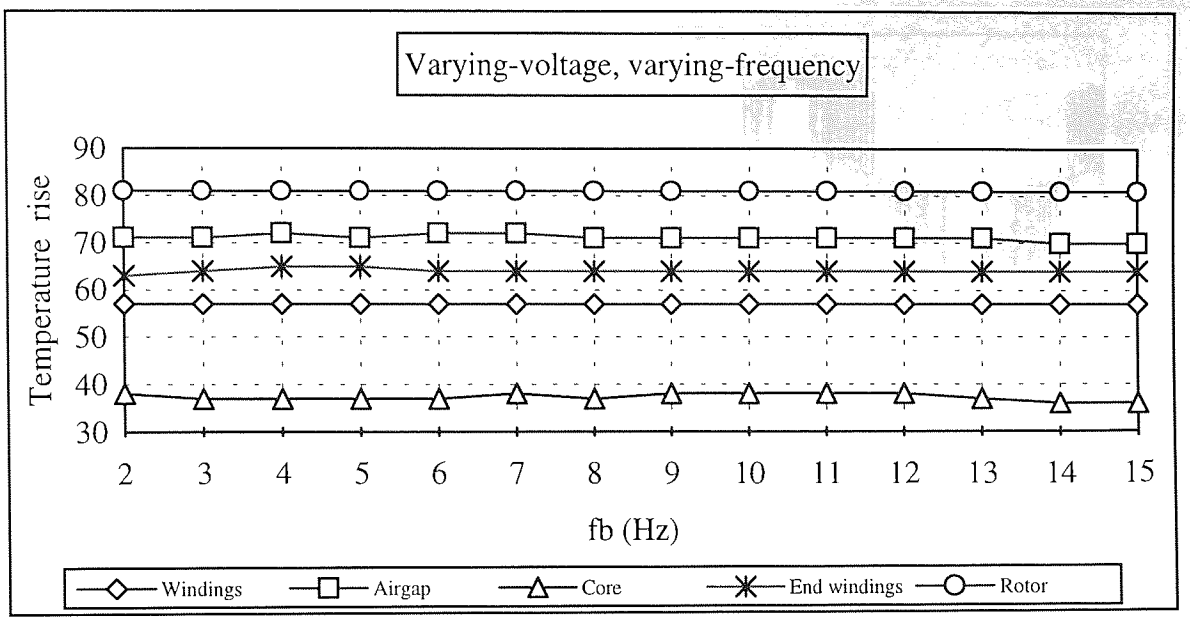

Fig. 6.3-2 Temperature rises of VVVF test of the squirrel-cage induction machine at various beat frequencies.

Output voltage of the inverter and its harmonic spectrum at 10 Hz beat frequency with 3 kHz switching frequency and 40 kHz sampling frequency of VVVF test are shown in Fig. 6.3-3. The frequency and the magnitude of voltage are changing with respect to the beat frequency. The maximum harmonic appears at about 50 Hz. The side band harmonics above and below 50 Hz are between 10% and 42% of the fundamental harmonics.

There are high frequency harmonics at 3 kHz switching frequency, but their magnitudes are about 5% of the fundamental harmonic because the inverter operates in transitional mode between full PWM and six-step. However, the high frequency harmonics can increase the core losses due to their high order.

The low order voltage harmonics of the order 5, 7, 11, and 13 in Fig. 6.3-3 are very small comparing the fundamental harmonic and their effects can be ignored.

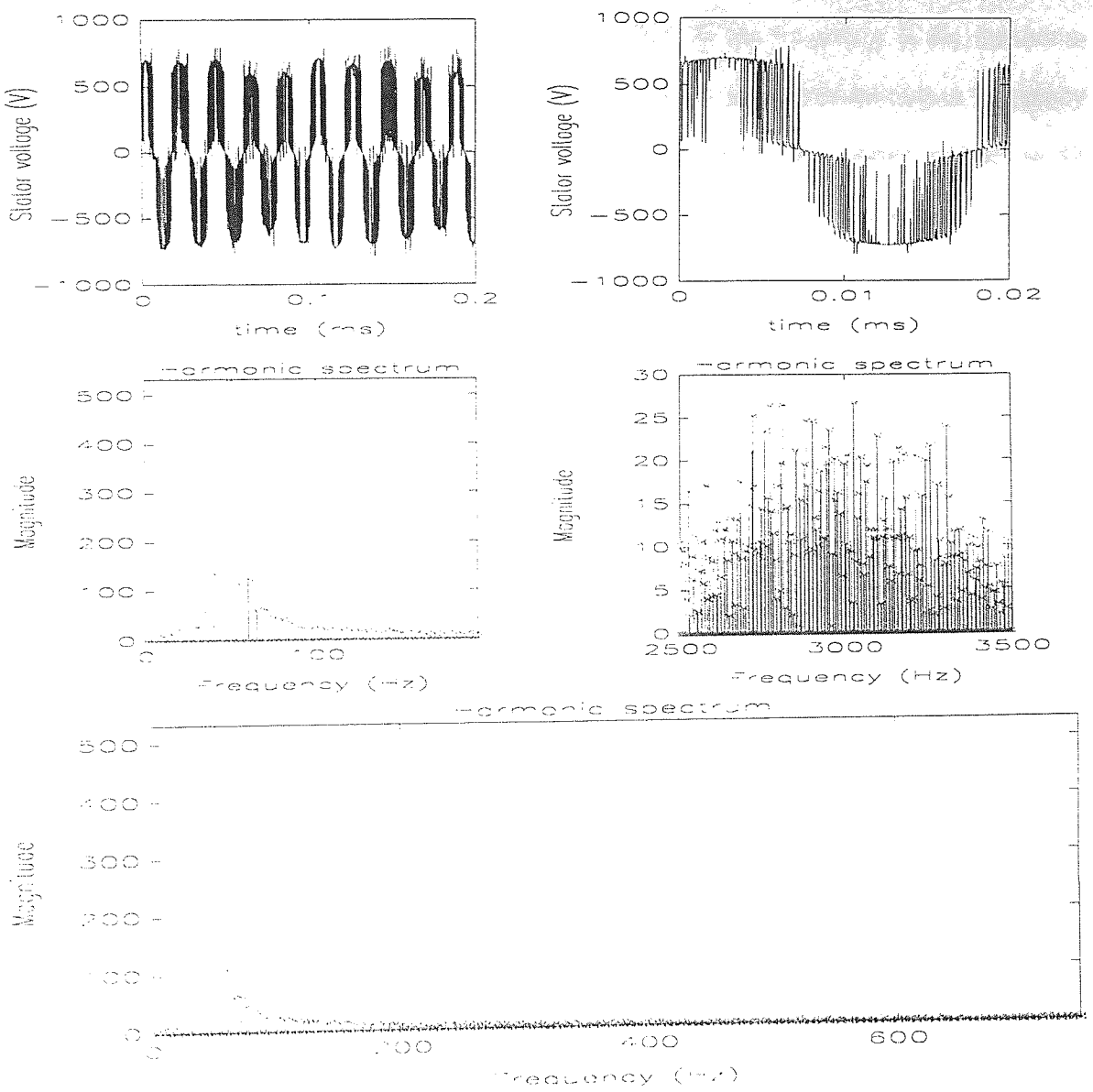

Fig. 6.3-3 Inverter output voltage and its harmonic spectrum of the VVVF test (f_b = 10 Hz, $f_{switching}$ = 3 kHz, $f_{sampling}$ = 40 kHz).

Fig. 6.3-4 shows the filtered stator line voltage and its harmonic spectrum of the VVVF test at 10 Hz beat frequency in where the variation of amplitude and frequency of the stator line voltage can be seen clearly. The rms voltage value was found to be 418.71 V, which is very close to rated voltage value of 415 V. As the beat frequency increases, the amount of variation in peak voltage decreases, as seen in Fig. 6.3-8. It is also clear that the stator line voltage has more than one significant harmonic component as seen in Fig. 6.3-4 although some of the low frequency harmonics appeared above and below 50 Hz in Fig. 6.3-3 have been either reduced in amplitude or disappeared due to the filter. The biggest harmonic

appears at 48 Hz and has a value of 565.3 Volts. This 48 Hz frequency is the maximum possible value for 10 Hz beat frequency of VVVF test since the maximum output frequency of the inverter is set to 48 Hz. There are other significant harmonics above and below 48 Hz. These are sidebands with spacings of 10 Hz due to the 10 Hz beat frequency. Above 58 Hz and below 38 Hz the magnitudes of the harmonics drop to very small values.

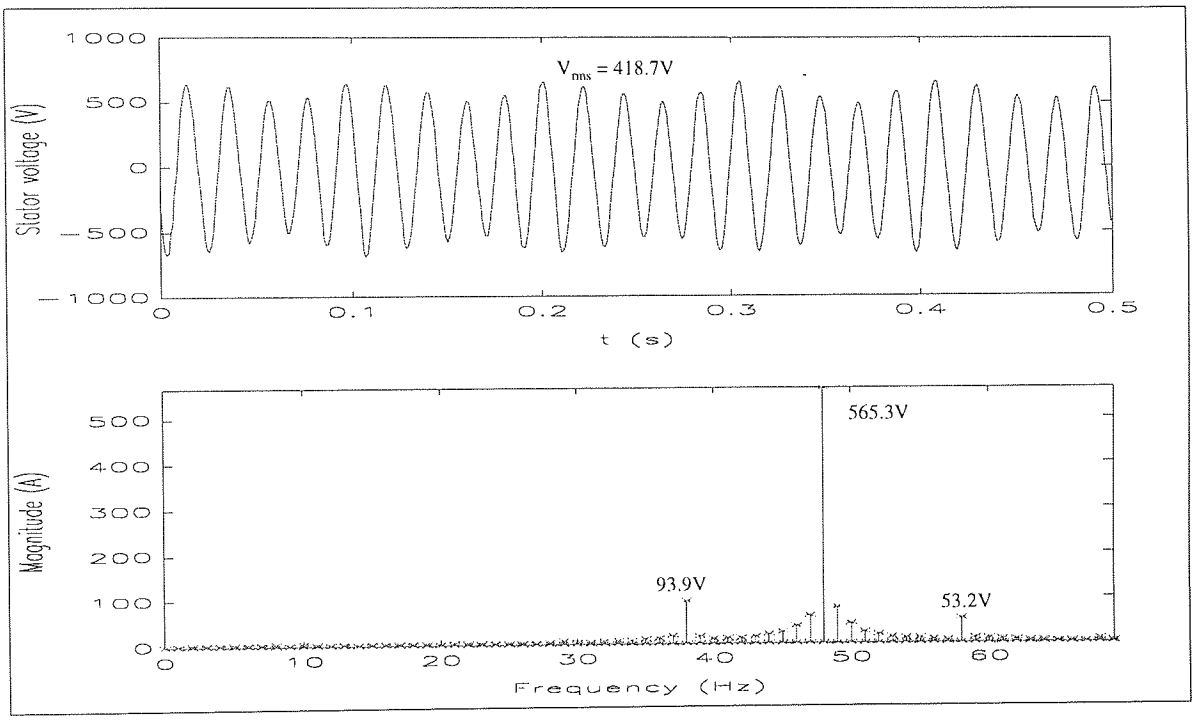

Fig. 6.3-4 Filtered stator line voltage and its harmonic spectrum at 10 Hz beat frequency of VVVF test of the squirrel-cage induction motor.

Fig. 6.3-5 shows the stator line current and its harmonic spectrum. The stator line current waveform has 7.2 A rated rms value and has harmonics almost at every 1 Hz, but the significant harmonics appear as sidebands around 48 Hz with 10 Hz steps between them. The maximum harmonic of the stator line current again appears at 48 Hz as a value of 5.7 Amperes, as does the maximum voltage harmonic.

The waveforms of the rotor speed and its harmonic spectrum are given in Fig. 6.3-6 for 10 Hz beat frequency with a mean speed value of 306.88 Rad/s. The measurement of the speed is described in appendix 5.

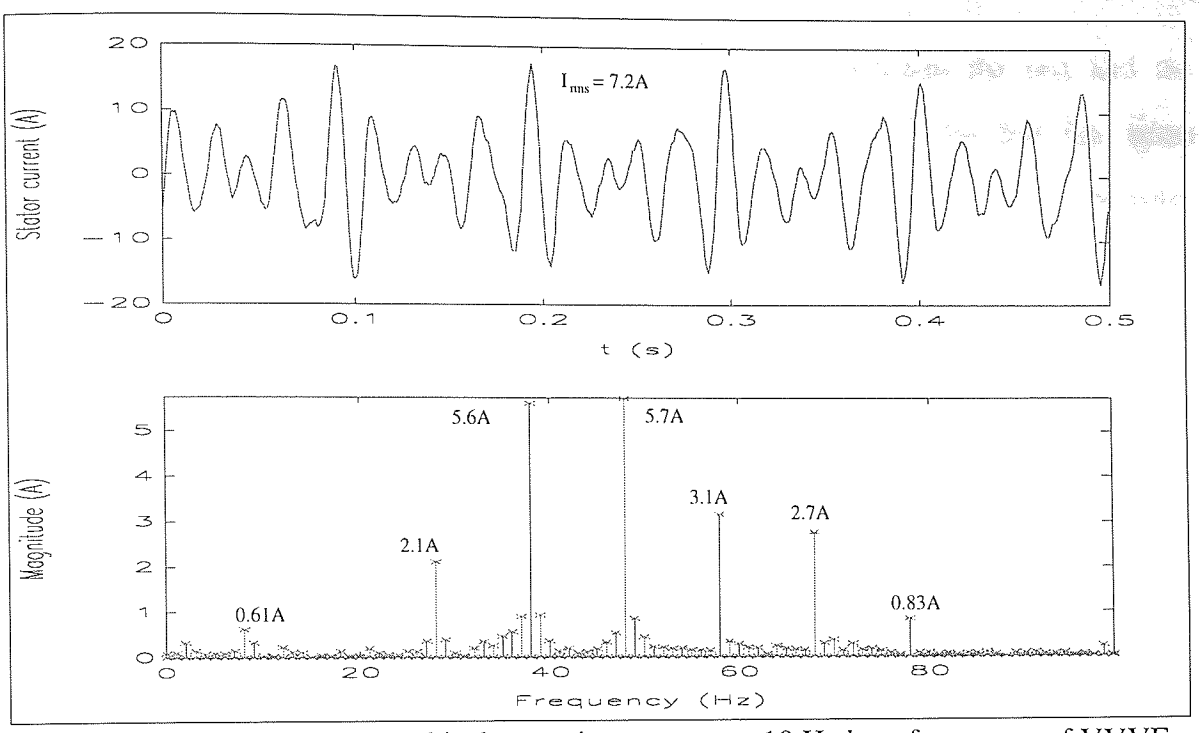

Fig. 6.3-5 Stator line current and its harmonic spectrum at 10 Hz beat frequency of VVVF test of the squirrel-cage induction motor.

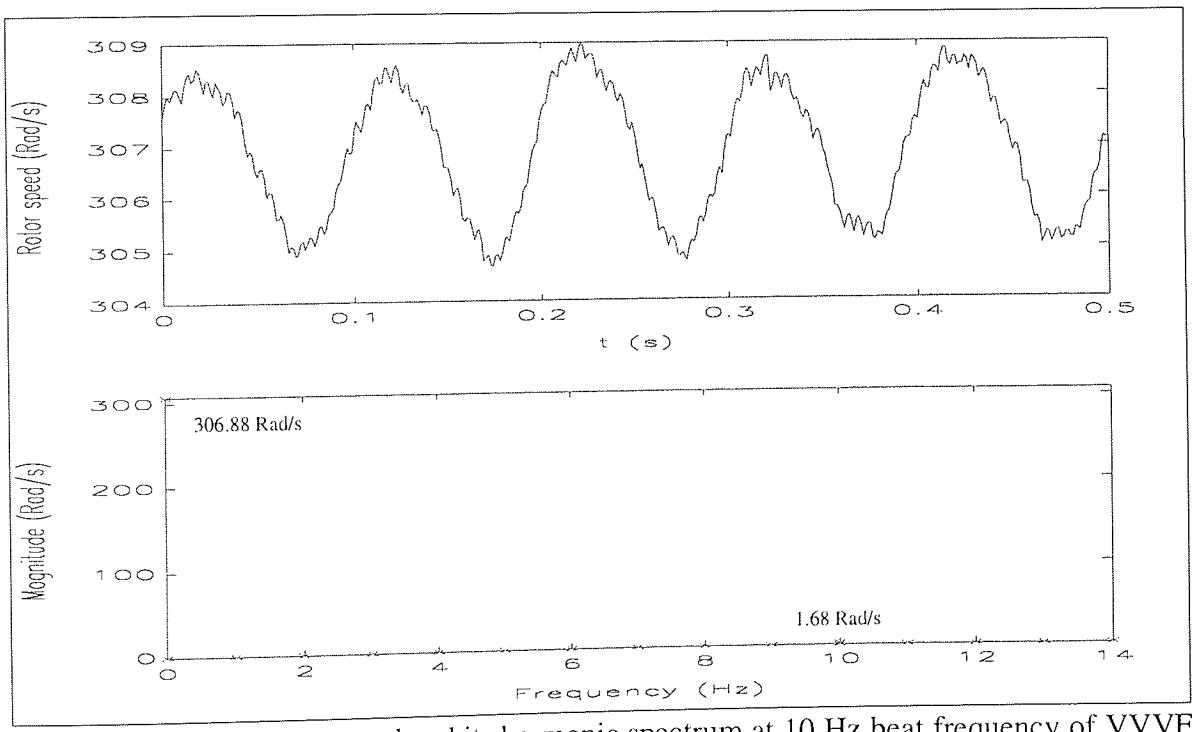

Fig. 6.3-6 Filtered rotor speed and its harmonic spectrum at 10 Hz beat frequency of VVVF test of the squirrel-cage induction motor.

Fig. 6.3-7 shows the comparison of the test and the simulation results of the stator current and the rotor speed of varying-voltage varying-frequency test at 10 Hz beat frequency. The right hand side of the figure shows the simulation results, the left hand side shows the test

results. This figure shows that there is a good agreement between the test and the simulation results. However, the speed waveform obtained from the test has some pulsations due to the tachometer used to measure the speed. Normally, the tachometer produces symmetrical pulses as given in Fig. A.4.1, but there is an RC circuit at the output of the tachometer, so that the RC circuit charges and discharges the capacitor and produces the speed waveform.

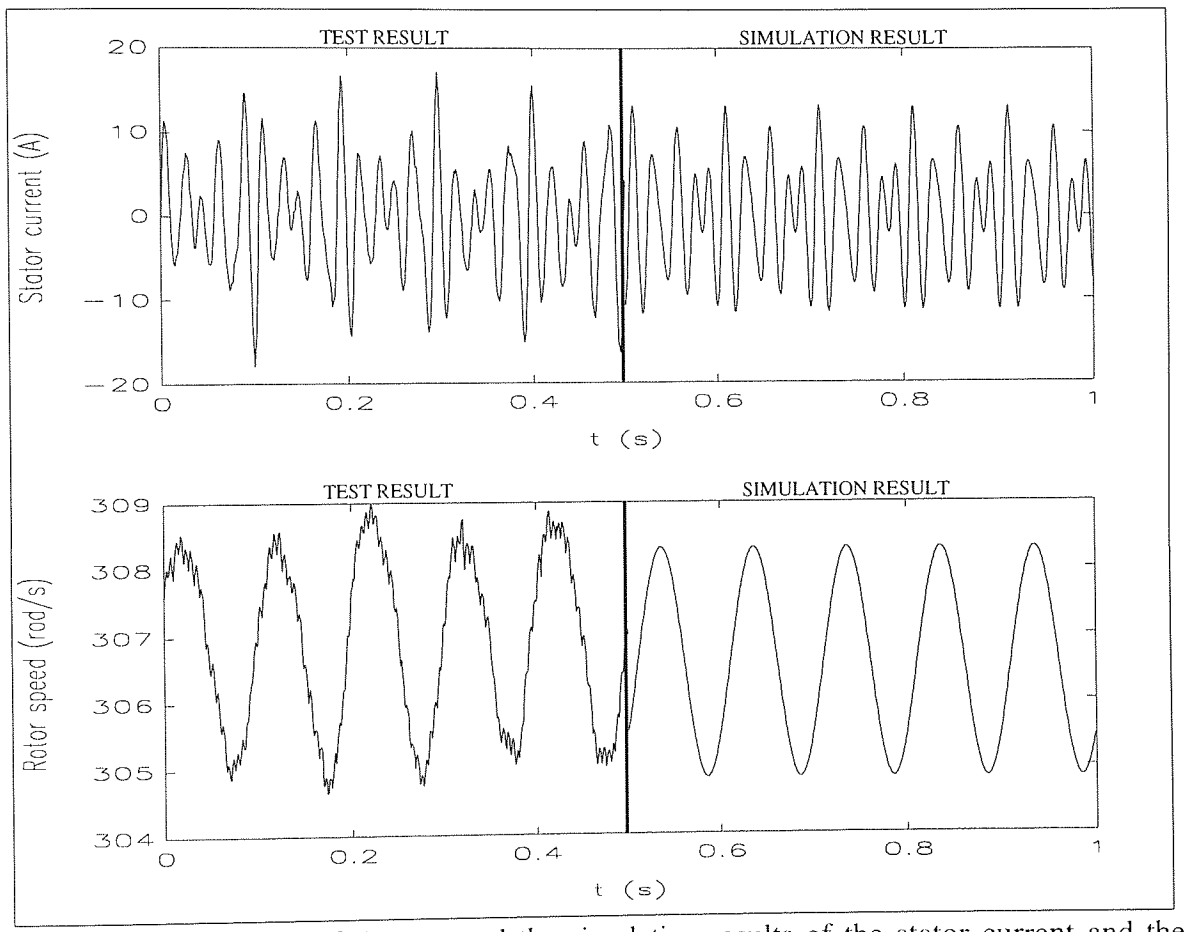

Fig. 6.3-7 Comparison of the test and the simulation results of the stator current and the rotor speed at 10 Hz beat frequency of VVVF test of the squirrel-cage induction motor.

Fig.'s 6.3-8, 6.3-9, 6.3-10 and 6.3-11 show waveforms of the filtered stator voltage, the stator current, the filtered rotor speed and the speed demand at various beat frequencies respectively. These figures show the variation in amplitude and frequency of stator voltage, stator current, rotor speed and speed demand.

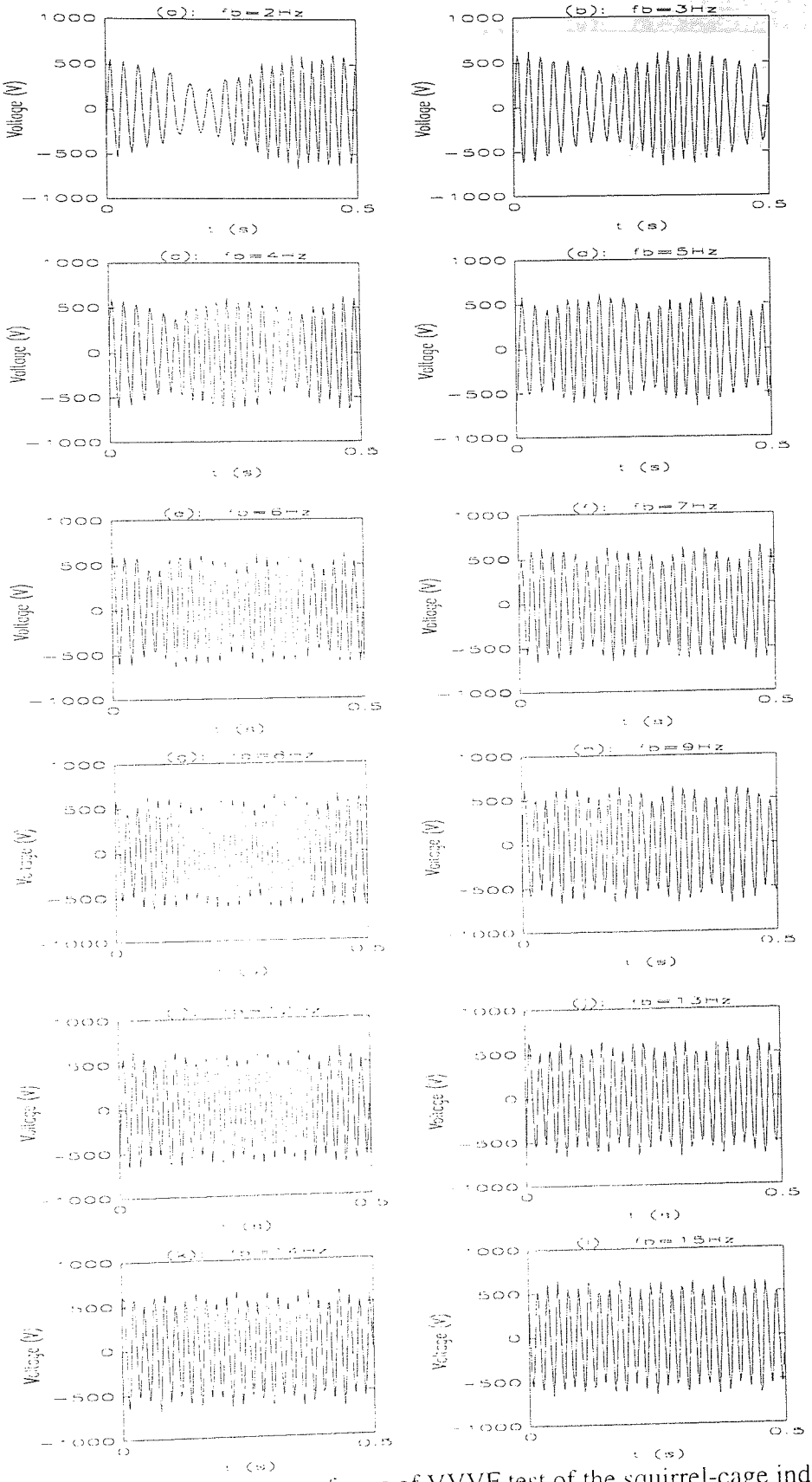

Fig. 6.3-8 Filtered stator voltage waveforms of VVVF test of the squirrel-cage induction machine at different beat frequencies.

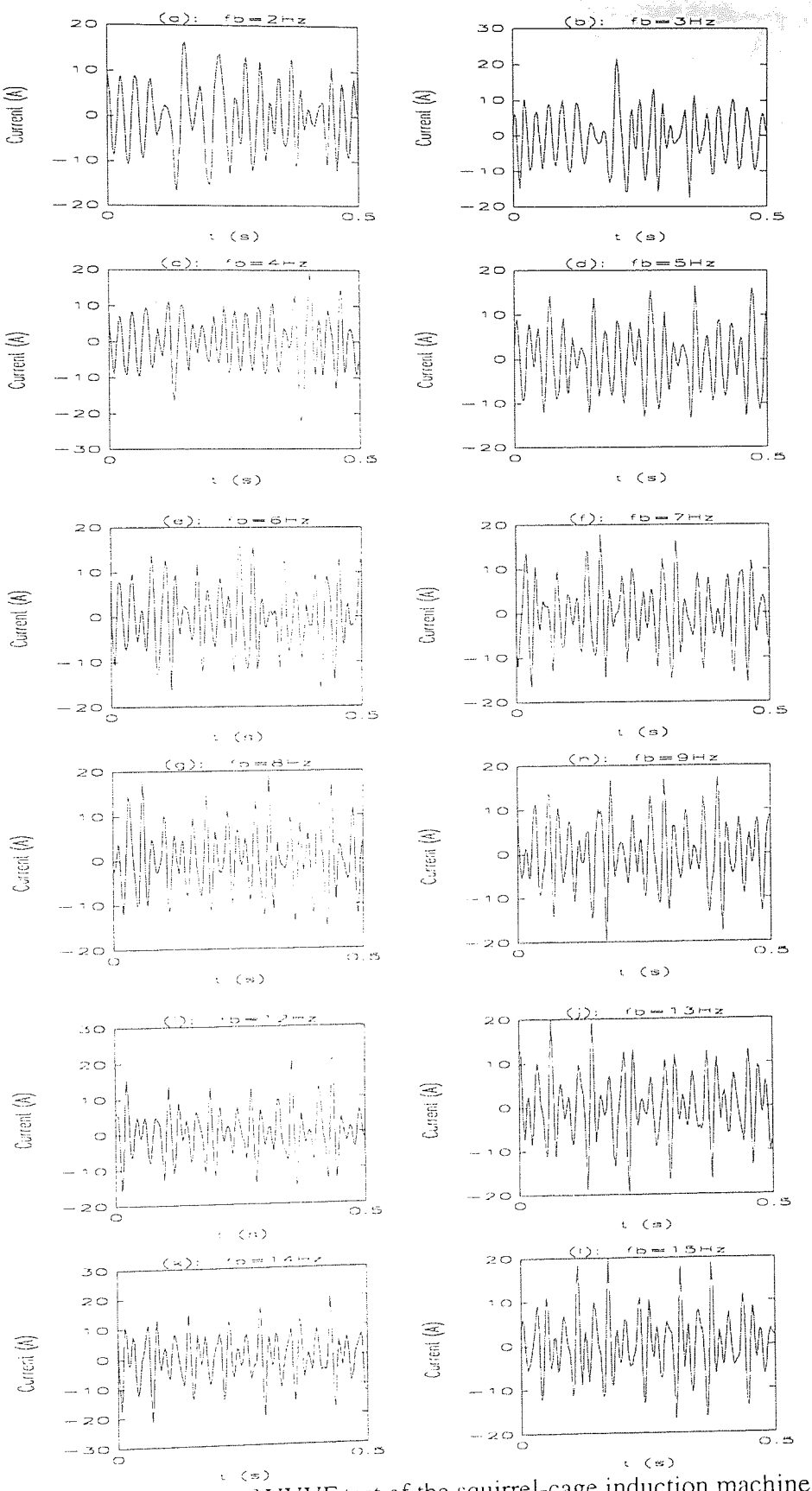

Fig. 6.3-9 Current waveforms of VVVF test of the squirrel-cage induction machine at different beat frequencies.

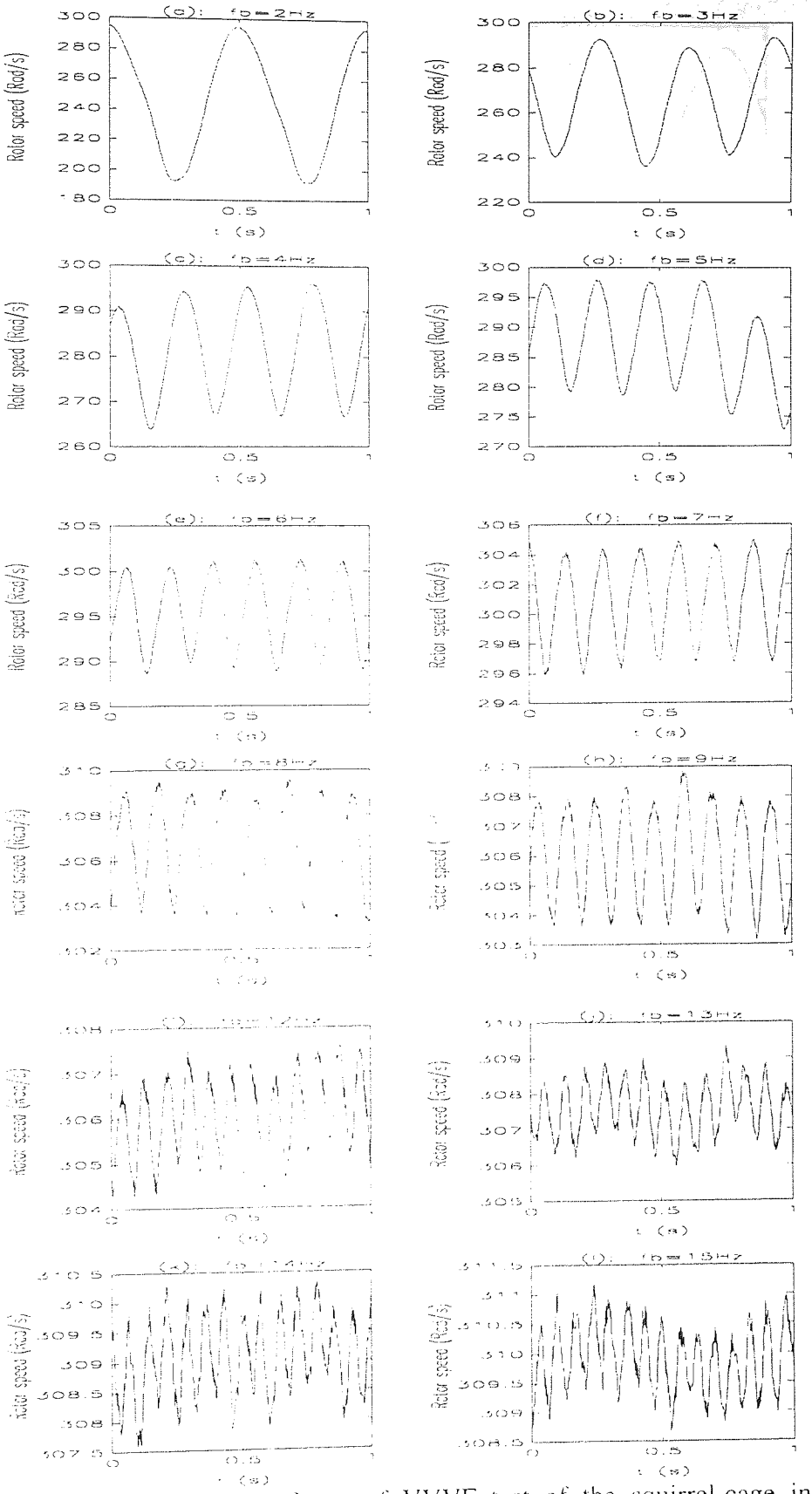

Fig. 6.3-10 Filtered speed waveforms of VVVF test of the squirrel-cage induction machine at different beat frequencies.

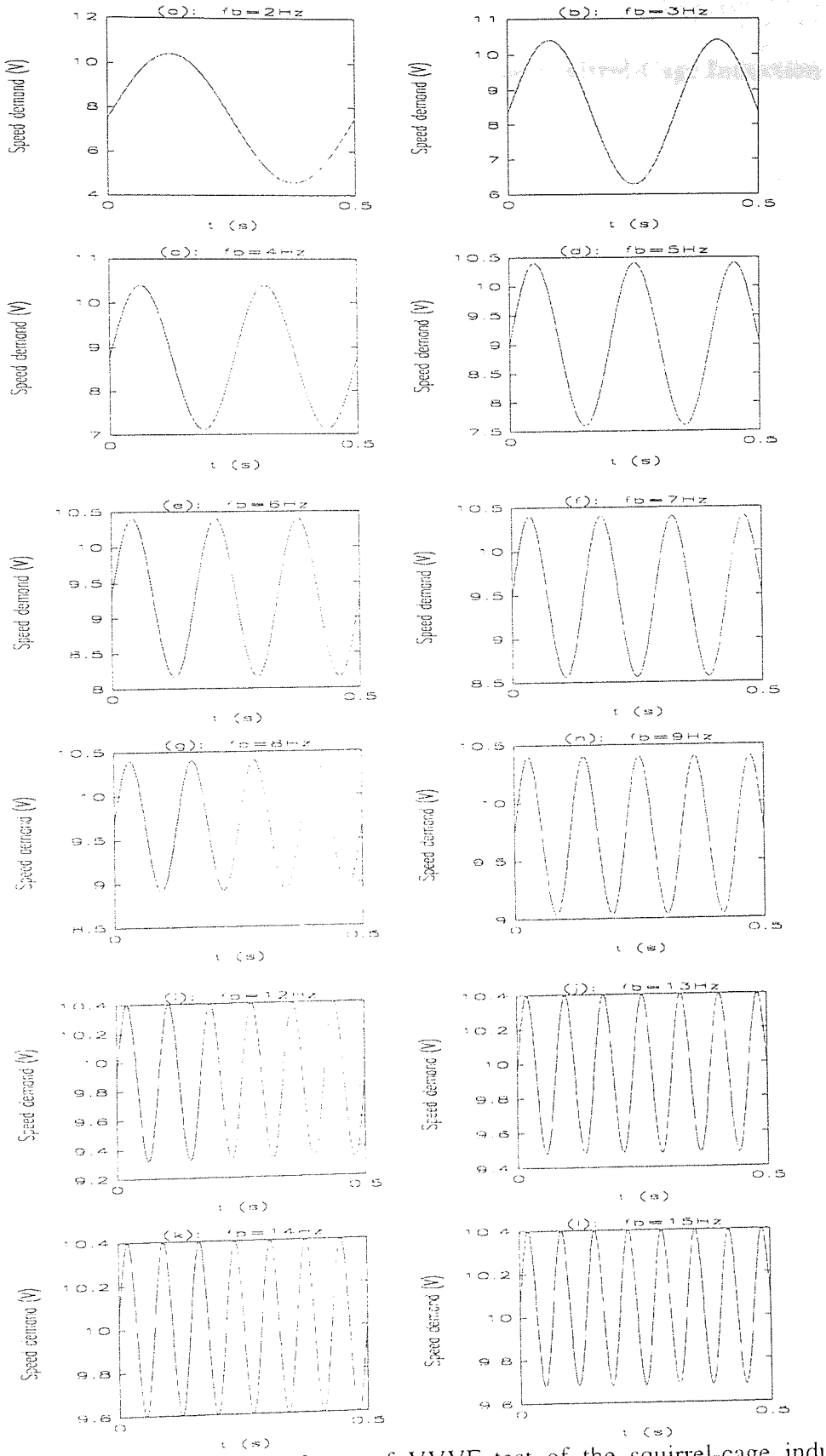

Fig. 6.3-11 Speed demand waveforms of VVVF test of the squirrel-cage induction machine at different beat frequencies.

6.4. Varying-Voltage, Varying-Frequency Test of the Squirrel-Cage Induction Machine With Increased Inertia

In this section, the effects of the increased inertia on the VVVF test are pointed out. The inertia was increased 3.21 times of the normal inertia of 0.0181 kgm^2 by adding extra weights to the rotor shaft. The VVVF test was then repeated on the machine. The increased inertia allowed the test to start at 1 Hz beat frequency. The variations of the speed demand and the rotor speed of the increased inertia test are similar to the normal inertia test. Fig. 6.4-1 illustrates the variation of speed demand at various beat frequencies.

fb (Hz)	Amplitude (V)	DC Offset (V)	Windings °C	Airgap °C	Core °C	End Windings °C	Rotor °C
1.0	4.20	6.20	57.0	70.0	35.0	64.0	70.0
2.0	2.60	7.80	57.0	71.0	37.0	65.0	70.0
3.0	1.74	8.66	57.0	71.0	38.0	65.0	70.0
4.0	1.26	9.14	57.0	71.0	38.0	65.0	76.0
5.0	1.00	9.40	57.0	71.0	38.0	65.0	76.0
6.0	0.78	9.62	57.0	71.0	38.0	65.0	76.0
7.0	0.66	9.74	57.0	71.0	38.0	65.0	81.0
8.0	0.62	9.78	57.0	71.0	38.0	64.0	81.0
9.0	0.56	9.84	57.0	72.0	38.0	65.0	81.0
10.0	0.52	9.88	57.0	71.0	37.0	65.0	81.0
11.0	0.48	9.92	57.0	71.0	37.0	65.0	81.0
12.0	0.46	9.94	57.0	71.0	37.0	64.0	81.0
13.0	0.44	9.96	57.0	71.0	37.0	64.0	81.0
14.0	0.50	9.90	57.0	71.0	37.0	65.0	81.0
15.0	0.58	9.82	57.0	71.0	37.0	64.0	81.0
Full-load temperature rises			**57.0**	**70.0**	**32.0**	**66.0**	**81.0**

Table 6.4-1 Data for VVVF increased inertia test of the squirrel-cage induction machine.

Fig. 6.4-2 shows that the variations of the temperature rise at various points within the machine during the VVVF increased inertia test are fairly constant, except for the rotor temperature. At low frequencies, up to 7 Hz of beat frequency, the rotor temperature was measured to be variable. It was found as 70 °C between 1 Hz and 3 Hz of beat frequency and 76 °C between 4 Hz and 6 Hz of beat frequency. After 6 Hz the rotor temperature rise was constant at 81 °C. So that the increased inertia test at low frequencies does not produce the rated rotor temperature rise as the normal inertia test does. All the other temperature

rises of this test are very close to the direct full-load temperature rises as shown in Table 6.4-1.

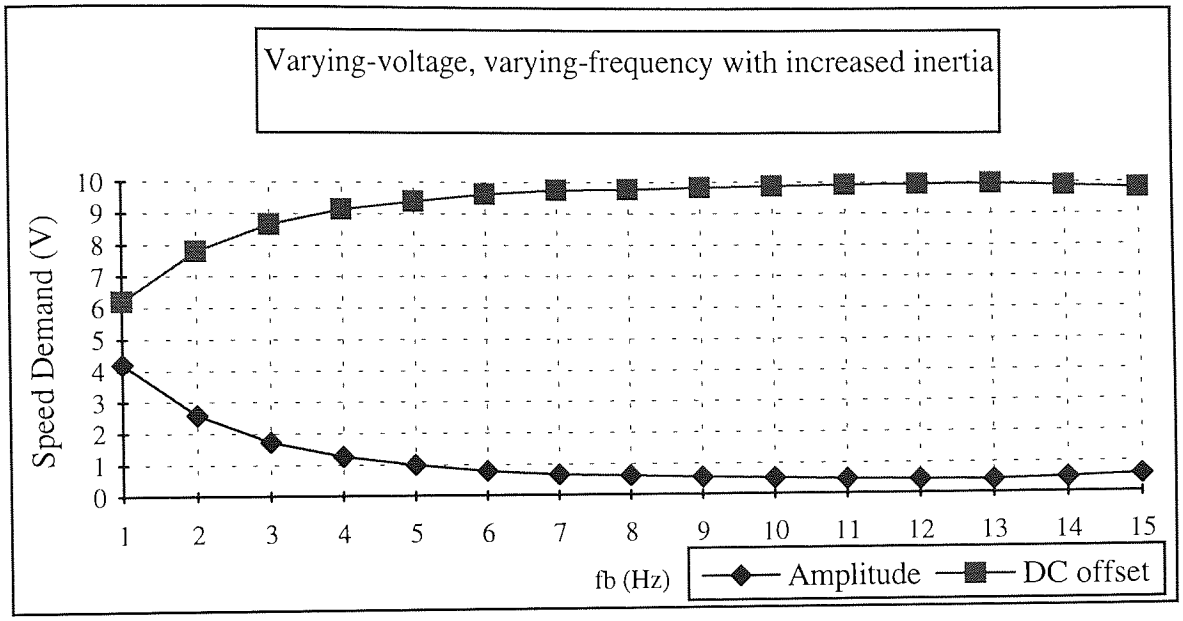

Fig. 6.4-1 Variation of DC offset and amplitude of speed demand for VVVF increased inertia test of the squirrel-cage induction machine.

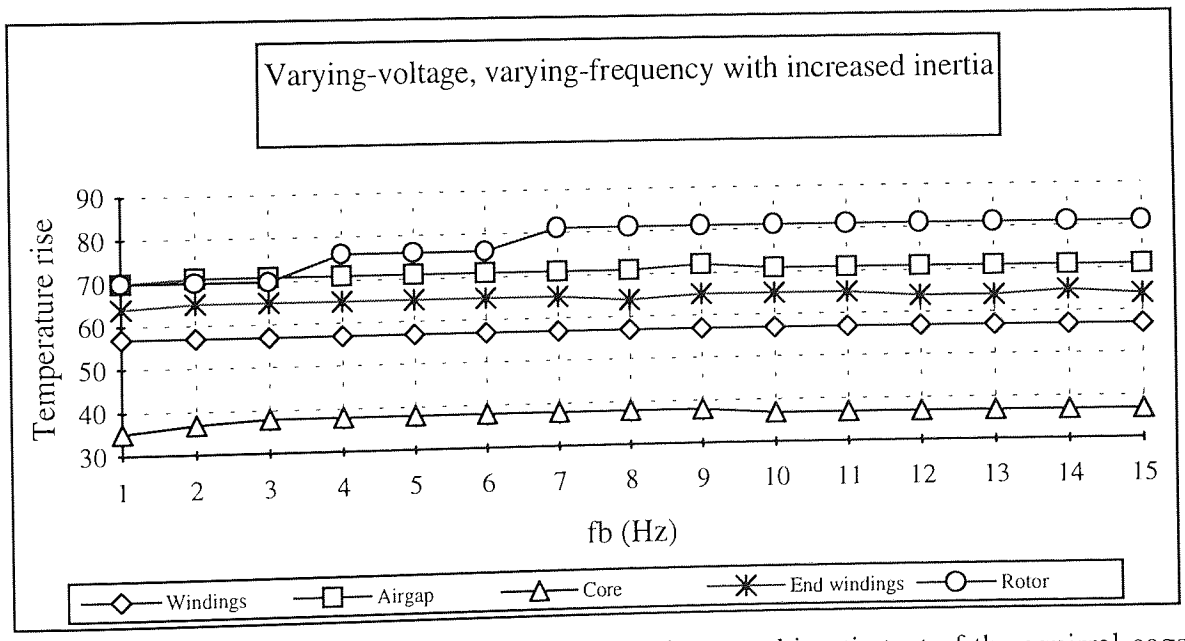

Fig. 6.4-2 Variation of temperature rises of VVVF increased inertia test of the squirrel-cage induction machine.

The filtered stator line voltages, stator line currents and filtered rotor speeds at different beat frequencies are given in Fig. 6.4-3, Fig. 6.4-4 and Fig. 6.4-5 respectively.

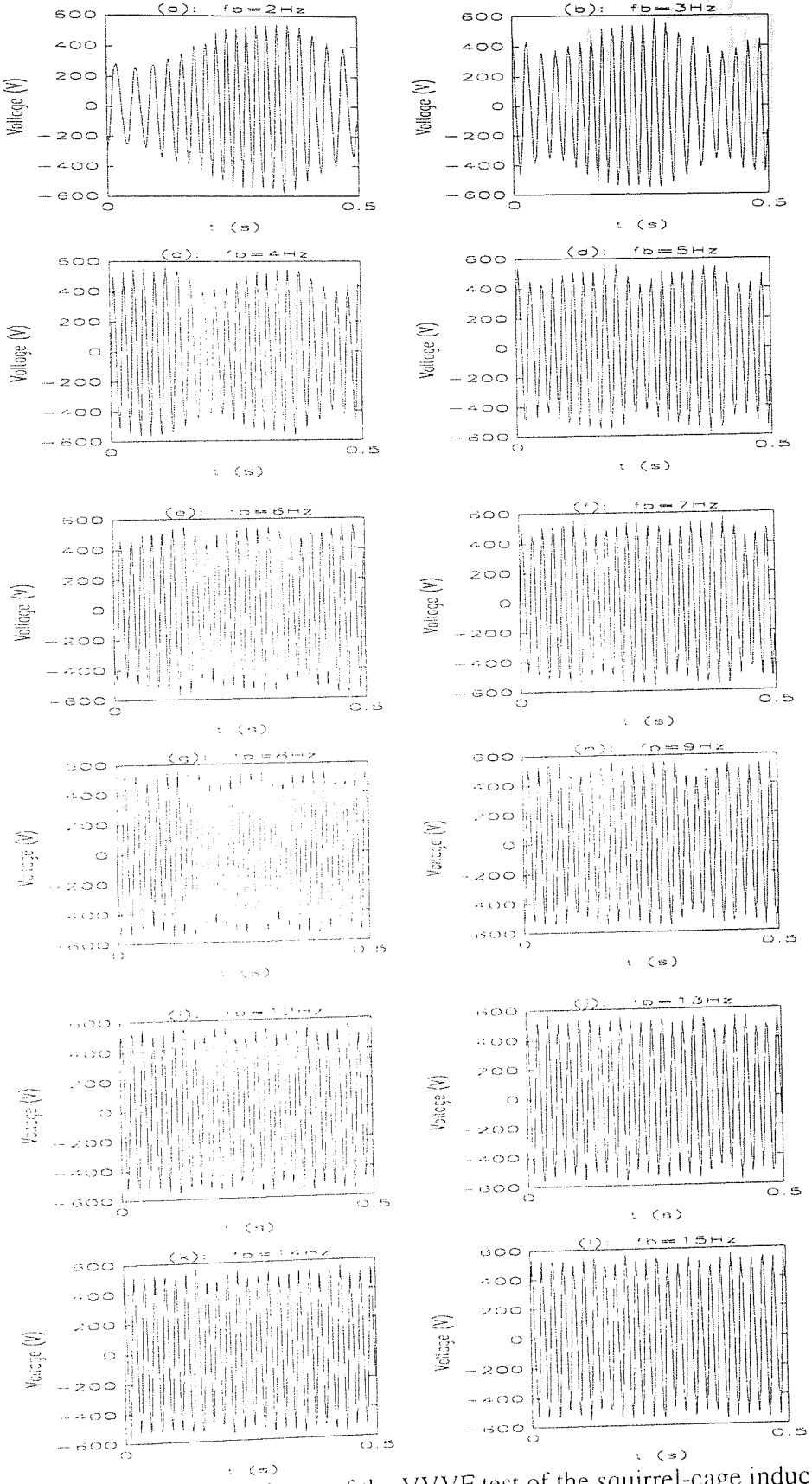

Fig. 6.4-3 Filtered voltage waveforms of the VVVF test of the squirrel-cage induction motor with increased inertia at various beat frequencies.

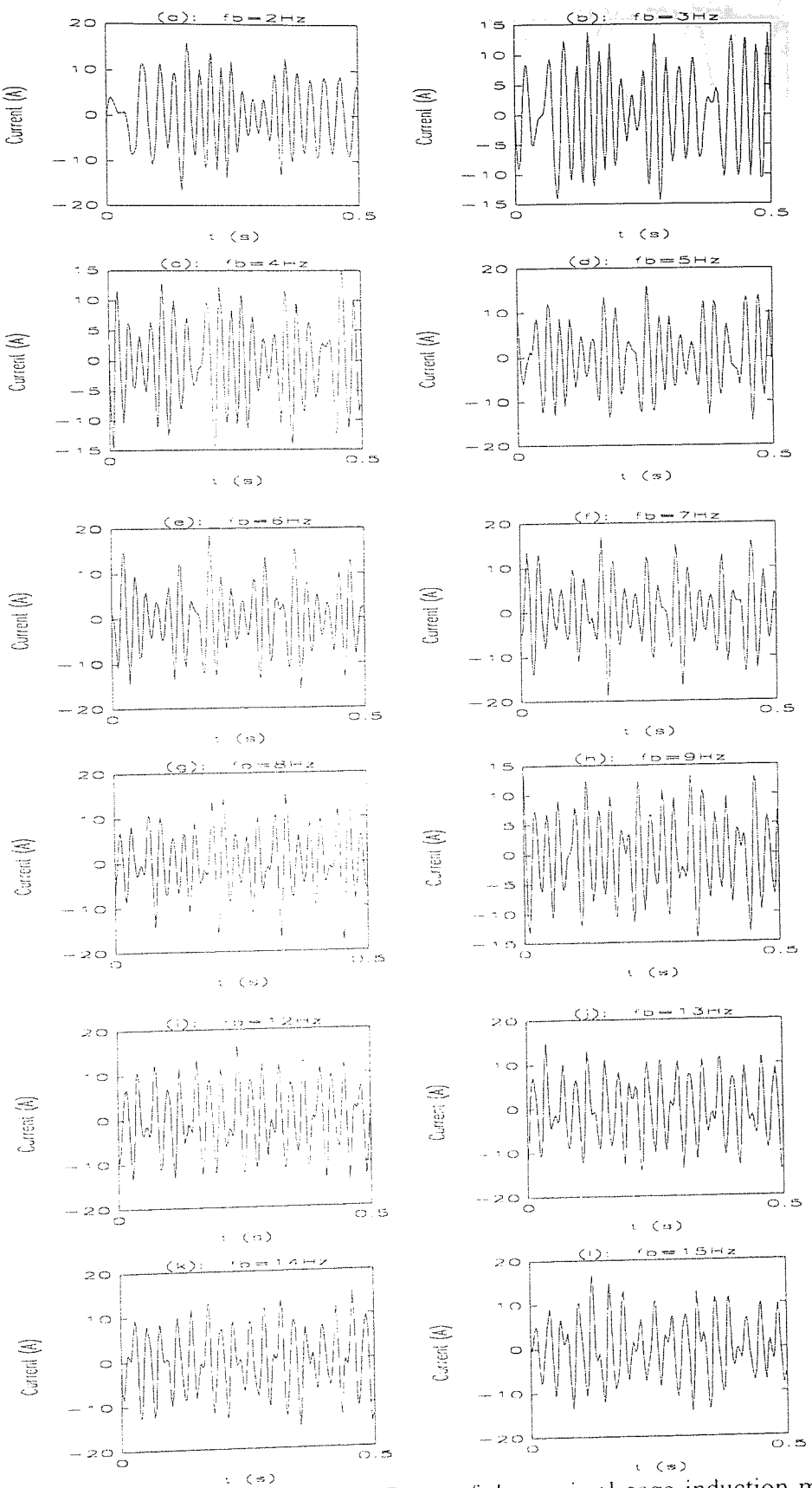

Fig. 6.4-4 Current waveforms of the VVVF test of the squirrel-cage induction motor with increased inertia at various beat frequencies.

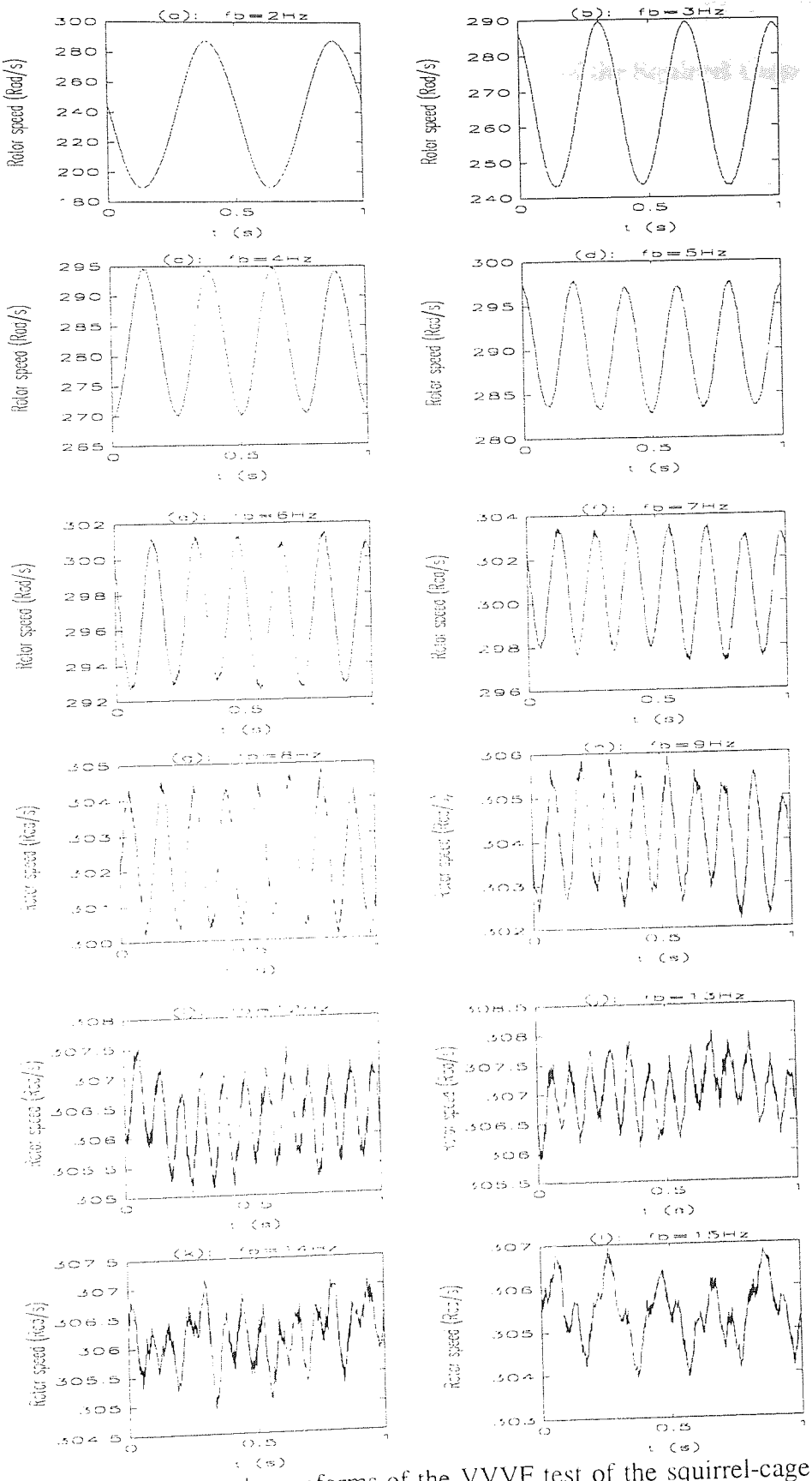

Fig. 6.4-5 Filtered rotor speed waveforms of the VVVF test of the squirrel-cage induction motor with increased inertia at various beat frequencies.

6.5. Constant-Voltage, Varying-Frequency (CVVF) Test of the Squirrel Cage Induction Machine

In this section the constant-voltage varying-frequency (CVVF) testing of a 4 kW squirrel-cage induction motor is examined in detail. An inverter is used as a power supply which is able to provide constant-voltage varying-frequency output as shown in Fig. 6.5-1 since its "base frequency" is set to a very small value of 20 Hz.

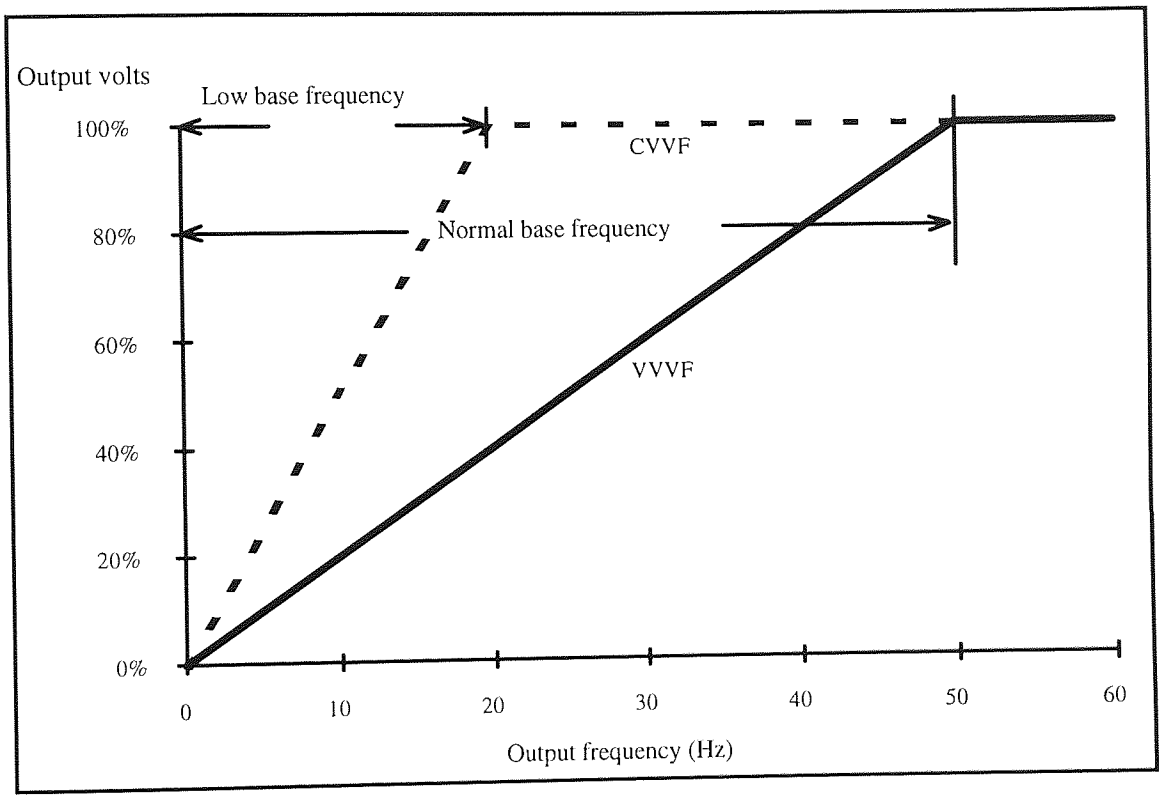

Fig. 6.5-1 Voltage-frequency relationship of the inverter.

The test was carried out at different beat frequencies, from 2 Hz to 15 Hz, at each beat frequency voltage, current, speed and speed demand, as well as the temperature rises from various points (windings, airgap, core, end windings and rotor) within the machine were recorded. It should be noted that, the rms stator current (read by an ammeter) and the winding temperature rise were kept constant at their rated values of 7.2A and 57°C respectively.

Data of the speed demand and temperature rises for the CVVF test at different beat frequencies are given in Table 6.5-1.

fb (Hz)	Amplitude (V)	DC Offset (V)	Windings °C	Airgap °C	Core °C	End Windings °C	Rotor °C
2.0	2.00	8.40	57.0	61.0	33.0	71.0	54.0
3.0	1.86	8.54	57.0	61.0	32.0	71.0	54.0
4.0	1.78	8.62	57.0	61.0	32.0	71.0	54.0
5.0	1.60	8.80	57.0	65.0	33.0	68.0	65.0
6.0	1.40	9.00	57.0	65.0	34.0	69.0	70.0
7.0	1.10	9.30	57.0	66.0	34.0	69.0	76.0
8.0	1.08	9.34	57.0	66.0	33.0	68.0	76.0
9.0	1.00	9.40	57.0	67.0	33.0	68.0	76.0
10.0	0.94	9.46	57.0	69.0	33.0	67.0	76.0
11.0	1.30	9.10	57.0	68.0	32.0	69.0	76.0
12.0	1.40	9.00	57.0	69.0	32.0	68.0	76.0
13.0	1.42	8.98	57.0	67.0	32.0	69.0	76.0
14.0	1.04	9.36	57.0	68.0	32.0	69.0	76.0
15.0	0.90	9.50	57.0	67.0	32.0	69.0	76.0
Full-load temperature rises			**57.0**	**70.0**	**32.0**	**66.0**	**81.0**

Table 6.5-1 Data for CVVF test of the squirrel-cage induction machine.

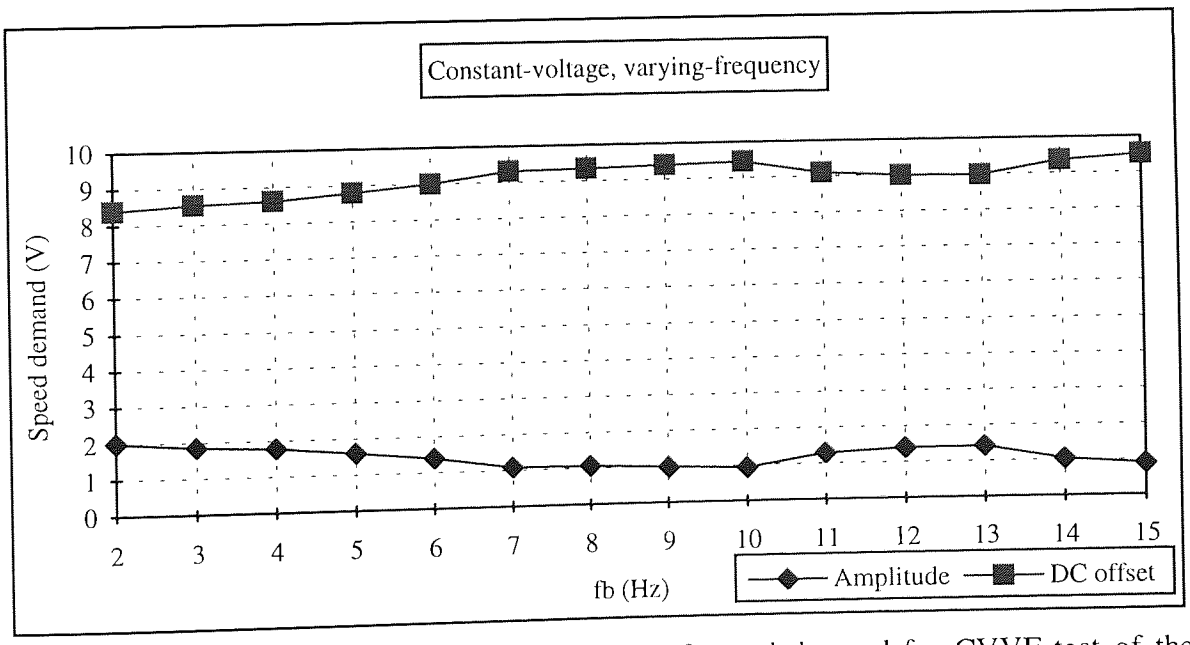

Fig. 6.5-2 Variation of DC offset and amplitude of speed demand for CVVF test of the squirrel-cage induction machine.

The beat frequency was adjusted by adjusting the frequency of the output sinewave (or speed demand waveform) from the arbitrary waveform generator. The sinusoidal speed

demand waveform has two components, DC offset and amplitude as illustrated in Fig. 6.5-2. Moreover, the sum of these two components is limited to 10.4V by the arbitrary waveform generator. There are therefore many different combinations of DC offset and amplitude of the speed demand to draw the rated rms stator current and to obtain the rated winding temperature rise during the test. In order to obtain higher rotor speed the DC offset value of the speed demand was always set to the maximum available value.

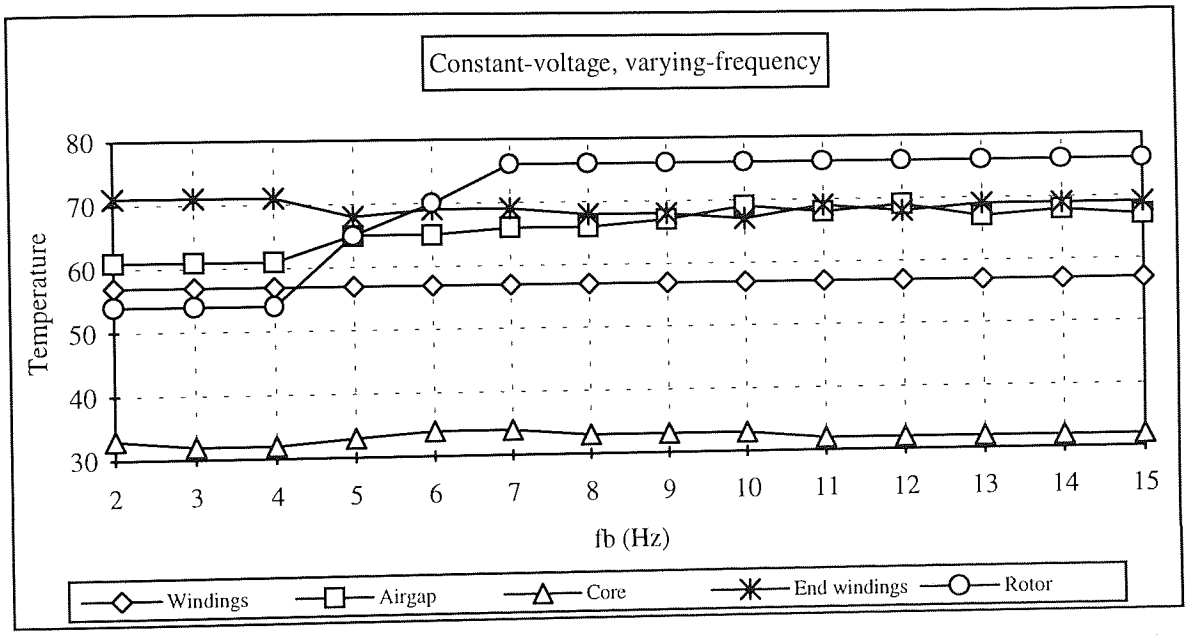

Fig. 6.5-3 Variation of temperature rises of CVVF test of the squirrel-cage induction machine.

The variation of the temperature rises from different points of the motor at various beat frequencies for the CVVF test are illustrated in Fig. 6.5-3. The windings' temperature rise is constant at 57 °C during the test which is the same as the full-load temperature rise of the windings. The airgap temperature rise was found to be less than the full-load value and varied from 61 °C to 69 °C during the test. The temperature rise of the core was found to be close to the full-load value and varied around the rated value of 32 °C during the test. At low beat frequencies, between 2 Hz and 4 Hz, the temperature rise of the end windings was found to be 71 °C, but after that, up to 15 Hz beat frequency, it was found to vary between 67 °C and 69 °C, which is higher than the full-load value. The rotor temperature rise

between 2 Hz and 4 Hz was found to be 54 °C, but after that it was found to be raised up to 76 °C, then remained constant at 76 °C between 7 Hz and 15 Hz beat frequency.

The conclusion of the above comparison is that the CVVF test produces the same temperature rises as the full-load test for the windings and the core, but it produces different temperature rises from the full-load test for the airgap, the end windings and the rotor. In Fig. 5.5-2 in chapter 5, simulation result of the rms rotor current at various beat frequencies was shown as to be rising up below the rated value as the beat frequency increases. This has been proved by the test results given in Table 6.5-1 and Fig. 6.5-3. It should be noted that, in Fig. 5.5-2, the rms rated stator voltage and rms rated stator current were kept constant at every beat frequency, which shows that the temperature rises of winding and core do not change during the test. These have been also proved by the test result as given in Table 6.5-1 and Fig. 6.5-3. Finally it was shown that good agreement between the simulation results and test results has been achieved.

Output voltage of the inverter and its harmonic spectrum at 10 Hz beat frequency with 3 kHz switching frequency and 40 kHz sampling frequency of CVVF test are shown in Fig. 6.5-4. The magnitude of the voltage is not varying with respect to the beat frequency, but the frequency of the voltage changes with respect to the beat frequency.

The maximum harmonic appears at about 50 Hz. The side band harmonics above and below 50 Hz are between 10% and 15% of the fundamental harmonics. There are high frequency harmonics at 3 kHz switching frequency, but their magnitudes are about 5% of the fundamental harmonic because the inverter operates in transitional mode between full PWM and six-step. However, the high frequency harmonics can increase the core losses due to their high order.

The low order voltage harmonics of the order 5, 7, 11, and 13 in Fig. 6.5-4 are very small comparing the fundamental harmonic so that their effects can be ignored.

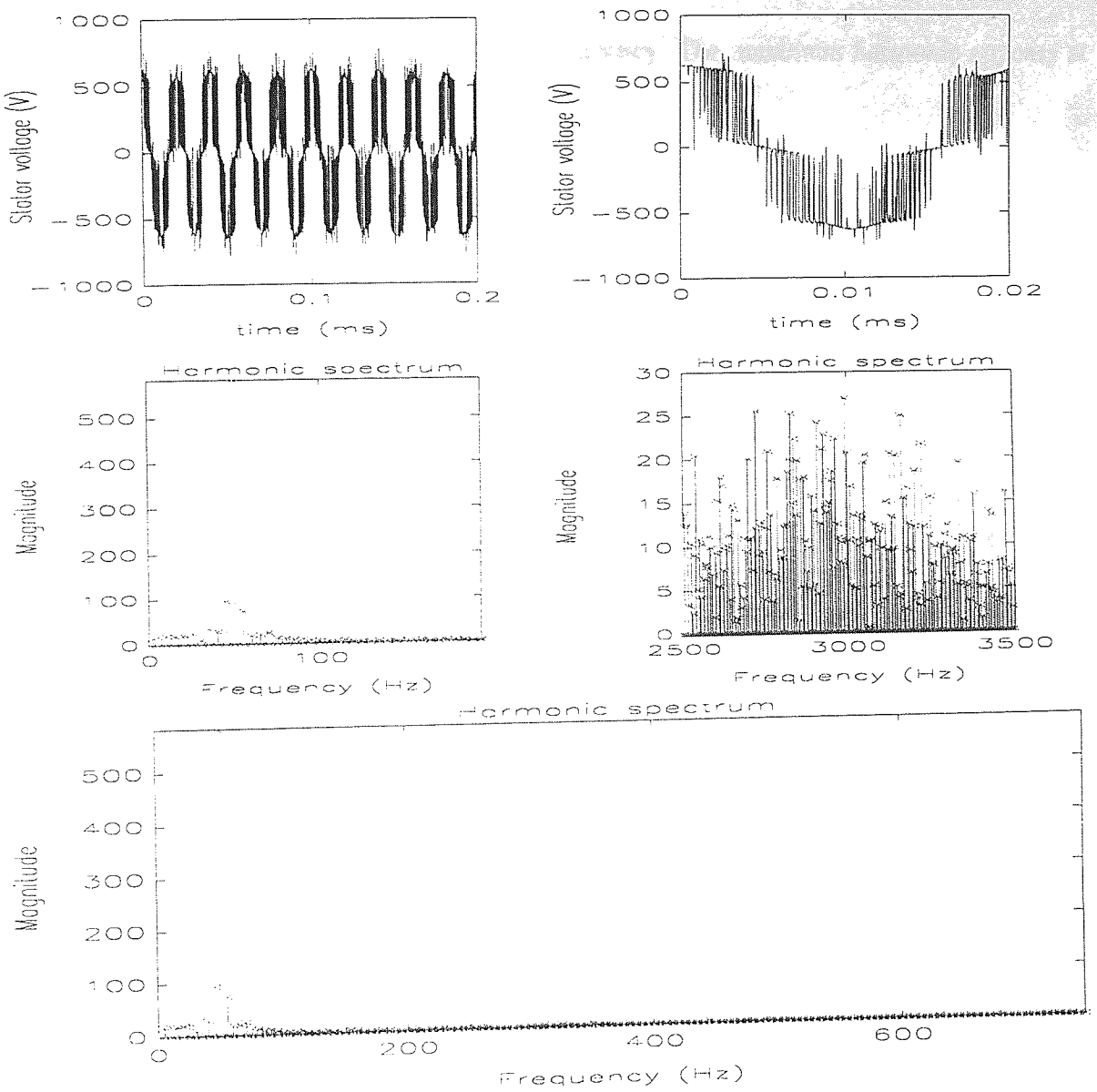

Fig. 6.5-4 Inverter output voltage and its harmonic spectrum of the CVVF test (f_b = 10 Hz, $f_{switching}$ = 3 kHz, $f_{sampling}$ = 40 kHz).

The instantaneous stator line voltage waveform, and the harmonic content of the squirrel-cage induction machine at 10 Hz beat frequency are given in Fig. 6.5-5. The amplitude of the voltage is fairly constant with 410 volts rms value, but its frequency is varying periodically. It is also clear that the stator line voltage has more than one significant harmonic component as seen in Fig. 6.5-5 although some of the low frequency harmonics appeared above and below 50 Hz in Fig. 6.5-4 have been either reduced in amplitude or disappeared due to the filter. The significant harmonics start to be seen at 38 Hz up to 58

Hz in steps of 10 Hz due to the 10 Hz beat frequency. The maximum harmonic appears at 48 Hz, and is 498 Volts.

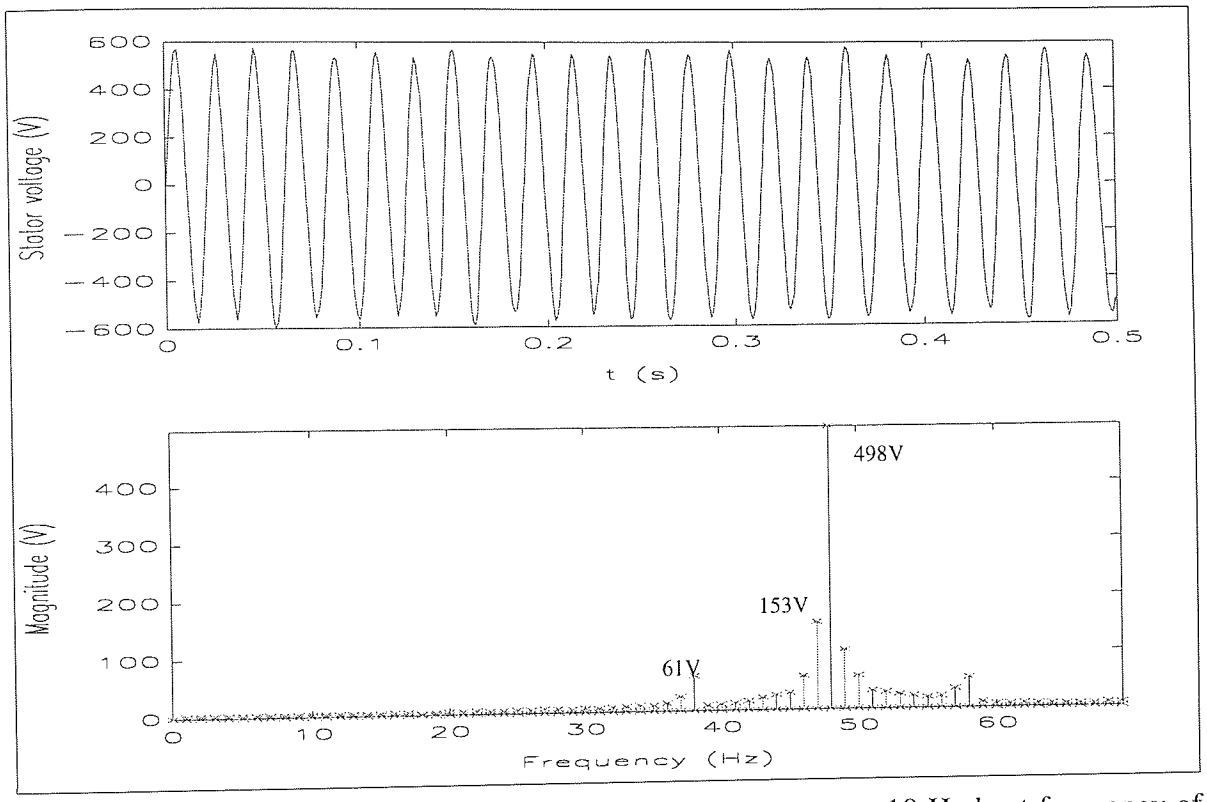

Fig. 6.5-5 Filtered stator line voltage and its harmonic spectrum at 10 Hz beat frequency of CVVF test of the squirrel-cage induction motor.

Similarly, Fig. 6.5-6 gives the instantaneous stator line current and its harmonic contents. The amplitude of the current is not constant but it has an rms value of 7.15 A. The significant harmonics of the current can be seen between 8 Hz up to 88 Hz. The maximum harmonics appear at 28 Hz, 38 Hz, 48 Hz and 68 Hz with magnitudes of 4.5A, 3.7A, 4.3A and 3.2A respectively.

Fig. 6.5-7 illustrates the filtered rotor speed waveform and the harmonic spectrum of the squirrel-cage induction machine at 10 Hz beat frequency. The rotor speed has a mean value and an oscillatory component which is quite smooth during the test with a mean speed of 300 Rad/s. It does not contain any significant harmonics.

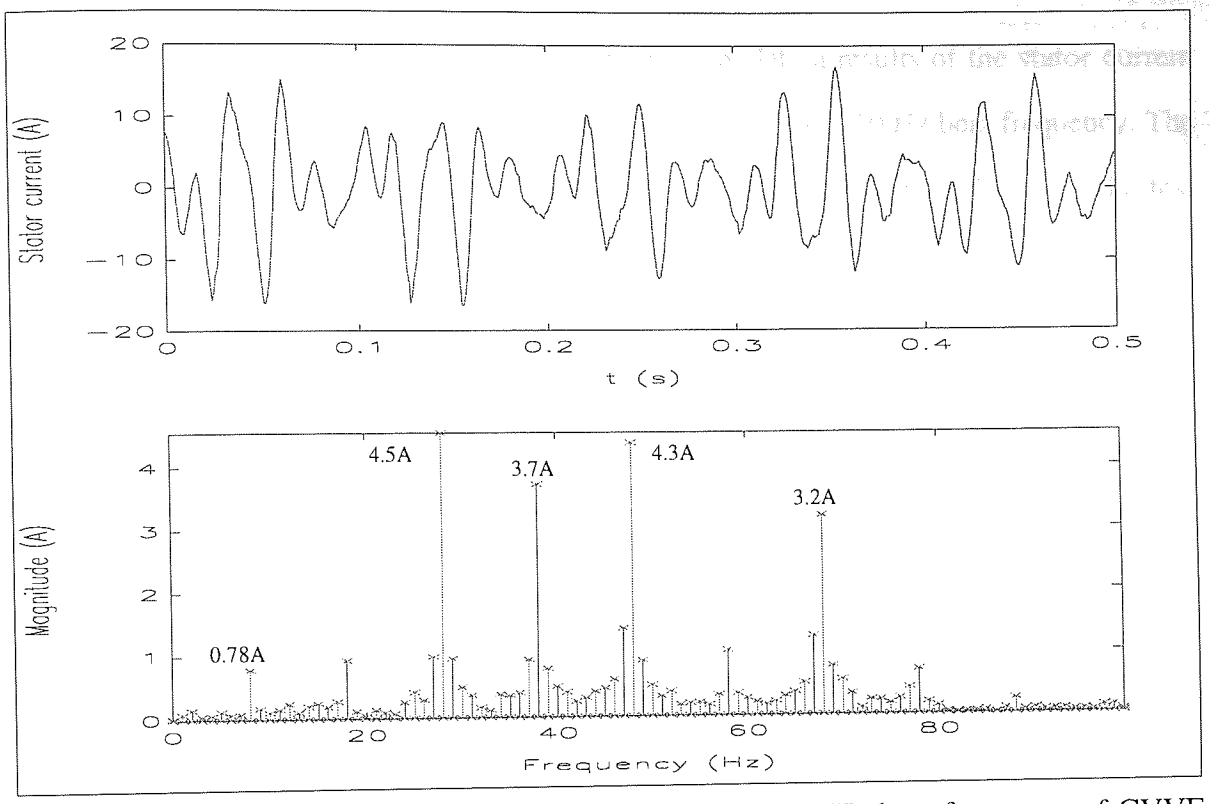

Fig. 6.5-6 Stator line current and its harmonic spectrum at 10 Hz beat frequency of CVVF test of the squirrel-cage induction motor.

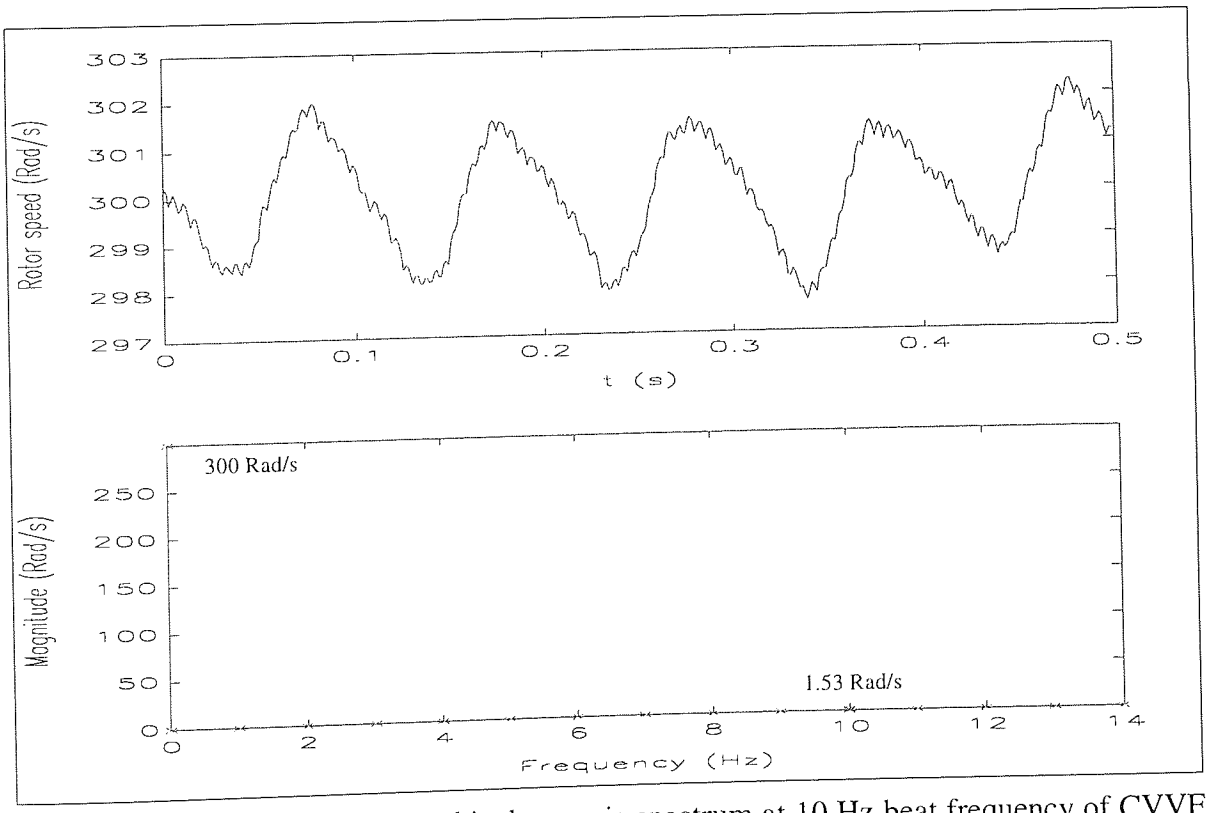

Fig. 6.5-7 Filtered rotor speed and its harmonic spectrum at 10 Hz beat frequency of CVVF test of the squirrel-cage induction motor.

Fig. 6.5-8 shows the comparison of the test and the simulation results of the stator current and the rotor speed of constant-voltage varying-frequency test at 10 Hz beat frequency. The right hand side of the figure shows the simulation results, the left hand side shows the test results. This figure shows that there is a good agreement between the test and the simulation results. However, the speed waveform obtained from the test has some pulsations due to the tachometer and the RC circuit at the output of the tachometer used to measure the speed.

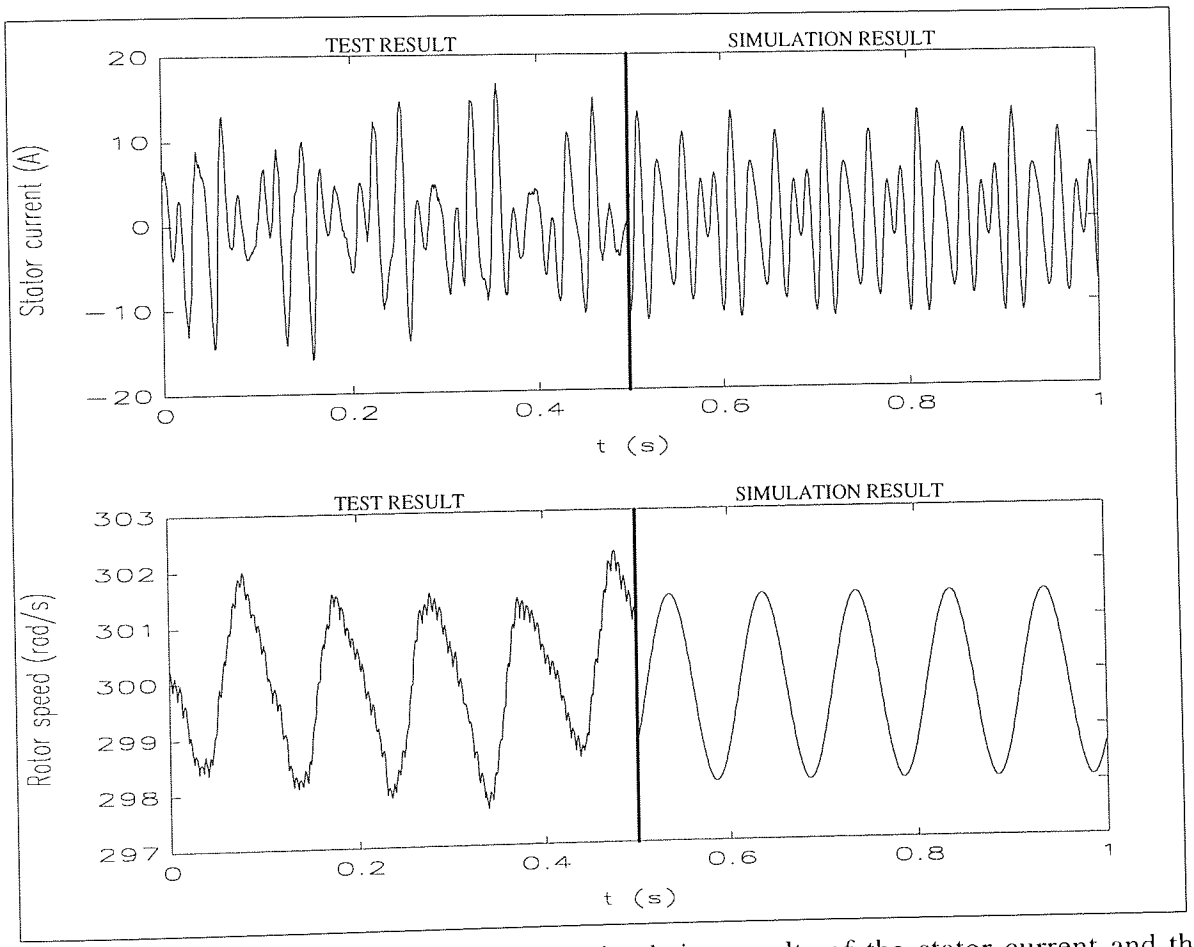

Fig. 6.5-8 Comparison of the test and the simulation results of the stator current and the rotor speed at 10 Hz beat frequency of the CVVF test of the squirrel-cage induction motor.

The stator voltage, the stator current, the rotor speed and the speed demand waveforms of the squirrel-cage induction machine at various beat frequencies are given in Fig. 6.5-9, Fig. 6.5-10, Fig. 6.5-11 and Fig. 6.5-12 respectively. Variation of the frequency of voltage can be seen clearly in Fig. 6.5-9.

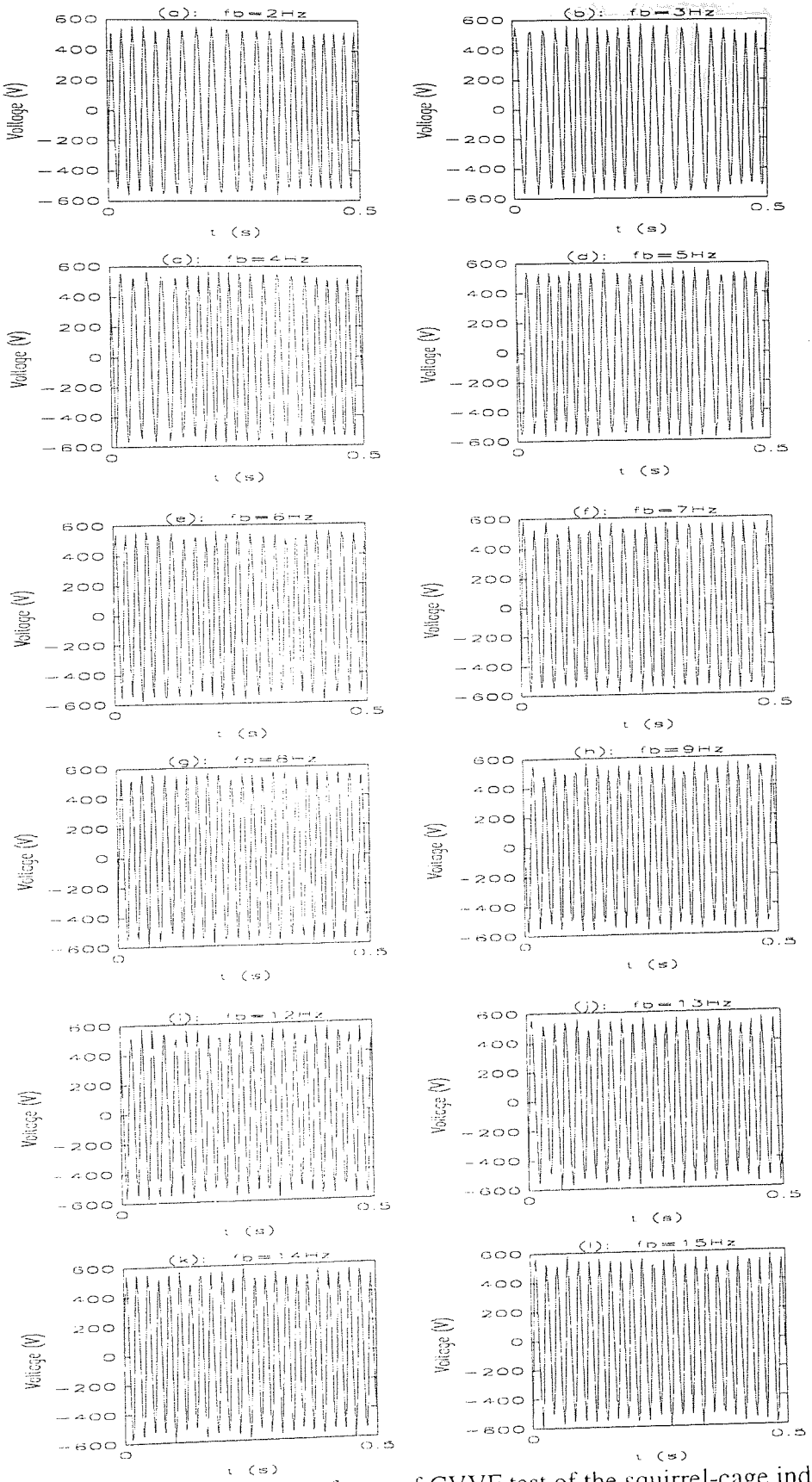

Fig. 6.5-9 Filtered stator voltage waveforms of CVVF test of the squirrel-cage induction motor at different beat frequencies.

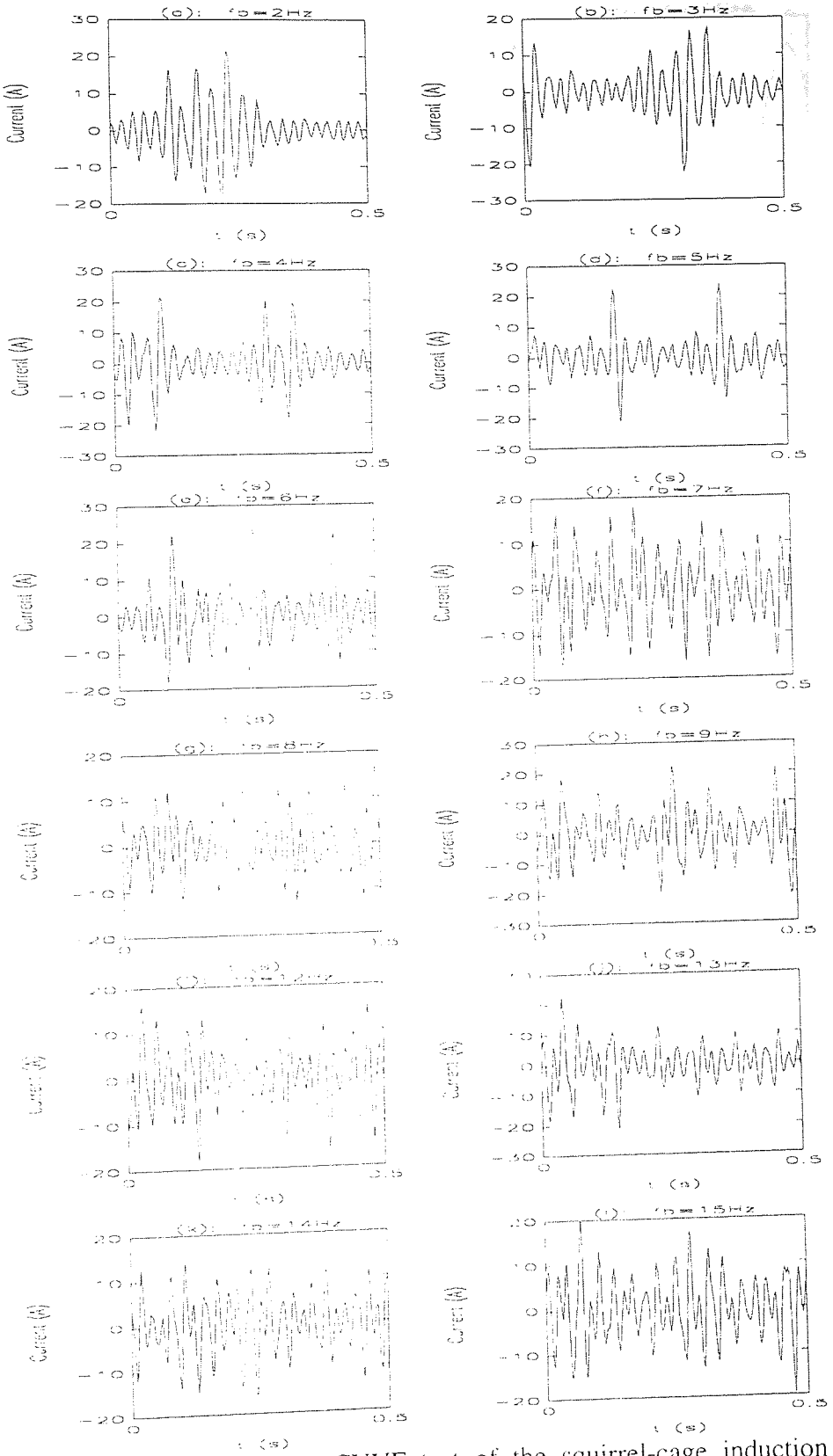

Fig. 6.5-10 Current waveforms of CVVF test of the squirrel-cage induction motor at different beat frequencies.

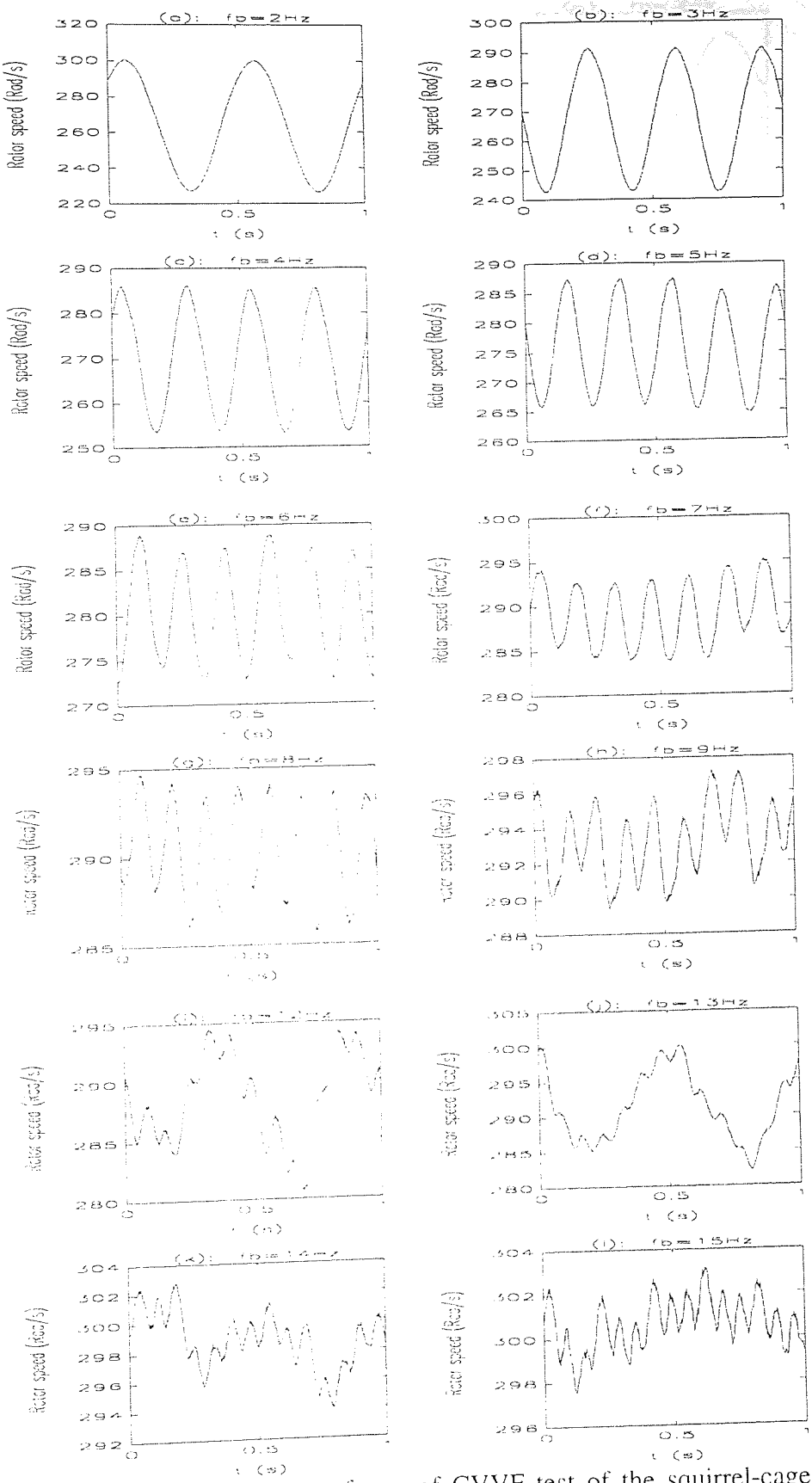

Fig. 6.5-11 Filtered rotor speed waveforms of CVVF test of the squirrel-cage induction motor at different beat frequencies.

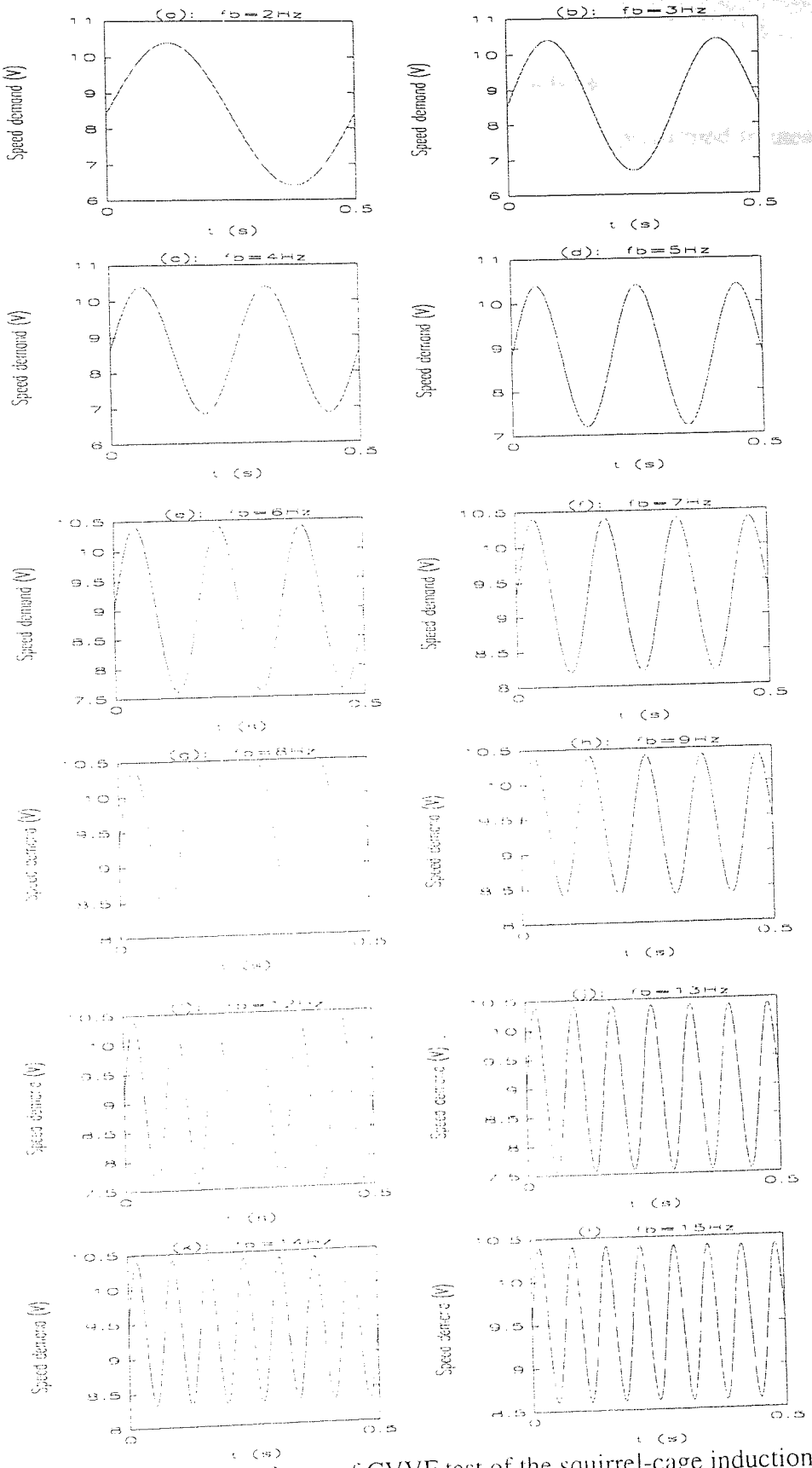

Fig. 6.5-12 Speed demand waveforms of CVVF test of the squirrel-cage induction motor.

6.6. Direct Loading Test of the Slip-Ring Induction Machine

A direct loading test of a 3.3 kW slip-ring induction machine was performed to measure the rated temperatures from the different points within the machine as well as to record the rated stator voltage, stator current, rotor current and rotor speed. Firstly, the delta connected slip-ring induction machine, whose parameters are given in appendix 1, was coupled to a DC generator which was also loaded by a resistive load. The rated sinewave voltage was applied to the terminal of the test machine. When the test machine was running at maximum rotor speed, the DC generator was loaded until the slip-ring induction machine was drawing its rated rms stator current from the supply at rated rotor speed. The full-load test of the machine was continued for a couple of hours to warm the test machine up. When the winding temperature rise had stabilised at 40 °C, all the temperature rises from different points of the test machine were recorded. In addition the stator phase voltage, the stator line current, the rotor phase current and the rotor speed were recorded through a D/A card in a PC.

Table 6.6-1 shows the full-load temperature rise of the slip-ring induction machine at different points within the machine. Due to the structure of the slip-ring induction machine, the temperature rises are found as not high as the temperature rises found in the squirrel-cage induction machines.

Windings (°C)	Airgap (°C)	Core (°C)	End windings (°C)	Rotor (°C)
40	36	25	36	24

Table 6.6-1 Full load temperature rise test results of the slip-ring induction machine.

Fig. 6.2.1-2 shows the vector diagram of the induction machine with the angle, γ, between the recorded current, I_{sa}, and voltage, V_{sa},. If γ can be found from Fig. 6.6-1, then the power factor, $\cos(\phi)$, of the slip-ring induction machine can easily be calculated.

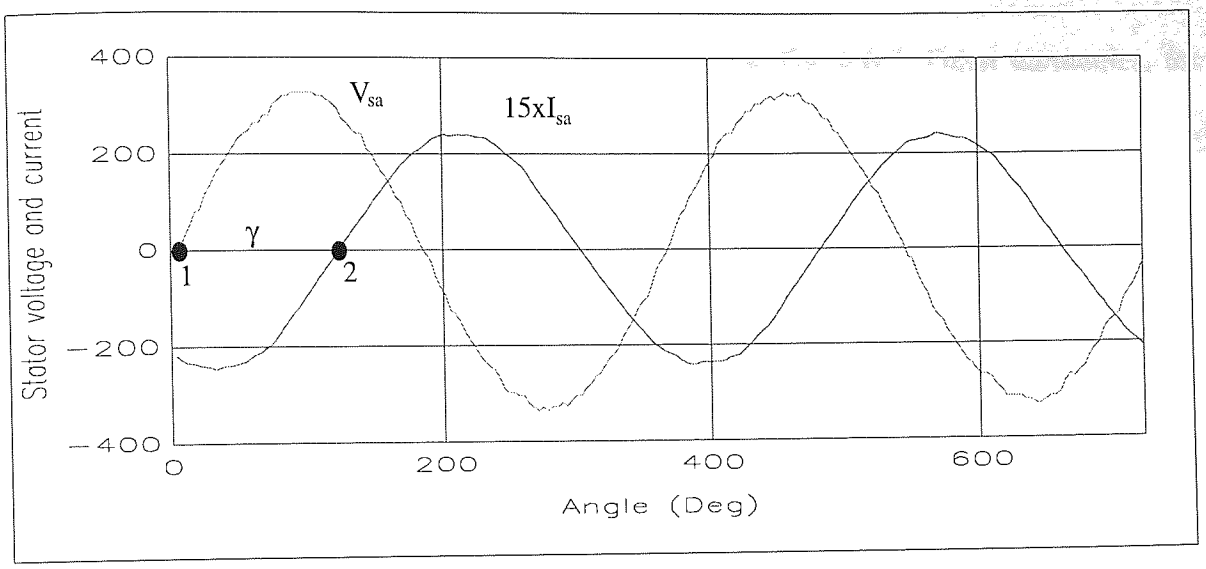

Fig. 6.6-1 Illustration of the angle, γ, of the slip-ring induction machine.

The angle, γ, between point 1 and point 2 in Fig. 6.6-1 is found as 112.4°. If γ = 112.4°, the angle (ϕ) between phase voltage (V_{sa}) and phase current (I_{s1}) is calculated as to be -22.4 with respect to $-I_3$, in Fig. 6.2.1-2 .

In Fig. 6.6-1, the current waveform was magnified 15 times in order to show the angle between voltage and current clearly. Since the power factor (cos(ϕ)), the rms line voltage (V_{sa}) and the rms line current (I_{sa}) are known, the input power of the induction machine can be calculated as to be 4184 W.

The efficiency of the machine is:

$$\eta = \frac{P_{out}}{P_{in}} = \frac{3300}{4184} = 78.87\ \% \qquad (8.2\text{-}3)$$

Waveforms of the direct full-load stator line voltage and stator line current of a delta connected slip-ring induction machine are given in Fig. 6.6-2. The rated rms value of the voltage and the current were found to be 230.1 Volts and 11.36 Amperes respectively. Maximum voltage and current harmonics were both appeared at 50 Hz and were found to

be 323.6 Volts and 16 Amperes respectively as shown in Fig. 6.6-3. Other harmonics, for voltage and current, were insignificant.

Waveforms of the rotor current and the rotor speed of the delta connected slip-ring induction machine are given in Fig. 6.6-4. The rms value of the rotor current is 8.94 Amperes and the mean value of the rotor speed is 148.94 Rad/s. The maximum harmonic of the rotor current appears, at 2.5 Hz, to be 12.6 Amperes. The rotor speed has a value of 149 Rad/s.

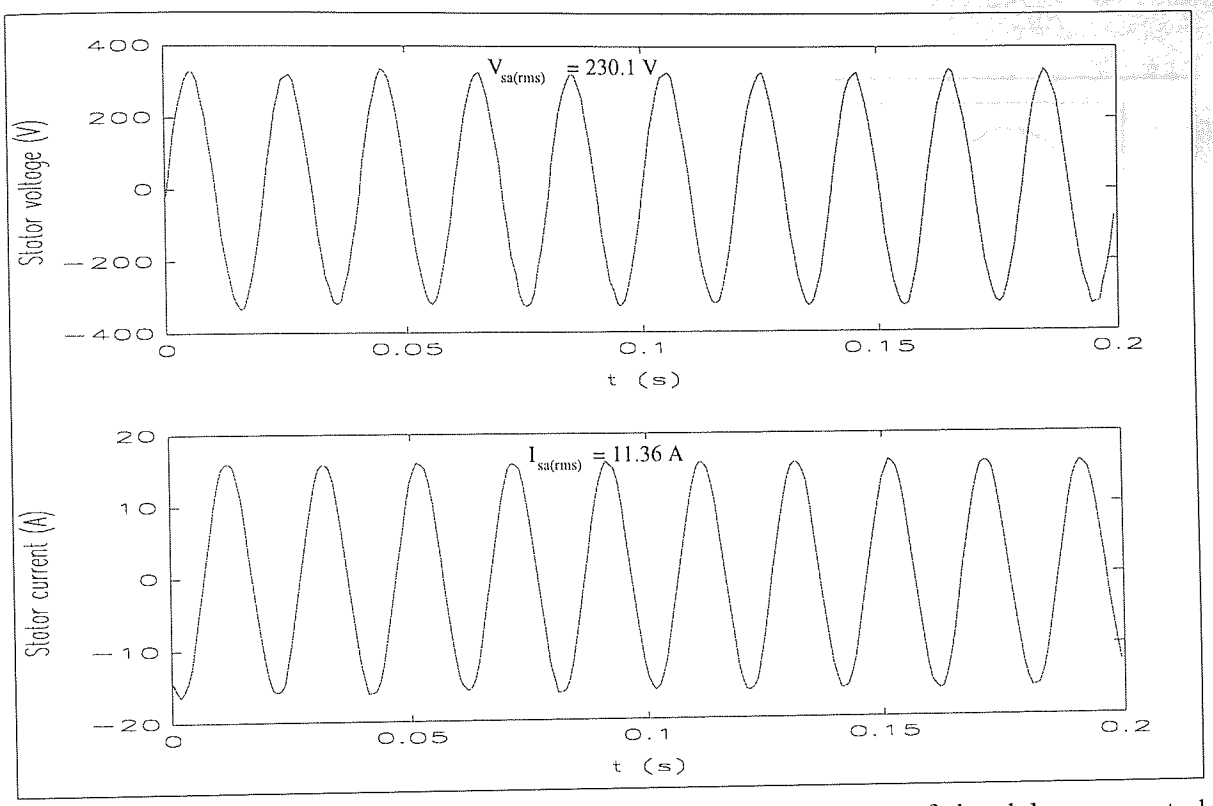

Fig. 6.6-2 Full-load instantaneous stator voltage and stator current of the delta connected slip-ring induction machine.

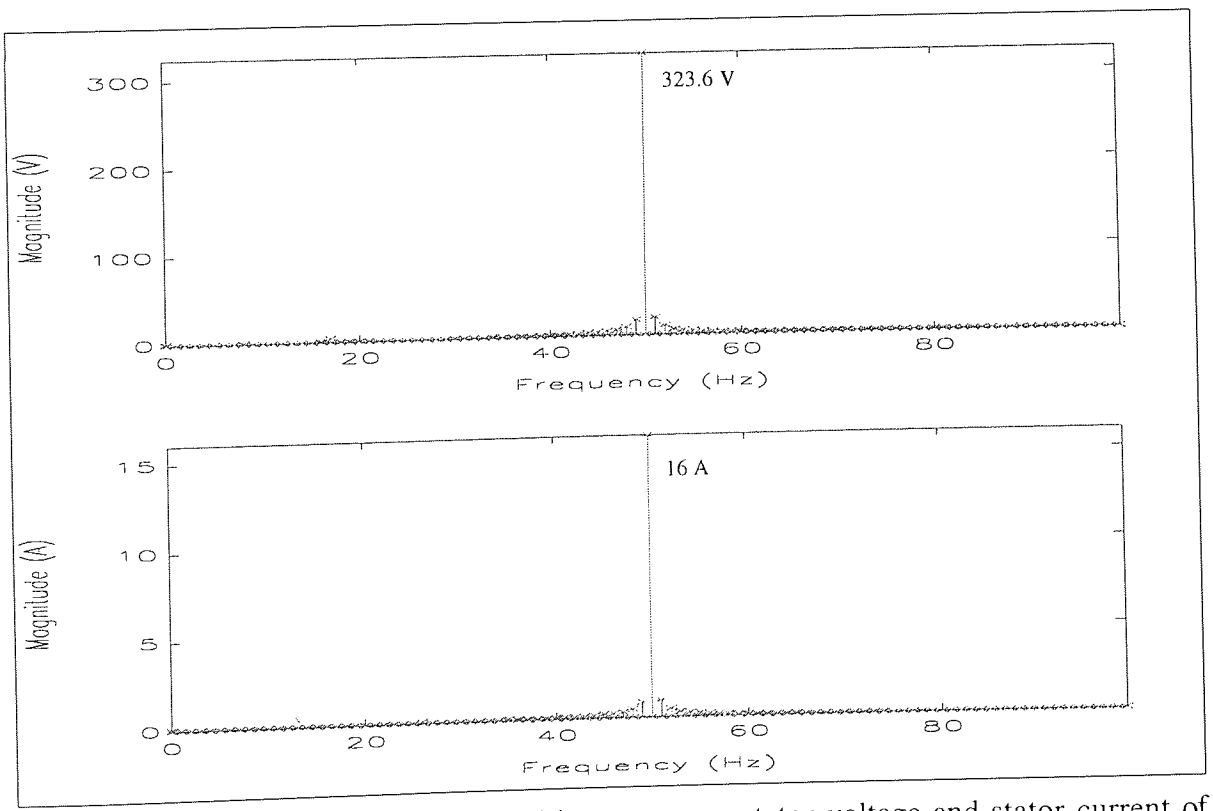

Fig. 6.6-3 Harmonic spectra of full-load instantaneous stator voltage and stator current of the delta connected slip-ring induction machine.

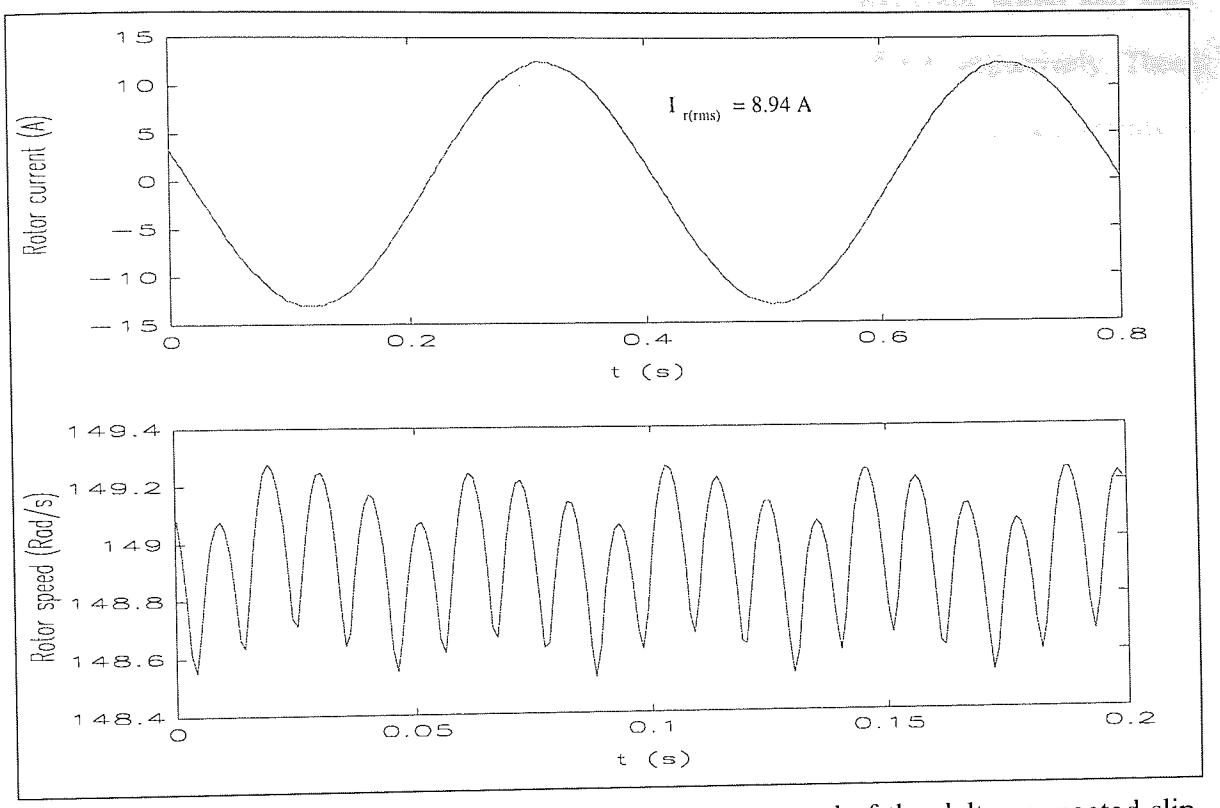

Fig. 6.6-4 Full-load instantaneous rotor current and rotor speed of the delta connected slip-ring induction machine.

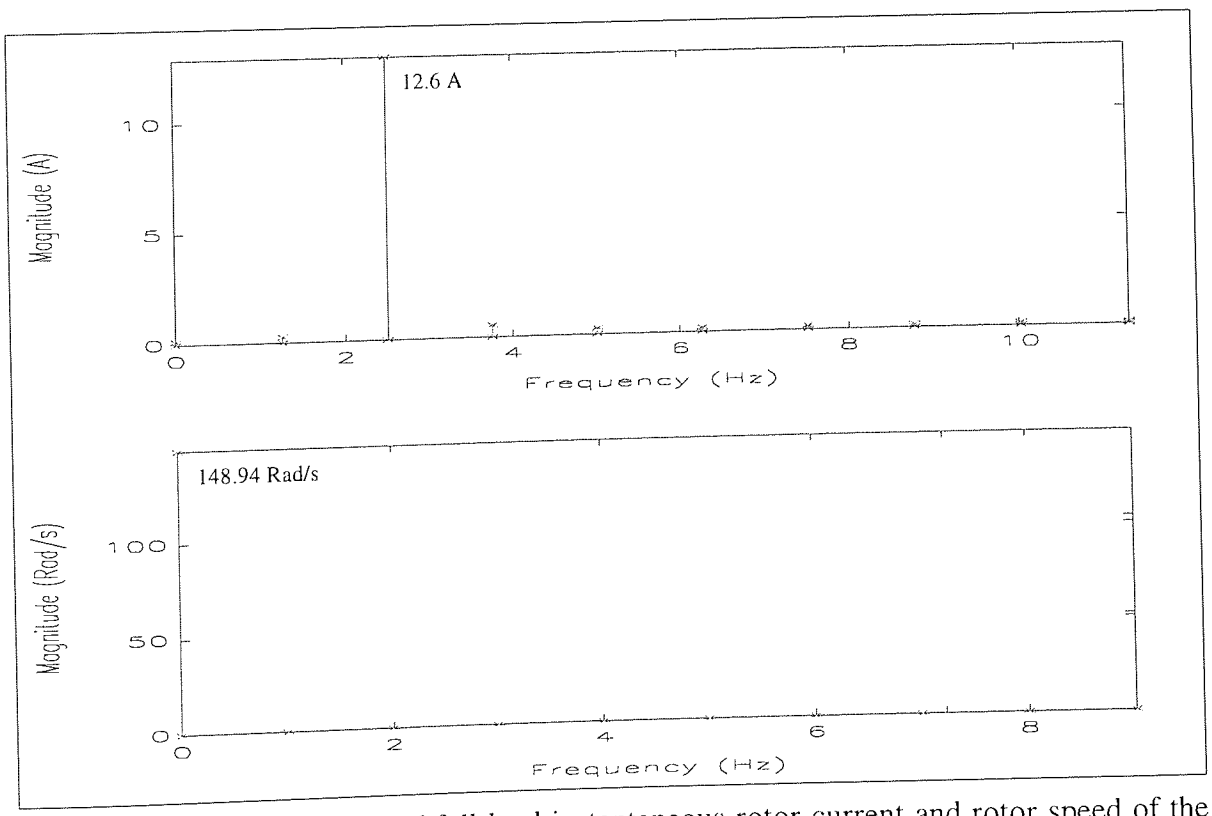

Fig. 6.6-5 Harmonic spectra of full-load instantaneous rotor current and rotor speed of the delta connected slip-ring induction machine.

Simulation results of the full-load stator current, rotor current and rotor speed and their harmonic spectra are illustrated in Fig. 6.6-6, Fig. 6.6-8 and Fig. 6.6-8 respectively. These results show that there are good agreements between the simulation and the test results in terms of the rms values and harmonic contents. The stator current has 11.41 Amperes rms value and 16.14 Amperes maximum harmonic at 50 Hz. The rms value of the rotor current was found as to be 9.1 Amperes and its maximum harmonic has appeared at 2.5 Hz as a value of 12.8 Amperes. The simulation result of the rotor speed is a pure DC and has a value of 148.9 Rad/s.

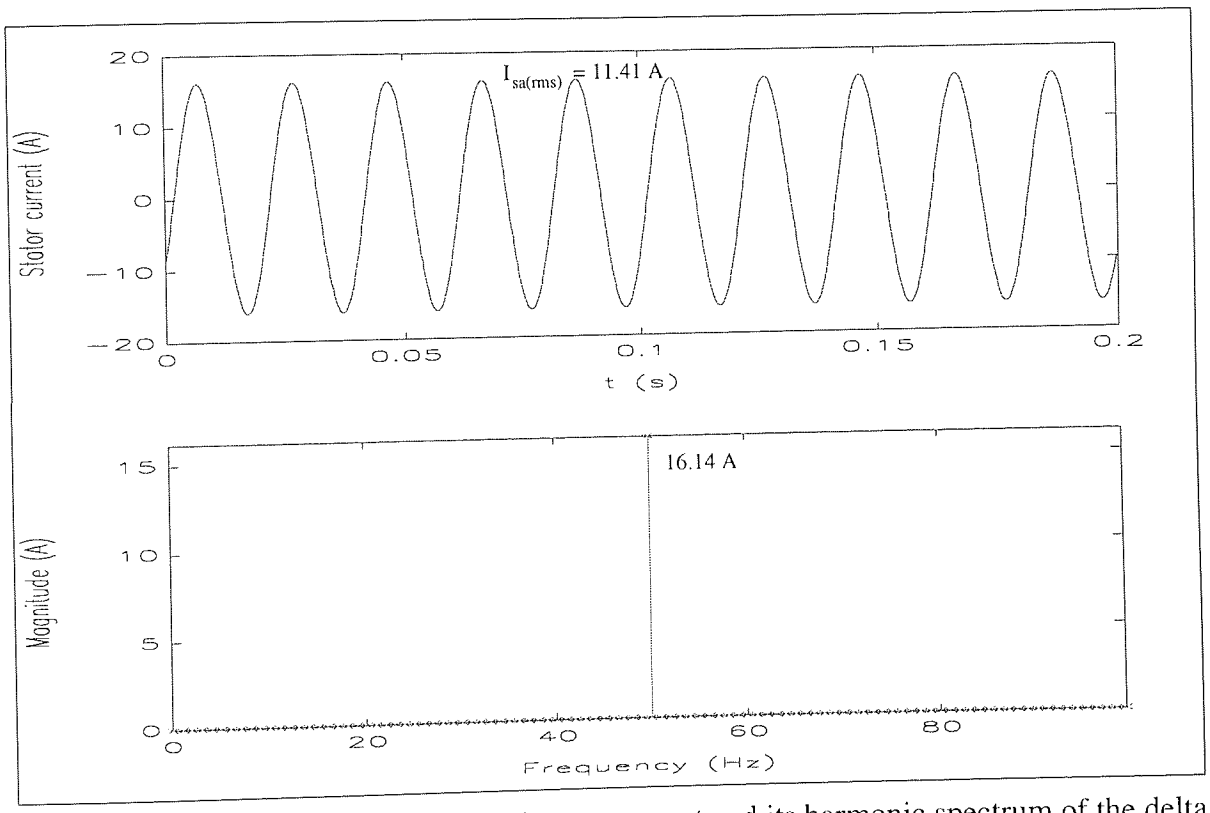

Fig. 6.6-6 Simulation result of full-load stator current and its harmonic spectrum of the delta connected slip-ring induction machine.

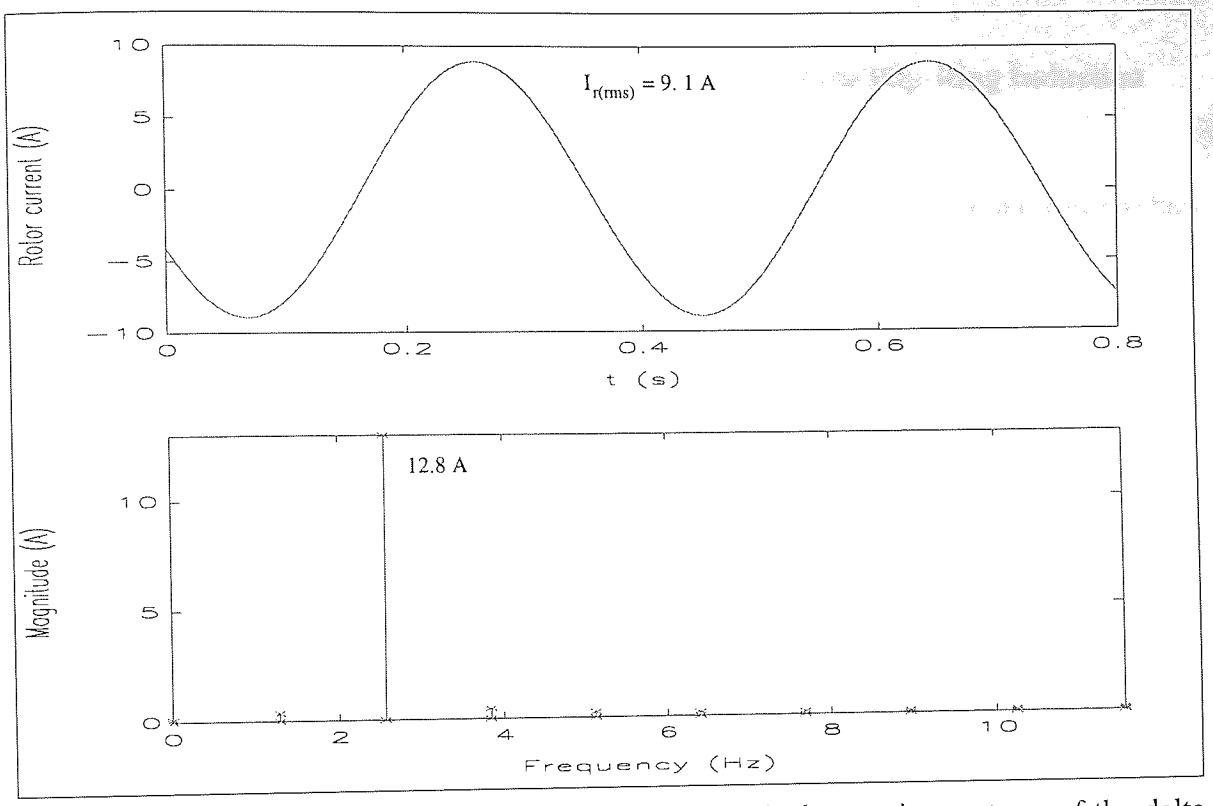

Fig. 6.6-7 Simulation result of full-load rotor current and its harmonic spectrum of the delta connected slip-ring induction machine.

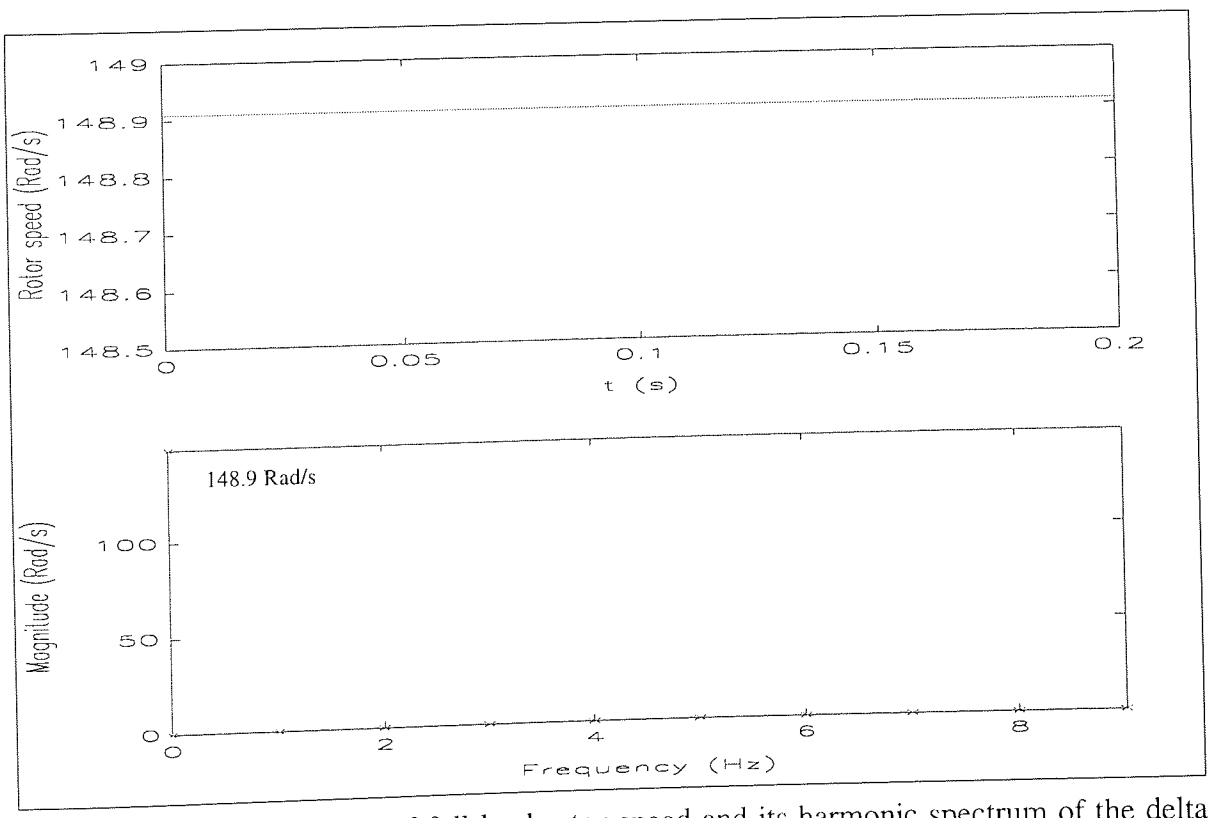

Fig. 6.6-8 Simulation result of full-load rotor speed and its harmonic spectrum of the delta connected slip-ring induction machine.

6.7. Varying-Voltage, Varying-Frequency (VVVF) Test of the Slip-Ring Induction Machine

The VVVF test of slip-ring induction machine was carried out to compare the rotor values in terms of full-load and VVVF tests. Due to the recordability of the rotor current, a reliable comparison of the rotor current obtained from full-load and VVVF tests and simulation can be done.

The test was carried out using the inverter available in the laboratory by applying sinusoidal speed demand signals from an arbitrary waveform generator to the inverter's external analogue speed demand terminals. The frequency of the speed demand was varied from 1.0 Hz to 15 Hz. In every case, the sinusoidal speed demand had two components, amplitude and DC offset, and sum of these components is limited to 10.4 Volts by the arbitrary waveform generator. When the speed demand is 10 Volts DC, the output frequency of voltage of the inverter is equal to 50 Hz which causes the rotor to run at rated speed. As the test motor (3.3 kW slip-ring machine) was drawing the rated rms stator current of 11.36 A from the supply at the rated winding temperature rise of 40 °C, the temperature rises at various points within the motor were recorded as well as the stator voltage, the stator current, the rotor current, the rotor speed and the instantaneous speed demands at different beat frequencies.

Table 6.7-1 shows data of the speed demand and temperature rises at various beat frequencies of the VVVF test of the slip-ring induction machine.

Fig. 6.7-1 shows that the speed demand waveform, at various beat frequencies, is varying smoothly with the normal inertia of the slip-ring induction machine. Temperature rises of the windings, the airgap and the rotor are the same as for the direct loading test. The temperature rises are 40 °C, 36 °C and 24 °C respectively. The temperature rises of the core and the end windings were also found to be very close to 25 °C and 36 °C of the direct

loading test. The variations of these temperatures with the different beat frequencies are shown in Fig. 6.7-2.

fb (Hz)	Amplitude (V)	DC offset (V)	Windings (°C)	Airgap (°C)	Core (°C)	End Windings (°C)	Rotor (°C)
1	4.40	6.00	40	37	29	40	24
2	2.60	7.80	40	37	27	37	24
3	1.80	8.60	40	36	27	36	24
4	1.30	9.10	40	36	26	36	24
5	1.08	9.32	40	36	26	35	24
6	0.96	9.44	40	36	25	35	24
7	0.88	9.32	40	36	27	36	24
8	0.80	9.60	40	36	26	35	24
9	0.76	9.62	40	36	26	35	24
10	0.80	9.60	40	36	26	36	24
11	0.90	9.50	40	36	26	35	24
12	0.94	9.46	40	36	26	36	24
13	1.00	9.40	40	36	26	36	24
14	1.04	9.26	40	36	25	36	24
15	1.20	9.20	40	36	25	36	24
Full-load temperature rises			**40**	**36**	**25**	**36**	**24**

Table 6.7-1 Data for VVVF test of the star connected slip-ring induction machine.

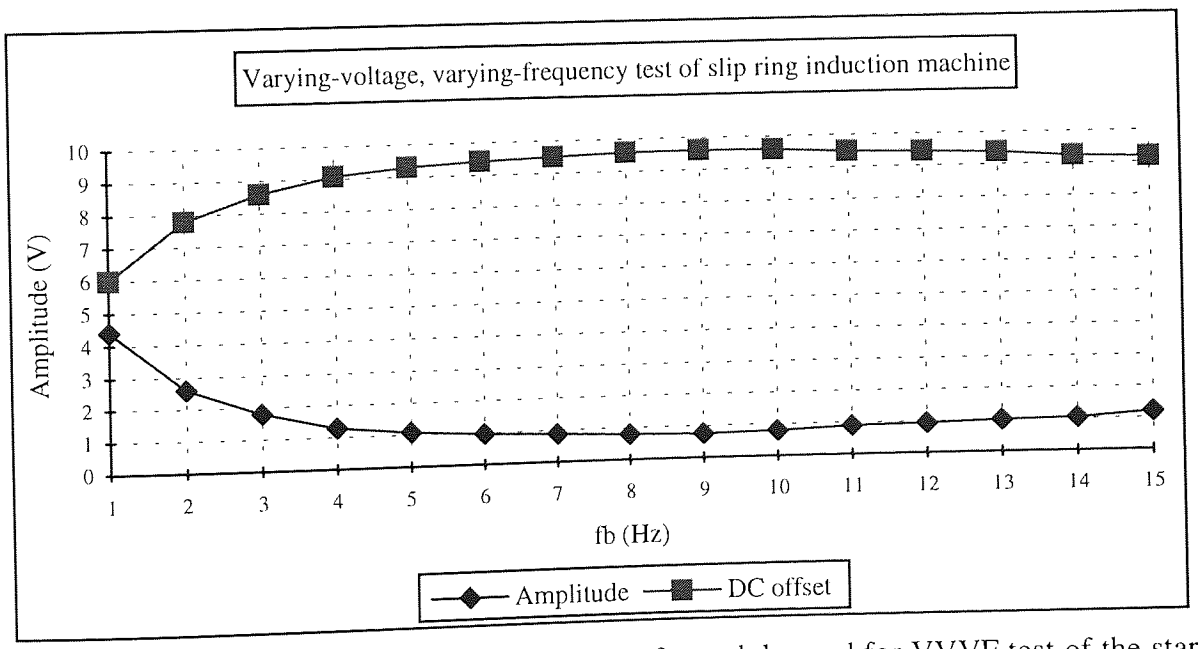

Fig. 6.7-1 Variation of DC offset and amplitude of speed demand for VVVF test of the star connected slip-ring induction machine.

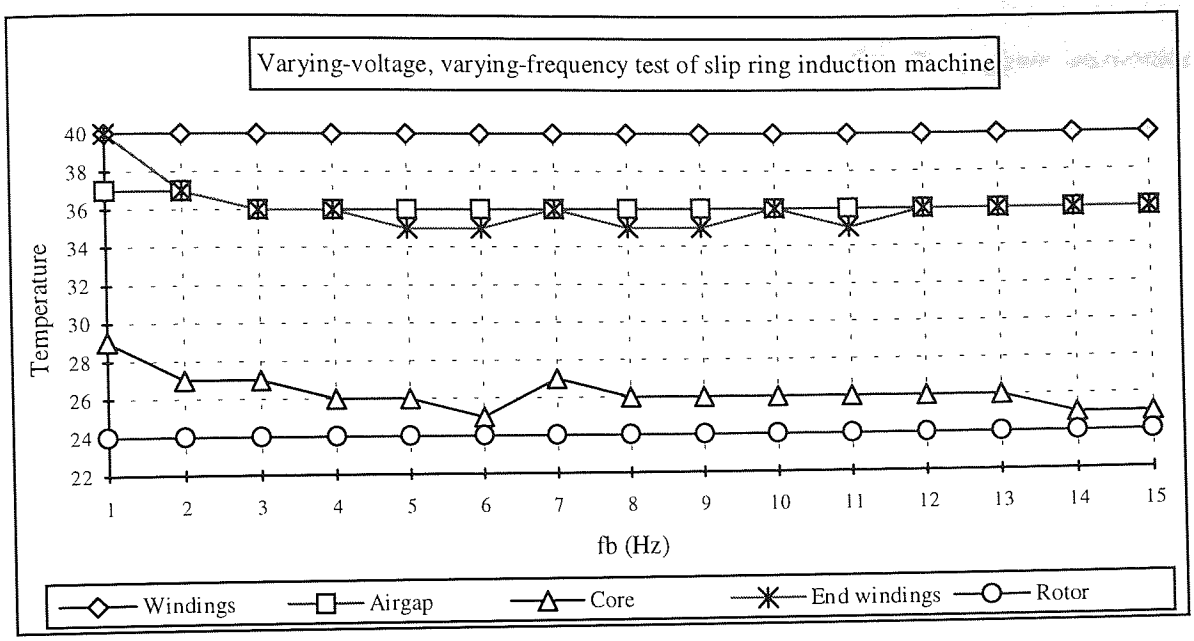

Fig. 6.7-2 Temperatures of VVVF test of the star connected slip-ring induction machine.

Variation of the stator line voltage and its harmonic spectrum for the star connected slip-ring induction machine are shown in Fig. 6.7-3 at 5 Hz beat frequency of VVVF test. The rms value of the voltage is 365.5 Volts. Significant harmonics of the voltage start to appear at 26 Hz and continue up to 56 Hz with 5 Hz difference between them. The maximum harmonic appears at 46 Hz with a value of 391 Volts.

The stator phase current and its harmonic spectrum are given in Fig. 6.7-4. The rms value of current, 6.25 Amperes, is equal to the rated rms value. Significant harmonics of the current start at 21 Hz and go up to 61 Hz. There are some harmonics below 10 Hz, particularly the harmonic at 1 Hz is quite significant. Normally the minimum beat frequency in this test is 5 Hz, but due to rotor frequencies below 10 Hz, as shown in Fig. 6.7-5, harmonics of stator current below 10 Hz appear. The maximum harmonic of the stator current appears at 46 Hz similar to the maximum voltage harmonic.

The rotor current and its harmonic spectrum are shown in Fig. 6.7-5. The rotor current has an rms value of 9.2 Amperes, equal to the rated rms value. The variation is not as smooth as the stator current. The significant rotor harmonics start to appear at 1 Hz, with a value of

2.8 Amperes and continue up to 60 Hz; but are mostly below 10 Hz. The biggest harmonics appear at 4 Hz and 5 Hz with a value of 7.5 Amperes.

The rotor speed and its harmonic spectrum are given in Fig. 6.7-6. The rotor speed varies between 148 Rad/s and 142 Rad/s with high frequency oscillations. However, the amplitudes of these oscillations are not significant. The DC value of the rotor speed was found as to be 144.5 Rad/s.

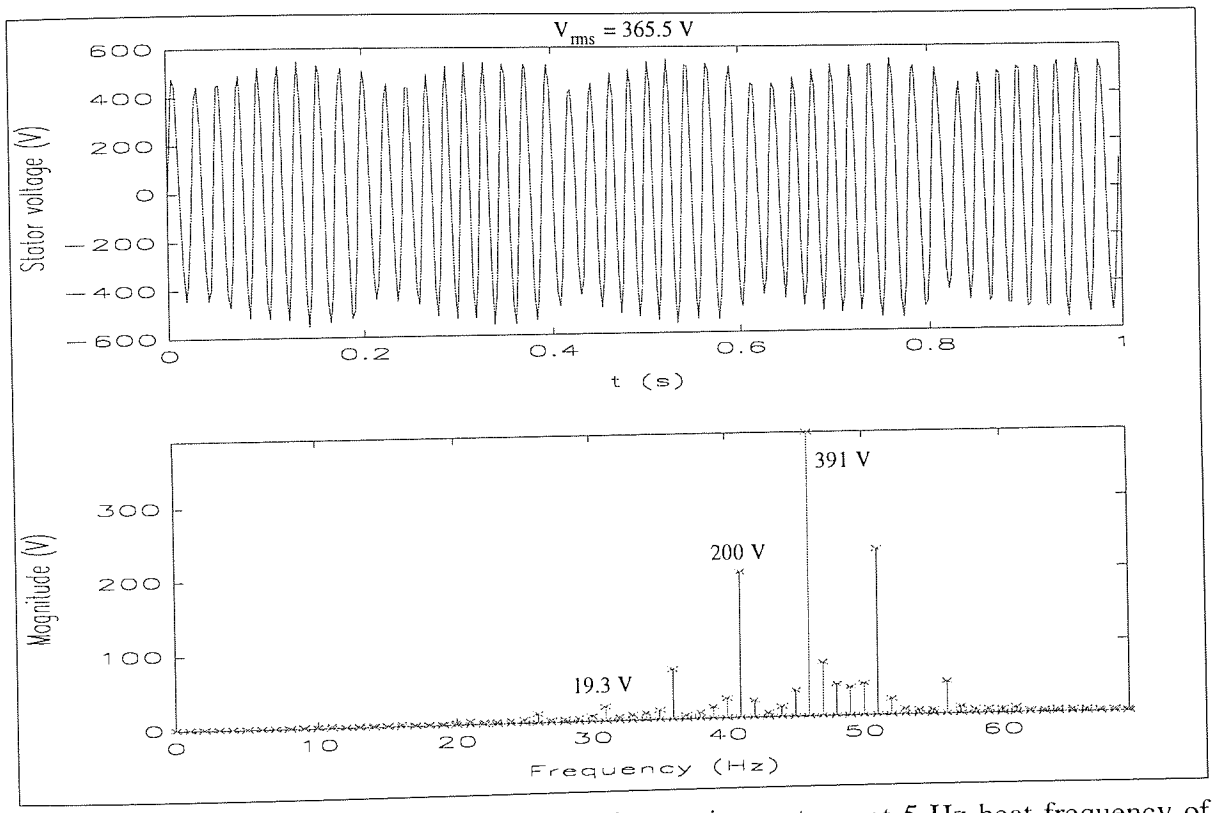

Fig. 6.7-3 Filtered stator line voltage and its harmonic spectrum at 5 Hz beat frequency of VVVF test of the star connected slip-ring induction machine.

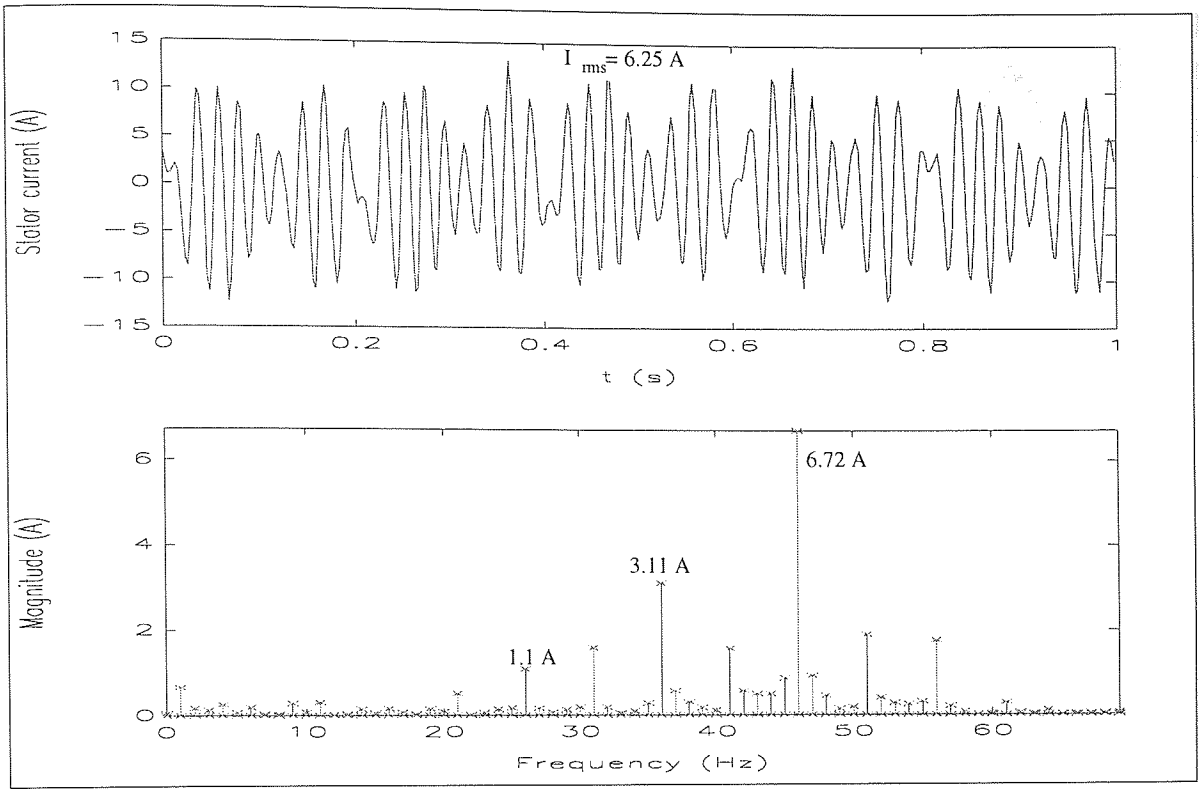

Fig. 6.7-4 Stator phase current and its harmonic spectrum at 5 Hz beat frequency of VVVF test of the star connected slip-ring induction machine.

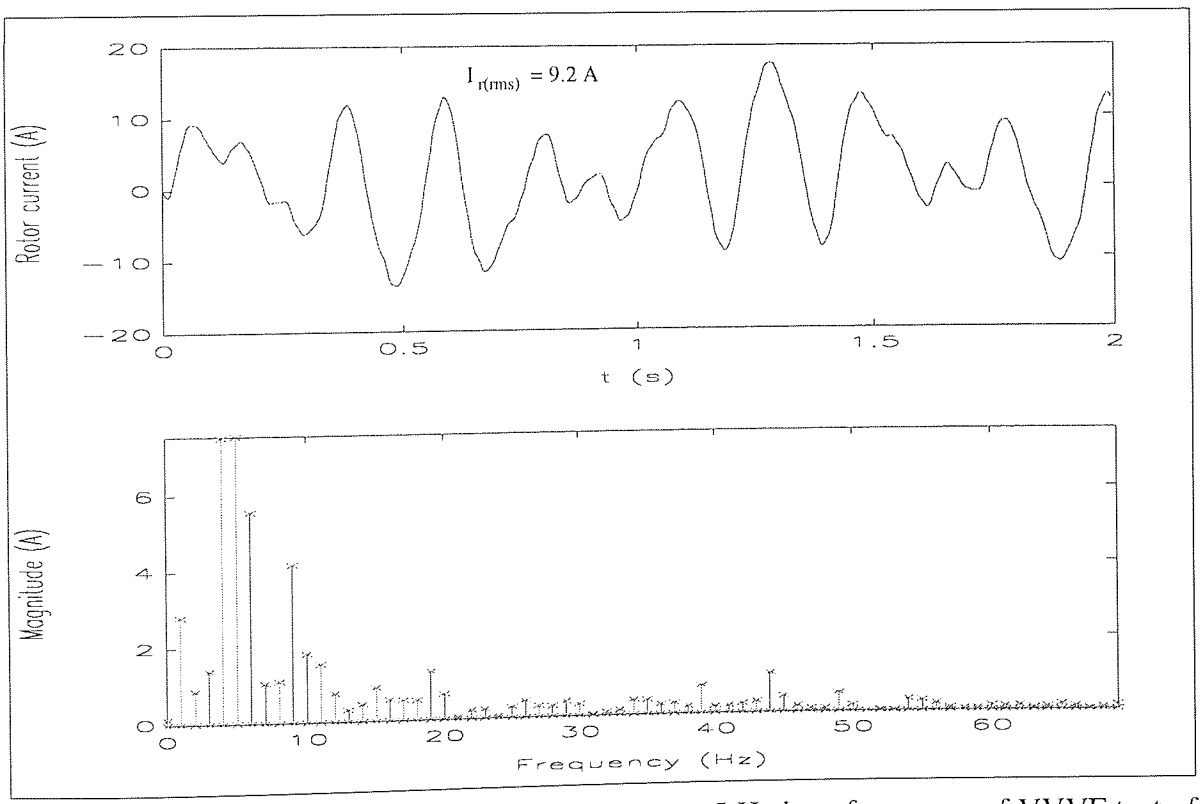

Fig. 6.7-5 Rotor current and its harmonic spectrum at 5 Hz beat frequency of VVVF test of the star connected slip-ring induction machine.

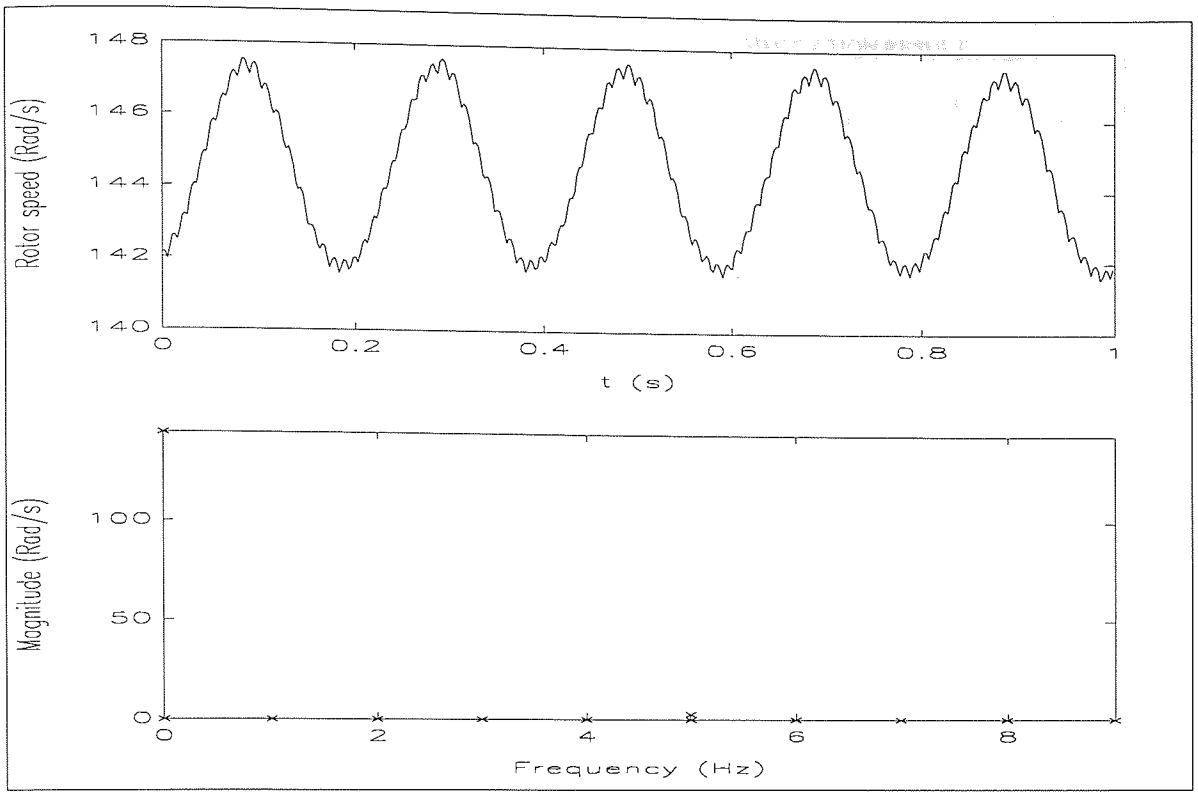

Fig. 6.7-6 Filtered rotor speed and its harmonic spectrum at 5 Hz beat frequency of VVVF test of the star connected slip-ring induction machine.

Fig. 6.7-7 shows the comparison of the test and the simulation results of the stator current and the rotor speed at 5 Hz beat frequency of varying-voltage varying-frequency test. Comparison of the rotor current is given in Fig. 6.7-8. The simulation results are illustrated on the second half of the figures and the first half of the figures show the test results. As seen from these figures, good agreement was achieved between the simulation and the test results.

Waveforms of the filtered stator voltage, the stator current, the rotor current and the filtered rotor speed of the star connected slip-ring induction machine at various beat frequencies are given in Fig. 6.7-9, Fig. 6.7-10, Fig. 6.7-11 and Fig. 6.7-12 respectively.

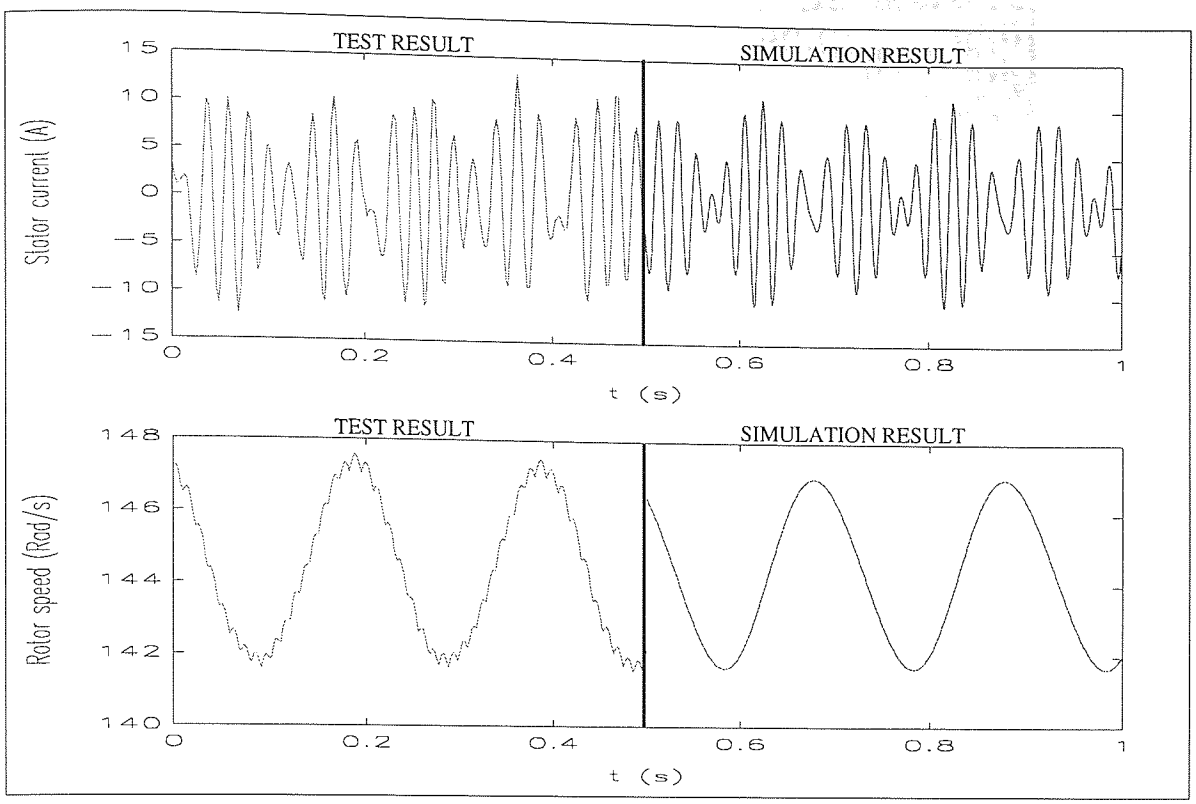

Fig. 6.7-7 Comparison of the test and the simulation results of the stator current and the rotor speed at 5 Hz beat frequency of VVVF test of the slip-ring induction machine.

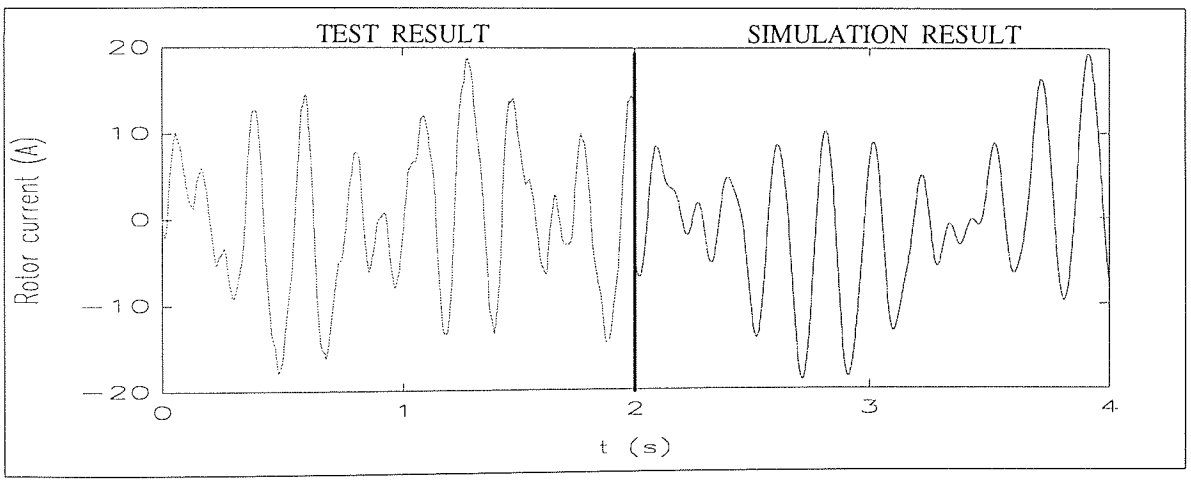

Fig. 6.7-8 Comparison of the test and the simulation results of the rotor current at 5 Hz beat frequency of VVVF test of the slip-ring induction machine.

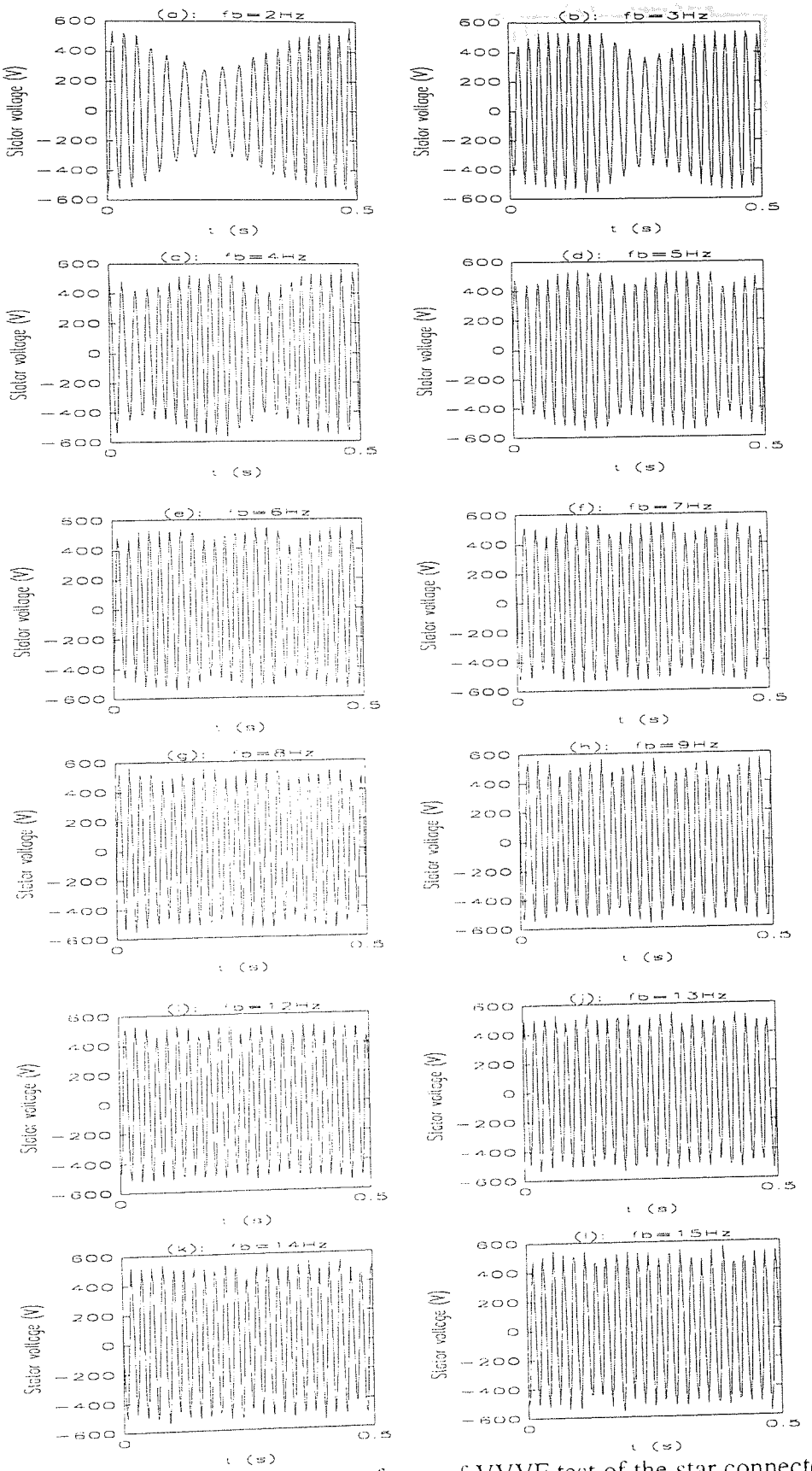

Fig. 6.7-9 Filtered stator line voltage waveforms of VVVF test of the star connected slip-ring induction machine at various beat frequencies.

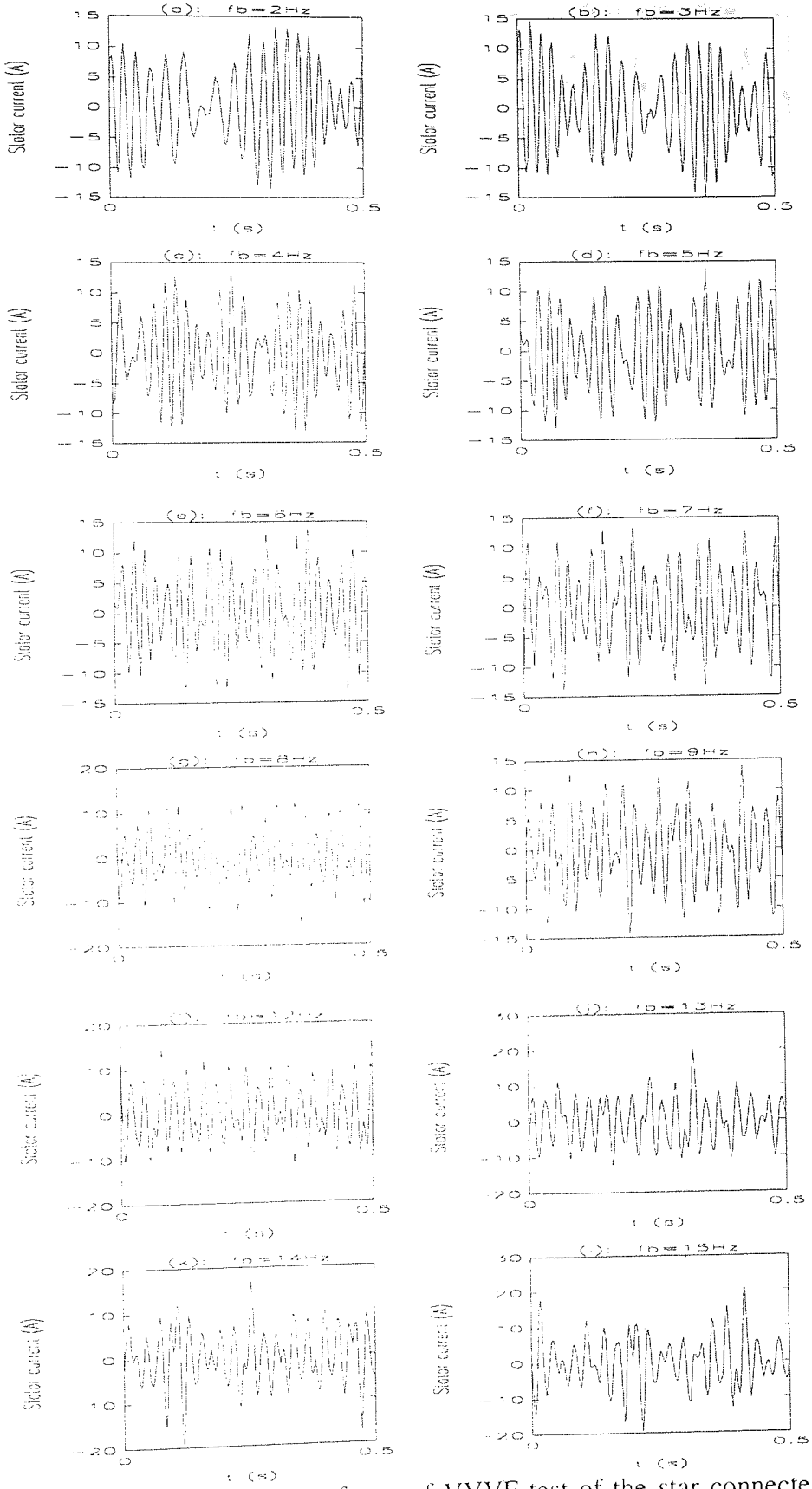

Fig. 6.7-10 Stator phase current waveforms of VVVF test of the star connected slip-ring induction machine at various beat frequencies.

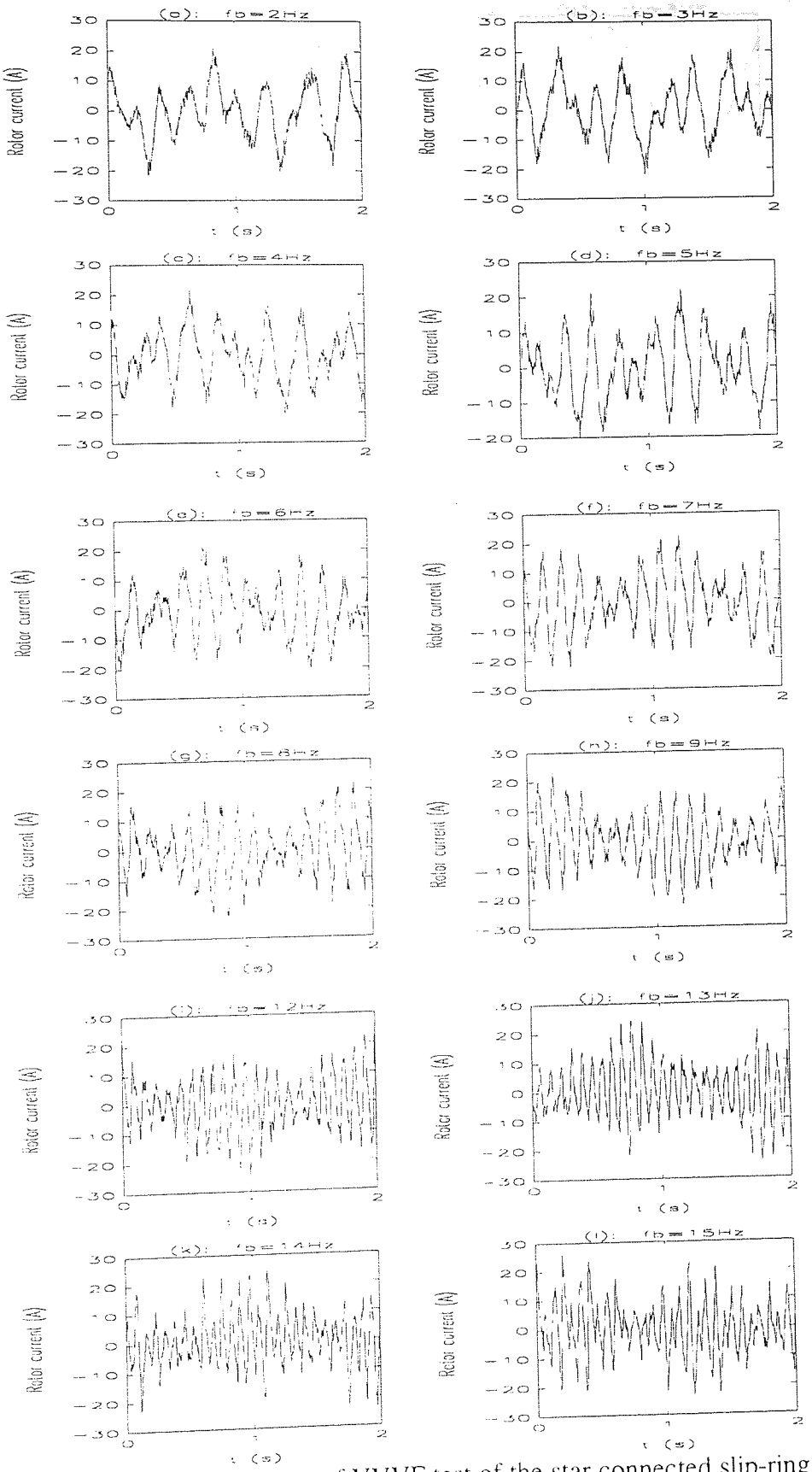

Fig. 6.7-11 Rotor current waveforms of VVVF test of the star connected slip-ring induction machine at various beat frequencies.

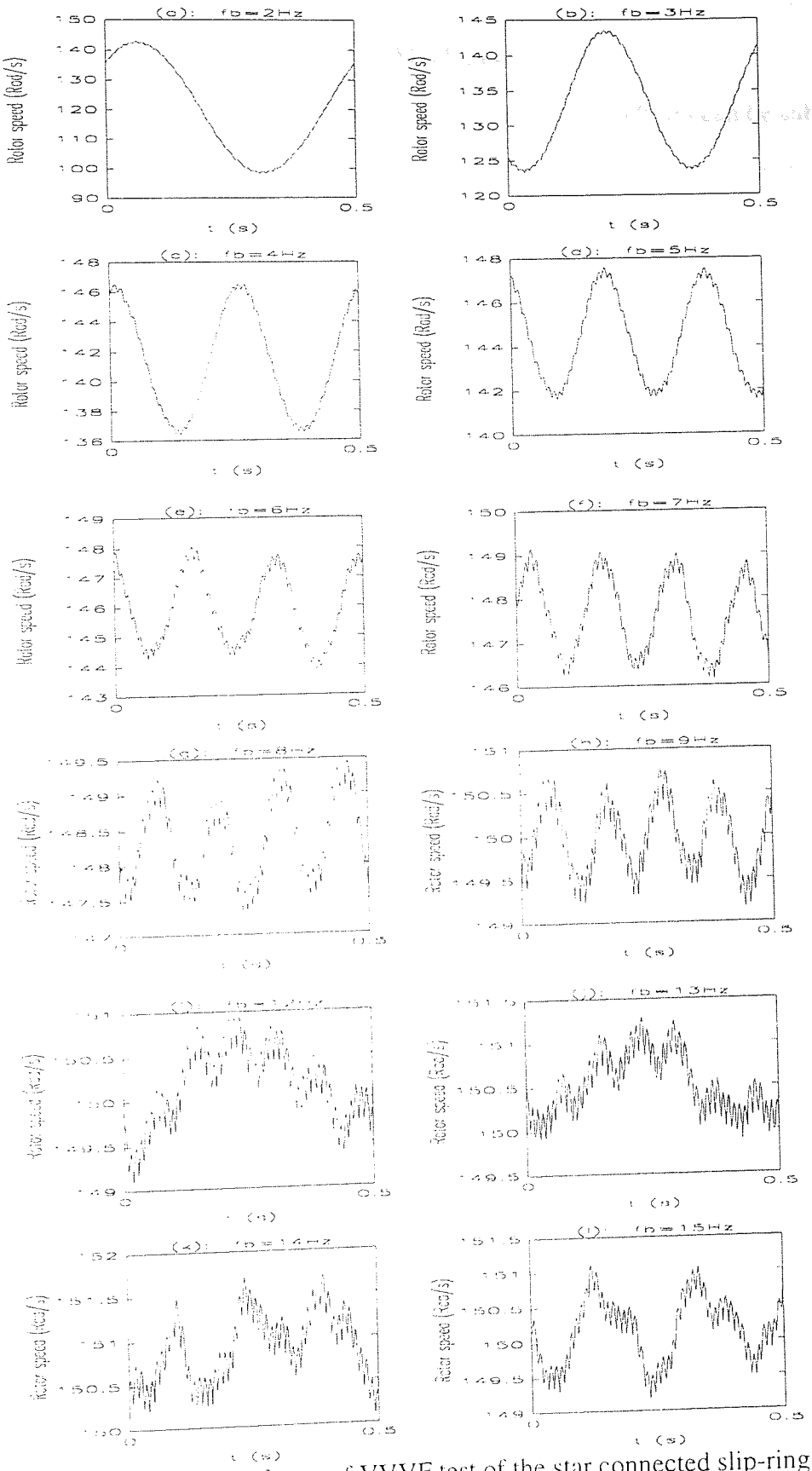

Fig. 6.7-12 Filtered speed waveforms of VVVF test of the star connected slip-ring induction machine at various beat frequencies.

6.8. Breakdown of the Losses in Induction Machines

As mentioned in the introduction section, the losses in induction machines can be subdivided into electrical losses and mechanical losses. The electrical losses are iron losses, stator and rotor copper losses, and stray load losses. The mechanical losses are windage and friction losses.

Although the input power measured from the mixed-frequency test is accepted as approximately equal to the total losses of the machine, when the input current is at rated value, that does not mean the losses are distributed correctly inside the machine. Some of the losses can be different from the full load values due to variations of voltage, current and frequency.

In this section, the losses within the induction machine have been examined carefully and the losses of the test motors are identified.

6.8.1. Stator Copper Loss

Achieving rated stator current is one of the principle criteria for a representative mixed-frequency test of an induction machine. In any good mixed-frequency test, the stator current will be at least approximately equal to the rated current. Achieving the exact stator current does not necessarily produce the most accurate mixed-frequency test. On the other hand, the stator copper loss is defined as the product of the stator current squared and the stator resistance. The stator resistance does not change during the test, but the stator current changes depending on the voltage and the type of the mixed-frequency test applied. Therefore, there is a direct relation between the stator current and the stator copper loss. As long as the rms stator current during the test is the rated value of the motor, the stator copper loss can be taken as the full-load loss. The stator current was considered to be at the rated value for all "four cases" given in the chapter 5. The stator copper loss is equal to the full-load loss. As seen from Fig. 6.8.1-1, for the simulated machine (12.6 MVA), the instantaneous stator copper loss ($P_s(t)=3I_s^2(t)R_s$) is varying in the positive area having a

maximum instantaneous power of 0.084518 MW (0.00670 p.u.) and a minimum instantaneous power of 0.014039 MW (0.00111 p.u.) with an average value of 0.0520879 MW (0.00413 p.u.).

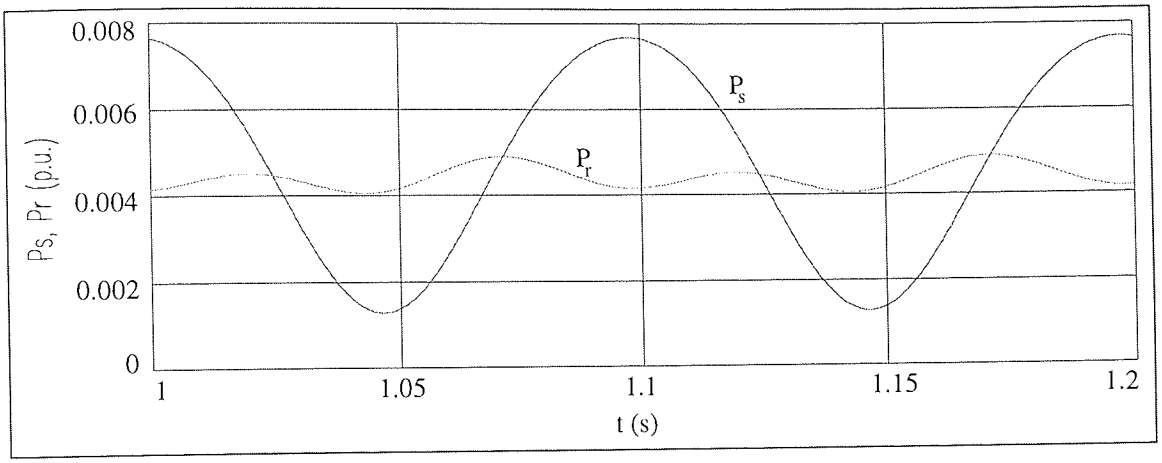

Fig. 6.8.1-1 Stator and rotor copper losses for case 1 (V_1 = 1.0 p.u., f_1 = 1.0 p.u., V_2/V_1 = 0.083907, f_b = 10 Hz).

6.8.2. Rotor Copper Loss

Since the rotor deep-bar effects were not considered, the rotor resistance is constant and the rotor copper loss is varied with respect to the rotor currents. As shown in chapter 5, for all four cases of the mixed-frequency test, the rotor current is varied with a beat frequency of f_b. In cases 1 and 3, at specific beat frequencies, it is possible to obtain the rated rotor current. The instantaneous rotor copper loss ($P_r(t)=3I_r^2(t)R_r$) for case 1 is shown in Fig. 6.8.1-1. It has a maximum instantaneous power of 0.053928 MW (0.00428 p.u.) and a minimum instantaneous power of 0.044553 MW (0.00353 p.u.) with an average value of 0.048522 MW (0.00385 p.u.) for a particular machine of 12.6 MVA.

If the rotor deep-bar effects are considered, the effective rotor AC resistance changes as the rotor slip frequency is varied. As an example of the change of the rotor resistance, the ratio of R_{ac}/R_{dc} was quoted as 7.0 at the rated frequency of 50 Hz, and 1.75 during the mixed-frequency test (Peebles Electrical Machines), so that the rotor copper loss is increased above the full load value.

6.8.3. Windage and Friction (Mechanical) Losses

Windage and friction losses are related to the rotor speed. Therefore, since the rotor speed is at the rated value, the mechanical loss is the normal full load value. The rotor speed for case 1 is illustrated in Fig. 2.3-4b. Although it is varying sinusoidally, its average value was found to be 1.0 p.u., which is the same for all other cases of the mixed-frequency test. Because the mechanical loss torque is not a linear function of the speed, it is important that speed fluctuations are kept reasonably small.

6.8.4. Iron (core) Loss

Since the main power supply alone feeds the motor with the rated values, the iron loss will then be the normal full load value. The auxiliary supply will further increase the iron loss due to the increment of the resultant stator voltage. Thus the total iron loss will be slightly higher than full load value (Peebles Electrical Machines). In the model of an induction machine given in appendix 2, the core loss was represented with a resistance (R_{sc}). Therefore, the total core loss is the square of stator voltage divided by R_{sc}. Fig's 5.4-2c, 5.5-2b, 5.6-2c and 5.7-2c show the variation of stator voltages with respect to the beat frequencies for all the cases of the mixed-frequency test. In the case of using an iverter as a mixed-frequency power supply, the core losses will be incresead further due to the high swithing frequency of the inverter.

6.8.5. Stray Load Losses

The stray-load losses are additional core losses, caused by the increase in air-gap leakage fluxes with load, and by the high frequency pulsations of these fluxes (Alger et al. (1959), Alger (1970), Bourne (1989)). Christofides (1965) and Jimoh et al. (1985) defined the stray load losses of an induction motor as the difference between the total power loss of the machine on load and the losses determined by the loss-segregation.

$$P_{load\text{-}loss} = P_t - (P_{f+w} + P_{fe1}) - P_{c1} - P_{c2} \qquad (4.5\text{-}1)$$

where

P_t = Total loss of the machine on full load,

P_{few} = Friction and windage losses deduced from the no-load test,

P_{fe1} = Stator core loss deduced from the no-load test,

P_{c1} = Stator copper loss on full load,

P_{c2} = Rotor copper loss on full load.

From above it is clear that the stray-load losses occur in both stator and rotor circuits of the machine as additional core losses. In terms of the mixed-frequency test, the accuracy of the load-losses depends on the accuracy of the other segregated losses given above.

6.8.6. Identification of Losses of the Test Machines

In this section, the losses of both the squirrel-cage induction machine and the slip-ring induction machine used in the test were identified using test results.

Normally some information about the machine is given on the name plate of the machine. This includes the number of phases, rated output power, stator voltage, full-load stator current, number of poles, connection type, full-load rotor speed, frequency and rated temperature. Other information about the machine (power factor, input power, output torque, efficiency, and total losses) can be calculated using these values. The separation of losses from the total loss is related to the machine parameters (stator resistance, rotor resistance, resistance which represents core loss and inertia). Therefore, since a good estimation of the machine parameters has already been achieved, the distribution of the losses will be reasonably accurate.

In section 6.2, the full-load values of the squirrel-cage induction machine were given. When the stator voltage is 415.2 Volts and the stator line current is 7.2 Amperes, the rotor phase current is 3.32 Amperes and the rotor speed is 302.4 Rad/s. The input power of the machine was calculated using the stator line voltage, the stator line current and the power factor (or phase angle between voltage and current) of the machine. The phase angle was found to be

-27° by using the instantaneous recorded voltage and current as illustrated in Fig. 6.2.1-3. Using this angle, the input power was calculated as to be 4611.28 Watts in section 6.2-1 and the efficiency of the motor was calculated as to be 86.74 % in equation (6.2.1-3). The total loss of the squirrel-cage induction machine was 611.28 W. The distribution of the losses of the squirrel-cage induction motor is given in Table 6.8.6-1.

In section 6.6, the full-load values (stator line voltage, line stator current, rotor current and rotor speed) of the delta connected slip-ring induction machine were given as 230 Volts, 11.36 Amperes, 12.6 Amperes and 148.9 Rad/s respectively. The phase angle was calculated from the instantaneous voltage and current waveform given in Fig. 6.6-1. The input power of the machine was also calculated using voltage, current and phase angle as to be 4184 Watts, therefore the efficiency of the machine was found as to be 78.87%. If the output power, 3300 Watts, is subtracted from the input power, then the total loss of the motor is found as to be 884 Watts. By using the parameters of the motor given in section 4.7, separation of the losses can be found as given in Table 6.8.6-1.

Power (Watt)	**Squirrel-cage induction machine**	**Slip-ring induction machine**
Total input power	4661.28	4184.00
Output power	4000.00	3300.00
Total loss	***611.28***	***884.00***
Stator copper loss	269.56	205.22
Rotor copper loss	102.50	389.20
Core loss	121.41	90.14
Mechanical loss	59.27	157.5
Stray load loss	58.54	41.94

Table 6.8.6-1 Distribution of the losses of the both squirrel-cage and slip-ring induction motors.

Distribution of power losses of both the squirrel-cage and slip-ring induction motors are shown as pie chart in Fig's. 6.8.6-1 and 6.8.6-2 respectively.

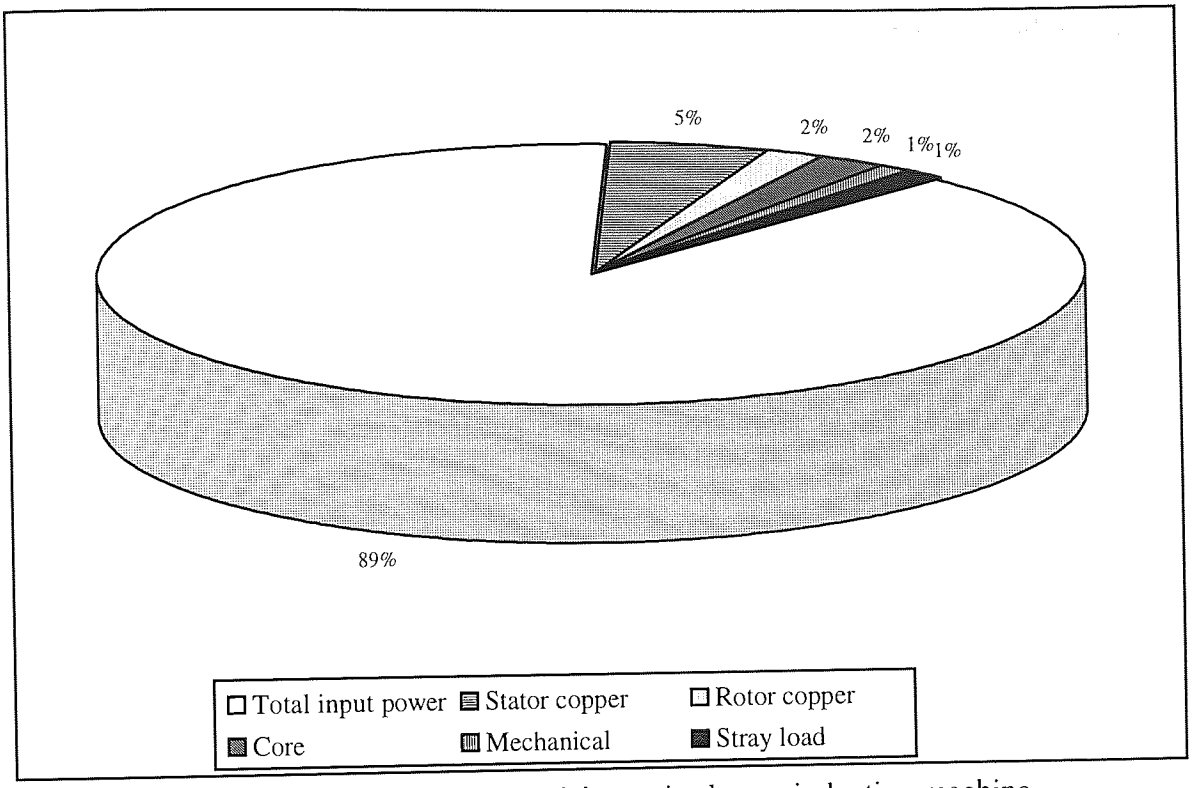

Fig. 6.8.6-1 Distribution of power losses of the squirrel-cage induction machine.

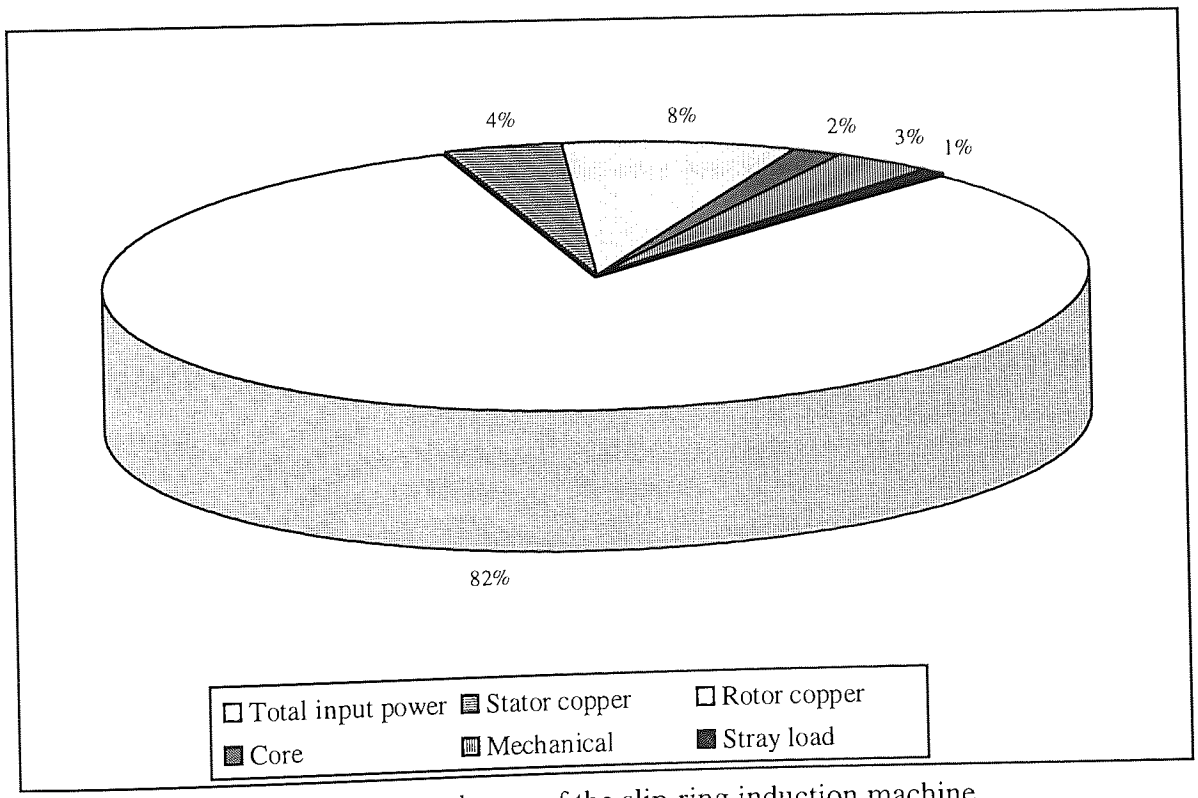

Fig. 6.8.6-2 Distribution of power losses of the slip-ring induction machine.

6.9. Summary

In this chapter, experimental work comprising full-load tests and mixed-frequency test, on two different induction motors, was explained in detail. One of the motors had a squirrel-cage rotor and the other had a wound rotor.

First of all, full-load tests of both motors were given. The full-load voltage, current, speed and temperature rise from different points of the machine were analysed. This was followed by two different modes of the mixed-frequency test namely VVVF and CVVF tests. The losses of both motors were calculated and the distributions of the losses were given in detail.

The temperature rise results obtained from the mixed-frequency tests were compared with the full-load values and good agreement was achieved. It was shown that, during the mixed-frequency test, since the stator voltage, the stator current and the rotor speed are only approximately equal to their rated values, the input power measured is not exactly equal to the rated full-load power of the motor. However, the stator copper loss and mechanical loss, if the rotor is running at about rated speed, can be excepted as equal to their rated values for both VVVF and CVVF tests. The core loss is also equal to its rated value in CVVF test because the voltage applied to the machine is kept constant during the test, but it was found to be less than the rated value for the VVVF test as, given in Table 8.3-1. The rotor copper loss is equal to its rated value for the VVVF test, but was found to be less for the CVVF test.

CHAPTER 7

ALTERNATIVE NEW METHODS OF FULL-LOAD TEMPERATURE RISE TESTING OF INDUCTION MACHINES

7.1 Introduction

This chapter introduces mainly two new alternative methods of full-load temperature rise testing of induction machines. In the first method, a "variable inertia test" is proposed. In the second method, a "new cheaper mixed-frequency test-rig for a lower current supply" is suggested.

7.2. The "Variable Inertia Test" For Full Load Temperature Rise Testing Of Induction Machines

Full load temperature-rise testing of induction machines can be done in various ways including the "back to back test", the "phantom-loading test" and various forms of what is referred to in this thesis as the "mixed-frequency test". This chapter proposes a new method of testing called the variable inertia test. The proposed test is purely mechanical in nature, it does not require any electrical connection of the test machine to any other machine and it can be very efficient in terms of space. It may, therefore, be attractive to manufacturers of large electrical machines. A simulation of this test indicates that full-load losses can be achieved relatively simply.

7.2.1. Full-Load Temperature Rise Testing of Induction Machines

The testing of induction machines for full load temperature rise is an inherent part of the approval procedure for these machines. To carry on this test exactly, the machine must be mechanically coupled to a load machine which will draw full load mechanical torque from the induction machine running at rated speed. This "exact test" is expensive for the manufacturer to set up for three reasons :

(1) It is time- and resource- consuming to mechanically couple each test machine to the load machine.

(2) It is expensive to retain and maintain a load machine having a high capital value with an associated facility for dumping (or converting) power. The cost for space alone can be significant.

(3) The electrical power drawn by the test machine is expensive (unless most of it is returned to the supply).

This chapter describes a new approximate test for full-load temperature-rise of induction machines called the "variable inertia test" which has an interesting set of advantages and disadvantages. The principal disadvantage must be that it does require mechanical coupling of the test machine to a load. Against this, however, is the fact that the "load" is very simple and compact compared with an electrical load machine and the only net electrical power drawn from the supply is that which appears as losses in the induction machine. By having a large free-running inertia, the variation in rotor speed can be very small indeed as the results in a later section show.

7.2.2. The Proposed Test

The physical layout of this new test is shown schematically in Fig. 7.2.2-1. It comprises three essential elements:

(a) the machine on test

(b) a gearbox having a non-constant speed-ratio

(c) a free-running inertia

The test proposed here is closely related to "mixed frequency test" family. The essence of the test lies in the non-constant speed-ratio gearbox which causes the inertia (referred to the machine shaft) to be a smooth function of the total rotation angle of that shaft. This

variation causes a varying shaft-torque which in turn results in a varying rotor speed and hence a finite mean absolute value of slip.

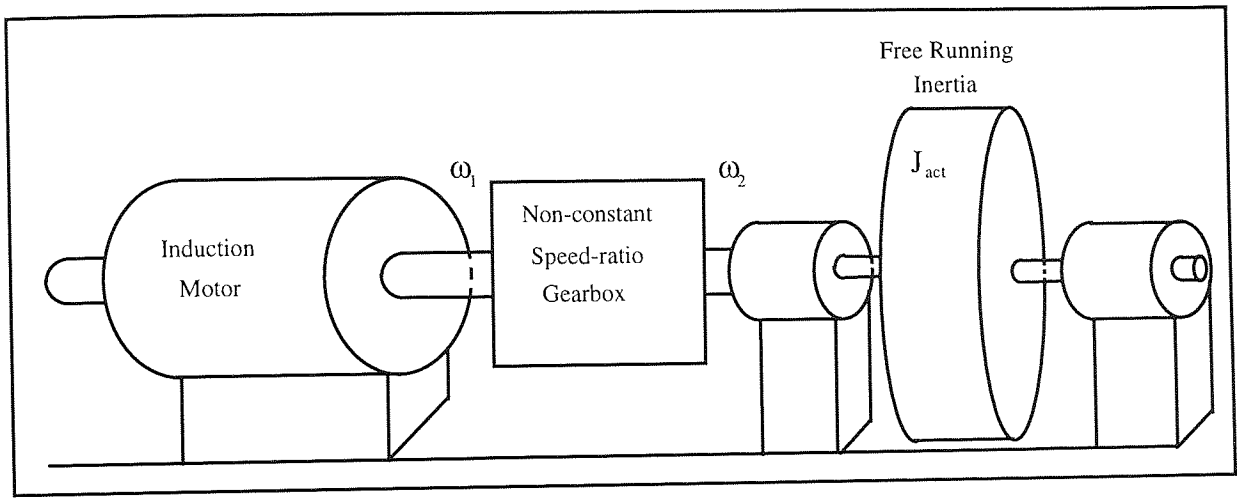

Fig. 7.2.2-1 Schematic diagram of proposed test arrangement.

The speed-ratio of the gearbox is related to the total angle of rotation, θ, of the machine shaft and depending on the exact nature of the changing-ratio gearbox used, this variation would be approximated by (7.2.2-1) in which it is implicitly assumed that speed-ratio (and hence the referred-inertia) will undergo one complete cycle for each ten revolution of the machine shaft.

$$R(\theta) = \frac{\omega_2}{\omega_1} \cong R_0 + R_1 \sin\left(\frac{\theta}{10}\right) \qquad (7.2.2\text{-}1)$$

where

R, R_0, R_1 = speed ratio parameters of the gearbox

ω_1 and ω_2 = angular speeds of the shaft on the two sides of the gearbox

θ = angle of the rotor

It is beyond the scope of this chapter to discuss in detail the many conceivable implementations of a gearbox having a non-constant ratio but two possible arrangements

are mentioned here. One uses an epi-cyclic gearbox in which the carrier for the planet-gears is rocked slowly forwards and backwards undergoing one complete cycle in every ten revolution of the shaft of the load machine. The other involves a conventional 20:1 speed-reduction gearbox connected to the shaft of the test machine with the low-speed side of this gearbox being connected through a Hooke's Joint to a large free-running inertia. In both cases it is relatively simple to adjust the actual value of the free-running inertia (by bolting-on or removing additional mass) and it is also possible to adjust the amount of variation in the speed-ratio. What cannot be adjusted easily is the period of the speed ratio function.

It should be noted that losses will accure in the gearbox which may be the same order as the induction motor losses, but it is possible to measure the net mechanical power flowing out of the induction motor using torque and speed transducers.

The referred inertia at the machine shaft-end is $J_L(\theta)$ given by (7.2.2-2) and its derivative with respect to θ is given in (7.2.2-3).

$$J_L(\theta) = J_{act} R^2(\theta) = J_{act}\left[R_0^2 + 2R_0R_1\sin\left(\frac{\theta}{10}\right) + R_1^2\sin^2\left(\frac{\theta}{10}\right)\right] \qquad (7.2.2\text{-}2)$$

$$\frac{dJ_L}{d\theta} = J_{act}\left[\frac{2R_0R_1}{10}\cos\left(\frac{\theta}{10}\right) + \frac{R_1^2}{10}\sin\left(\frac{\theta}{5}\right)\right] \qquad (7.2.2\text{-}3)$$

where

J_L, J_{act} = load inertia referred to motor shaft and external free running inertia

In a mechanical system, the kinetic energy can be calculated as:

$$V = \frac{1}{2}J(\theta)\left(\frac{d\theta}{dt}\right)^2 \qquad (7.2.2\text{-}4)$$

where

V = Energy

J = Inertia of the system

The derivative of the kinetic energy gives the power flowing into the mechanical system- assuming that no significant energy is stored elastically. This must be equal to the rate at which work is being done on the system by the torque imposed.

$$\text{Power} = T\left(\frac{d\theta}{dt}\right) = \frac{dV}{dt} = \frac{d}{dt}\left(\frac{1}{2}J(\theta)\left(\frac{d\theta}{dt}\right)^2\right) \qquad (7.2.2.\text{-}5)$$

$$T\left(\frac{d\theta}{dt}\right) = \left[\left(\frac{1}{2}\frac{dJ(\theta)}{dt}\left(\frac{d\theta}{dt}\right)^2\right) + J(\theta)\left(\frac{d\theta}{dt}\right)\left(\frac{d^2\theta}{dt^2}\right)\right] \qquad (7.2.2.\text{-}6)$$

$$T\left(\frac{d\theta}{dt}\right) = \left[\left(\frac{1}{2}\frac{dJ(\theta)}{d\theta}\left(\frac{d\theta}{dt}\right)^3\right) + J(\theta)\left(\frac{d\theta}{dt}\right)\left(\frac{d^2\theta}{dt^2}\right)\right] \qquad (7.2.2.\text{-}7)$$

Using arguments based on the conservation of energy given above, it is found that the shaft torque, T, at the drive end of the induction machine is related to the total shaft angle θ, by (7.2.2-8).

$$T = \left[\left(\frac{1}{2}\frac{dJ_L(\theta)}{d\theta}\left(\frac{d\theta}{dt}\right)^2\right) + J_L(\theta)\left(\frac{d^2\theta}{dt^2}\right)\right] \qquad (7.2.2\text{-}8)$$

When (7.2.2-8) is combined with the set of equations giving the dynamic behaviour of the induction machine (i.e. Çolak et al. (1993), EPE'93), a simulation of the "variable-inertia test" can be performed.

7.2.3. Simulation of the Variable Inertia Test

Using a particular set of parameters for a large 12.6 MVA induction machine, whose parameters are given in appendix 1, and a fixed mean-speed ratio R_0 = 0.2, a number of

simulations were carried out to establish a combination of J_{act} and R_1 which would produce rated copper losses on both the stator and the rotor. These values were found to be J_{act} =

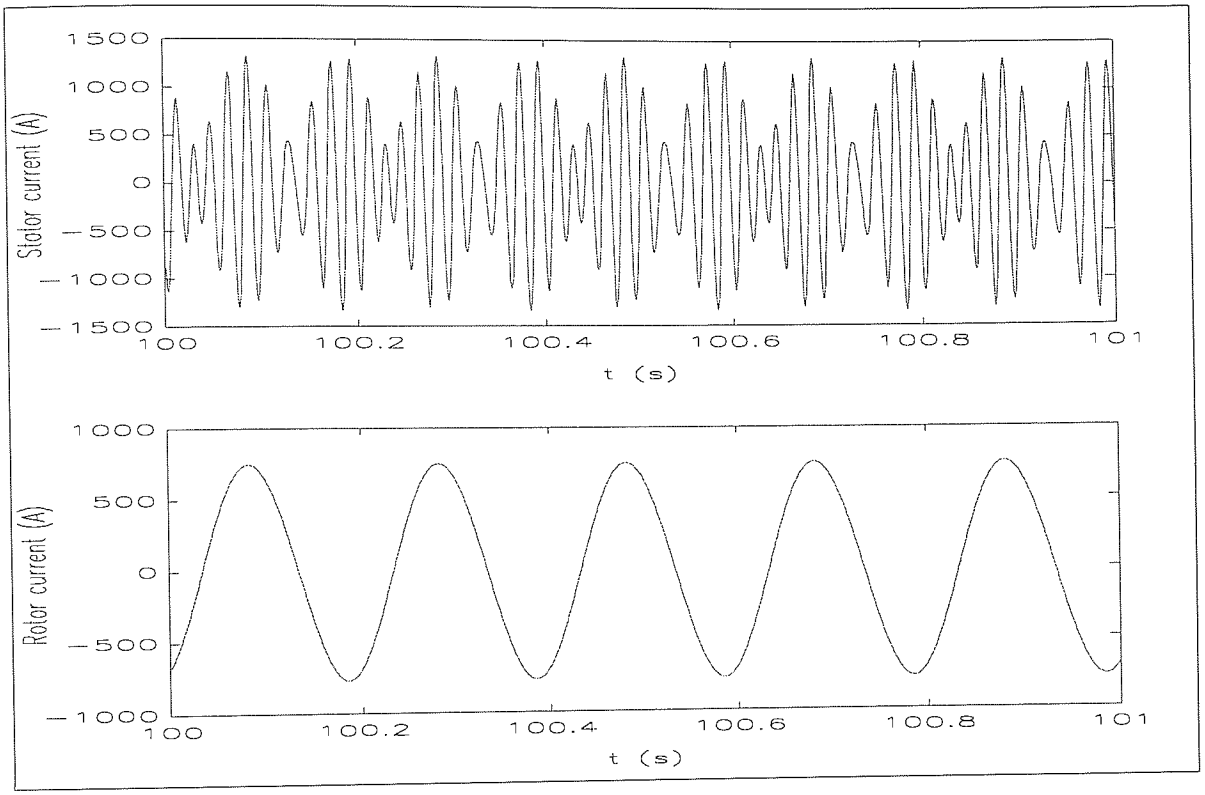

Fig. 7.2.3-1 Waveforms of stator and rotor currents.

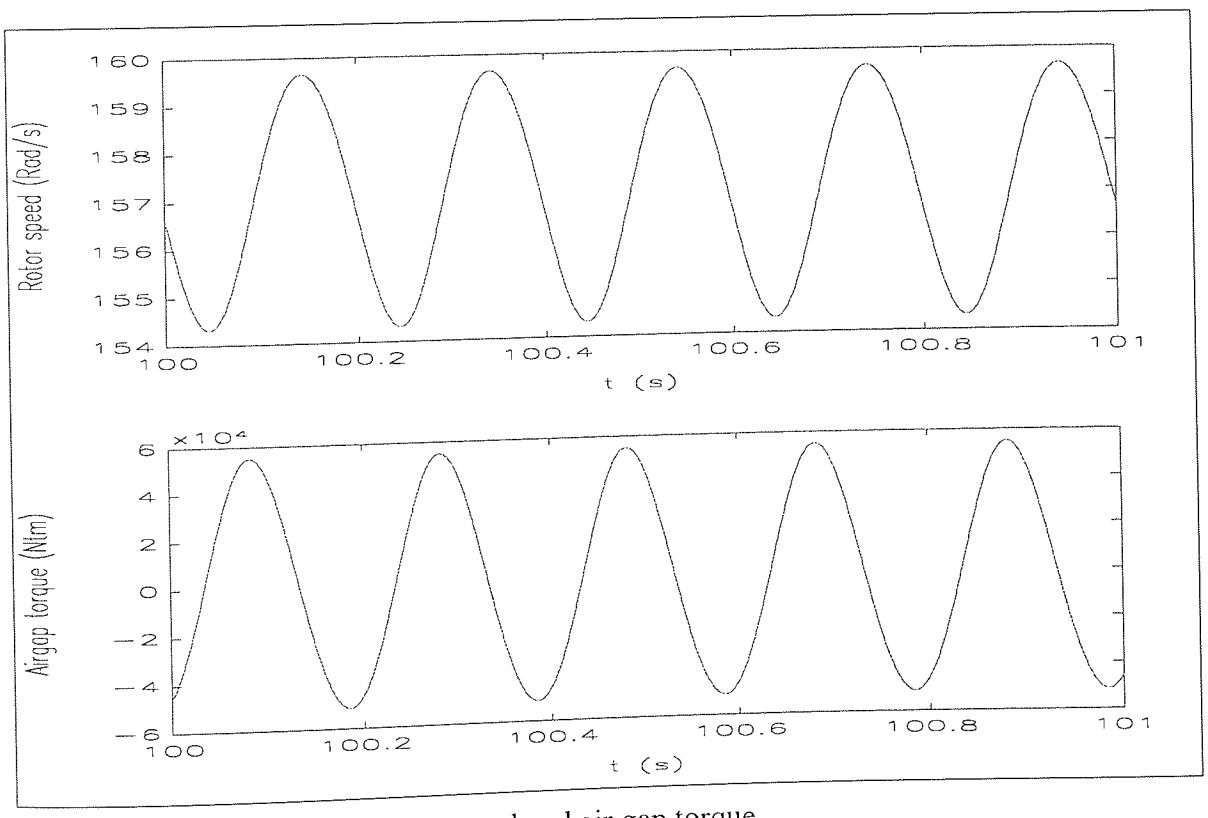

Fig. 7.2.3-2 Waveforms of rotor speed and air gap torque.

6250.0 kgm^2 and R_1 = 0.06. The steady-state behaviour of the system with these values of inertia and speed-ratio variability is shown on Fig's. 7.2.3-1 and 7.2.3-2. The effect of varying the referred inertia is found to be very similar to the effect of the usual mixed-frequency test.

7.2.4. Summary

The testing of induction machines to determine the full load temperature rise can be done by smoothly varying the referred-inertia of the load using a special gearbox between the machine and an external free running inertia. This test is primarily mechanical and does not require any electrical connection of the test machine to other machines. The fact that the values of the free-running inertia and the variation in speed ratio of the gearbox can both be influenced relatively easily means that in many cases losses can be disposed accurately on rotor and stator.

7.3. A New Mixed-Frequency Test-Rig For A Lower Current Supply

In chapter 1, several established methods of testing the induction machine for full-load temperature rise without coupling it mechanically to a load machine were introduced. A large subset of testing methods was found to be members of a family of tests which have been collectively named mixed-frequency tests. However, different names have been given to these methods depending on the authors' preference and the particular voltage waveform employed. So far, all of the methods discussed have had the accuracy of the test as a primary concern.

The essence of the mixed frequency test is that the test machine runs alternately as a motor and as a generator. The long term rms current flowing between the supply and the machine is quite high being approximately equal to rated current. Therefore, although the net average power flowing into the test machine is equal to the total losses of the machine, the connection to the supply must be rated for currents which may be twice the rated current of

the machine. If the correct rms currents are to flow in the rotor of the induction machine, there is no alternative to transmitting energy across the airgap. The ideal testing-station for large induction machines in a manufacturers' works would be one which did not involve drawing large currents from the supply. This requires that the testing-station itself has some facility for the controlled storage and release of significant amounts of energy.

This chapter proposes two cheaper testing methods whereby the mixed-frequency testing can be conducted on a large induction machine without drawing substantial currents from the supply. In the one, a resonant bank is used between the inverter and the main supply as an energy storage. In the other, an ideal electromechanical energy storage mechanism is proposed.

7.3.1. Mixed Frequency Testing Using a Resonant Link Inverter

Resonant link inverters are becoming increasingly popular as drives for AC machines in conventional applications because of their reduced switching losses. In the context of mixed-frequency testing, these inverters appear initially to have two additional advantages :

1. The losses in the machine can be computed more accurately because the sharp voltage fronts associated with conventional switching arrangements are much reduced in the resonant link devices and the significant additional losses in the machine due to these fronts can be avoided.

2. The resonant bank could potentially be used to store and release energy for the mixed-frequency test so that the exchange of energy with the supply (and the corresponding high currents) can be largely avoided.

Fig. 7.3.1-1 shows a block-diagram of a resonant-link voltage-source inverter connected to an induction machine. It is relatively straightforward to use a resonant-bank inverter directly

to drive a mixed-frequency test of an induction machine if the energy-storage possibility is not pursued. The example presented here relates to one particular large induction machine (12.6 MVA) represented by the parameters given in appendix 1.

From trial simulations of this machine on the varying voltage, varying frequency test, it can be established that rated stator current can be caused to flow for $\delta_T = 7.648$ and $\Re = 0.2$. A voltage waveform can readily be generated using a standard natural sampling PWM switching-strategy for a constant-voltage DC link inverter such that the low-frequency content of this voltage waveform closely matches the desired voltage waveform.

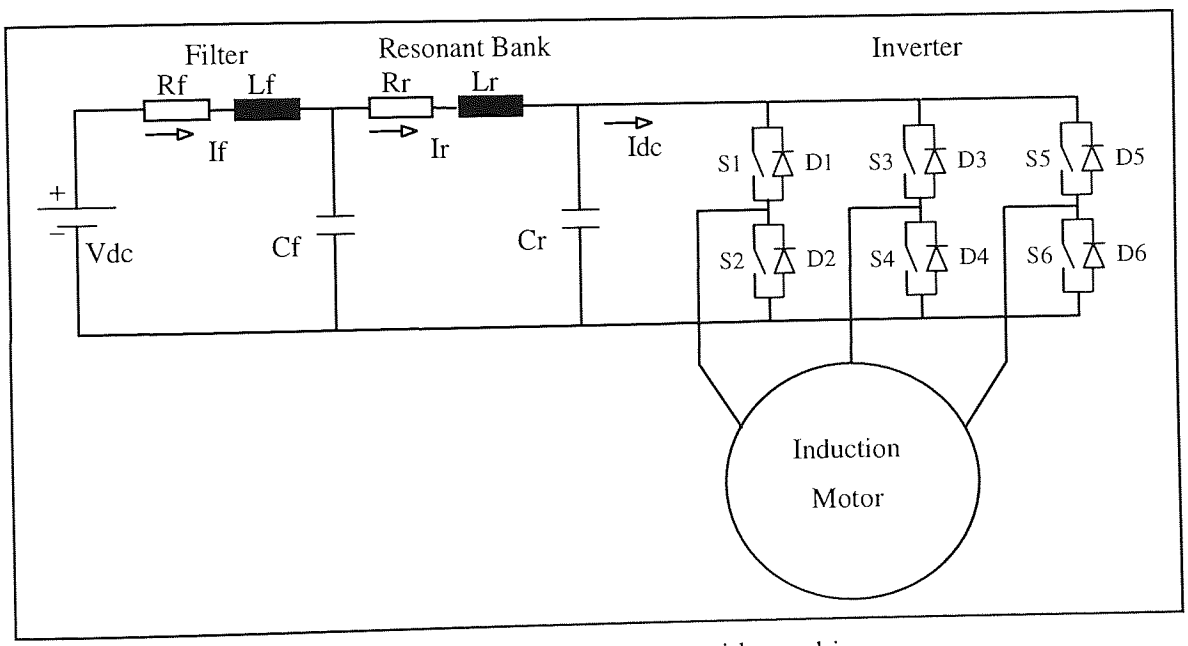

Fig. 7.3.1-1 Block diagram of voltage source inverter with machine.

The inverter switching frequency and the values of components used in the filter and resonant circuits are chosen according to the machine parameters for the simulation purposes as given below. They can be optimised further for the experimental purposes, but this is out of scope of this study.

$V_{dc} = (11000)\sqrt{(2/3)}$ V $\quad f_r = 5.0e3$ Hz

$R_f = 4.0e\text{-}3\ \Omega$ $\quad R_r = 5.0e\text{-}3\ \Omega$

$L_f = 5.0e\text{-}5$ H $\quad L_r = 6.7547e\text{-}5$ H

$C_f = 5.0$ F $\qquad\qquad$ $C_r = 1.5e\text{-}5$ F

Using a resonant-link inverter requires that the dynamic elements of the inverter be simulated as well as the machine's own dynamics if an accurate prediction of the system behaviour is to be obtained. The equations describing the filter and resonant-bank of the inverter are given concisely below.

$$\left.\begin{aligned} \frac{di_f}{dt} &= \frac{\left(V_{dc} - i_f R_f - v_{cf}\right)}{L_f}, \quad \frac{dv_{cf}}{dt} = \frac{i_f + i_r}{c_f} \end{aligned}\right\} \qquad (7.3.1\text{-}1)$$

$$\left.\begin{aligned} &\frac{di_r}{dt} = \frac{\left(v_{cf} - i_r R_r - v_{cr}\right)}{L_r}, \quad \frac{dv_{cr}}{dt} = \frac{i_r + I_{dc}}{c_r} \\ &\text{if resonant capacitor is short circuited by the inverter ;} \\ &\frac{di_r}{dt} = \frac{\left(v_{cf} - i_r R_r\right)}{L_r}, \quad \frac{dv_{cr}}{dt} = 0.0 \end{aligned}\right\} \qquad (7.3.1\text{-}2)$$

A switching strategy can be chosen for the resonant bank inverter based on shifted natural sampling PWM (Çolak et al. (1994)) such that a voltage waveform is generated having approximately the desired low-frequency content.

The results of simulations of the conventional inverter and the resonant bank inverter (filter voltage and current, bank voltage and current, inverter output voltage and DC link current, rotor speed and stator current, airgap energy and input power) for this machine are presented in figure 7.3.1-2.

No attempt was made in the above simulation of the resonant-bank inverter to cause the resonant bank of the inverter to act as an energy store which would swap energy with the induction machine and thereby isolate the supply from such energy exchanges. However, it

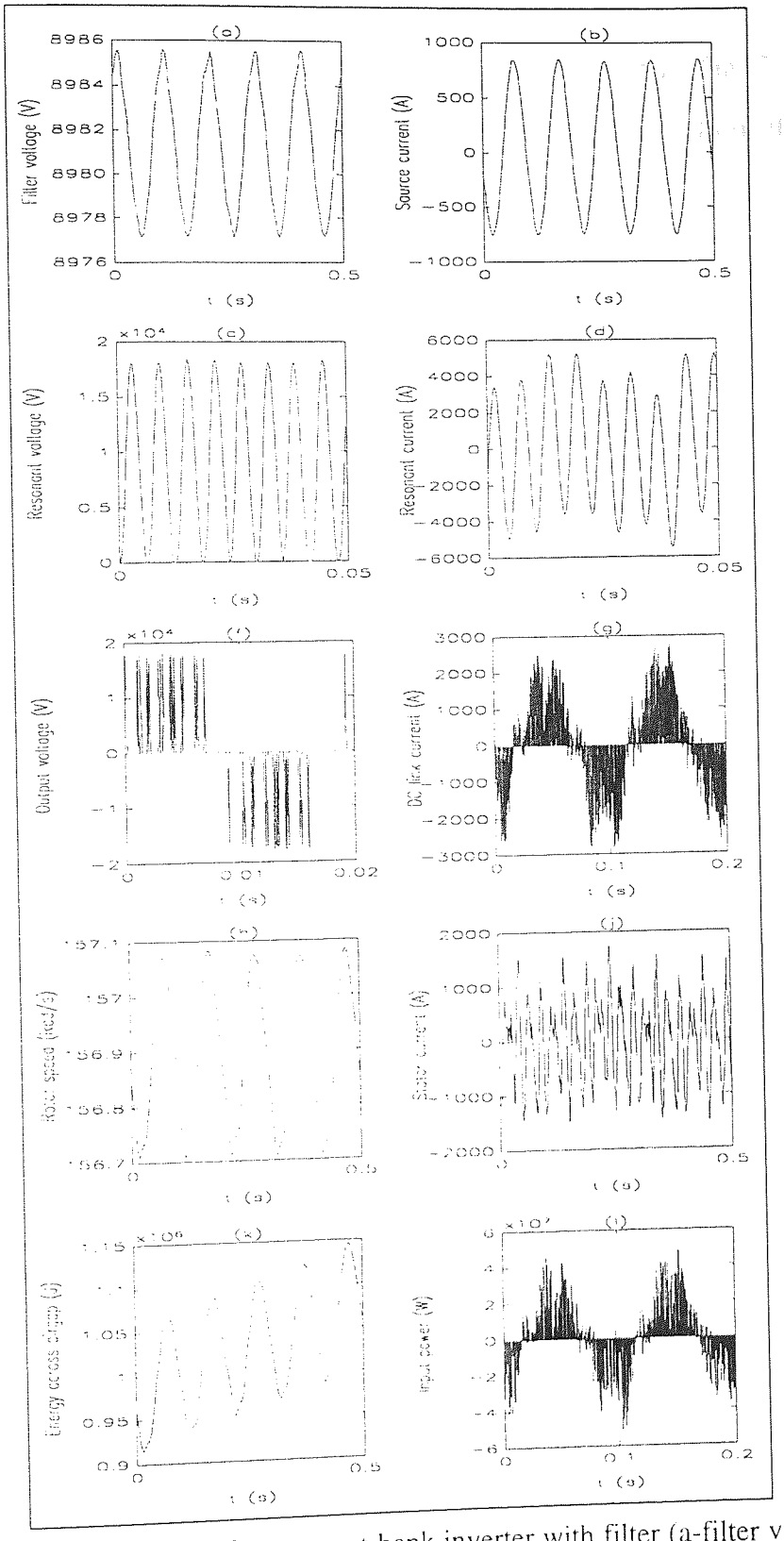

Fig. 7.3.1-2 Simulation results for resonant-bank inverter with filter (a-filter voltage, b-filter current, c-bank voltage, d-bank current, f-inverter output voltage, g-DC link current, h-rotor speed, j-stator current, k-airgap energy, l-input power of the machine).

is evident from the graph of net energy transferred across the airgap (Fig. 7.3.1-2) that a bundle of energy as large as 85 kJ must be fed into and taken out from this induction machine several times per second if the supply is not to be required to act as an energy store. Moreover, in a simple resonant circuit containing inductance and capacitance, energy stored within the circuit over several cycles of a resonance frequency must be stored completely in the inductances at one instant of the resonant cycle and completely stored in the capacitances at another instant. The cost of providing sufficient capacity in inductance and capacitance to store quantities of energy of this order is prohibitively large. This much energy could be stored in battery banks at realistic levels of expense for periods of hours but it could not be stored and released at the rates required for a mixed-frequency test (5 Hz to 15 Hz usually).

7.3.2. The Ideal Mixed-Frequency Testing Station

It is well known that storage of energy in a mechanical form is frequently several orders of magnitude cheaper than storage in other forms. Saraiva and Freris (1979) proposed the use of electromechanical filter units as economical alternatives to purely electrical filters. They designed and tested a vibrating unit. One of the principal drawbacks which they identified with their filter was the fact that it is far more difficult to obtain a "lumped-parameter" mechanical system than it is to obtain a lumped-parameter electrical system and therefore, a system which had only one clear resonant peak could not be realised.

Mixed-frequency testing of induction machines is possibly an ideal application for electromagnetic energy-storage units and vice-versa. Fig. 7.3.2-1 shows schematically how an electromagnetic energy-storage unit could be used to exchange energy across a "DC-link" through an inverter unit and connected induction machine.

Fig. 7.3.2-2 presents a schematic of a suitable homopolar electromagnetic energy storage unit. It comprises two equal lumps of mass (each one M kg) connected by stiff springs (total

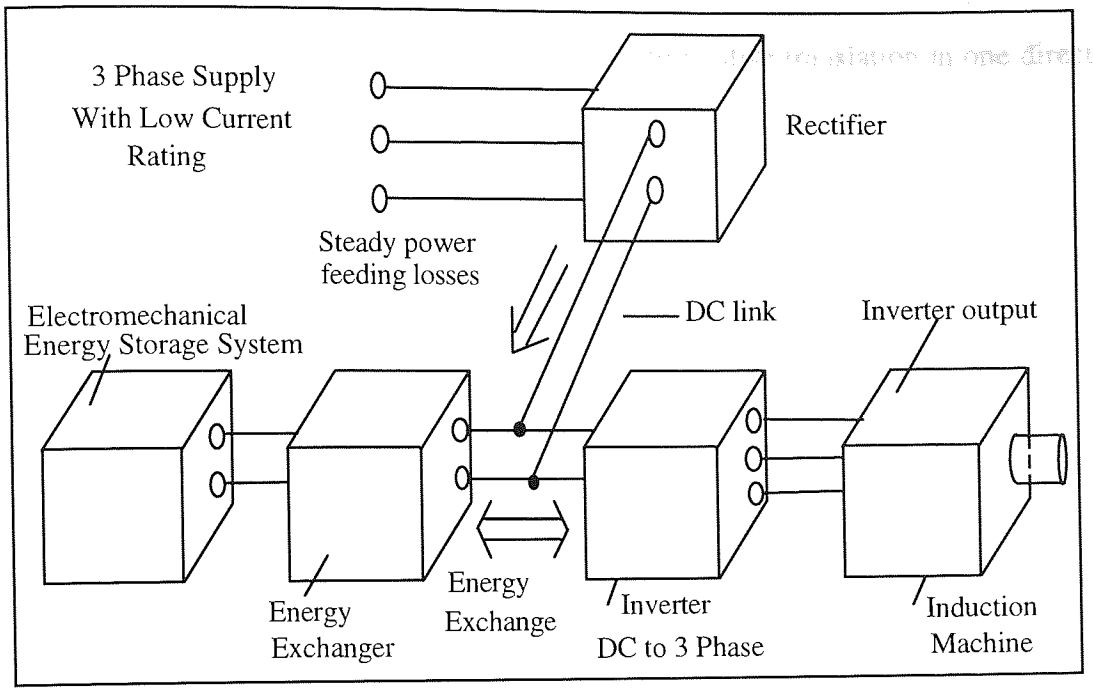

Fig. 7.3.2-1 Illustration of role of elements in proposed mixed-frequency testing method.

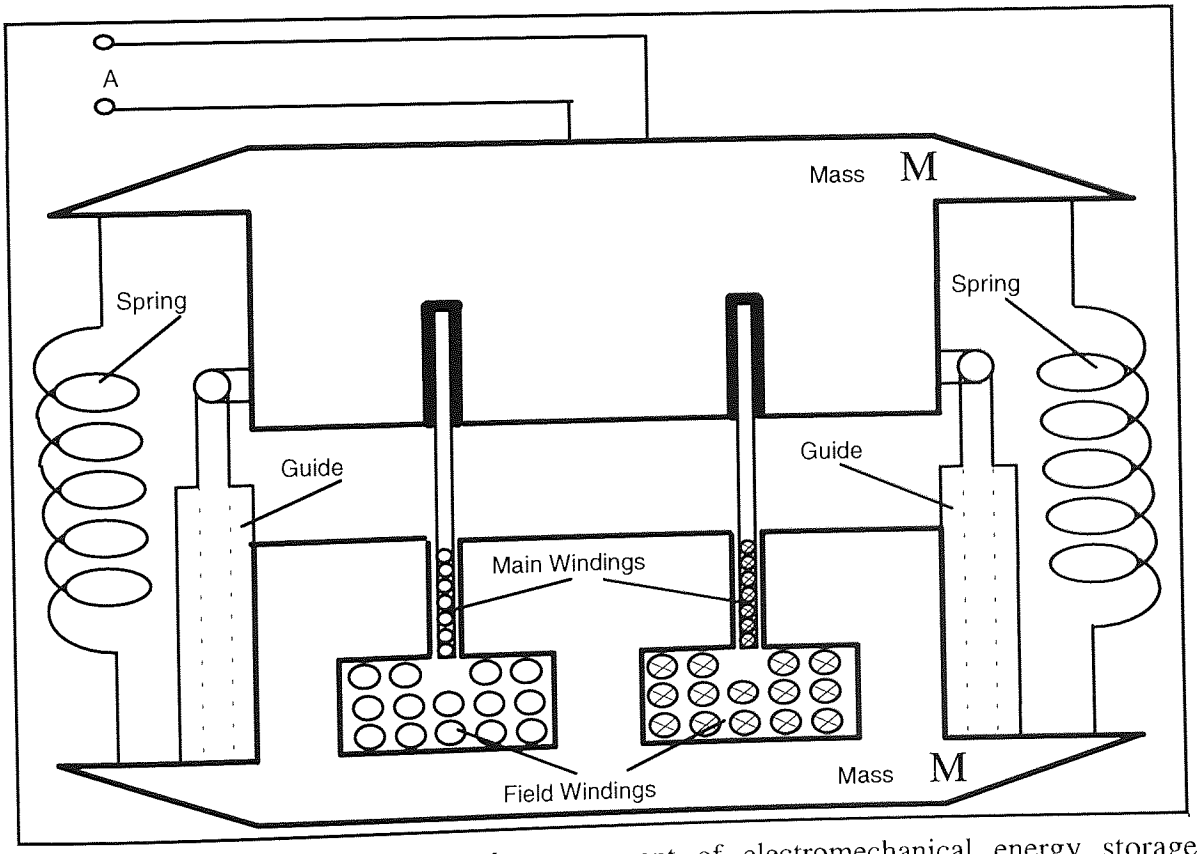

Fig. 7.3.2-2 Schematic of physical arrangement of electromechanical energy storage systems.

stiffness of SN/m) and constrained by guide elements to relative translation in one direction only and no relative rotation.

The electromagnetic part of the "machine" is concentrated at one end with field-windings providing a homopolar field, which drives flux through an airgap in the lower mass. The flux passes across the main windings which are formed into a rigid tube and this is rigidly attached to the upper mass. Some electromagnetic shakers operate on a similar principle. Two masses are used so that the unit can be supported on very flexible supports and thereby transmit no significant force into any other body which might dissipate the energy. This contrasts with the filter of Saraiva and Freris (1979) which was fixed-down rigidly on one side. The ideal fixing-location for this system would be at the central plane of the springs where translations are zero for the first natural mode of vibration.

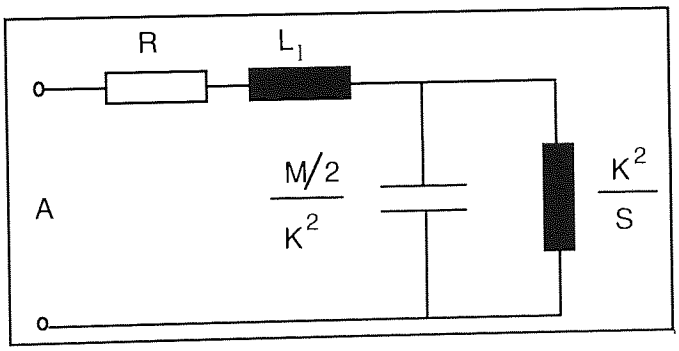

Fig. 7.3.2-3 Equivalent circuit of electromechanical energy storage systems.

The equations governing the dynamics of this system are given below and from these, it is clear that an equivalent circuit of the form of Fig. 7.3.2-3 applies in representing this unit.

$$\left.\begin{aligned} F = Ki_a &= S2u + M\frac{d^2u}{dt^2} \\ V_a &= Ri_a + L_1\frac{di_a}{dt} + EMF \\ EMF &= 2K\frac{du}{dt} \end{aligned}\right\} \qquad (7.3.2\text{-}1)$$

where

F = Force

i_a = Armature current

V_a = Applied voltage

L_l = Leakage inductance

R = Resistance

EMF = Back electromagnetic force

K = Machine constant

M = Mass

u = Vibration

S = Stiffness

An energy storage unit of this kind has the following advantages with respect to mixed-frequency testing of large machines :

1. The cost per MJ of energy stored is substantially lower than a purely electrical or electrochemical alternative.

2. Compared with a rotating electrical machine fixed to a large flywheel, this system can be virtually maintenance free. (The guides in the system need not necessarily involve sliding contact. In electromagnetic shakers, the guides are often based on a combination of flexure and twisting of sheet material).

3. The losses in this unit can be very small if a quality spring steel is chosen and if the connections between springs and masses are firm. Moreover, the average energy stored in the unit would normally be only 0.5 - 0.75 of the peak energy capacity.

4. The level of coupling between the terminals of the unit and the mechanical "part" of the unit can be relatively small. That is to say, it is not necessary that the main winding should be capable of injecting or extracting any more than a small fraction of the total energy capacity of the unit in a single cycle or part thereof.

It is useful, for interest, to put approximate values on such a unit which could be used for storing energy in a system for mixed-frequency testing machines such as the one described above.

The value of M can be set arbitrarily. Let M = 1000 kg. The total spring stiffness, S, determines the resonant frequency of the device. For a resonance of 500 Hz, S = 4940 MN/m. The energy stored in the device swings between strain energy (S.E.) in the spring and kinetic energy (K.E.) in the masses and the maximum amplitude of vibration can be determined either from an equation for either K.E. or S.E. To store 200 kJ, (Fig. 62.2-2k shows that a capacity of at least 85 kJ is necessary) an amplitude of vibration (u_{max}) equal to 4.5 mm peak is required. It is not appropriate to carry out a complete spring design here but it is useful to observe that a strain energy density of 1 MJ/m^3 is easily achieved with spring steel and therefore the volume of working steel in the springs (if they were to be made from steel) would be approximately 0.2 cubic metres (about 1560 kg). Clearly with such a design, suitable account should be taken of the amount of mass which the spring contributes to the "rigid-mass" at either end.

Devising a switching strategy (for both DC to 3 phase and DC to single phase inverters) which ensures that energy is exchanged with supply is not trivial if the switching strategy for the DC to 3 phase inverter is based on a desired low-frequency content of a voltage waveform. However, it is not necessary that a prescribed voltage waveform be imposed on an induction machine to conduct a mixed-frequency test. An alternative view of the mixed frequency test is possible as a test whereby an oscillatory power is imposed on the machine and where the rms power is equal to the rated power of the machine. This delivers a very representative test. If two current transducers are placed between the three lines to the machine, it is straightforward to determine, in real time, an average voltage vector which will deliver any desired "average" power to the machine - positive or negative. Clearly, whenever the power feed to the induction machine is positive, the same power should be

drawn from the electromagnetic energy storage device less the sum of the losses from the induction machine and the storage device.

7.3.4. Summary

It has been shown that the application of resonant link inverters as sources for mixed-frequency tests have been examined and found to be feasible although using the resonant bank of such inverters to store the quantities of energy which would be necessary to prevent drawing large currents from the supply has been shown to be impractical for large induction machines.

A system has been proposed, however, which utilises a special electro-mechanical energy-storage unit to store and release energy cyclically to counterbalance the energy flows to and from an induction machine on mixed-frequency test. Preliminary examination makes this system seem very attractive.

CHAPTER 8

CONCLUSIONS AND FURTHER STUDY

8.1. Conclusions

This study is about the mixed-frequency testing of induction machines to determine their temperature rise at full-load without mechanical coupling to a load machine. It consists of modelling, simulation and experimental work as well as alternative methods for the full-load temperature rise testing of induction machines. Three different induction machines, a 4 kW squirrel-cage induction machine, a 3.3 kW slip-ring induction machine and a 12.6 MVA squirrel-cage induction machine have been considered in this study. The experimental work was performed only on the smaller machines. The conclusions of this study are given chapter by chapter as follows.

In chapter 1, a detailed literature survey of the testing methods of induction machines was given. These testing methods are:

- Direct loading test
- Superimposed frequency test
- Back-to-back test
- Phantom loading test
- Forward short circuit test
- Mixed-frequency tests

All of these tests were explained and their respective advantages and disadvantages were summarised.

In chapter 2, a detailed historical background of the mixed-frequency testing of induction machines has been summarised, from 1921 up to 1993. In the literature reviewed, the mixed-frequency testing was applied to different sizes of machines from a few kilowatts to 12 MVA. Different supply arrangements for mixed-frequency testing of induction machines as well as the concepts of mixed-frequency testing have been given. In addition, the main parameters for the mixed-frequency testing have been explained. Further, besides the conventional mixed-frequency testing power supplies, low and high-frequency contents of voltage waveforms from inverters have been examined.

In chapter 3, a detailed analysis of the modelling of induction machines based on the phase co-ordinate model and d-q axis model were introduced. After explaining the advantages and disadvantages of these models, it was highlighted that the inverse of the inductance matrix of the induction machine in phase equation model was previously not known explicitly and required much computational time to evaluate numerically. The explicit form of the inverse of the inductance matrix was shown to exist and the simulation time almost halved as a result in appendix 2. The phase equation model was expanded by incorporating the core losses, saturation and the rotor deep-bar effects into the model in appendix 2. In addition to the phase equation model, chapter 3 gives the relative advantages and disadvantages of the d-q axis model. The advances reported in this chapter have been prepared for the publication in IEE, Part-B (Çolak et al. (1993)).

In chapter 4, the DC test, the no-load test and the locked-rotor test were explained and performed on the test motors using the main source. The no-load test of a squirrel-cage induction motor using an inverter was also performed at different frequencies and different levels of fluxing to calculate the motor impedance at different levels of voltages. The locked-rotor test was repeated at different voltages and frequencies using an inverter to calculate various locked-rotor impedances of the motor.

For the slip-ring induction machine, only the DC test, the no-load test and the locked-rotor test were performed. The run-up and the run-down tests were applied to both squirrel-cage and slip-ring induction motors to calculate the mechanical losses and the inertia of both machines. The inertia was established by measuring run-up and run-down rotor speeds in each case with and without an additional known inertia on the rotor shaft. As a result of the above tests, the parameters of both test motors were calculated. The method for parameter estimation developed in this chapter has been published (Çolak et al. (1993), Oxford).

In chapter 5, four different forms of the mixed-frequency test have been investigated. First of all, the voltage equations were given in closed form for each case of the mixed-frequency test. The relationship between the degree of torque modulation and the degree of voltage and frequency modulation was expressed in the equations given. It has been shown that, in order to produce rated stator current, the degree of torque modulation has different values at different frequency ratios for each form of the mixed-frequency test. In addition, the stator voltages and rotor currents were examined in detail for a given degree of torque modulation and frequency ratio. It was shown that the voltage waveforms in cases 2, 3 and 4 were symmetrical and their harmonics increased between 40 Hz and 50 Hz then decreases between 50 Hz and 60 Hz gradually in the same order with the same steps according to the same frequency ratio. Case 1 has only two harmonics at 45 Hz and 50, because, in case 1, one of the sinewaves, with a low amplitude at low frequency, was superimposed on to the other one which has rated amplitude at rated frequency.

In addition, the investigation on each case was carried on by running the simulation program for wide range of frequency ratio, from zero to 0.3. At each step of the frequency ratio, the simulation program was run several times with different values of the degree of torque modulation to get the rated rms stator current. After every successful running of the simulation program, the degree of torque modulation, the stator voltage and the rotor current were recorded. The variations of these three components with respect to the frequency ratio were found as an odd function of the torque-speed curve of an induction

motor. Each of the curves of these components has a deep point where they have their minimum values. The stator voltage was found to be above the rated value for case 1 and case 3, but it was found to be equal to the rated value for the case 2 and case 4. The rotor current was found to be close to the rated value at low frequency ratios below 0.02 for all the three cases. At about 0.04 the rotor current has its minimum value, but above 0.04 it starts to increase. In case 3, the rotor current always decreases as the frequency ratio increases. Furthermore, the effects of the increased inertia test on the rotor current are also given by increasing the rotor inertia to 10 and 25 times the normal inertia for case 1. It has been shown that the increased rotor inertia test provides the rated rotor current at almost every step of the frequency ratio. The results of this chapter were published (Çolak et al. (1993), Brighton).

In chapter 6, the experimental work, comprising full-load tests and mixed-frequency tests, on two different induction motors were explained in detail. First of all, the full-load tests of both motors were given. The full-load voltage, current, speed and temperature rise from different points of the machine were analysed. This was followed by two different modes of the mixed-frequency test namely VVVF and CVVF tests. The losses of both motors were calculated and the distribution of the losses was given in detail.

The results obtained from the mixed-frequency tests of the squirrel-cage induction motor were compared with the full-load values. The stator copper losses for both mixed-frequency tests were found to be same as the direct full-load test results due to the rated rms stator current drawn from the supply. The mechanical losses of both mixed-frequency tests were also the same as the full-load value providing that the rotor was running at rated speed. The VVVF test proved the rated rotor temperature rise as constant during the test. However, there might be slight changes in terms of temperature rises, but it was not possible to see these changes due to the high level ranges (5°C or 6°C) of the temperature labels used. The temperature rises of the core of the VVVF test was shown to be lees than the rated value, due to the variation of the stator voltage with respect to the beat frequency. The CVVF test

provided lower temperature rise of the rotor than the rated value but provided about the rated temperature rise of the core due to the rated stator voltage applied to the motor. The temperature rises within the slip-ring induction motor obtained from the VVVF test were found to be about the same as the temperature rises of the full-load test.

Chapter 7 includes two different alternative methods of full-load temperature rise testing of induction machines. In the first method, a new method of testing called the variable inertia test was proposed which is purely mechanical in nature and does not require any electrical connection of the test machine to any other machine. It can also be very efficient in terms of space and may, therefore, be attractive to manufacturers of large electrical machines. A simulation of this test indicates that full-load losses can be achieved relatively simply. A paper describing the "variable inertia test" has been accepted for publication (Garvey et al. (1994), IEE).

In secod method of chapter 7, two cheaper testing methods were proposed whereby the mixed-frequency testing can be conducted on large induction machines without drawing substantial currents from the supply. In one, a resonant bank was used between the inverter and the main supply as an energy store. It has been shown that the application of resonant link inverters as source for mixed-frequency tests has been examined and found to be feasible although using the resonant bank of such inverters to store the quantities of energy which would be necessary to prevent drawing large currents from the supply has been shown to be impractical for large induction machines. In the other, an ideal electromechanical energy storage mechanism was proposed to store and release energy cyclically to counterbalance the energy flows to and from an induction machine on mixed-frequency test. Preliminary examination makes this system seem very attractive. The findings of this chapter were published (Garvey et al. (1994), Paris).

8.2. Further Study

In this thesis the modelling, and the mixed-frequency testing of induction machines have been studied in detail. In addition, alternative methods of the modelling and the full-load temperature rise testing of induction machines have also been introduced and initial simulation results of the alternative full-load temperature rise tests have been given. Detailed analysis and applications of the modelling and the full-load temperature rise testing of induction machines have been recommended for the further study as explained in the following subsections.

8.2.1. Modelling of Machines

The modelling of induction machines, including the phase equation model, the d-q axis model, and the one phase T equivalent circuit model, have been given in detail in this thesis. The advantages and the disadvantages of the use of d-q axis model and the phase equation model were also discussed. In the simulation programs the basic phase equation model was used to solve the differential equations of the induction machine in their original forms; i.e. without transforming them into any other forms. Harmonics, saturation, rotor deep-bar effects and the unbalance of the machine can easily be included in the phase equation model. The major problem of the phase equation model was that the inverse of the inductance matrix of the induction machine was not known explicitly and it was required to be solved at every step of the simulation, therefore, the phase equation model took a longer simulation time than the d-q axis model.

The explicit form of the inverse of the inductance matrix for a symmetrical induction machine has been given and the simulation time was almost halved. The explicit form of the inverse of the inductance matrix is still valid for an unbalanced machine, if the machine unbalance is slight. In this case the inverse of the inductance matrix can be solved explicitly by assuming the machine to be balanced and the errors due to the unbalance can then be added to the result.

The method presented in this thesis for calculating the explicit form of the inductance matrix for the induction machine can also be adapted to other electrical machines, such as the synchronous and the brushless DC machines.

8.2.2. Testing of Large induction Machines

This thesis consists of the test results of VVVF and CVVF tests on 4 kW squirrel-cage and 3.3 kW slip-ring induction machines. The mixed-frequency testing of large induction machines using an inverter, including all four cases given in this thesis, will be very useful for future study. In addition, the application of the mixed-frequency test to synchronous machines and brushless DC machines, will also extend the use of this test in industry.

8.2.3 Generalised View of the Mixed-Frequency Test

A generalised view of the mixed-frequency test can be developed as a test in which the rms power across the airgap is equal to the rated rms airgap power of the machine. Whilst this concept has been introduced, it has not yet been fully explored and it points to some particularly interesting work on switching strategies for achieving power waveforms instead of opposed to voltage or current waveforms.

8.2.4. Application of Cheaper Test-Rig for the Mixed-Frequency Testing of Induction Machines

There were two methods suggested in chapter 7 to set up a cheaper test-rig for the mixed-frequency testing of induction machines without drawing large currents from the power supply. In the one, a resonant bank was proposed between the main supply and the inverter. In the other, an ideal electromechanical energy storage mechanism was proposed. The experimental work from these methods will be very interesting for further study.

8.2.5. Application of Variable Inertia Test-Rig for Full-Load Temperature Rise Testing of Induction Machines

A new test called the "variable inertia" test for the full-load temperature rise testing of induction machines was explained in chapter 7, but it has not yet been tested. Therefore the experimental work of this method will be another important part of the family of the full-load temperature rise testing of induction machines.

REFERENCES

Acarnley P. P., Chai H., and Atkinson D. J., (1991), "Induction motor parameter estimation using on-line spectral analysis", EPE'91, 4th European Conference on Power Electronics and Applications, pp. 3-326, 3-331, Firenze.

Adkins B. and Harley R. G., (1975), "The general theory of alternating current machines", Chapman and Hall, London.

Alger P. L., Angst G. and Davies E. J., (1959), "Stray-load losses in polyphase induction machines", A.I.E.E., Trans., Vol. 78, Part III A, pp. 349-355, June.

Alger P. L., (1970), "Induction machines", Gordon and Breach, Science Publishers, New York.

Andrade D. A., Hughes A. and Corda J., (1994), "Principles of vector control in cage motors: An easy quantitative approch via space-phasors", IEE Power Electronics and Variable-Speed Drives Conference, No. 399, pp. 204-210, 26-28 October.

Ansuj S. Shokooh F. and Schinzinger R., (1989), "Parameter estimation for induction machines based on sensitivity analysis", IEEE Trans. on Industry Applications, Vol. 25, No. 6, pp. 1035-1039, November \ December.

Atkinson D. J., Acarnley P. P. and Finch J. W., (1989), "Parameter identification techniques for induction motor drives", European Power Electronics (EPE'89) Proceedings, EPE Aechen, pp. 307-311.

Artime J., Diez A. and Sanz J., (1987), "New method for on-line estimation of induction motor parameters", IEE Third International Conference on Electrical Machines and Drives, pp. 226-230, 16th - 18th November.

Bal G. and Grant D. M., (1992), "Parameter estimation of field-oriented controlled induction motor fed by CR-PWM via EKF using stator reference currents", ICEM'92, International Conference on Electrical Machines, 15th-17th September, pp. 597-601, Manchester, UK.

Boldea I. and Nasar S. A., (1987), "Unified treatment of core losses and saturation in the orthogonal-axis model of electrical machines", IEE Proceedings, Vol. 134, Pt. B, No. 6, November.

Bowes S. R., Clements R. R., (1983), "Digital computer simulation of variable-speed PWM inverter machine derives", IEE Proc., Vol. 130, Pt. B, pp. 149-160, May.

Bowes S.R. and Clare J. C., (1988), "Computer-aided design of PWM power-electronic variable-speed drives", IEE Proceedings, Vol. 135, Pt. B, No. 5, pp. 240-260, September.

Bourne R., (1989), "No load method of estimating stray load losses in small cage induction motors", IEE Proc. Vol. 136, Pt. B, No. 2, pp. 92-95, March.

Bresnahan K., Zelaya de la Parra H., D. L., Teodorescu R. and Evans P. D., (1994), "Harmonic analysis of SVM and experimental verification in a general purpose induction motor test rig", IEE Power Electronics and Variable-Speed Drives Conference, No. 399, pp. 352-356, 26-28 October.

Brown J. E., Kovacs K. P. and Vas P., (1983), "A method of including the effects of main flux path saturation in the generalised equations of AC machines", IEEE Transactions on Power Apparatus and System, Vol. PAS-102, No. 1, January.

Cecconi V., Pagano E. and Perfetto A., (1986), "A contribution to test standardisation for inverter-fed asynchronous machines", IEEE Trans. on Industry Applications, Vol IA-22, No. 1, pp. 25-31, January\Fabruary.

Chapman S. J., (1987), "Electric machinery fundamentals", McGraw-Hill Company, Singapore.

Christensen L. Mathiassen O., Rasmussen L. B., Ritchie A. E. and Rosholm J. R., (1994), "Iron losses in electrical machines driven from non-sinusoidal waveforms", Universities Power Electronics Conference (UPEC'94), pp. 935-938.

Christofides N., (1965), "Origins of load losses in induction motors with cast aluminium rotors", Proc. IEE, Vol. 112, No. 12, pp. 2317, December.

Christofides N. and Adkins B., (1966), "Determination of load losses and toques in squirrel-cage induction motors", Proc. IEE, Vol. 113, No. 12, pp. 1995-2005, December.

Çolak İ., Elmas Ç., Bal G., Coşkun İ., (1994), "High frequency resonant DC link PWM inverters", in Proceedings of IEEE Mediterranean Electrotechnical Conference MELECON, Antalya Turkey, April.

Çolak İ., Garvey S. and Wright M.T., (1993), "Estimation of induction machine parameters for simulation of a mixed-frequency test", 6th International Conference on Electrical Machines and Drives, 8-10 September, pp. 208-212, Oxford, UK.

Çolak İ., Garvey S. and Wright M.T., (1993), "Mixed-frequency testing of induction machines using inverters", EPE'93, 5th European Conference on Power Electronics and Applications, 14-17 September, vol. 5, pp. 317-322, Brighton, UK.

Çolak İ., Garvey S. and Wright M.T., 1993, "Simulation of induction machines using phase variables and the explicit inverse of the inductance matrix", A modified version of this paper is being prepared for re-submission to IEE Part-B.

Eurotherm Drives Variable "Frequency Inverter 584/585/586 Product Manual", HA385329, Issue 1.

ERA Report, (1993), "Indirect testing of rotating electrical machines to determine temperature rise", 93-0319R, April , Surrey UK.

Ferreira de Jesus J. M., (1988), "A model for saturation in induction machines", IEEE Trans. on Energy Conversion, Vol. 3, No. 3, pp. 682-687, September.

Fitzgerald A. E., Kingsley C. and Umans S. D., (1983), "Electric machinery", McGraw-Hill Book Company, Fourth Edition, Singapore.

Fong W., (1972), "New temperature test for polyphase induction motors by phantom loading", Proc. IEE, Vol. 119, No. 7, pp. 883-887, July.

Fuches E. F., Chang L. H. and Appelbaum J., (1984), "Magnetising current, iron losses and forces of three-phase induction machines at sinusoidal and nonsinusoidal terminal voltages. Part 1: Analysis", IEEE Trans. on Power Apparatus and Systems, Vol. PAS-103, No. 11, pp. 3303-3312, November.

Fuches E. F., Chang L. H. and Appelbaum J., (1984), "Magnetising current, iron losses and forces of three-phase induction machines at sinusoidal and nonsinusoidal terminal voltages. Part 2: Results", IEEE Trans. on Power Apparatus and Systems, Vol. PAS-103, No. 11, pp. 3313-3319, November.

Fudeh H. R. and Ong C. M., (1983), "Modelling and analysis of induction machines containing space harmonics. Part 1: Modelling and transformation", IEEE Transaction on Power Apparatus and System, Vol. PAS-102, No. 8, pp. 2608-2615, August.

Fudeh H. R. and Ong C. M., (1983), "Modelling and analysis of induction machines containing space harmonics. Part 2: Analysis of asynchronous and synchronous actions", IEEE Transaction on Power Apparatus and System, Vol. PAS-102, No. 8, pp. 2616-2627, August.

Garvey S., Çolak İ. and Wright M.T., (1994), "Aspects of mixed-frequency testing of induction machines", ICEM'94 International Conference on Electrical Machines, 5-8 September, pp. 623-628, Paris, France.

Garvey S., Çolak İ. and Wright M.T., (1994), "The "variable inertia test" for full-load temperature rise testing of induction machines", This paper has been accepted for the publication in IEE-part B.

Gerald Curtis F. and Wheatley Patrick O., (1994), "Applied numerical analysis", California Polytechnic State University, Fifth Edition.

Grantham C. and Rahman F., (1993), "A novel machineless dynamometer for load testing three-phase induction motors", Sixth International. Conference on Electrical Machines and Drives, 8-10 September, pp. 202-207, Oxford, UK.

Grantham C., (1993), "Full load testing of three phase induction motors without the use of a dynamometer", International. Conference on Electrical Machines, 5 September, pp. 147-152, Kensington, Australia.

Grantham C., Spooner E. D. and Sheng M., (1990), "Synthetic loading of machines using microprocessor-controlled power electronics", Fourth International Conference on Power Electronics and Variable Speed Drives, IEE Conf. Publ. No. 324, London, UK, 17-19 July, pp. 121-126.

Grzesiak L. M. and Reichert K., (1992), "Equivalent circuit determination of an AC-machine based on catalogue data and values of no-load current and stator resistance", International Conference on Electrical Machines (ICEM'92), pp. 303-306, 15th-17th September, UMIST, Manchester, UK.

Hall J. and Pickering C., (1989), "Data acquisition toolbox for use with MATLAB", version 1.0, December, Signal Processing Technology Limited, P.O. Box 68, Southampton, SO9 7EP, UK.

Hill W., (1965), "Discussion on Stray Load Losses in Squirrel-Cage Induction Motor", IEE Proc., Vol. 112, No. 9, pp. 1752, September.

Ho S.L., (1992), "Further development of phantom loading in induction motors", ICEM'92, International Conference on Electrical Machines, 15th-17th September, pp. 298-302, Manchester, UK.

Hoffman Joe D., (1992), "Numerical methods for engineers and scientists", McGraw-Hill, Inc., Purdue University, New York.

Holliday D., Green T. C. and Williams B. W., (1994), "On-line measurement of induction machine stator and rotor winding parameters", IEE Power Electronics and Variable-Speed Drives Conference, No. 399, pp. 465-469, 26-28 October.

Holtz J. and Thimm T., (1991), "Identification of the machine parameters in a vector-controlled induction motor drive", IEEE Trans. on Industry Applications, Vol. 27, No. 6, pp. 1111- 1117, November\December.

Illango B. and Ramamoorty M., (1974), "Steady state analysis of thyristor controlled three phase induction motors using state space techniques", 1973 Annual Meeting of the IEEE Industry Applications Society, pp. 1165-1172, February 27.

Jacovides L. J., (1973), "Analysis of cycloconverter-induction motor drive system allowing for stator current discontinuities", IEEE Transactions on Industry Applications, Vol. IA-9, No. 2, pp. 206- 215, March/April.

Jimoh A. A., Findlay R. D. and Poloujadoff M., (1985), "Stray losses in induction machines. Part 1: Definition, origin and measurement", IEEE Trans. on Power Apparatus and Systems, Vol. PAS-104, No. 6, pp. 1500-1505, June.

Jimoh A. A., Findlay R. D. and Poloujadoff M., (1985), "Stray losses in induction machines. Part 2: Calculation and reduction", IEEE Trans. on Power Apparatus and Systems, Vol. PAS-104, No. 6, pp. 1506-1511, June.

Jordan H. E., (1965), "Analysis of induction machines in dynamic systems", IEEE Trans. on Power Apparatus and Systems, Vol. PAS- 84, No. 11, pp. 1080-1088, November.

Jordan H. E., (1967), "Digital computer analysis of induction machines in dynamic systems", IEEE Trans. on Power Apparatus and Systems, Vol. PAS-86, No. 6, pp. 722-727, June.

Jordon H. E., Cook J. H. and Smith R. L., (1977), "Synthetic load testing of induction machine", IEEE Transactions on Power Apparatus and Systems, Vol. PAS-96, No. 4, pp. 1101-1104, July/August.

Kerkman R., (1985), "Steady-state and transient analyses of an induction machine with saturation of the magnetising branch", IEEE Trans. on Industry Applications, Vol. IA-21, No. 1, pp. 226-234, January\Fabruary.

Khenfer N., Rezzoug A., Gudefin E. J. and Meidbody-Tabar F., (1992), "Identification of parameters of asynchronous machines. Experimental methods and results", ICEM'92, International Conference on Electrical Machines, 15th-17th September, pp. 283-287, Manchester, UK.

Koopman R. J. W. and Trutt F., (1969), "Direct simulation of AC machinery including third-harmonic effects", IEEE Transaction on Power Apparatus and Systems, Vol. PAS-88, No. 4, pp. 465-474, April.

Krause P. C. and Thomas C. H., (1965), "Simulation of symmetrical induction machinery", IEEE Trans. on Power Apparatus and systems, Vol. PAS-84, No. 11, pp. 1038-1053, November.

Krause P. C., (1968), "Method of multiple reference frames applied to the analysis of symmetrical induction machinery," IEEE Trans. on Power Apparatus and Systems, Vol. PAS-87, No. 1, pp. 218-226, January.

Krause P. C, (1986) "Analysis of electric machinery", McGraw-Hill Book Company, London.

Krause P. C. and Wasynczuk O., (1989), "Electromechanical motion devices", McGraw-Hill Book Co., Singapore.

Kron A. W., (1973), "Messungen an Asychronmotoren bei bifrequenter Speisung", ETZ-A94 (2), pp. 77-82.

Levi Emil, Rauski D., (1993), "Self-excitation modelling in deep-bar and double-cage induction generators", Sixth International Conference on Electrical Machines and Drives, pp. 162-167, 8-10 September, Oxford, UK.

Levi Emil, (1994), "Iron core loss effects in indirect rotor flux oriented induction machines", in Proceedings of IEEE Mediterranean Electrotechnical Conference MELECON, Antalya Turkey, April.

Limebeer D. J. N. and Harley R. G., (1981), "Subsynchronous resonance of deep-bar induction motors", IEE Proc., Vol. 128, Pt. B, No. 1, pp. 43-51, January.

Lipo T. A. and Consoli A., (1984), "Modelling and simulation of induction motors with saturable leakage reactances", IEEE Trans. on Industry Applications, Vol. IA-20, No. 1, pp. 180-189, January\Fabruary.

Lloyd M. R., (1982), "Transient performance of induction motors in electromechanical systems", IEE. Conf. Public. on Electrical Machines-Design and Applications, pp. 52-56.

Melkebeek J. A. A., (1983), " Magnetising-field saturation and dynamic behaviour of induction machines. Part 1: Improved calculation method for induction machine dynamics", IEE Proc., Vol. 130, Pt. B, No. 1, pp. 1-9, January.

Mendes E., Razek A., (1994), "A simple model for core losses and magnetic saturation in induction machines adapted for direct stator flux orientation control", IEE Fifth International Conference on Power Electronics and Variable-Speed Drives, PEVD'94, No. 399, pp. 192-197, London , UK.

Meyer A. and Lorenzen H. W., (1979), "Two-frequency heat run - a method of examination for three-phase induction motors", IEEE Transaction on Power Apparatus and Systems, Vol. Pas-98, no. 6, pp. 2338-2347, November/December.

Mohan N., Undeland T. M. and Robbins W. P., (1989), "Power Electronics: Converters, Applications and Design", Printed in the Republic of Singapore.

Monro, Donald M., (1987), "FORTRAN 77", Imperial College of Science and Technology University of London.

Morris D.G.O., (1968), "Back-to-back test for induction machines: Floating gearbox", Proc. IEE, Vol. 115, No. 4, pp. 536-537, April.

Nath G. and Berg G. J., (1981), "Transient analysis of three-phase SCR controlled induction motors", IEEE Trans. on Industry Applications, Vol. IA-17, No. 2, pp. 133-142, March/April.

O'Kelly D., (1991), "Performance and control of electrical machines", McGraw-Hill Book Company, London.

Ojo J. O., Consoli A. and Lipo T. A, (1990), "An improved model of saturated induction machines", IEEE Trans. on Industry Applications, Vol. 26, No. 2, pp. 212-221, Marc\April.

Palit B. B., (1980), "Temperature rise in a synthetically loaded induction machine", International Conference on Electrical Machines, Athens, Greece, 15-17 September, Vol. 3, pp. 2082-2088

Peebles Electrical Machines, Publication No. MG 510X, "The use of continuously varied frequency (C.V.F) for induction motor heat runs".

Plevin D. H., (1988), "Test Simulation of full load heating for large cage type induction motors."

Radic P. and Strupp H., (1976), "Measurement of temperature rise in induction motors using the continuously varied frequency method", Brown Boveri Rev. Vol. 63, No 8, pp. 517-520, August.

Rajan S. D., Jacovides L. J. and Lewis W. A., (1974), "Digital simulation of a high-performance AC drive system-part 1-2", IEEE Transactions on Industry Applications, Vol. IA-10, No. 3, pp. 391- 402, May/June.

Rahman S., Shepherd W., (1977), "Thyristor and diode controlled variable voltage drives for 3-phase induction motors", Proc. IEE, Vol. 124, No. 9, pp. 784-790, September.

Ramminger P. and Andresen E., (1992), "Prediction of performance characteristics of small induction motors from measurements without load machine", International Conference on Electrical Machines ICEM'92, pp. 288-292, 15th-17th September, UMIST, Manchester, UK.

Ramshaw R. S., Padiyar K. R., (1973), "Generalised system model for slip-ring machines", IEE Proc. Vol. 120, No. 6, pp. 647-658, June.

Robertson S. D. T. and Hebbar K. M., (1969), "A digital model for three-phase induction machines", IEEE Transaction on Power Apparatus and Systems, Vol. PAS-88, No. 11, pp. 1624- 1634, November.

Romeira M. P., (1948), "The "superimposed frequency test" for induction motors, or S. F. test", AIEE Trans., Vol. 67, pp. 952-955, April 7.

Russel A. P. and Pickup I. E. D., (1982), "An analysis of the induction motor, part 1- steady-speed operation", IEE Proc., Vol. 129, Pt. B, No. 5, pp. 229-237, September.

Russel A. P. and Pickup I. E. D., (1982), "An analysis of the induction motor, part 2- damping and synchronising torque production", IEE Proc., Vol. 129, Pt. B, No. 5, pp. 238-242, September.

Russel A. P. and Pickup I. E. D., (1982), "An analysis of the induction motor, part 3- power/frequency relationships", IEE Proc., Vol. 129, Pt. B, No. 5, pp. 243-247, September.

Salvatore L. and Stasi S. (1994), "Monitoring of inverter drives in time-frequency domain", International Conference on Electrical Machines (ICEM'94), Vol. 2, pp. 72-78, Paris, France.

Saraiva E. de S. and Freris L. L., (1979) "Development of electromechanical filter and performance evaluation in dc. link", Proc. Inst. Elect. Eng. (GB), vol. 126, pp. 1282-1286.

Sarkar A. K. De and Berg G. J., (1970), "Digital simulation of three-phase induction motors", IEEE Trans. on Power Apparatus and Systems, Vol. PAS-89, No. 6, pp. 1081-1037, July/August.

Schwenk H.R., (1975), "Equivalent loading of induction machines for temperature tests", Conf. Record of IAS Meeting, pp. 1053-1058.

Slemon Gordon R., (1989), "Modelling of induction machine for electric drives", IEEE Transaction on Industry Applications, Vol. 25, No. 6, pp. 1126-1131, November/December.

Smith K. S. and Yacamini R., (1993), "Time domain modelling of elctrical machines and drives using modern computer aided engineering (CEA) software", Sixth International Conference on Electrical Machines and Drives, pp. 323-327, 8-10 September, Oxford, UK.

Spooner E. D., Grantham C. and Largent R., (1986), "Synthetic loading of machines", Electrical Energy Conference 1986, Electrical Energy Systems - Today and Tomorrow, Institution of Engineers, Australia, Brisbane, Australia, 20 -22 October, pp. 194 -197.

Sull S. K., (1989), "A novel technique of rotor resistance estimation considering variation of mutual inductance", IEEE Trans. on Industry Applications, Vol. 25, No. 4, pp. 578-587, July\August.

Szabados B., Dableh J. H., Findlay R.D. and Stafford D., (1989), "A new approach for measurement of the torque-speed characteristics of induction motors", IEE Fourth International Conference on Electrical Machines and Drives, pp. 246-250, 13-15 September.

Timar P. L., Bajza L., Krisch E. and Solymoss E., (1992), "Parameter identification of asynchronous motors with special attention to fast response measuring methods", ICEM'92, International Conference on Electrical Machines, 15th-17th September, pp. 307-311, Manchester, UK.

Vas P., (1990), "Vector control of AC machines", Oxford University Press, Valton Street, Oxford.

Von der Embse U. A., (1968), "New theory of nonlinear commutator machines", IEEE Trans. on Power Apparatus and systems, Vol. PAS87, No. 9, pp. 1804-1809, September.

APPENDIX 1

A.1.1. Parameters of the small squirrel-cage induction machine:

BROOK CROMPTON 3 phase, 4 kW, 2 pole, 415 V, 50 Hz, Δ,

Full-load stator line current = 7.2 amperes,

No-load stator current = 2.31 amperes,

Full load winding temperature = 80 °C,

R_s = 5.2 Ω, R_r ≈ 3.1 Ω,

L_{sl} ≈ 0.031 H, L_{rl} ≈ 0.031 H,

L_{sr} ≈ 0.93 H, J ≈ 0.00478 kgm^2,

A.1.2. Parameters of the slip-ring induction machine:

3 phase, 3.3 kW, 4 pole, 50 Hz, Δ,

Stator voltage = 230 volts,

Rotor voltage = 240 volts,

Full load stator line current = 11.4 amperes,

Full load rotor current = 9.3 amperes,

Full load winding temperature = 65 °C,

R_s = 1.58 Ω, R_r = 1.5 Ω,

L_{sl} ≈ 0.0245 H, L_{rl} ≈ 0.0245 H,

L_{sr} ≈ 0.62 H, J ≈ 0.074 kgm^2.

A.1.3 Parameters of the large squirrel-cage induction machine:

3 phase, 11 kV/line, 12.6 MVA, 4 pole,

R_s = 0.03975 Ω, R_r = 0.1037 Ω,

L_{ss} = 0.08438 H, L_{rr} = 0.08325 H,

M_{sr} = 0.0811 H, J = 2534.4 kgm^2,

Full load stator current = 661.3 amperes,

Full load rotor current = 406.8 amperes,

Full load core losses = 36 kW.

A.1.4 Time constants of test machines:

Machines	T_1	T_2	T_3	T_4	T_5	T_6
4 kW	0.4873	0.0060	0.0075	0.0100	0.4873	0.0075
3.3 kW	0.0158	0.8213	0.0167	0.8213	0.0162	0.0162
12.6 MVA	0.0001	3.7927	0.0005	0.0005	5.1760	3.7927

Table A.1-1 Time constants of test machines in seconds.

APPENDIX 2

A.2.1. Explicit Form of the Inverse of the Inductance Matrix of an Induction Machine

The inductance matrix $\mathbf{L}(\theta)$ defined in (3.3-4) above can be regarded as being composed of four blocks as in (A.2.1-1) below.

$$\mathbf{L}(\theta) = \begin{bmatrix} \mathbf{L}_{ss} & \mathbf{L}_{sr}(\theta) \\ \mathbf{L}_{rs}(\theta) & \mathbf{L}_{rr} \end{bmatrix} \qquad \text{(A.2.1-1)}$$

where

$\mathbf{L}_{ss}$, $\mathbf{L}_{sr}(\theta)$, $\mathbf{L}_{rs}(\theta)$ and $\mathbf{L}_{rr}$ are all (3x3) blocks as defined in (A.2.1-2) below. Clearly $\mathbf{L}_{ss}$ and $\mathbf{L}_{rr}$ do not vary with θ.

$$\left.\begin{aligned} \mathbf{L}_{ss} &= \begin{bmatrix} L_{ss} & -\frac{1}{2}L_{sm} & -\frac{1}{2}L_{sm} \\ -\frac{1}{2}L_{sm} & L_{ss} & -\frac{1}{2}L_{sm} \\ -\frac{1}{2}L_{sm} & -\frac{1}{2}L_{sm} & L_{ss} \end{bmatrix}, \qquad \mathbf{L}_{rr} = \begin{bmatrix} L_{rr} & -\frac{1}{2}L_{rm} & -\frac{1}{2}L_{rm} \\ -\frac{1}{2}L_{rm} & L_{rr} & -\frac{1}{2}L_{rm} \\ -\frac{1}{2}L_{rm} & -\frac{1}{2}L_{rm} & L_{rr} \end{bmatrix} \\ \mathbf{L}_{sr}(\theta) &= M_{sr}\begin{bmatrix} \cos(\theta) & \cos(\theta+\frac{2\pi}{3}) & \cos(\theta-\frac{2\pi}{3}) \\ \cos(\theta-\frac{2\pi}{3}) & \cos(\theta) & \cos(\theta+\frac{2\pi}{3}) \\ \cos(\theta+\frac{2\pi}{3}) & \cos(\theta-\frac{2\pi}{3}) & \cos(\theta) \end{bmatrix} = \left[\mathbf{L}_{rs}(\theta)\right]^{T} \end{aligned}\right\} \qquad \text{(A.2.1-2)}$$

Now, we introduce a certain 3x3 matrix $\mathbf{H}(\theta)$ defined in (A.2.1-3) which has the very useful property of orthogonality as expressed by (A.2.1-4).

$$\mathbf{H}(\theta) = \frac{1}{3}\begin{bmatrix} [1+\ 2\cos(\theta)] & [1-\ \cos(\theta)+\sqrt{3}\sin(\theta)] & [1-\ \cos(\theta)-\sqrt{3}\sin(\theta)] \\ [1-\ \cos(\theta)-\sqrt{3}\sin(\theta)] & [1+\ 2\cos(\theta)] & [1-\ \cos(\theta)+\sqrt{3}\sin(\theta)] \\ [1-\ \cos(\theta)+\sqrt{3}\sin(\theta)] & [1-\ \cos(\theta)-\sqrt{3}\sin(\theta)] & [1+\ 2\cos(\theta)] \end{bmatrix} \tag{A.2.1-3}$$

$$\left.\begin{aligned} \mathbf{L}(\theta) = \begin{bmatrix} \mathbf{L}_{ss} & \mathbf{L}_{sr}(\theta) \\ \mathbf{L}_{rs}(\theta) & \mathbf{L}_{rr} \end{bmatrix} &= \begin{bmatrix} \mathbf{I} & 0 \\ 0 & \mathbf{H}(\theta)^{T} \end{bmatrix}\begin{bmatrix} \mathbf{L}_{ss} & \mathbf{L}_{sr}(0) \\ \mathbf{L}_{rs}(0) & \mathbf{L}_{rr} \end{bmatrix}\begin{bmatrix} \mathbf{I} & 0 \\ 0 & \mathbf{H}(\theta) \end{bmatrix} \\ \mathbf{L}(\theta)^{-1} &= \begin{bmatrix} \mathbf{I} & 0 \\ 0 & \mathbf{H}(\theta)^{T} \end{bmatrix}\left[\mathbf{L}(0)^{-1}\right]\begin{bmatrix} \mathbf{I} & 0 \\ 0 & \mathbf{H}(\theta) \end{bmatrix} \end{aligned}\right\} \tag{A.2.1-4}$$

It is relatively simple to verify that equations (A.2.1-4) below are true. (Numerical verification is easiest.)

$$\left.\begin{aligned} [\mathbf{L}_{sr}(\theta)] = [\mathbf{L}_{sr}(0)][\mathbf{H}(\theta)], \qquad [\mathbf{L}_{rs}(\theta)] &= [\mathbf{H}(\theta)]^{T}[\mathbf{L}_{rs}(0)] \\ [\mathbf{H}(\theta)]^{T}\mathbf{L}_{rr}[\mathbf{H}(\theta)] &= \mathbf{L}_{rr} \end{aligned}\right\} \tag{A.2.1-5}$$

The consequence of equation (A.2.1-4) is that the complete inductance matrix, $\mathbf{L}(\theta)$, can be written as in (A.2.1-6) and that its inverse, $\mathbf{L}(\theta)^{-1}$, can therefore be written in closed form also as in (A.2.1-6).

$$\left.\begin{aligned} \mathbf{L}(\theta) = \begin{bmatrix} \mathbf{L}_{ss} & \mathbf{L}_{sr}(\theta) \\ \mathbf{L}_{rs}(\theta) & \mathbf{L}_{rr} \end{bmatrix} &= \begin{bmatrix} \mathbf{I} & 0 \\ 0 & \mathbf{H}(\theta)^{T} \end{bmatrix}\begin{bmatrix} \mathbf{L}_{ss} & \mathbf{L}_{sr}(0) \\ \mathbf{L}_{rs}(0) & \mathbf{L}_{rr} \end{bmatrix}\begin{bmatrix} \mathbf{I} & 0 \\ 0 & \mathbf{H}(\theta) \end{bmatrix} \\ \mathbf{L}(\theta)^{-1} &= \begin{bmatrix} \mathbf{I} & 0 \\ 0 & \mathbf{H}^{T}(\theta) \end{bmatrix}\mathbf{L}(0)^{-1}\begin{bmatrix} \mathbf{I} & 0 \\ 0 & \mathbf{H}(\theta) \end{bmatrix} \end{aligned}\right\} \tag{A.2.1-6}$$

The inverse of the inductance matrix for $\theta = 0$, $\mathbf{L}(0)^{-1}$, has five unknown scalars u, v, w, and y.

$$\mathbf{L}(0)=\begin{bmatrix} L_{ss} & -\frac{1}{2}L_{sm} & -\frac{1}{2}L_{sm} & M_{sr} & \frac{-M_{sr}}{2} & \frac{-M_{sr}}{2} \\ L_{sm} & L_{ss} & -\frac{1}{2}L_{sm} & \frac{-M_{sr}}{2} & M_{sr} & \frac{-M_{sr}}{2} \\ -\frac{1}{2}L_{sm} & -\frac{1}{2}L_{sm} & L_{ss} & \frac{-M_{sr}}{2} & \frac{-M_{sr}}{2} & M_{sr} \\ M_{sr} & \frac{-M_{sr}}{2} & \frac{-M_{sr}}{2} & L_{rr} & -\frac{1}{2}L_{rm} & -\frac{1}{2}L_{rm} \\ \frac{-M_{sr}}{2} & M_{sr} & \frac{-M_{sr}}{2} & -\frac{1}{2}L_{rm} & L_{rr} & -\frac{1}{2}L_{rm} \\ \frac{-M_{sr}}{2} & \frac{-M_{sr}}{2} & M_{sr} & -\frac{1}{2}L_{rm} & -\frac{1}{2}L_{rm} & L_{rr} \end{bmatrix}, \quad \mathbf{L}(0)^{-1}=\begin{bmatrix} u & v & v & w & \frac{-w}{2} & \frac{-w}{2} \\ v & u & v & \frac{-w}{2} & w & \frac{-w}{2} \\ v & v & u & \frac{-w}{2} & \frac{-w}{2} & w \\ w & \frac{-w}{2} & \frac{-w}{2} & x & y & y \\ \frac{-w}{2} & w & \frac{-w}{2} & y & x & y \\ \frac{-w}{2} & \frac{-w}{2} & w & y & y & x \end{bmatrix}$$

(A.2.1-7)

The five unknowns can be defined in terms of the motor parameters obtained by multiplying the selected rows of $\mathbf{L}(0)$ with the selected columns of $\mathbf{L}(0)^{-1}$. The solutions of these equations are then as in (A.2.1-8).

$$\left.\begin{aligned} u &= \frac{\left[4\left(L_{ss}+L_{sm}\right)\left(L_{rr}-L_{rm}\right)-3M_{sr}^{\,2}\right]}{\left(L_{ss}+2L_{sm}\right)\left[4\left(L_{ss}-L_{sm}\right)\left(L_{rr}-L_{rm}\right)-9M_{sr}^{\,2}\right]}, \qquad v = \frac{-\left[4L_{sm}\left(L_{rr}-L_{rm}\right)+3M_{sr}^{\,2}\right]}{\left(L_{ss}+2L_{sm}\right)\left[4\left(L_{ss}-L_{sm}\right)\left(L_{rr}-L_{rm}\right)-9M_{sr}^{\,2}\right]} \\ w &= \frac{-4M_{sr}}{\left[4\left(L_{ss}-L_{sm}\right)\left(L_{rr}-L_{rm}\right)-9M_{sr}^{\,2}\right]} \\ x &= \frac{\left[4\left(L_{rr}+L_{rm}\right)\left(L_{ss}-L_{sm}\right)-3M_{sr}^{\,2}\right]}{\left(L_{rr}+2L_{rm}\right)\left[4\left(L_{ss}-L_{sm}\right)\left(L_{rr}-L_{rm}\right)-9M_{sr}^{\,2}\right]}, \qquad y = \frac{-\left[4L_{rm}\left(L_{ss}-L_{sm}\right)+3M_{sr}^{\,2}\right]}{\left(L_{rr}+2L_{rm}\right)\left[4\left(L_{ss}-L_{sm}\right)\left(L_{rr}-L_{rm}\right)-9M_{sr}^{\,2}\right]} \end{aligned}\right\}$$

(A.2.1-8)

Now, because $\mathbf{L}(0)^{-1}$ has exactly the same form as $\mathbf{L}(0)$ and because $\mathbf{L}(\theta)^{-1}$ is related to $\mathbf{L}(0)^{-1}$ in exactly the same way that $\mathbf{L}(\theta)$ is related to $\mathbf{L}(0)$, it follows that $\mathbf{L}(\theta)^{-1}$ can be written in closed form as follows:

$$\mathbf{L}(\theta)^{-1} = \begin{bmatrix} u & v & v & w\cos(\theta) & w\cos\left(\theta+\frac{2\pi}{3}\right) & w\cos\left(\theta-\frac{2\pi}{3}\right) \\ v & u & v & w\cos\left(\theta-\frac{2\pi}{3}\right) & w\cos(\theta) & w\cos\left(\theta+\frac{2\pi}{3}\right) \\ v & v & u & w\cos\left(\theta+\frac{2\pi}{3}\right) & w\cos\left(\theta-\frac{2\pi}{3}\right) & w\cos(\theta) \\ w\cos(\theta) & w\cos\left(\theta-\frac{2\pi}{3}\right) & w\cos\left(\theta+\frac{2\pi}{3}\right) & x & y & y \\ w\cos\left(\theta+\frac{2\pi}{3}\right) & w\cos(\theta) & w\cos\left(\theta-\frac{2\pi}{3}\right) & y & x & y \\ w\cos\left(\theta-\frac{2\pi}{3}\right) & w\cos\left(\theta+\frac{2\pi}{3}\right) & w\cos(\theta) & y & y & x \end{bmatrix}$$

(A.2.1-9)

As seen from (A.2.1-9), the scalars are not a function of the θ and need to be calculated only once in a normal simulation run. The elements related by the cosine function are the same for all three phases with a phase shifting of $2\pi/3$. The total numbers of these elements are 18, but if three of them are calculated for one phase during each simulation step, the others will be known. The author has tested this method in a simulation program written in FORTRAN 77 on a 486 PC. The improved method takes 26.17 seconds for 0.8 seconds of real time of the machine using 50μs time steps. Using the conventional Gauss-Jordan method it takes 45.40 seconds, with the same time step.

A.2.2. Incorporating Core Losses and Deep-Bar Effect into the Model of the Induction Machine

Incorporating the core losses and the deep-bar effect into either the phase equation model or the d-q axis model of a machine is the same.

The core losses of an induction machine are generally ignored when calculating the machine losses since the machine is fed from a sinusoidal power supply. Nevertheless, the value of the core losses increase considerably if the machine is fed from a nonsinusoidal power supply, therefore, the core losses cannot be ignored and must be included in the machine model. The core losses are often included into the machine equations as a DC resistance placed in parallel to the magnetising branch (Fitzgerald et al. (1985), Chapman (1987),

Fuchs et al. (1984), Christensen et al (1994)) or in serial with the mutual inductance (Mendes and Razek (1994)). Alternatively, Boldea and Nasar (1987) represented the core losses with one stator and one rotor winding along each axis of the d-q axis model. Later Levi (1994, Antalya) used the same representation of the core losses, referring to Boldea and Nasar (1987), for the space vector modelling of an induction motor.

The rotor deep-bar effect causes the rotor current to shift to the tops of the rotor bars during starting, resulting in an increase in rotor resistance and a decrease in leakage inductance with increasing slip frequency (Lipo and Consoli (1981)). Representation of the deep-bar effect is given by splitting the rotor conductors radially (into three 'current sheets' in the diagram below) as suggested by Alger (1970) Limebeer and Harley (1981) and also used by Çolak et al. (1993, EPE'93). Levi and Rauski (1993) treated the deep-bar winding as an equivalent double cage winding.

The basic model of the induction machine given in (3.3-5) can be enhanced so that the core losses and the deep-bar effect can be included into this model easily. The schematic circuit diagram given below (Çolak et al. (1993, EPE'93)) illustrates the new model of the induction machine which includes the core losses and the deep-bar effect. The inductance and resistance quantities are emboldened to indicate that they represent 3x3 matrix quantities as opposed to scalar quantities. The current quantities ($\mathbf{I}_{s1}$, $\mathbf{I}_{s2}$ and $\mathbf{I}_{r1}$) are also emboldened to indicate that they are 3x1 vectors. The voltage quantities are given as $\mathbf{V}_s$, $\mathbf{E}_s$ and $\mathbf{E}_r$ where $\mathbf{E}_s$ and $\mathbf{E}_r$ are induced electromotive forces on the stator and rotor sides of the airgap respectively.

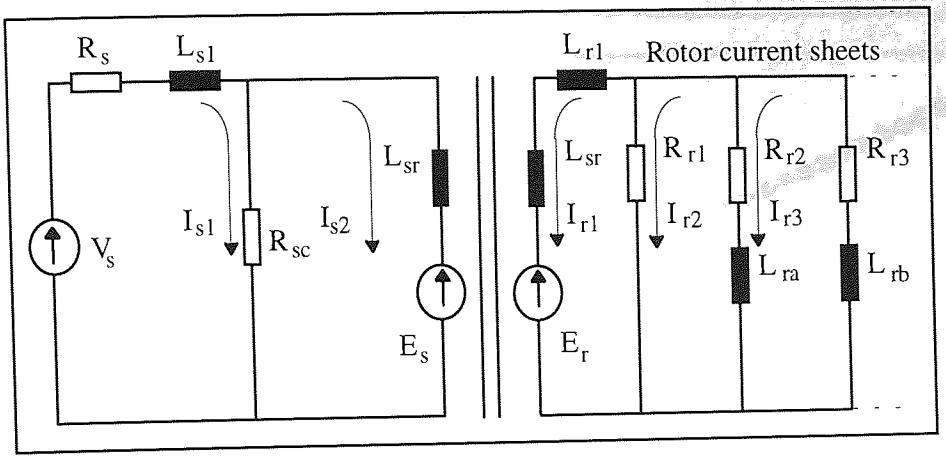

Fig. A.2.2-1 Equivalent circuit of an induction motor.

The core losses of the machine are represented by $\mathbf{R}_{sc}$. This model of representing the core loss in the machine equations is the simplest one which is based on the phase equivalent circuit of the machine.

One phase equivalent rotor circuit can be shown separately as in Fig. A.2.2-2. The variation of the one phase equivalent rotor impedance is shown as in Fig. A.2.2-3 for particular values of R_{r0}, R_{r1}, R_{r2}, R_{r3}, L_{r1}, L_{r2} and L_{r3} (in this case 10Ω, 10Ω, 10Ω, 10Ω, 0.2mH, 0.3mH and 0.4mH respectively).

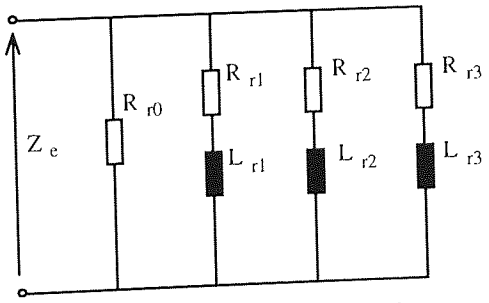

Fig. A.2.2-2 Representation of one phase equivalent rotor circuit.

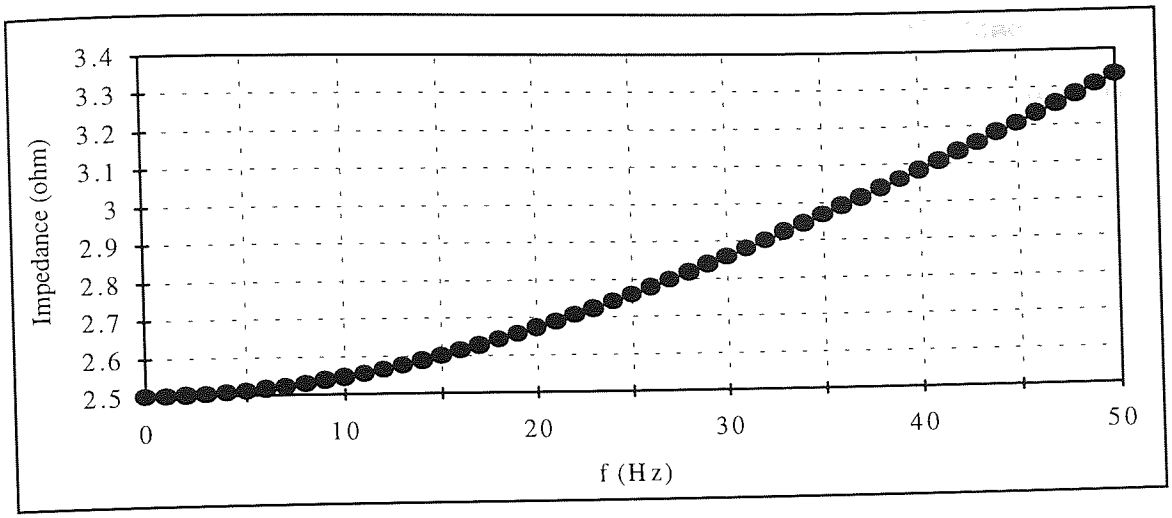

Fig. A.2.2-3 Variation of one phase equivalent rotor impedance verses frequency.

The complete electrical dynamics of the induction machine including core losses and rotor deep-bar effects are then expressed in the above equations.

$$\begin{bmatrix} \mathbf{V}_s \\ -\mathbf{E}_s \\ -\mathbf{E}_r \\ 0 \\ 0 \end{bmatrix} = \begin{bmatrix} \mathbf{R}_s+\mathbf{R}_{sc} & -\mathbf{R}_{sc} & 0 & 0 & 0 \\ -\mathbf{R}_{sc} & \mathbf{R}_{sc} & 0 & 0 & 0 \\ 0 & 0 & \mathbf{R}_{r1} & -\mathbf{R}_{r1} & 0 \\ 0 & 0 & -\mathbf{R}_{r1} & \mathbf{R}_{r1}+\mathbf{R}_{r2} & -\mathbf{R}_{r2} \\ 0 & 0 & 0 & -\mathbf{R}_{r1} & \mathbf{R}_{r2}+\mathbf{R}_{r3} \end{bmatrix} \begin{bmatrix} \mathbf{I}_{s1} \\ \mathbf{I}_{s2} \\ \mathbf{I}_{r1} \\ \mathbf{I}_{r2} \\ \mathbf{I}_{r3} \end{bmatrix} + \begin{bmatrix} \mathbf{L}_{sl} & 0 & 0 & 0 & 0 \\ 0 & \mathbf{L}_{sr} & \mathbf{L}_{sr}\mathbf{H}(\theta) & 0 & 0 \\ 0 & \mathbf{H}^T(\theta)\mathbf{L}_{sr} & \mathbf{H}^T(\theta)\mathbf{L}_{sr}\mathbf{H}(\theta)+\mathbf{L}_{rl} & 0 & 0 \\ 0 & 0 & 0 & \mathbf{L}_{ra} & -\mathbf{L}_{ra} \\ 0 & 0 & 0 & -\mathbf{L}_{ra} & \mathbf{L}_{ra}+\mathbf{L}_{rb} \end{bmatrix} \frac{d}{dt} \begin{bmatrix} \mathbf{I}_{s1} \\ \mathbf{I}_{s2} \\ \mathbf{I}_{r1} \\ \mathbf{I}_{r2} \\ \mathbf{I}_{r3} \end{bmatrix} \quad \text{(A.2.2-1)}$$

$$\left.\begin{aligned} \mathbf{E}_s &= \mathbf{L}_{sr}\left[\frac{d(\mathbf{H}(\theta))}{dt}\right]\mathbf{I}_{r1} \Rightarrow \mathbf{E}_s = \mathbf{L}_{sr}\frac{d\mathbf{H}(\theta)}{d\theta}\omega_r\mathbf{I}_{r1} \\ \mathbf{E}_r &= \frac{d\mathbf{H}^T(\theta)}{d\theta}\mathbf{L}_{sr}\omega_r\mathbf{I}_{s2} + \left(\frac{d\mathbf{H}^T(\theta)}{d\theta}\mathbf{L}_{sr}\omega_r\mathbf{H}(\theta)+\mathbf{H}^T(\theta)\mathbf{L}_{sr}\frac{d\mathbf{H}(\theta)}{d\theta}\omega_r\right)\mathbf{I}_{r1} \end{aligned}\right\} \quad \text{(A.2.2-2)}$$

$$\mathbf{L}_{sr} = \begin{bmatrix} l_{sr} & \frac{-l_{sr}}{2} & \frac{-l_{sr}}{2} \\ \frac{-l_{sr}}{2} & l_{sr} & \frac{-l_{sr}}{2} \\ \frac{-l_{sr}}{2} & \frac{-l_{sr}}{2} & l_{sr} \end{bmatrix}, \quad \mathbf{L}_{sl} = \begin{bmatrix} l_{sl} & 0 & 0 \\ 0 & l_{sl} & 0 \\ 0 & 0 & l_{sl} \end{bmatrix}, \quad \mathbf{L}_{rl} = \begin{bmatrix} l_{rl} & 0 & 0 \\ 0 & l_{rl} & 0 \\ 0 & 0 & l_{rl} \end{bmatrix} \quad \text{(A.2.2-3)}$$

A.2.3. Incorporating Saturation into the Model of the Induction Machine

Induction machines are non-linear due to the characteristics of the magnetic steel which is used to build up the machine's body. Every magnetic element has a different limitation for carrying the flux linkages produced by the machine currents. If the flux linkages reach this limit, then the magnetic elements start to saturate the iron and the rate at which flux rises (with respect to increasing MMF) begins to drop. Figure A.2.3-1 shows the form of the saturation curve.

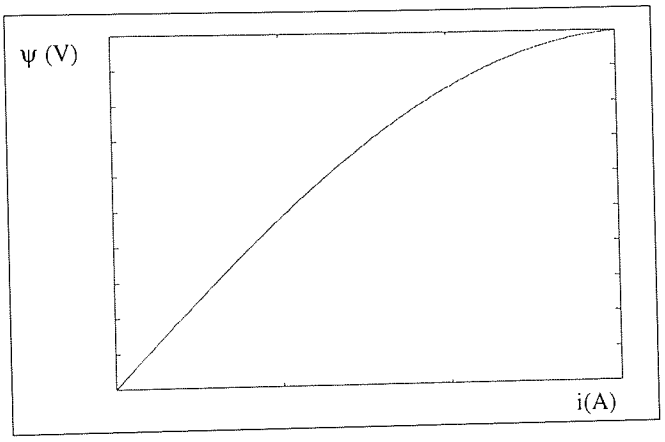

Fig. A.2.3-1 Variation of flux linkage versus current.

The theoretical basis for the consideration of saturation in the generalised equations of the single-circuit electrical machine was first established by Von der Embse in 1968. Incorporation of the saturation into the three phase machine models (phase equation, d-q axis, space vector models) was adapted by different authors. Lipo and Consoli (1981), Ojo et al. (1990) discussed the saturation of the leakage inductance in detail. Then, Brown et al. (9983) incorporated the saturation of the main flux path into the generalised equations of alternating current machines in which the currents are chosen as the state variables. The saturation effects of the magnetising filed were studied by Melkebeek (1983), Kerkman (1985) and Boldea and Nasar (1987). Ferreira de Jesus (1988), developed a model that accounts for saturation in an induction machine, based on Von der Embse's (1968) concepts.

Generally, induction machines are used near the saturation limit to get a balance between the cost and the efficiency of machine. Therefore modelling the saturation is necessary for modelling of an induction machine. For a machine in steady state at constant voltage, it is acceptable to drive an equivalent inductance which will produce the correct component of current at fundamental frequency, but there will be harmonics associated with both stator and rotor currents.

Since the flux linkages of the machine are the only variables which saturate, the saturation can be included into the flux linkages. The flux linkages are a function of the current and the inductance of the machine. For a linear machine, the relationship between the flux and the current can be given as:

$$\boldsymbol{\psi} = \mathbf{L}\mathbf{i} \tag{A.2.3-1}$$

For the general machine, the vector of flux linkages, $\boldsymbol{\psi}$, can be expressed directly in terms of the current and inductance as:

$$\boldsymbol{\psi} = \mathbf{L}(\mathbf{i})\mathbf{i} \tag{A.2.3-2}$$

Alternatively, $\boldsymbol{\psi}$ can be tracked as it proceeds from the linear region to the saturated region using equation (A.2.3-3) below.

$$\Delta\boldsymbol{\psi} = \mathbf{L}(\boldsymbol{\psi})\Delta\mathbf{i} \tag{A.2.3-3}$$

For several reasons, the expression of $\mathbf{L}$ as a function of $\boldsymbol{\psi}$ is more satisfactory. In the inductance matrix, stator leakage ($\mathbf{L}_{sl}$), rotor leakage ($\mathbf{L}_{rl}$), and mutual ($\mathbf{L}_{sr}$) inductances are symmetrical as given in equation (A.2.2-3). If all three elements of each flux linkage vector ψ_{sl}, ψ_{rl} and, ψ_{sm} are less then the threshold values ϕ_{sl}, ϕ_{rl} and, ϕ_{sr} then $\mathbf{L}_{sl}$, $\mathbf{L}_{rl}$, and $\mathbf{L}_{sr}$ can be given as:

$$\mathbf{L}_{sl}(\psi_{sl}) = \mathbf{L}_{sl}(0), \quad \mathbf{L}_{rl}(\psi_{rl}) = \mathbf{L}_{rl}(0), \quad \mathbf{L}_{sr}(\psi_{sm}) = \mathbf{L}_{sr}(0) \tag{A.2.3-4}$$

It will be convenient to show the saturation effects on the inductances of one phase. When only one of the phases of machine is energised and saturated, then the distribution of the flux linkages will be as shown below:

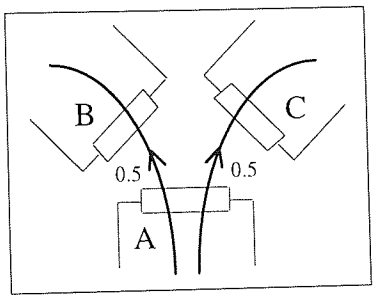

Fig. A.2.3-2 Distribution of flux linkages.

The distribution of the flux linkages for the other two phases can be treated in exactly the same way as shown in Fig. A.2.3-2. Three phase mutual inductance $\mathbf{L}_{mabc}$, and stator leakage $\mathbf{L}_{slabc}$ inductance can be separated as individually energised phases respectively:

$$\left.\begin{aligned} \mathbf{L}_{mabc} &= \frac{2}{3}L_{sr}\begin{bmatrix} 1.5 & -0.75 & -0.75 \\ -0.75 & 1.5 & -0.75 \\ -0.75 & -0.75 & 1.5 \end{bmatrix} = \mathbf{L}_{ma} + \mathbf{L}_{mb} + \mathbf{L}_{mc} \\ \mathbf{L}_{ma} &= \frac{2}{3}L_{sr}\begin{bmatrix} 1 & -0.5 & -0.5 \\ -0.5 & 0.25 & 0.25 \\ -0.5 & 0.25 & 0.25 \end{bmatrix}, \quad \mathbf{L}_{mb} = \frac{2}{3}L_{sr}\begin{bmatrix} 0.25 & -0.5 & 0.25 \\ -0.5 & 1 & -0.5 \\ 0.25 & -0.5 & 0.25 \end{bmatrix}, \quad \mathbf{L}_{mc} = \frac{2}{3}L_{sr}\begin{bmatrix} 0.25 & 0.25 & -0.5 \\ 0.25 & 0.25 & -0.5 \\ -0.5 & -0.5 & 1 \end{bmatrix} \end{aligned}\right\} \tag{A.2.3-5}$$

$$\left.\begin{aligned} \mathbf{L}_{slabc} &= L_{sl}\begin{bmatrix} 1 & 0 & 0 \\ 0 & 1 & 0 \\ 0 & 0 & 1 \end{bmatrix} \\ \mathbf{L}_{sla} &= L_{sl}\begin{bmatrix} 1 & 0 & 0 \\ 0 & 0 & 0 \\ 0 & 0 & 0 \end{bmatrix}, \quad \mathbf{L}_{slb} = L_{sl}\begin{bmatrix} 0 & 0 & 0 \\ 0 & 1 & 0 \\ 0 & 0 & 0 \end{bmatrix}, \quad \mathbf{L}_{slc} = L_{sl}\begin{bmatrix} 0 & 0 & 0 \\ 0 & 0 & 0 \\ 0 & 0 & 1 \end{bmatrix} \end{aligned}\right\} \tag{A.2.3-6}$$

If ψ_{sma} exceeds ϕ_{sm} and ψ_{sla} exceeds ϕ_{sl}, the equations below show how $\mathbf{L}_{sr}(\psi_{sm})$ and $\mathbf{L}_{sl}(\psi_{sl})$ are affected.

$$\text{If } \psi_{sma} > \phi_{sm}, \text{ then } \mathbf{L}_{sr}(\psi_{sm}) = \mathbf{L}_{sr}(0) - S_{sm}(\psi_{sma} - \phi_{sm}) \begin{bmatrix} 1.0 & -0.5 & -0.5 \\ -0.5 & 0.25 & 0.25 \\ -0.5 & 0.25 & 0.25 \end{bmatrix} \quad \text{(A.2.3-7)}$$

$$\text{If } \psi_{sla} > \phi_{sl}, \text{ then } \mathbf{L}_{sl}(\psi_{sl}) = \mathbf{L}_{sl}(0) - S_{sl}(\psi_{sla} - \phi_{sl}) \begin{bmatrix} 1.0 & 0 & 0 \\ 0 & 0 & 0 \\ 0 & 0 & 0 \end{bmatrix} \quad \text{(A.2.3-8)}$$

Saturation in $\mathbf{L}_{lr}$ is treated in exactly the same way as ($\mathbf{L}_{ls}$). Saturation parameters for the stator and the rotor are set artificially as:

$$\phi_{sl} = \phi_{rl}, \qquad S_{sl} = S_{rl} \quad \text{(A.2.3-9)}$$

The scalar parameters ϕ_{sm}, S_{sm}, ϕ_{sl}, S_{sl} describe the saturation of main and leakage flux paths and $\mathbf{L}_{sr}(0)$, $\mathbf{L}_{sl}(0)$, $\mathbf{L}_{rl}(0)$ describe the unsaturated mutual and leakage inductance matrices. If the machine is not saturated, the parameters of saturation (S_{sm} and S_{sl}) given in equations (A.2.3-7) and (A.2.3-8) are not used. If the machine is saturated, equations (A.2.3-7) and (A.2.3-8) show that the impedance of the machine will start to decrease at saturation point. Figure 4.7-2b shows the changes of the machine impedance with respect to the base voltage from the no-load test of the machine.

APPENDIX 3

DESCRIPTIONS OF EQUIPMENT USED IN THE TEST

A.3.1. Inverter

Company name	: Eurotherm Drives
Code number	: 584
Supply voltage	:380V to 460V ±%, 50/60 Hz
Supply current	: 18A
Power factor lag	: 0.86
Max. motor power	: 7.5kW
Output voltage	: Depend on input voltage
Cont. O/P current	: 16A
Overload	: 150% for 30 sec.
Output frequency	: 0 to 120Hz/240Hz/480Hz
Approx. power loss	:250W
Operating temperature	: 0 to 50°C

A.3.2. Signal Generator

Wavetek Arbitrary Waveform Generator

model 75

Max. output voltage : 5V peak to peak.

A.3.3. Data Acquisition Toolbox

Specification of Data Acquisition Toolbox for use with MATLAB:

Analogue to digital conversion:

Number of inputs	: 8 Single ended
ADC throughput	: 60K samples/sec overall

Sample and hold : 1 CH multiplexed

Resolution : 12 bits

Max. data transfer to disk : 60 K samples/sec overall

Input voltage range : ±5V

Input coupling : AC

Over voltage protection : 240v ac continuous

Input SNR :> 70dB per channel

External sample rate : dc-160,000Hz

Triggering : Keyboard or free run

Digital to analogue conversion:

No. of outputs : 2 Single ended

DAC throughput : 300K samples/sec

Resolution : 12 bits

Max. data transfer from disk : 2K samples/sec

Output voltage range : ±5V

Output coupling : DC

Over voltage protection : 240V ac continuous

Output SNR : > 70dB per channel

Triggering : Keyboard or free run

A.3.4. Temperature Labels

Stock numbers	Temperature limits	Sensitive levels	Level ranges
555-409	71-110°C	8	6-5-6-5-6-5-6°C
285-942	99-127°C	6	5-6-6-5-6°C
285-920	44-62°C	6	2-3-5-6-2°C

Table A.3.4.1 Temperature labels supplied from RS Compony.

A.3.5. Tachometer

Comark Tachometer Type 2101.

This tachometer detects the black and white colours on the rotor shaft and produces both analogue and digital signals.

A.3.6. Power scope

Type : PWD 880 Power Scope.

This scope has 4 input channels which are insulated from the output. The ratio between the input and output is 3200.

A.3.7. Current transducer

Company	: RS
Stock number	: 286-327
Rating	: 50A
Output	: 5V instantaneous
Turns ratio	: 1:1000
Supply voltage	: ±15V

APPENDIX 4

A.4.1 Calibration of Tachometer

The speed signals were measured with a tachometer which counts the black and white labels on the rotor shaft and produces periodical signals as shown in Fig. A.4.1. with a fundamental frequency of 8 times shaft speed. When the harmonic spectrum of the speed signal of no-load test is checked between 398 Hz and 400 Hz, the fundamental frequency is found as to be 399.05 Hz due to the four black labels and twice the fundamental frequency of 200 Hz. Therefore, the exact rotor frequency is found as to be 49.88125 Hz and the rotor speed is found 313.413 Rad/s for the no-load test.

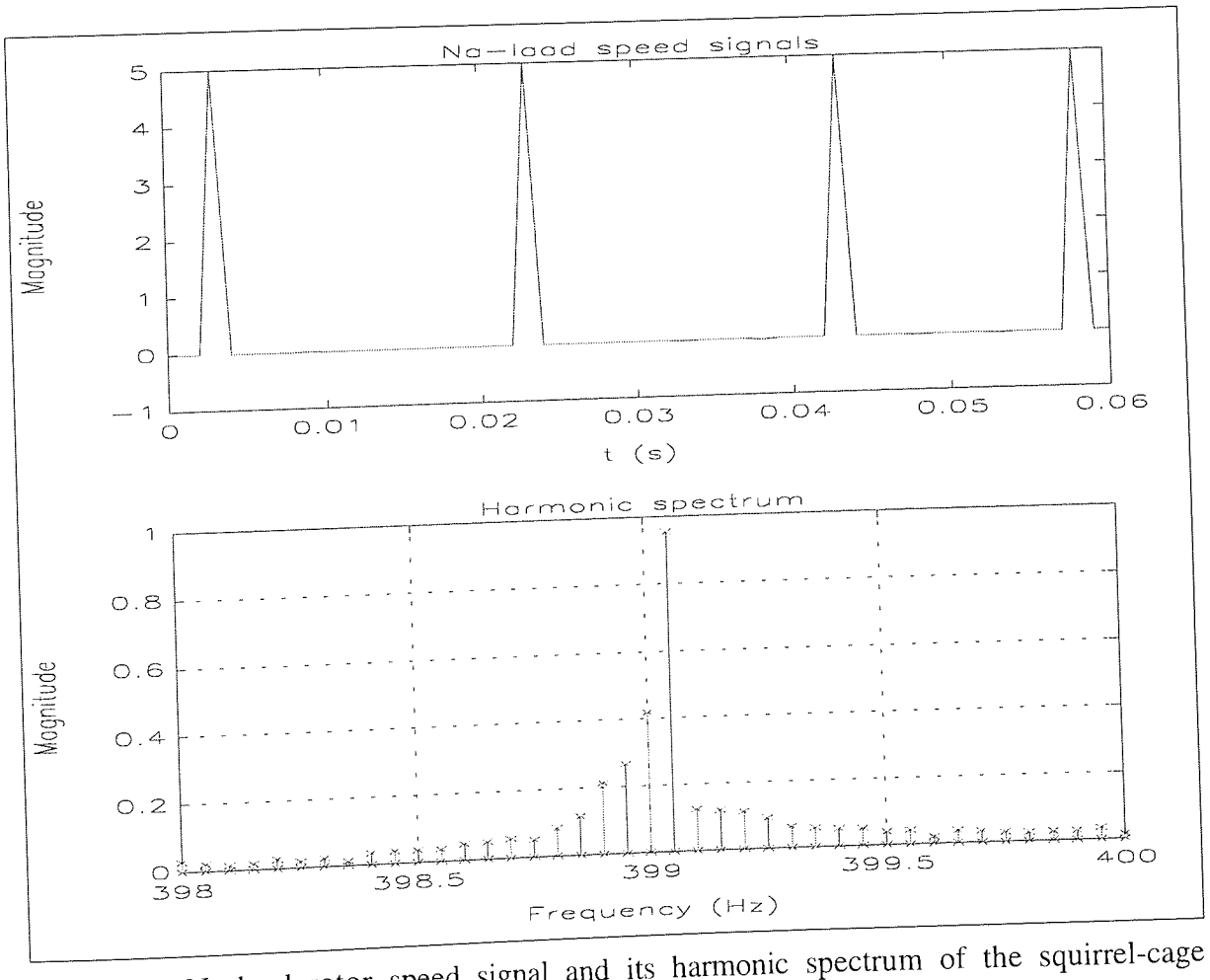

Fig. A.4.1 No-load rotor speed signal and its harmonic spectrum of the squirrel-cage induction motor.

As seen from the above figure, the speed signal is only varying between zero and 5 Volt. To produce the right speed shape, an RC circuit is connected to the output of the tachometer. The capacitor of the RC circuit is charged and discharged during each cycle due to the applied voltage and resistance. So that, the voltage across the capacitor gives the right speed shape. The correct speed ratio (499.2744) is found by dividing the calculated speed value of 313.413 Rad/s by the average capacitor voltage.

APPENDIX 5

PUBLICATIONS

A.5.1 Publication 1

"Estimation of induction Machine Parameters for Simulation of a Mixed-Frequency Test"

This paper has been published in the proceedings of the "6th International Conference on Electrical Machines and Drives", 8-10 September, pp. 208-212, Oxford, UK., 1993.

Aston University

Content has been removed for copyright reasons

A.5.2 Publication 2

"Mixed-Frequency Testing of Induction Machines Using Inverters"

This paper has been published in the proceedings of the "5th European Conference on Power Electronics and Applications", 14-17 September, Vol. 5, pp. 317-322, Brighton, UK., 1993.

A.5.3 Publication 3

"Aspects of Mixed-Frequency Testing of Induction Machines"

This paper has been published in the proceedings of the "ICEM'94 International Conference on Electrical Machines", 5-8 September, Vol. 2, pp. 623-628, Paris, France., 1994.

Aston University

Content has been removed for copyright reasons

A.5.4 Publication 4

"The "Variable Inertia Test" for the Full-Load Temperature Rise Testing of Induction Machines"

This paper has been accepted to be published in the IEE Part-B., 1993.

Aston University

Content has been removed for copyright reasons

Simulation of Induction Machines Using Phase Variables and the Explicit Inverse Inductance Matrix

İ. Çolak, PhD
S. D. Garvey, BEng, CEng, PhD
M. T. Wright, FEng, BSc, PhD, FIEE, FIMechE, SenMemIEEE [1]

Dynamics, Control & Vibrations Research Group, Aston University.

Indexing term: Power electronics, Induction motor, Phase equation, Simulation, Mixed-Frequency Test.

Aston University

Content has been removed for copyright reasons

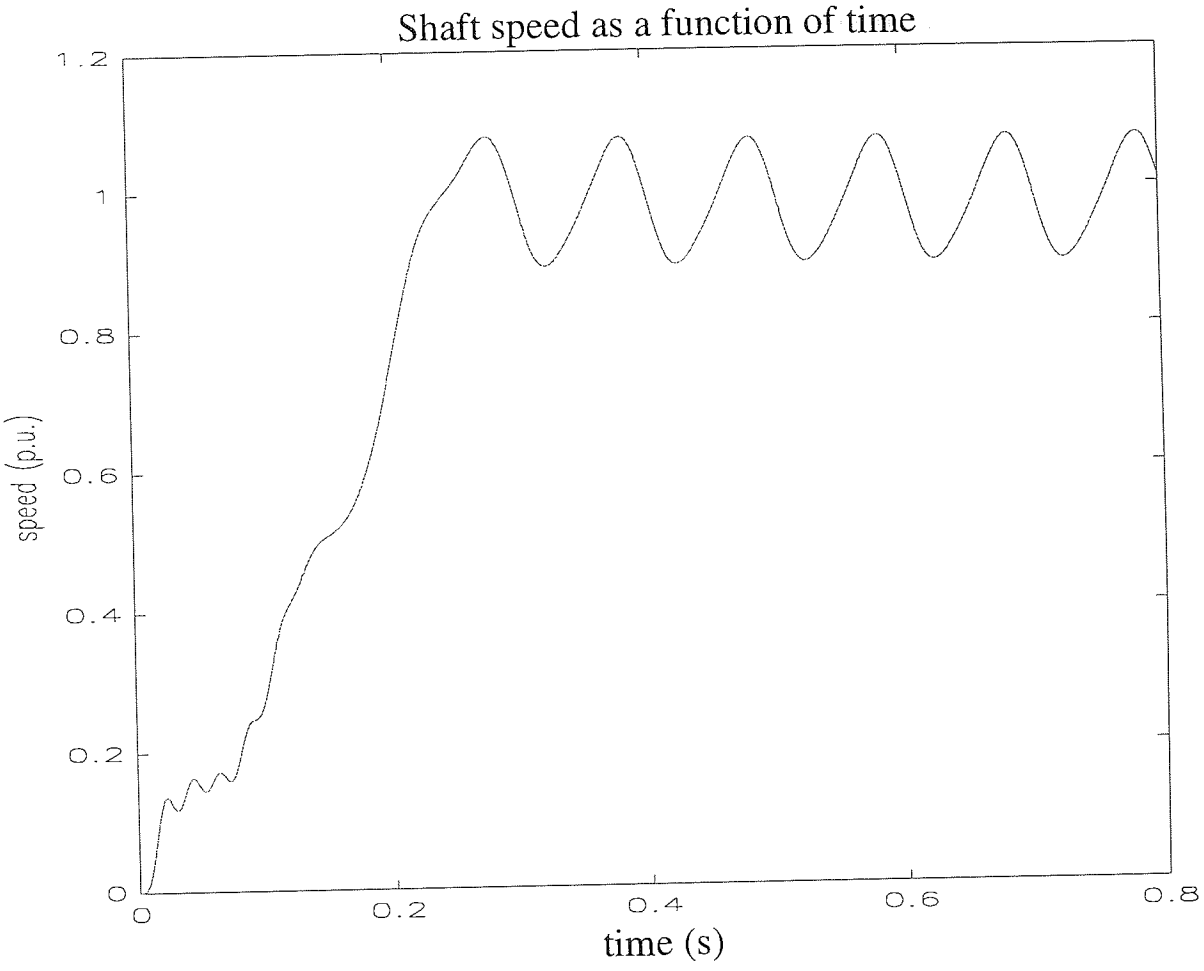

Fig. 1. Shaft speed as a function of time.

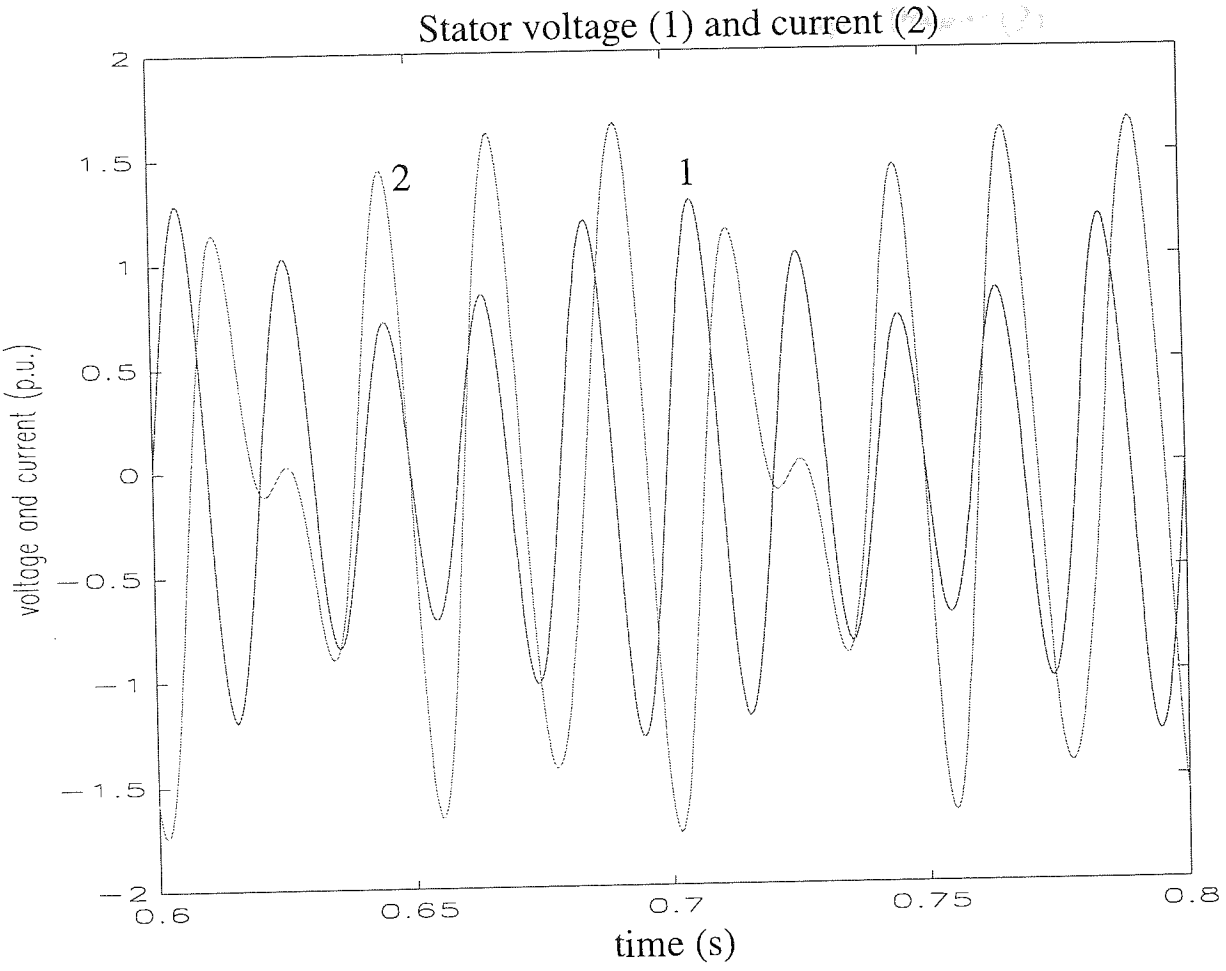

Fig. 2. Stator phase voltage and current.

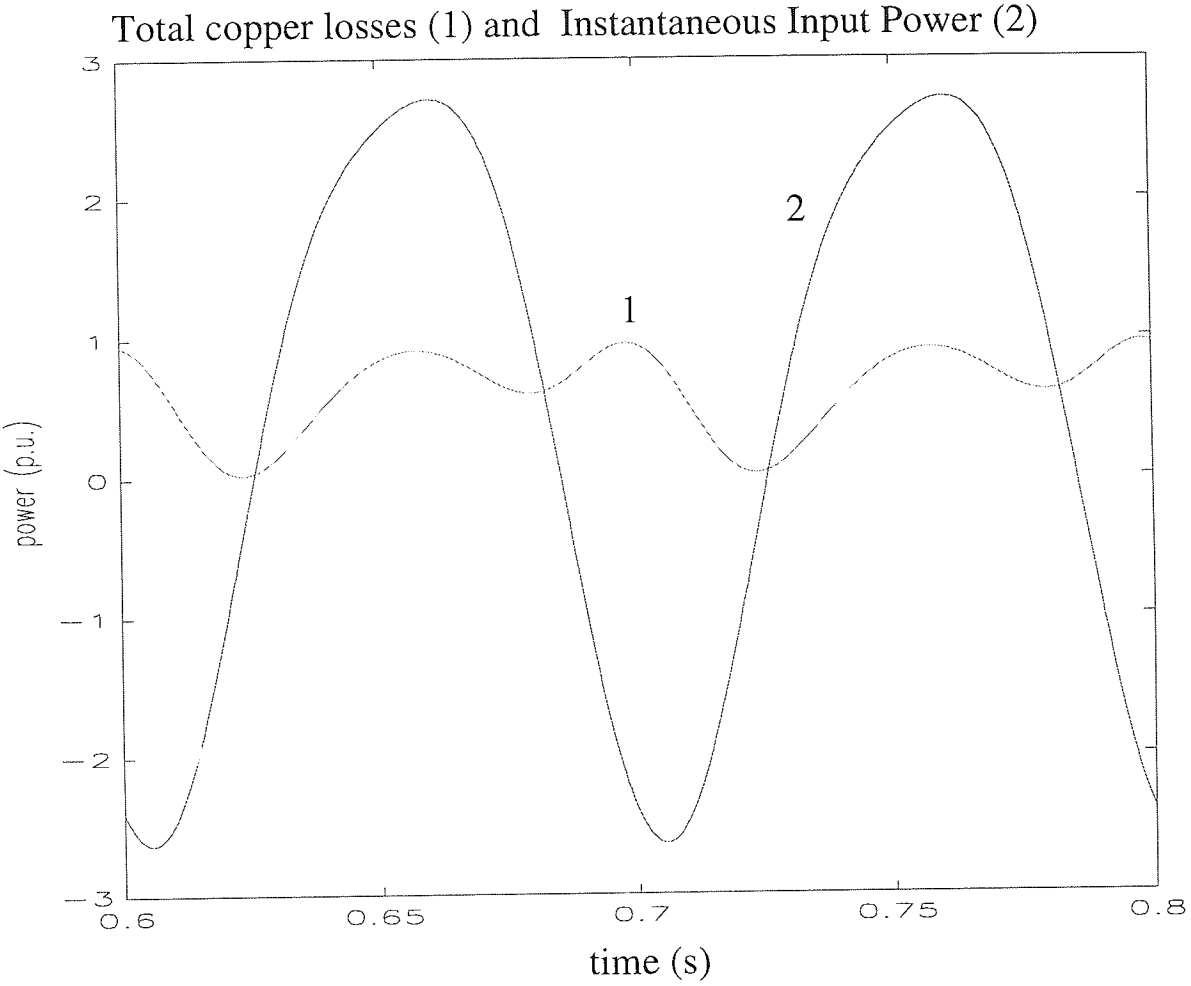

Fig. 3. Total instantaneous copper losses and total instantaneous input power.